PREPRINTS OF PAPERS

11th AEROSPACE
MECHANISMS SYMPOSIUM

NASA
National Aeronautics and
Space Administration

CALTECH

LOCKHEED

APRIL 28-29, 1977

GSFC — **GODDARD SPACE FLIGHT CENTER** —
GREENBELT, MARYLAND

PREPRINTS OF PAPERS

11th AEROSPACE

MECHANISMS SYMPOSIUM

APRIL 28-29, 1977

GODDARD SPACE FLIGHT CENTER
Greenbelt, Maryland

PREFACE

The Aerospace Mechanisms Symposium is devoted exclusively to the interchange of information relative to aerospace mechanisms. Information gathered from the formal presentations is but one of the benefits to be gained from this two-day meeting. Another important reward is gained from the professional and technical discussions and associations which begin here and are carried on long after the 11th Symposium is brought to a close. It is our sincere desire that you profit from the many opportunities presented during the planned break periods and social activities.

We hope your visit to the Goddard Space Flight Center is both enjoyable and rewarding.

Frank T. Martin
Host Chairman

ORGANIZING COMMITTEE

Charles W. Caole, General Chairman, LMSC
Ernest E. Sechler, Administrative Chairman, CIT
Alfred L. Rinaldo, Operations Chairman, LMSC
Frank T. Martin, Host Chairman, NASA-GSFC

Paul W. Bomke, NASA-JPL

Kenneth S. Bush, NASA-LRC

Kenneth C. Curry, NASA-JPL

John D. Ferrera, NASA-JPL

Angelo Giovannetti, NASA-ARC

James H. Parks, NASA-LRC

Bowden W. Ward, Jr., NASA-GSFC

David F. Welch, CIT

The Twelfth Aerospace Mechanisms Symposium is planned for April 1978 at
the NASA-Ames Research Center, Moffett Field, California

CONTENTS

CONTENTS (Continued)

CONTENTS (Continued)

DESIGN AND DEVELOPMENT OF THE

SPACE SHUTTLE TAIL SERVICE MASTS

By S.R. Dandage, N.A. Herman, S.E. Godfrey, and R.T. Uda

Planning Research Corporation

ABSTRACT

The successful launch of a Space Shuttle vehicle depends on the proper operation of two tail service masts (TSMs). Reliable TSM operation is assured through a comprehensive design, development, and testing program. In a previous paper (ref. 1), the TSM concept verification test (CVT) was described. This paper presents the results of the CVT and the resulting impact on prototype TSM design. The design criteria are outlined, and the proposed prototype TSM tests are described.

INTRODUCTION

Major requirements of the TSM mechanism are to:

o Provide physical support for the lines and cables connected to the Orbiter T-0 umbilicals.

o Support Orbiter checkout and launch preparations in an environment of salt air, sand, wind, and rain as defined in reference 2.

o Provide the capability for a test ("plugs out") umbilical disconnect and retract.

o Allow the carrier and supporting lines to remain connected to the Orbiter during payload exchange, external tank (ET) pressurization and tanking, solar and wind deflections, and Space Shuttle main engine (SSME) ignition, thrust buildup vibration, and acoustics.

o Rotate the 2250-pound carrier 11-15 degrees to detach it from the Orbiter and retract it (on command) into the TSM housing in approximately 1500 milliseconds.

o Be ready to reconnect a new Orbiter within 100 hours after launch.

o Provide the capability to pre-position the carrier with quick disconnects (Q/Ds) and lines installed, to support installation of the carrier on the Orbiter.

Two TSMs, identified as LOX TSM and LH$_2$ TSM, are located separately on two sides of the Orbiter. Figure 1 shows the concept of the TSM and its major components. Telescopic links are used to avoid excessive vibration traveling to and from the Orbiter. Power for disconnecting and retracting the umbilical carrier is supplied by a dropweight. Tension latches in the upper links and compression shock absorbers in the lower links effectively secure the carrier to the mast during the retract process. Belleville springs are used to minimize the instantaneous tensile force peaks in the upper links which also contain shock absorbers for compression.

TSM DEVELOPMENT PROGRAM

A comprehensive TSM design and development program (figure 2) is in progress at John F. Kennedy Space Center, Florida. The design is performed with the help of a kinematic study (a detailed stress analysis and an acoustic analysis of the blast structure) performed on the PDP-11 computer graphic system (a dynamic analysis program using the GE-635 computer).

Two test facilities (figure 3) are utilized in the TSM test program. The concept verification test facility (CVTF) consists of a liftoff simulator erected inside a building. The launch equipment test facility (LETF) includes a random motion simulator, cryogenic supplies, and a test control room (ref. 3).

CONCEPT VERIFICATION TESTING

The CVT provided early confidence in the feasibility of the TSM concept before a full scale prototype was fabricated. Only critical TSM concepts, those involving the disconnect process using lanyards and telescoping links, were tested. In effect, only the top portion of the mast was modeled. The dropweight power system, bonnet operation, blast structure, and retract phase of the TSM operation were not included in the CVT model. Figure 4 shows an overall view of the CVT rig. Further details of the rig and its design are included in reference 1.

CVT RESULTS

The concept verification testing included a number of component tests as well as seven dynamic system tests. A full account of these tests is available in the Test Report, TR-1443 (ref. 4). The following is a brief summary of the results.

The first dynamic test was conducted at about half the maximum anticipated operating speed (at 0.6 g nominal masthead acceleration) in order to avoid structural damage due to any unexpected problems.

The test was highly successful, and the disconnect operation took place without any problems. Therefore, the second test was performed at the maximum anticipated operating speed (1.2 g nominal masthead acceleration). The test indicated the feasibility of the TSM concept. However, two minor problems were discovered during the test which were resolved before the next test. Tests 3 to 7 obtained proper chronological sequence of operations and effects of various modifications. These tests were performed at the minimum anticipated nominal acceleration (0.8 g). It was determined during initial tests that the flexhose was not as stiff as anticipated, and the motion of the masthead was a result of the bottoming out of the lower links (which did not have shock absorbers). The link lengths, lanyard lengths, and initial masthead position had to be adjusted to achieve the desired sequence and to compensate for the flexhose effect. One disconnect (test 4) was conducted from a 2-inch higher initial position of the umbilical carrier. The link forces in this test were high due to the carrier descending through a larger distance under gravity. Disconnects from any higher carrier position were postponed until prototype testing due to the absence of shock absorbers in the links. The desired chronological sequence was obtained in test 7.

The force levels in the lanyards, links, and other components of the rig generally were as anticipated. Forces exerted on the liftoff simulator were acceptable. During independent side loading tests, the link-masthead assembly was found to be considerably stiffer than anticipated. This, however, was still within the expected side motion requirements of the TSM.

Useful data on the vacuum jacketed (VJ) flexhose were unavailable prior to CVT. Independent investigation of the hose characteristics and its effect on masthead dynamics were undertaken. A hysteresis type behavior of the hose and a significantly large dead band were observed. However, the TSM operation did not seem to be significantly affected by the VJ flexhose properties.

During deceleration of the masthead, both upper and lower links experienced compression which consequently raised the umbilical carrier. As anticipated, carrier rise was too low to cause any problems during the CVT. However, in the prototype, the masthead-carrier assembly traces an arc. Therefore, carrier inertia, together with some carrier rise, conceivably could have caused the carrier to overturn. This potentially hazardous situation was corrected in the prototype design by raising the upper link attachment point on the mast, thus making the upper link angle more acceptable.

PROTOTYPE TSM DESCRIPTION

The prototype TSM is a full-scale model of the production design with only minor differences. The basic components are briefly described in the following paragraphs (refer to figure 1).

T-0 Umbilical Carrier. The time-zero (T-0) umbilical carrier interfaces with the airborne Orbiter skin panel. It includes the fluid couplings and electrical connectors required to service the Orbiter vehicle at or near T-0 in the countdown. It also provides the capability for simultaneously disconnecting these couplings and connectors at liftoff.

Links. Two sets of telescopic links support the carrier to the mast. Each set consists of an upper and lower link. The prototype upper links contain two latches and belleville springs for tension. All prototype links are equipped with compression shock absorbers to reduce impact forces at the end of the telescoping action. A new, improved design of links has been made for the production TSM. This new design contains ratchet type latches. Figure 5 shows the carrier and the prototype links as assembled to the mast.

Mast. The mast supports the flexhoses and lines going from the mobile launcher platform (MLP) to the umbilical carrier interface. During carrier retract, the mast rotates about a pivot located near the base of the TSM structure until the action is stopped by mast shock absorbers. Figure 6 shows the completely fabricated mast being transported to the CVTF for assembly and testing.

Bonnet. The bonnet, along with the blast structure, provides blast protection for the TSM assembly. It is held in the "up" position until the carrier is safely inside the blast structure. At this point, the bonnet is "kicked" down by the bonnet thruster to completely enclose the assembly.

Dropweight. The dropweight provides power for TSM retraction. When the separation bolt is pyrotechnically released, energy is transferred using a lanyard system from the dropweight through the carrier to the mast.

Separation Bolt. For prototype TSM testing, the separation bolt will be replaced with a pneumatically released separation nut designed to operate at 2000 psig of GN_2.

Lanyard System. This system consists of a pair of identical lanyard assemblies. Each assembly has two lanyards connecting the upper and lower sides of the carrier to a common lanyard tiepoint. The main lanyards run from this tiepoint over the mast sheaves to the dropweight through a mechanical advantage system.

Shock Absorbers. In addition to shock absorbers in the four links, one shock absorber is used to dissipate energy from the falling dropweight. Two shock absorbers are used for decelerating the rotating mast and two for the bonnet.

Blast Structure. The blast structure provides structural support and protection for the TSM subsystems. It is designed to withstand dynamic, blast, acoustic, and vibrational loads, and temperature gradients created by vehicle exhaust blast at liftoff. Figure

7 shows the blast structure after being completely fabricated.

OBJECTIVES OF PROTOTYPE TESTING

The main objective of prototype testing is to validate/verify that the test model will operate as intended under simulated launch conditions prior to fabrication of production units. If any anomalies or failures occur, necessary redesign and/or changes will be made to rectify the inadequacy. In addition to the above, the prototype testing will serve the following purposes:

o A highly sophisticated computer model of the TSM has been developed (ref. 5). The system equations are obtained by Lagrange Formulation and are accurately solved by using a fourth order Runge-Kutta algorithm. By comparing prototype TSM results with the computer predictions, the model will be validated and improved if necessary. The model has previously been used in prototype design and will be used further for the production TSM.

o The prototype tests will provide early familiarity of TSM to test crews and operations personnel. The tests will also help develop and refine operations concepts and criteria.

o Tests will be conducted to verify hardware operation under nominal and off-nominal launch environments and umbilical release configurations.

o The prototype tests will demonstrate reliability and maintainability of the TSMs.

PROTOTYPE TEST PHASES

Testing of the prototype TSM will be accomplished in three phases. These phases are described in the following paragraphs.

Phase I Testing. Phase I testing includes TSM system testing without using the upper housing (hood), bonnet, bonnet thruster, and bonnet decelerator. Testing will be accomplished in the CVTF. Dynamic tests will be performed with the liftoff simulator airborne skin panel at a fixed position at test initiation. No induced environmental dynamic simulations such as liftoff and random motion simulations will be applied.

Phase II Testing. Phase II testing includes testing of the complete TSM system which includes using the upper housing (hood), bonnet, bonnet thruster, and bonnet decelerator. Testing will be accomplished in the CVTF. Dynamic testing will be performed with the simulator panel at a fixed position at test initiation and also with liftoff simulation. No induced environmental dynamic simula-

5

tions will be applied other than liftoff simulation.

Phase III Testing. Phase III testing includes full dynamic testing of the TSM including liftoff and random motion simulations. Testing will be accomplished in the LETF. Induced environments such as cryogenic fluid flows, simulated blast temperatures and pressures, and acoustic effects will be excluded.

PROTOTYPE TEST REQUIREMENTS

General test and data requirements are published in the Test Plan (ref. 6). Detail test requirements and procedures are presented in the Test Requirements document (ref. 7).

Prior to dynamic testing, weights and inertial properties of major moving assemblies were measured. A test fixture was designed and fabricated to measure mass moments of inertia by the quadrifilar torsional pendulum method.

Sixty-three strain gages, 25 accelerometers, 6 linear potentiometers, 2 angular potentiometers, 4 microswitches, 4 load cells, 1 pressure transducer, and 1 event marker will record sufficient data to evaluate complete performance of the TSM. Nineteen critical dynamic measurements will be available for "quick look" within minutes after the test for test engineers to obtain adequate information to reconfigure the system for the next test. All recorded data will be computer-processed (digitized, filtered, integrated, and plotted) as required. A computer program for reducing and integrating accelerometer data on the Raytheon RDS 500 computer has been developed and tested. In addition, three cameras will take motion pictures of the TSM from different angles during each dynamic test. Still photographs will record pre- and post-test static observations.

Phase I tests consist of three parts. Part 1 includes component and subsystem tests such as lanyard spring rate test, mast and dropweight shock absorber tests, link shock absorber tests, mast torsion, carrier to blast structure clearance test, and various adjustments. Part 2 includes seven dynamic tests at the minimum nominal operating speed. The tests cover disconnects from various initial carrier heights. Four additional tests at maximum nominal operating speeds are proposed under Part 3 testing.

Phase II testing also consists of two parts. Part 1 consists of bonnet and bonnet system tests, and Part 2 includes six complete system tests.

Requirements for Phase III testing have not been determined as of November 1976.

CONCLUSION

The concept of disconnecting and retracting the umbilical carrier by using lanyards, telescoping links, and a rotating mast is feasible. Forces in various components of the TSM as well as forces on the Orbiter can be controlled within reasonable limits.

REFERENCES

1. Uda, Robert T., "Space Shuttle Tail Service Mast Concept Verification," 10th Aerospace Mechanisms Symposium Proceedings, JPL Technical Memorandum 33-777, Pasadena, California, July 1, 1976.

2. "Space Shuttle Ground Support Equipment General Design Requirements," SW-E-0002, Lyndon B. Johnson Space Center, Houston, Texas, January 6, 1976.

3. Uda, R.T., Dandage, S.R., and MacDonald, D.C., "Simulation Testing of Launch Critical Shuttle Ground Support Equipment at the Launch Equipment Test Facility, Kennedy Space Center, Florida," Ninth NTEC/Industry Conference Proceedings, Technical Report NAVTRAEQUIPCEN IH-276, Orlando, Florida, November 1976.

4. Dandage, S.R., "Space Shuttle Tail Service Mast: Concept Verification Test Report," TR-1443, Kennedy Space Center, Florida, July 1976.

5. Dandage, S.R., "Space Shuttle Prototype Tail Service Mast: Dynamic Analysis," TR-1440, Kennedy Space Center, Florida, to be published.

6. Dandage, S.R., "Space Shuttle Prototype Tail Service Mast: Test Plan," TR-1439, Kennedy Space Center, Florida, May 1976.

7. Uda, R.T., "Space Shuttle Prototype Tail Service Mast: Test Requirements," TR-1473, Kennedy Space Center, Florida, September 1976.
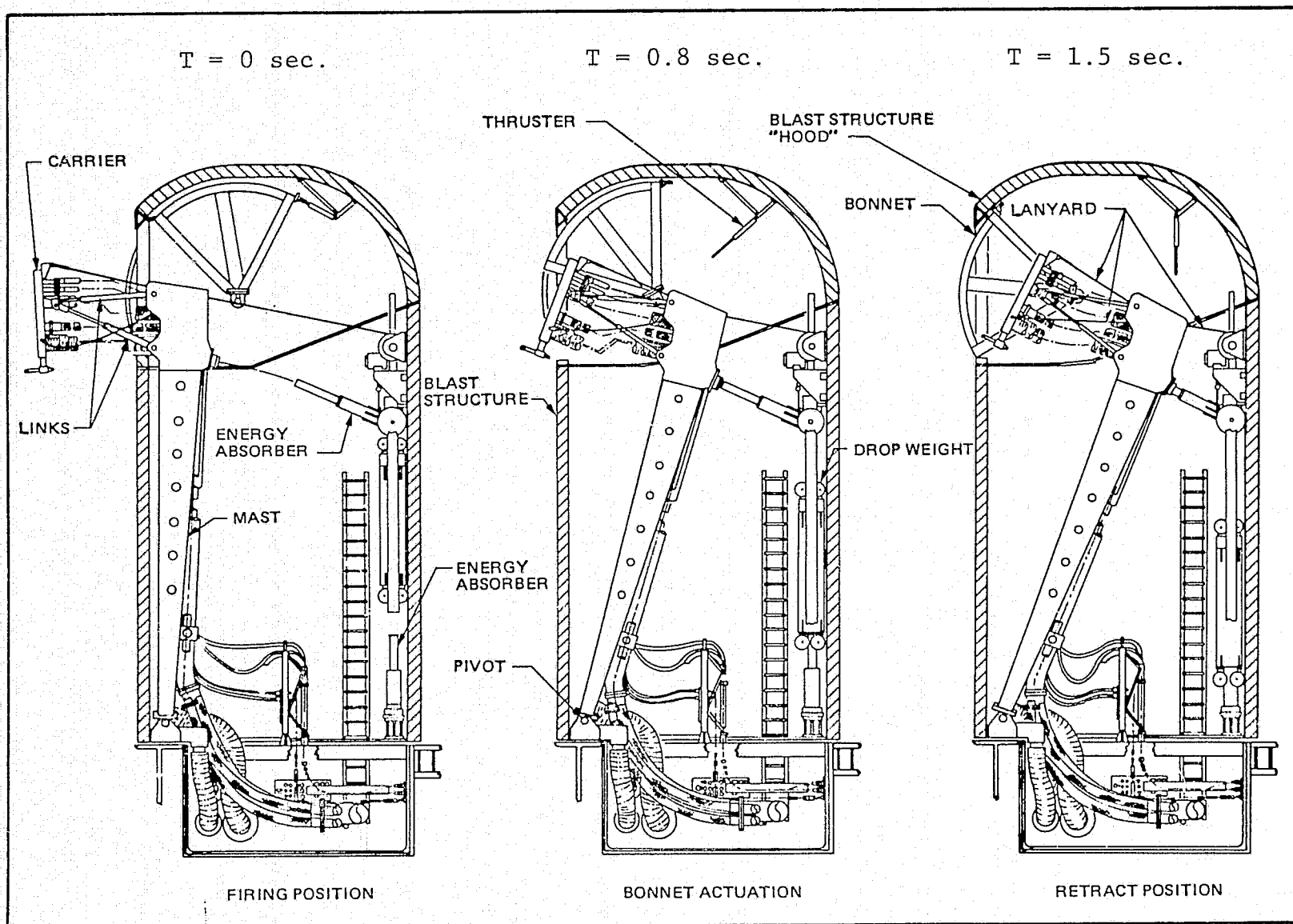
Figure 1. Conceptual Operation of the TSM

```
                    ┌─────────────────────┐
                    │   PROTOTYPE TSM      │
                    │      DESIGN          │
                    └─────────────────────┘
        ┌────────────────┬──────────────────┬──────────────────────┐
        ▼                                                           ▼
┌─────────────────────┐                        ┌─────────────────────────────┐
│  PROTOTYPE TSM      │                        │  CONCEPT VERIFICATION TEST  │
│   FABRICATED        │                        │     RIG FABRICATED          │
│                     │                        │   (ONLY THE TOP HALF OF     │
└─────────────────────┘                        │     TSM FABRICATED)         │
         │                                     └─────────────────────────────┘
         ▼                                                  ▼
┌──────────────────────────┐              ┌───────────────────────────────┐
│   PROTOTYPE TESTING      │              │   CONCEPT VERIFICATION        │
│ (PERFORMANCE OF COMPLETE │              │        TESTING                │
│    TSM VERIFIED)         │              │ (ONLY THE CRITICAL CONCEPTS   │
└──────────────────────────┘              │       VERIFIED)               │
                                          └───────────────────────────────┘
              ┌─────────────────────┐
              │  PRODUCTION TSM     │
              │     DESIGN          │
              └─────────────────────┘
                       │
                       ▼
        ┌──────────────────────────────┐
        │  QUALIFICATION TESTING        │
        │   (TESTING UNDER ALL          │
        │  OPERATING CONDITIONS)        │
        └──────────────────────────────┘
```

PAST

FUTURE

STATUS AS OF NOVEMBER 1976
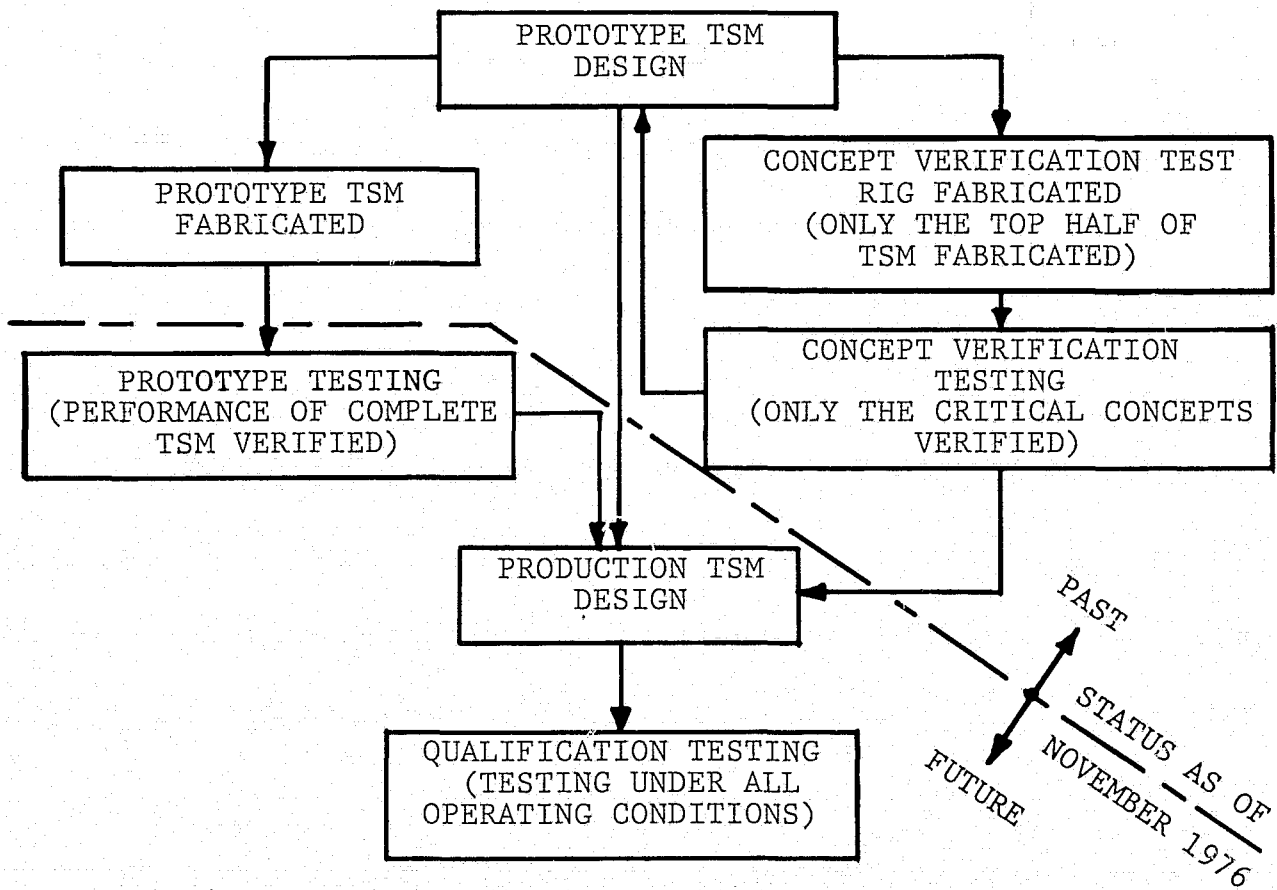
Figure 2.   TSM Design and Development Program
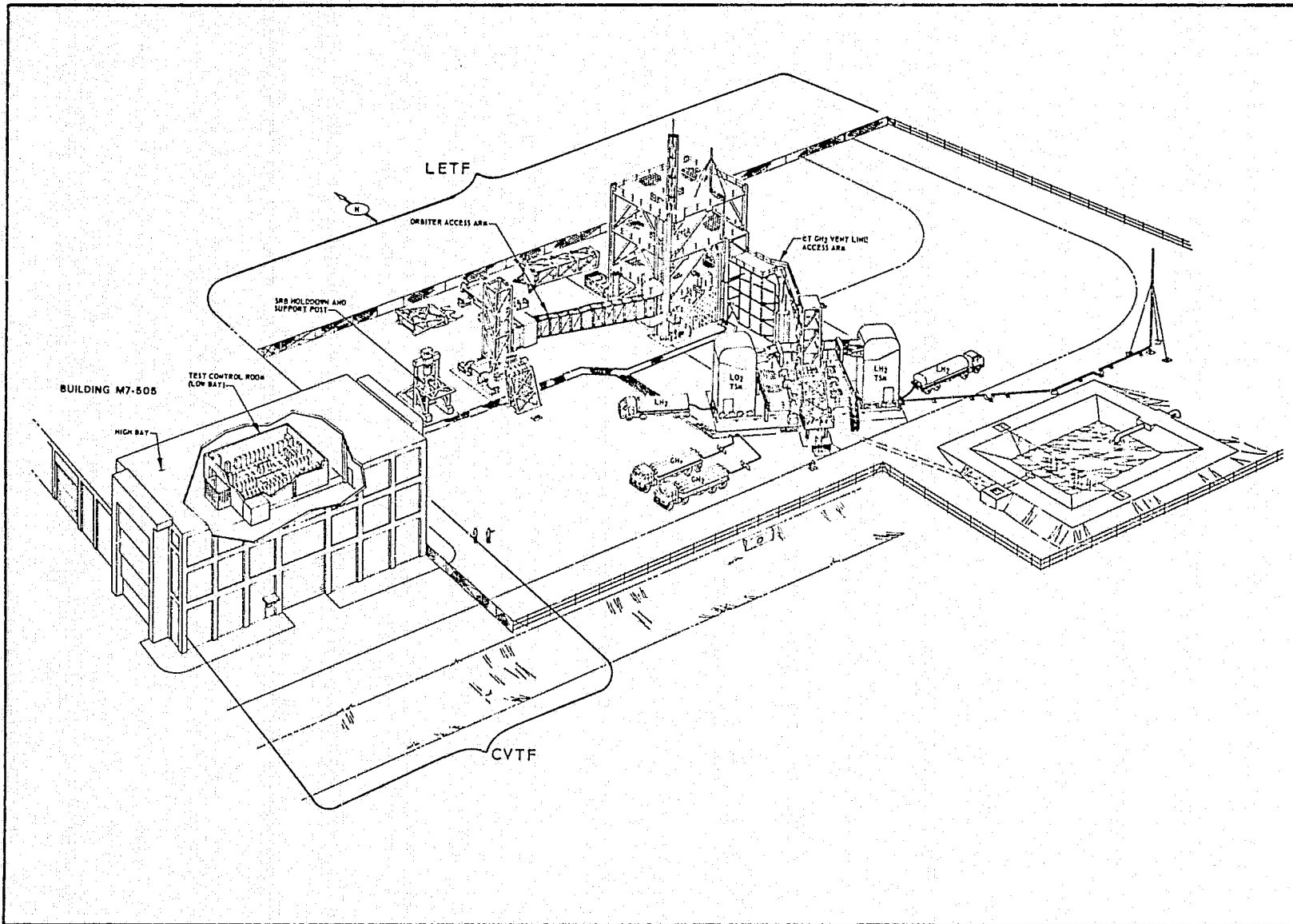
Figure 3.   CVTF and LETF Isometric Diagram
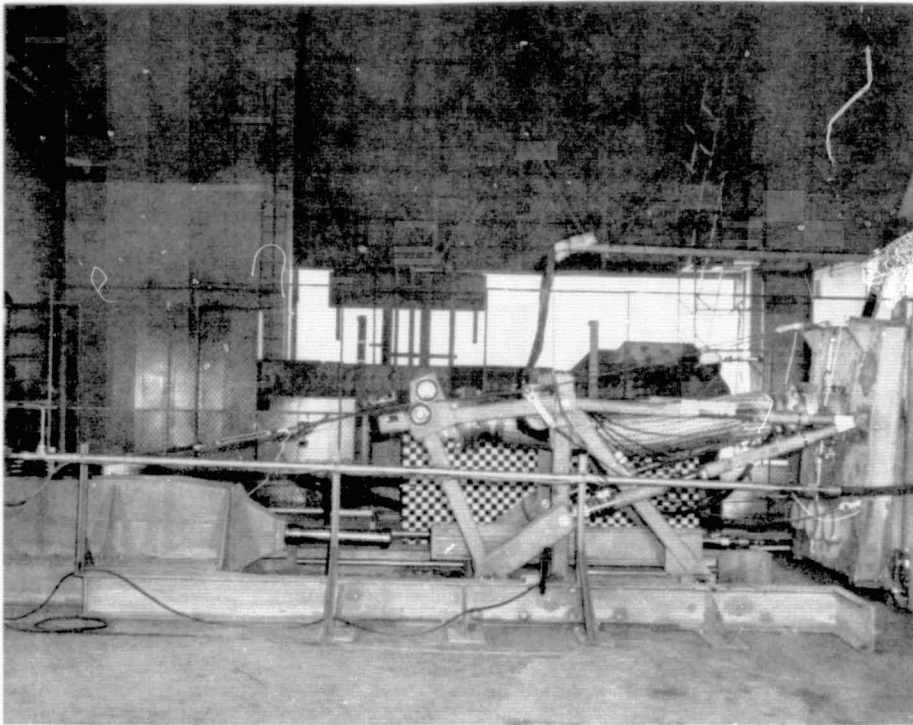
Figure 4.   Overall View of the CVT Rig
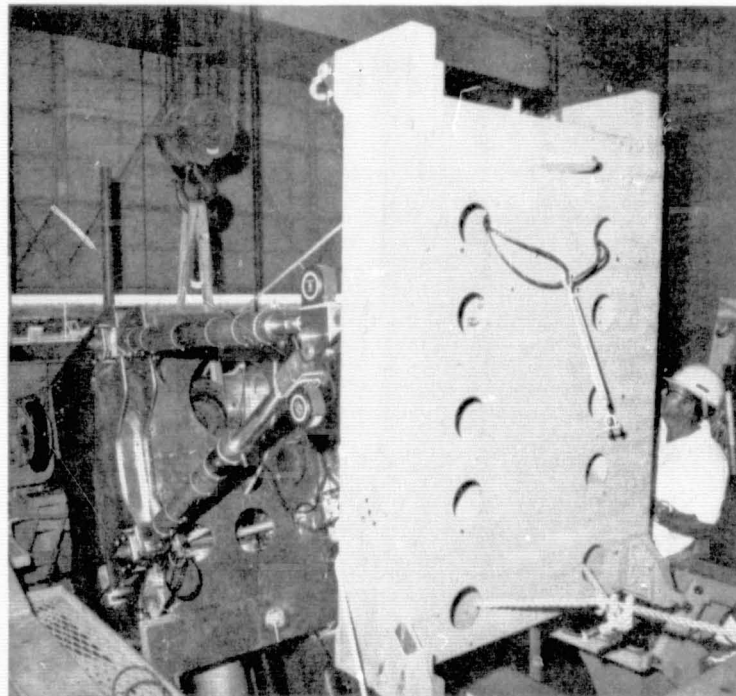
Figure 5.   Umbilical Carrier and Links, TSM Prototype

11
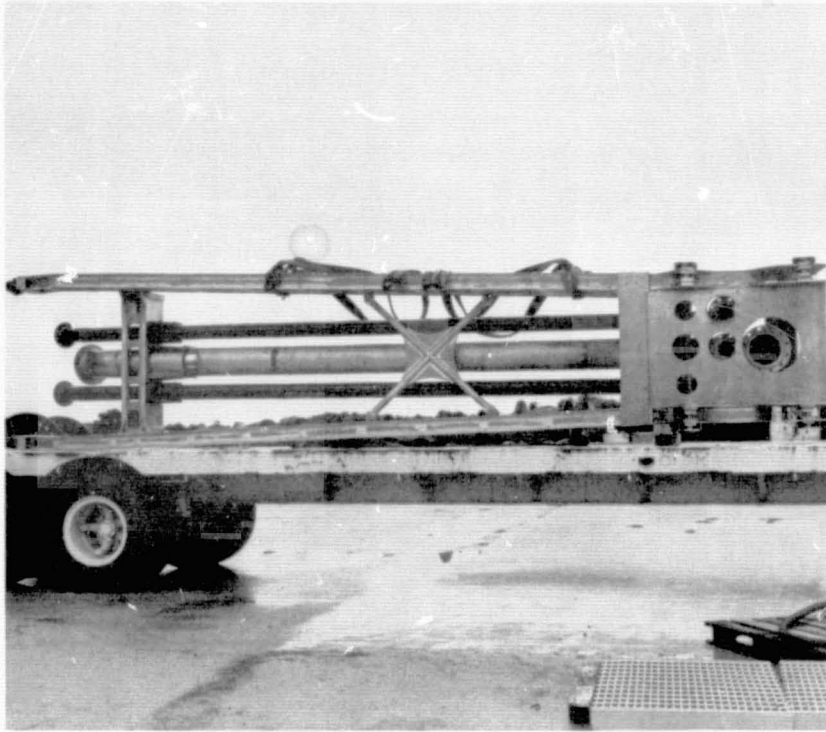
Figure 6. Completely Fabricated Prototype Mast

Figure 7. Completely Fabricated Blast Structure, TSM Prototype

12

SCANNING AND FOCUSING MECHANISMS OF METEOSAT RADIOMETER

By J. JOUAN Société MATRA (France)

1. ABSTRACT

Two mechanisms, both of screw-jack type are described. The scanning mechanism, an oil lubricated and sealed unit drives and accurately positions the telescope of the METEOSAT radiometer. The dry lubricated focusing mechanism is used to adjust the focus of this telescope.

These two mechanisms have been designed developped and tested within the METEOSAT Radiometer programme under a contract from the «Centre National d'Études Spatiales» followed at the beginning of 1973 by a contract from the European Space Agency.

The METEOSAT programme is nearly completed now and the first flight model will be launch at the end of this year.

2. INTRODUCTION

The scanning and focusing mechanisms are settled onboard the METEOSAT Radiometer, a large Camera which will take line by line pictures of the earth from a geostationary satellite in the same manner as a TV picture using both the spin of the spacecraft and the tilt of a telescope. An overall view of the radiometer is given on Fig. 1.

The scanning mechanism provides the $\pm 9^0$ degrees tilt angle of the telescope through 2 500 elementary steps of $1.256 \ 10^{-4}$ radian. Twenty five minutes are needed to perform the 2 500 steps corresponding to one image and the mechanism is able to drive back the telescope ten time faster.

As the radiometer image quality is closely dependent on the characteristics of the scanning law, the mechanism is required to fulfil functional performances specifications particularly severe in terms of linearity of the scan curve, accuracy of each steps as well as repeatability of the short-term scanning. Moreover, the mechanism is required to work during three years in deep space environment conditions, which represents about 50 000 cycles.

The focusing mechanism allows ± 12 millimiters shift of the telescope focus by step increments of 0.140 mm. The focus adjustment is achieved by moving a dihedral reflector according to a pure straight-line motion.

In the following the main requirements of each mechanism are summarized and their design and performances are described in detail. Finally the main problems encountered during development and the way they have been solved are reviewed.

3. SCANNING MECHANISM

3.1 - Summary of the requirements

The main requirements derived from the radiometer system requirements are summarized in the following table. The scanning law requirement is related to the tilt angle of the moving telescope considered as a rigid body.

PARAMETER	NOMINAL VALUE	ACCURACY
● **Functional performances**		
* Scanning law requirements		
— number of steps	2 700	
— step increment	$4 \pi \ 10^{-5}$ rd	10 %
— 50 steps increment	$2 \pi \ 10^{-3}$ rd	$2 . 10^{-4}$ rd
— slope of the global law	$\dfrac{0,054 \pi}{1\ 350}$	1 %
— repeatability of positioning at constant temperature		$2.5 \ 10^{-6}$ rd
* Step period	0.6 s	
* Rise time of each step	0.180 s	10 %
* Number of cycles over 3 years	50.000	
● **Physical parameters**		
* Mass	< 5 Kg	
* Electrical consumption		
- peak	8 W	
- average	3 W	

Since the beginning of the development, the high degree of criticality of the scanning drive mechanism has been recognized, and the baseline has been selected primarily in such a way as to achieve the highest possible reliability. For that reason, well proved state-of-the art solutions have been preferred to more sophisticated ones which could have presented higher development risks and associated costs. Moreover the presence of optical components and cooled detectors have led to avoid any risk of contamination and by the way to seal the mechanism.

Therefore the main features of the selected baseline are :

● Screw-jack unit driven by a stepper motor.
● Conventional oil lubrication of the sealed unit.
● Antibacklash links between moving parts.
● Telescope bearings made of flexural pivots.

After comparative study, the screw-jack device has been preferred to the servo-loop direct drive with optical encoder. The screw-jack offers excellent performances which may be achieved with existing technologies and standard components. Its basic advantage is that a high reduction ratio is obtained withing moderate size and weight : as a result, a high torque margin is available, and the accuracy mainly depends on the last stage, i.e. the screw nut assembly itself ; because of the irreversibility, the telescope position remains fixed when the motor is not supplied with electric power ; a screw jack unit combined with a stepper motor is easily controlled in an open loop manner without the need of a position pickoff.

The drive electronics is thus simplified, and consist mainly of a set of power amplifiers feeding the motor windings, and digital circuits generating the logic sequence. Furthermore, the line identification system being not in the control loop is not essential for the operation of the drive mechanism, which improves significantly the overall reliability.

3.2 - Detailed description (Ref. Fig. 2)

Screw-jack unit (Ref. Fig. 3)

The screw jack comprises a stepper motor, a gear box, the lead screw/nut assembly and a potentiometer. All these components are enclosed in a hermetically sealed housing. A set of two metallic bellows provides for relative translation motion of the screw.

The stepper motor, a 200 steps per revolution SLOSYN HS 25 device drives the nut through a gear box having a reduction factor of 3.

The nut is mounted on two pairs of pre-loaded ABEC 7 MPB ball bearings. The rotation of the nut causes the screw to move in translation, as the leading frame prevents the screw from rotating. A potentiometer with two triangular plastic film paths is driven by the motor through the same reduction ratio of 3. The whole unit is splash lubricated, which avoids the difficult problem of dry lubrication in hard vacuum conditions. The screw-jack design has some noticeable advantages : the stepper motor has accurate and steady position at rest ; torque marging of 14 insures that no step can be missed except in the case of a command failure. The scanning accuracy is further improved by the control logic/motor design, as each telescope angular increment corresponds to 12 elementary steps at the motor. Actually, due to the high overall reduction ratio, only the screw/nut assembly is critical as far as the scanning accuracy is concerned. High performances may readily be achieved by a carefull machining and running of the screw. Gears are antibacklash type ; materials are selected to minimize the effects of a temperature variation.

Leading frame and capstan device (Ref. Fig. 4)

The screw is fastened to a rectangular frame at its two tips. The linear motion of the frame is transformed into telescope rotation by the use of flexible metallic blades. One end of each blade is clamped to a curved sector fixed to the telescope, the other end being fastened to a small bar which is tightly connected to the frame by a set of prismatic shapes when being on orbit. A tensioning spring applies a constant load to the blades, in order to prevent from any backlash.

During launch phase, the telescope bearing latching device performs two functions which prevent the screw and the flexible blades from being overloaded by differential vibration motions.

— When the telescope is pulled down, the bars supporting the blades are disconnected from the leading frame so that not any effort can be transmitted through the blades.
— The leading frame itself is pushed again the main structure by the mean of calibrated springs fixed on the sectors.

15

When releasing the telescope, the bars, pushed up by a set of springs connect again with the leading frame. In the same time, the leading frame being free of any load comes back to its nominal scanning position.

3.3 - Modes of operation

Normal mode

Once per spacecraft revolution, i.e. every 600 ms, the motor drive electronics, stimulated by a signal, generates a sequence of logic signals which supply by groups of two the windings of the motor. 12 steps corresponding to a rotation of $21°6$ are then performed during a time lapse of 180 ms. Taking account of the reduction ratios, the nut and the potentiometer turn through $7°2$ in the same time and the screw moves of $35\ \mu$. The distance between the screw axis and the telescope axis of rotation being 278.5 mm, the corresponding angular increment of the telescope is 1.2566×10^{-4} rd.

The analog signal supplied by the potentiometer is digitalized and transmitted by telemetry. The lower bit corresponds to 4 motor steps, i.e. 1/3 rd telescope step.

A low voltage (2.5 V) ensuring a locking of the motor on the step is applied to the windings during the following 432 ms time interval during which the scanning of a line on the earth is situated.

Retrace mode

The sequence of operations is similar when the telescope moves back. However, a reduction of the rise time for each step (45 ms) and the higher rate of input timing signals allow to perform the 2700 steps 10 times faster i.e. in about 2.5 minutes.

An accurate reference position of the telescope is obtained by multiplexing the signal supplied by end of frame switches to the line identification signal coming from the potentiometer.

3.4 - Performances

The scanning laws are measured by using a laser interferometer the resolution of which is 0.1 second of arc. The measurements are handled through a Hewlett Packard computer.

The linearity requirement is readily met and the step accuracy is well within the specification : the 2700 increments measured on flight models is constant within 3 % (10 % specified) (see Fig. 5).

Step repeatability has been checked and the maximum deviation measured does not exceed $1.5\ 10^{-6}$ rd.

Life tests up to 300.000 cycles representing nearly 20 years life have been performed without any degradation of the scanning law.

3.5 - Main problems encountered

— On the first breadboard built at the beginning of the contract, a modulation of the scanning law at the period of the screw turn has been identified so that the accuracy requirement was not met. This modulation was induced by a pitch movement of the leading frame around an axis passing through the screw at the center of the nut. This movement was amplified by the arm level between the screw axis and the capstan sectors. A minor modification of the leading frame allowing the screw axis to lie in the plane containing the blades and tangential to the sectors results in completely avoiding such a perturbation.

16

— Achievement of a perfectly sealed housing (leak rate below 2.10^{-9} cm³ at m/sec of helium) has been the most worrying problem and has led to a large amount of development tests.

● sealing of materials of the same nature, stainless steel waves of bellows, aluminium caps of the housing has been obtain by electronic beam welding.

● sealed assembly of parts of different nature i.e. stainless steel element on aluminium element has been obtain by using the so-called "incrustation" technic developped for nuclear application.

This consist to sink a shaped stainless steel block in the aluminium block heated at a correct temperature before machining the whole assembly.

These welding technics have been developped and applied by the «Centre d'Études Nucléaires de Grenoble».

● The final sealing of the housing after filling of the mechanism with oil is obtained by pinching and cold welding of the aluminium filling pipe.

4. FOCUSING MECHANISM

The focusing mechanism is mainly characterized first by the high stability of the dihedral reflector required along the focusing range : less than 1 arc minute deviation all along the 12 mm motion amplitude and secondly by the choice of a dry lubrication technic of the unit using new technologies.

The mechanism consist of a size 11 stepper motor connected to a screw through a 5 : 1 gear. This screw drives a nut which supports the reflector and which is prevented from rotating by using a copper bellow. (Ref. Fig. 6)

The stability requirement has been met by the use of two accurately machined journal bearings which guide the nut.

The following technologies have been chosen for lubrication :

— Sliding surfaces i.e. journal bearings and screw-nut device are coated with bonded molybdenum disulphide film.

— Ball bearings, supplied by RMB (Switzerland) are ABEC 7 bearings the rings of which are coated with titanium carbide, a new technology already discuss in an other paper (ref. to «wear-resistant ball bearings for space applications» by M. BOVING, LSRH).

— The gear train is composed of one pinion made of DELRIN AF coupled to stainless steel pinions.

Main problems have been raised from the stability requirement which has led to tighly tolerance the journal bearings and a careful choice of the material regarding thermal effect.

Extensive life tests in ultra-high vacuum both on bearings and on a complete model have shown the ability of the chosen technologies to perfectly work in deep space environment. The evolution of the global resistive torque measured during life-test is shown on Fig. 7.

17

5. CONCLUSION

The two screw-jack mechanisms described above successfully meet their requirements through the application of completely different technologies. The scanning mechanism, characterized by its very high positioning accuracy has led to successfully solve the difficult problem of complete sealing. On the other hand promising dry lubrication technics have been qualified within the development of the focusing mechanism.

Acknowledgement
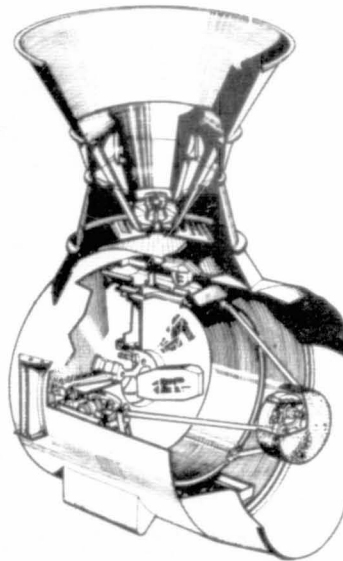
Overall view of METEOSAT
Radiometer
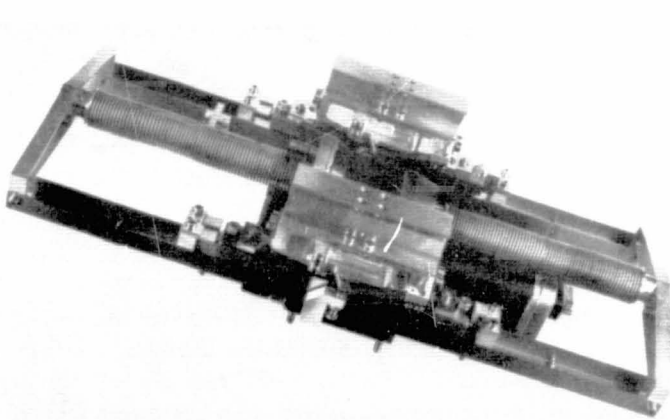
Scanning Mechanism
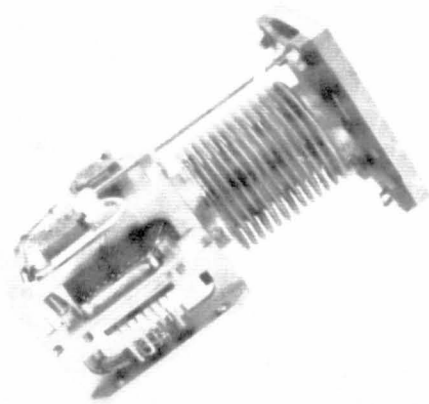
Focusing Mechanism

Fig. 1 – METEOSAT Radiometer

SECTION AA

Screw-jack

Mechanism
fitting

A

Leading frame

Telescope   Sector   Structure frame
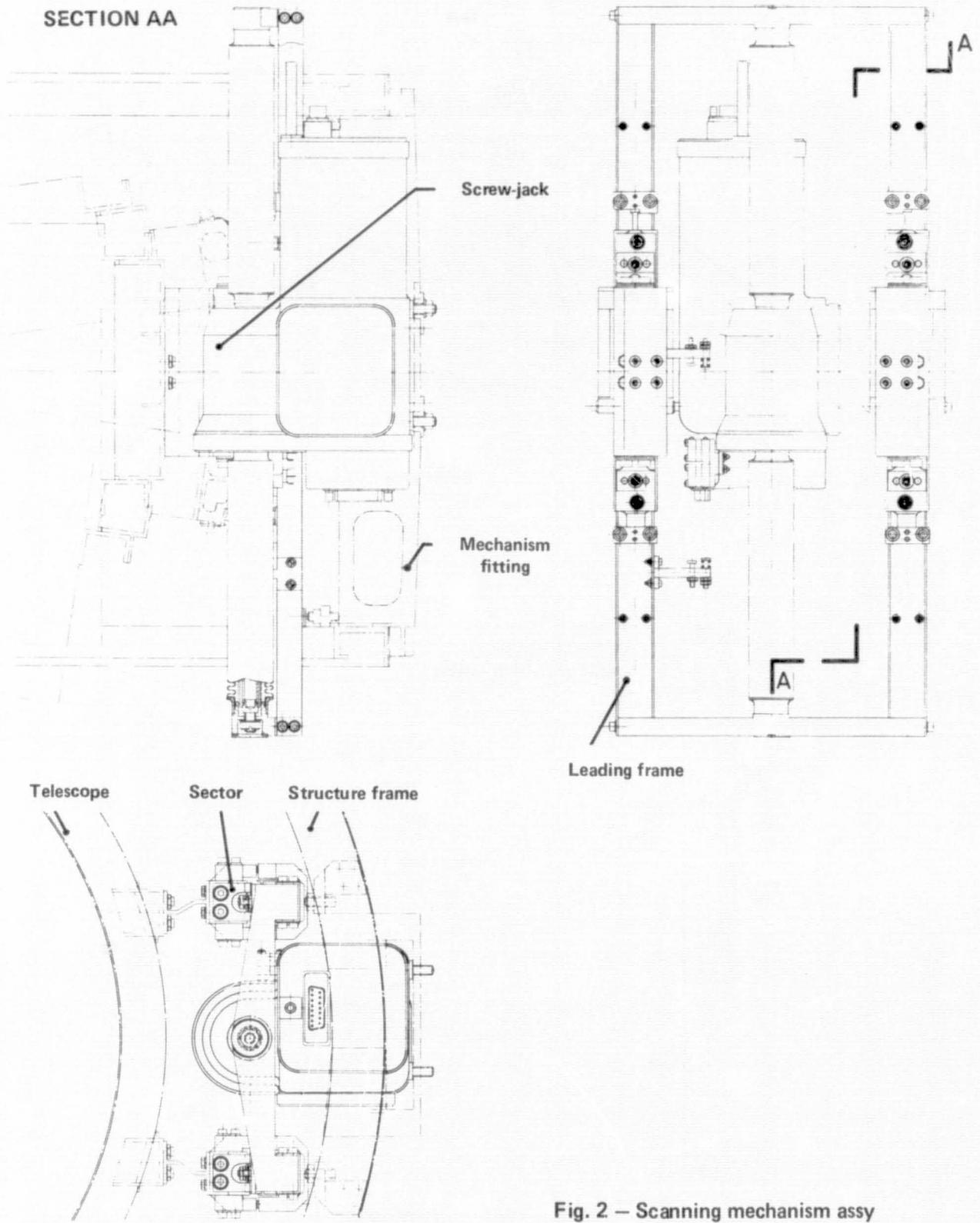
Fig. 2 – Scanning mechanism assy

19
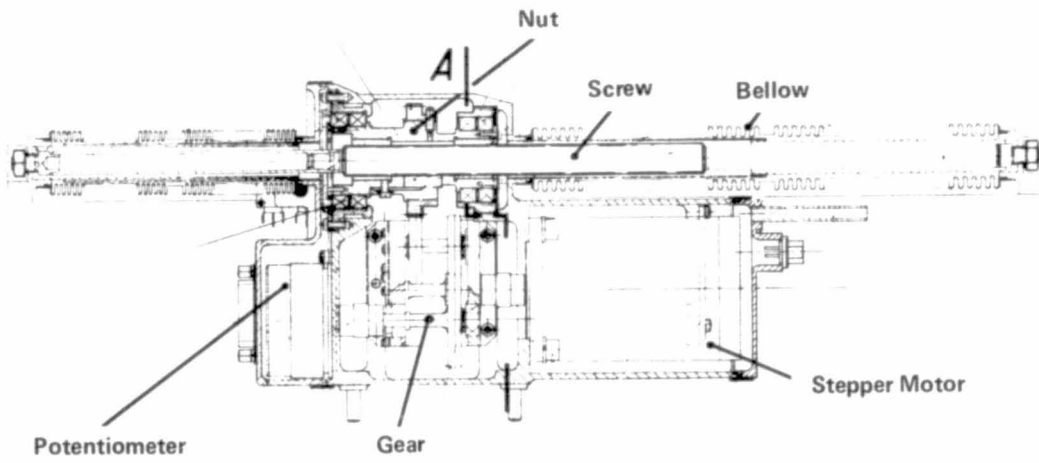
Fig. 3 — Screw-Jack unit
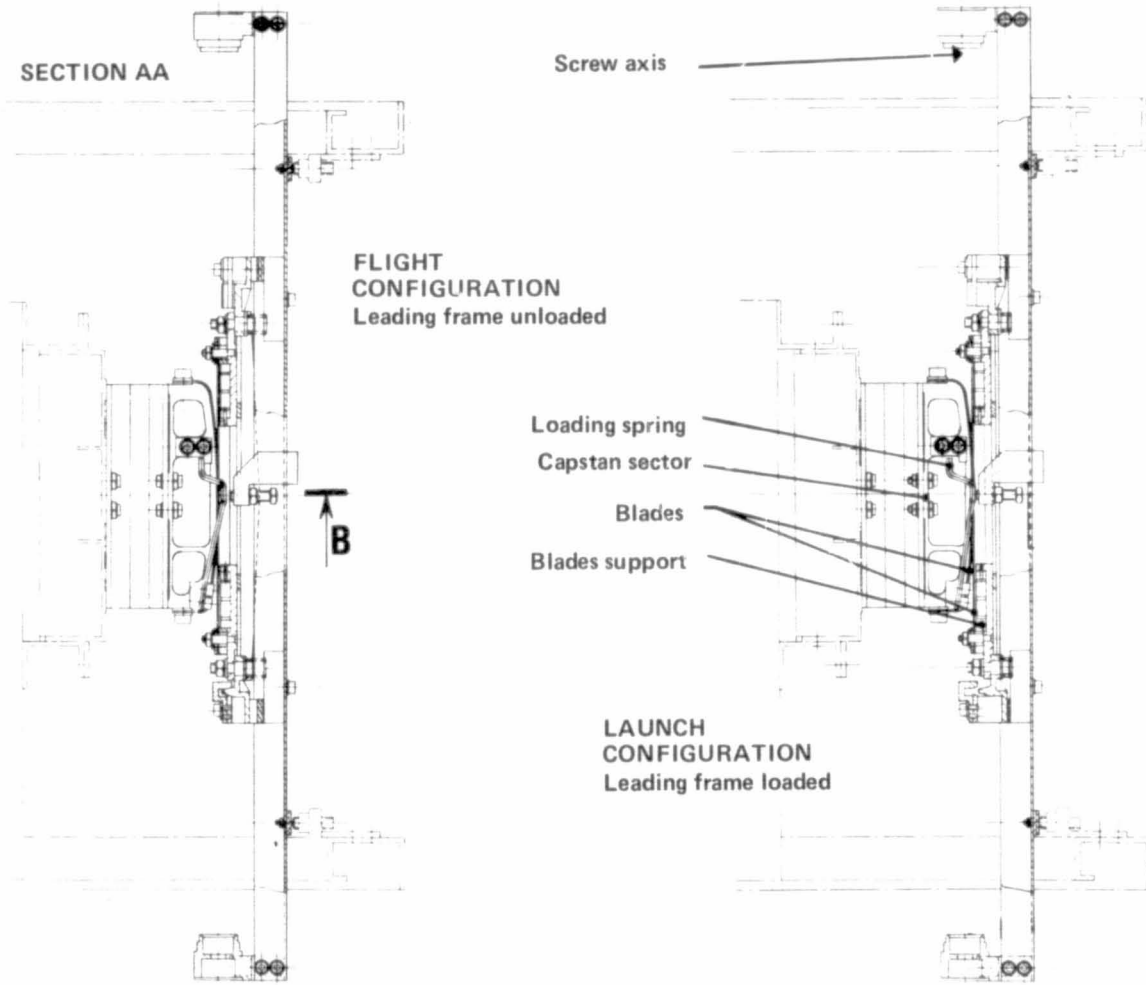
Fig. 4 — Leading frame assy
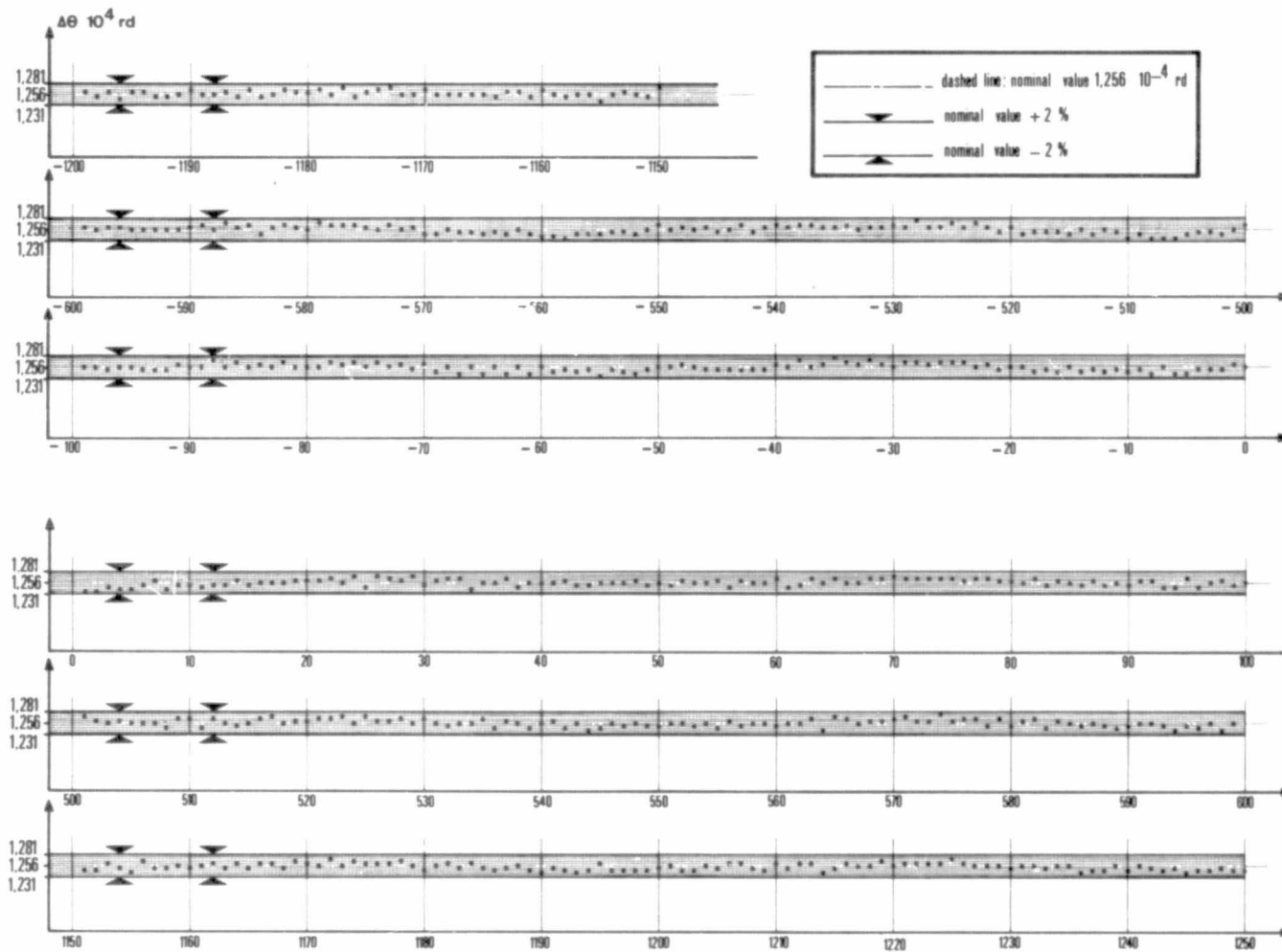
Fig. 5 — Step increments versus step number measured with a laser interferometer test equipment
(accuracy : 0.1 arc sec i.e. 5.10⁻⁴ mrd)
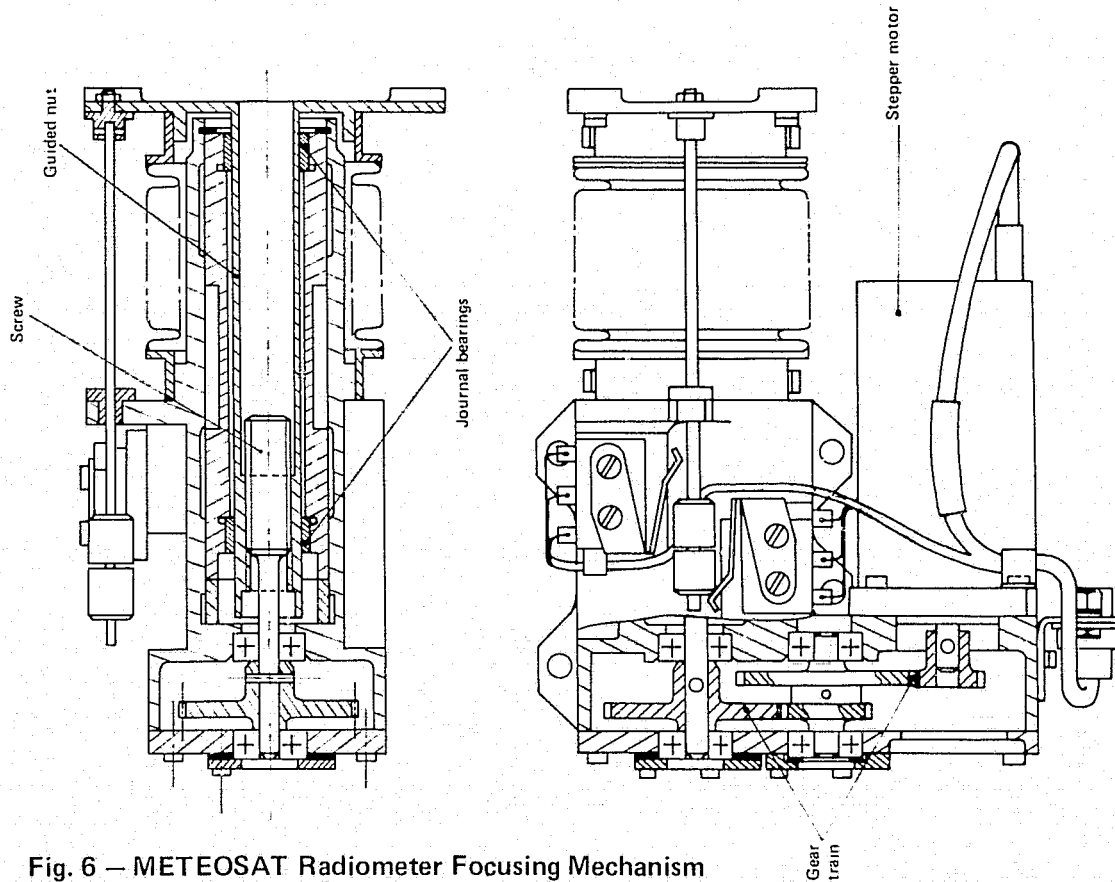
Fig. 6 — METEOSAT Radiometer Focusing Mechanism

Vacuum pressure : 5.10⁻⁹ Torv

Torque measured
in lab conditions

Outgassing
period

Number of cycles

130 140 150 160 170 180 190 200 210 220 230 240 250

Fig. 7 Evolution of the resistive torque measured at the motor
output during life tests in ultra-high vacuum

22

MAGNETOMETER DEPLOYMENT MECHANISM FOR PIONEER VENUS*

By William L. Townsend
Hughes Aircraft Company

ABSTRACT

A three segment, 15-foot boom mechanism was developed to deploy magnetometers from the Pioneer Venus orbiter spinning shelf. The stowage mechanism is designed to contain the magnetometers during launch and to deploy these instruments by centrifugal force upon pyrotechnic release. Unique graphite-epoxy boom segments are used for a lightweight design with sufficient strength to withstand a 7.5 g orbit insertion force while extended. The detailed design is described along with the test methods developed for qualification in a one-g field.

INTRODUCTION

The Pioneer Venus 1978 mission includes magnetometers on the spinning orbiter, Figure 1, to map the magnetic fields around Venus. These measurements require a 15-foot separation from the edge of the spinning shelf in order to minimize spacecraft magnetic effects. A 2-axis magnetometer is placed at the 15-foot position, and a single axis magnetometer is located at a 10-foot position for a magnetic gradient measurement.

The Magnetometer Deployment Mechanism (MDM) supports the magnetometers in a three-segment folded condition for launch, spacecraft separation and spin-up. The mechanism is pyrotechnically released to deploy the magnetometers approximately four hours after launch. Figure 2 shows the MDM in a partially deployed position. Early deployment is necessary for mass balance of the spinning shelf and to permit magnetometer calibration while still in the known magnetic field of the earth. The MDM reliability must be emphasized since failure to deploy will leave the spacecraft with a wobble angle unacceptable to most of the scientific instruments.
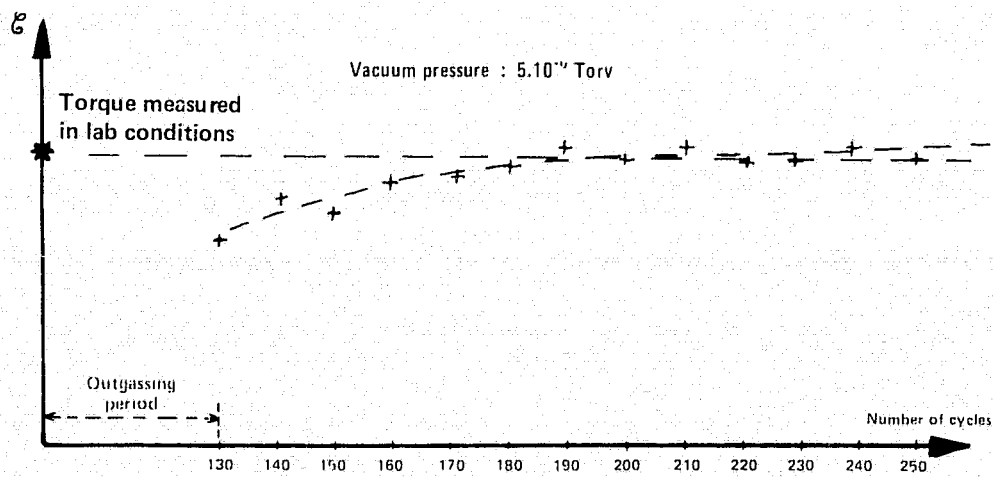
When the spacecraft arrives at Venus, a 7.5 g orbit insertion maneuver is required while the MDM is locked in the extended position. In addition, the spin stabilization during orbit insertion requires that the MDM deflection be limited so that spacecraft wobble angles are not excessive. This combination of strength and deflection requirements dictates a boom designed mainly for stiffness rather than material strength.

Once the spacecraft is in Venus orbit, the MDM must maintain magnetometer axes alignment within 1° of the prelaunch condition. The error must be allocated to include thermally induced distortion, latch repeatability, initial alignment uncertainty and elastic deformation due to centrifugal forces.

DESIGN REQUIREMENTS

The mission profile places design requirements for the Magnetometer Deployment Mechanism (MDM) into the following four distinct modes. Values are listed in Table 1.

1) <u>Launch</u> - The MDM must be folded and stowed to fit on the edge of the spacecraft shelf and to be within the 111 inch shroud diameter. The stowage system must limit launch accelerations on the magnetometer instruments to 22.5 g's.

2) <u>Deployment</u> - The MDM stowage mechanism must be designed with redundant pyrotechnic release for reliability. The MDM must be centrifugally deployed from the shelf while spinning at approximately 6 rpm. The mechanism must be designed with high reliability to latch after extension and with sufficient strength margin to absorb excess latching energy.

3) <u>Orbit Insertion</u> - The extended MDM must withstand 150% of the 7.5 g orbit insertion forces without damage and must be stiff enough to limit tip deflection to 10.5 inches when subjected to 7.5 g force.

4) <u>Orbit Operation</u> - The MDM must be designed using magnetically clean materials to limit magnetic effects to 0.04 gamma at the tip. The magnetometer alignment must remain within 1° of initial installation.

TABLE 1
REQUIREMENTS SUMMARY

Launch Mode (Stowed)		
Sine Vibration Thrust	5 to 2000 Hz	11.5 g Max.
Lateral	5 to 2000 Hz	5.5 g Max.
Random Vibration	20 to 2000 Hz	11.5 g - RMS
Natural Frequency		> 4.0 Hz
Magnetometer Max. Acceleration		< 22.5 g's
Deployment Mode		
Spin Speed		6.0 to 7.0 rpm
Release		Redundant pyrotechnic devices
Deployment Shock		< 8 g's
Temperature		0° to 100°F
Orbit Insertion (Deployed)		
Spin Speed		30 rpm
Insertion Acceleration (⊥ to boom ₵)		7.5 g's (11.25 g design)
Natural Frequency		> 1.0 Hz
Deflection Maximum		10.5 inches at tip
Temperature		+100°F to + 150°F
Orbital Operation (Deployed)		
Spin Speed		up to 65 rpm
Magnetics		< 0.04 gamma
Temperature		-200°F to + 150°F
Mechanism Boom Length		> 15.7 ft
Alignment Accuracy		± 1.0 degree
Weight Deployable Portion		10.36 lbs
Non-Deployable Portion		6.08 lbs
Total		16.44 lbs

In addition to the mission requirements, a ground test requirement was imposed to permit deployment demonstration during system test. Although the ground test imposes gravity induced frictional forces and aerodynamic forces not encountered in orbit, it does provide a set of data for analytical comparison to orbital conditions.

BOOM DESIGN

As can be seen on Figure 3, the boom segments are tapered tubular members for lightness, high stiffness and strength. The design loads including the 50% margin above 7.5 g orbit insertion mode are as follows.

a) Inboard Hinge   892 ft-lb
b) Center Hinge   380 ft-lb
c) Outboard Hinge   94 ft-lb

In addition to orbit insertion loads, the boom segments must be designed to absorb the residual energy for the worst case latching condition. For example, the middle segment must absorb 7 foot-pounds of excess energy. There is also a torsional strength requirement because of mass asymmetry of the hinges and magnetometers.

Graphite-epoxy material was selected for the boom segments because of its low density, high modulus of elasticity, magnetic cleanliness and ease of fabrication in a tapered tubular form. Beryllium was seriously considered but could not be easily obtained with sufficient magnetic cleanliness. Fiberglass-epoxy and aluminum tubing have structural properties significantly inferior to those of graphite-epoxy. The extent of the taper is dramatic with a 4.125 inch diameter at the root and 1.5 inch diameter at the tip. The tube ends are reinforced by bonding into the sockets of the titanium hinge fittings. Intermediate load points are reinforced by fiberglass bulkheads bonded inside the segments and fiberglass rings bonded outside the segments.

HINGE AND LATCH DESIGN

The engineering model hinge and latch are shown on Figure 4. The hinge pin, a beryllium copper cylinder, forms a journal bearing with the 6AL-4V titanium hinges. Redundant journals are provided by a sliding fit on each hinge half. There are redundant beryllium copper locking pins spring loaded against the titanium semi-circular tracks. The half-hinge and track are machined from one 6 AL-4V titanium piece. In order to meet redundancy requirements, each locking pin has sufficient strength to withstand all loading conditions.

The preloaded locking pins have the disadvantage of friction drag along the tracks throughout deployment. On the other hand, this design insures that the pins remain cocked until the proper latch position is reached. The drag friction torque is constant throughout deployment and is predictable using phenolic bonded MoS_2 dry lubrication. Wear during ground test was shown to be of little concern since an excess of 100 deployment cycles caused no significant change in friction torque.

The locking pin is designed with a tip radius to ride on the track, with a lead-in tapered section, and with a final cylindrical section to absorb stopping forces without being driven back out of engagement. The tapered section provides a 4 degree pull-in range to encompass a possible offset angle should the hinge stop rotating prior to full closure. When the locking pin is fully engaged, it is spring preloaded into a tapered socket for a repeatable latch position. Latch reliability is also enhanced by using a preload to impart locking pin acceleration of 50 to 100 g's. Even in the highest conceivable hinge closing rate of 300 degrees/second, the locking pin fully seats prior to overshooting the socket centerline.

The hinge shown on Figure 4 is typical of the middle and outer hinge designs. The root hinge as seen in Figure 3 has a cantelevered hinge pin to be compatible with the shelf structural load path. The locking pins are designed as described above except the latching action is parallel to the hinge.

ELECTRICAL CABLE DESIGN

The electrical cable is a special design for this application to achieve specific electrical performance for low level signals and to achieve low repeatable bending torque over the deployment temperature range of 0° to $100^\circ F$.

The conductor complement to meet the magnetometer excitation and signal feedback requirements is listed below. The cable bending torques were measured to be as high as 18 in-oz at low temperature and less than 1 in-oz at high temperature. Silicone encapsulation is molded around the conductors to form the necessary flat cross-section. In order to save weight, the silicone encapsulation provides the necessary insulation resistance for the single conductors and braided shields without separate teflon jackets.

Electrical Cable Conductors	Quantity	Type
	3	Twisted-Shielded Pairs
	2	Twisted-Pairs
	6	Shielded Singles
	2	Singles

MDM STOWAGE SYSTEM

The MDM is folded for launch in the manner shown on Figure 2. The three segments are supported by two cradles placed close to the mass concentrations of the hinges. Both cradles have hinged segments that are released by redundant pyrotechnic pin pullers. The outboard cradle (more distant from the root hinge) contains a spring-loaded plunger to push the three segments clear of the cradle despite any misalignment forces induced by distortion. The plunger also breaks lose any static friction in the cradle linkage to insure a predictable deployment sequence. The cradle linkage and plunger are shown on Figure 5.

The cradle structure is made of aluminum with MoS_2 dry lubrication on the hinge pins. Two links are hinged and contain torsion springs for deployment to provide redundant mechanisms for clearing the path for boom motion. Each boom segment has fiberglass support spacers to contact the aluminum cradle structure. These spacers are bonded to the boom segments so that the aluminum support brackets provide a clean unobstructed track-like surface for the different shapes that must pass during deployment.

Since both cradles must be pyrotechnically released for successful MDM deployment, both contain redundant pin pullers to eliminate single point mechanical failures. This redundancy concept is shown on Figure 6. At each cradle both pin pullers are retracted. The intermediate link permits release even if any one of the 2 pins per cradle remains engaged.

DEPLOYMENT SEQUENCE

The deployment sequence was modeled on a nine-degree-of-freedom dynamic simulation to include spacecraft dynamics as well as boom deployment. The hinge and cable friction torques were included with cases to cover a range of coefficient of friction from zero to 0.5. Although the spin speed will be selected for the deployment, the setting tolerance is included in the simulation to combine low friction with high spin speed for maximum residual energy. On the other hand, high friction is combined with low spin speed as a check on latch reliability.

The deployment sequence is displayed in Figure 7. The deployment time is 9.75 seconds for a nominal case from electrical initiation of the squib to full extension. The middle hinge latches first with the outer hinge latching only about 0.1 seconds later. At this point the root hinge actually reverses direction momentarily and then resumes the deployment.

When the root hinge finally latches at 9.75 seconds, the outer hinge receives its maximum bending moment. Table 2 displays an analytical comparison of the levels of energy, bending moment and rates encountered.

TABLE 2
MECHANISM LATCH CHARACTERISTICS IN ORBIT

	High Energy High rpm-Low Friction			Low Energy Low rpm-High Friction		
	Root Hinge	Middle Hinge	Outer Hinge	Root Hinge	Middle Hinge	Outer Hinge
Order of Lock	3	1	2	2	1	3
Closing Rate (deg./sec.)	22	274	6.9	9.6	104	72
Locking Energy (ft-lb)	0.53	4.78	0.48	0.23	0.73	0.11
Fundamental Freq. (Hz)	3.2	17.0	6.9	3.2	17.4	6.4
Transverse Moment (ft-lb)	165	230	45	105	77	30
Moment Capacity (ft-lb)	234	554	106	234	554	106

TEST VERIFICATION

The MDM has undergone a complete qualification at the unit level in-so-far-as practical without the exact spacecraft interface. The qualification will not be fully complete until the MDM can be integrated with the spacecraft. The two most important aspects are vibration with true spacecraft structural coupling and thermal-vacuum with realistic thermal inputs. However, the following tests are appropriate for unit level design verification. The data will be discussed in regard to only the first three items since the last two are purely survival exposures or a pass-fail criterion.

1) Release and deployment in room ambient conditions
2) Static loads and deflection
3) Alignment repeatability
4) Thermal cycling with high and low temperature release
5) Workmanship vibration

DEPLOYMENT DEMONSTRATION

Room ambient release and deployment were conducted with a rate controlled spin table to set the proper initial spin speed. Film coverage was used to visually record the latch sequence, and potentiometer readings were recorded from each hinge to verify latching velocity and exact timing. Strain gages were used to record boom strain at each hinge during latch-up to verify actual bending moments resulting from excess latch energy.

Initial testing was planned in room ambient conditions despite the aerodynamic drag and increased friction due to 1 g forces. A simplified math model showed that a slight increase in spin speed over the planned six rpm would provide sufficient energy for a deployment demonstration. However, even at speeds up to 9 rpm in air, the root hinge would not deploy to the latch position. A subsequent more detailed math model verified that most of the initial excess momentum was dissipated at latch of the middle hinge and that aerodynamic drag prevented a continuation of the deployment to the latch position of the root hinge. The test was then repeated in a 40 foot diameter tent filled with helium, 1/7 the density of air. The deployment was successful in helium, and the closure times and rates closely compared with the math model as shown on Table 3. A graphic plot of displacement versus time is shown on Figure 8.

TABLE 3
DEPLOYMENT TEST RESULTS IN 95% He ATMOSPHERE

	9.0 RPM SPIN		7.5 RPM SPIN	
	TEST RESULT	SIMULATION	TEST RESULT	SIMULATION
LATCH TIMES (sec.)				
Root	8.4	7.7	11.1	10.3
Middle	2.4	2.5	3.2	3.3
Outer	2.9	3.0	3.6	4.3
VELOCITY AT LATCH (deg/sec.)				
Root	28	32	13	18
Middle	236	235	140	150
Outer	83	83	50	40
PEAK BENDING MOMENT (ft-lb)				
Root	201	191	132	122
Middle	237	227	131	127
Outer	52	52	16	34

ALIGNMENT REPEATABILITY

Most of the factors contributing to alignment error are small compared to the 1.0 degree requirement and compared to the repeatability of the latch mechanism. The effects of temperature gradient, for instance, are minimized by the low coefficient of expansion of graphite-epoxy. Initial alignment uncertainty is minimized by the use of optical surfaces on the spacecraft, the MDM mounting points and on the magnetometers. These optical references are calibrated on the MDM while suspended with the root hinge fixed to the ceiling. The one-g acting along the axis of the suspended boom approximates the effect of centrifugal force in orbit. This arrangement places an approximate elastic strain on the hinges as in the spinning orbital condition. Three-axis alignment data are then used to align instruments on the spacecraft at a later stage of integration.

Repeatability data were collected while the MDM was vertically suspended to verify the alignment error for this predominant factor. Ten readings were taken in each direction of both lateral axes using an 18-ounce force at the tip prior to each reading. The alignment in the boost direction was the more repeatable with an uncertainty of $\pm$ 0.1 inches at the tip. The deployment axis alignment includes the hysteresis of the locking pin engagement which showed a tip repeatability of $\pm$ 1.1 inches. Although 1.1 inches at the tip seems excessive, the angular error is only 0.35 degrees of the 1.0 degree error allowed.

STATIC LOADS

Two static load tests were conducted using sand bags for incremental loading at the middle hinge, at the outer hinge and at the tip. Deflection measurements were made at each loading point after each weight was added and after each weight was removed. Strain gages were monitored to verify material stress at each loading condition up to the 9.0 g qualification load. The resulting data after interpolation to the 7.5 g condition are shown on Table 4.

TABLE 4
STATIC LOADS TEST RESULTS

		Middle Hinge	Outer Hinge	Tip
A.	Orbit Insertion 7.5 g's Deflection (inches)	1.80	6.77	14.59
		Root Hinge	Middle Hinge	Outer Hinge
B.	Deployment Loading Equilvalent Hinge Rotation (radians)	0.026	0.052	0.054
	Equilvalent Moment (ft-lb)	638	270	67
	Equilvalent Stiffness (ft-lb/rad.)	24,560	5,240	1,240

In the 7.5 g limit load of orbit insertion the tip deflection was 14.59 inches, 38% greater than the design analysis. Although the deflection was greater than planned, the boom met the strength margins according to the strain gage data and the increased wobble of 1.1 degrees during orbit insertion is acceptable.

CONCLUSIONS

The Magnetometer Deployment Boom has been successfully developed to meet the objectives of the Pioneer Venus mission. The development was conducted without benefit of a full development model. Only one of the three hinges was machined from aluminum to verify fits prior to commitment of the titanium flight hardware. Aside from static deflection and deployment in air, the analytical simulations were sufficiently successful to eliminate the need for extensive ground testing. As a low cost approach the only MDM constructed was used for both qualification and flight.
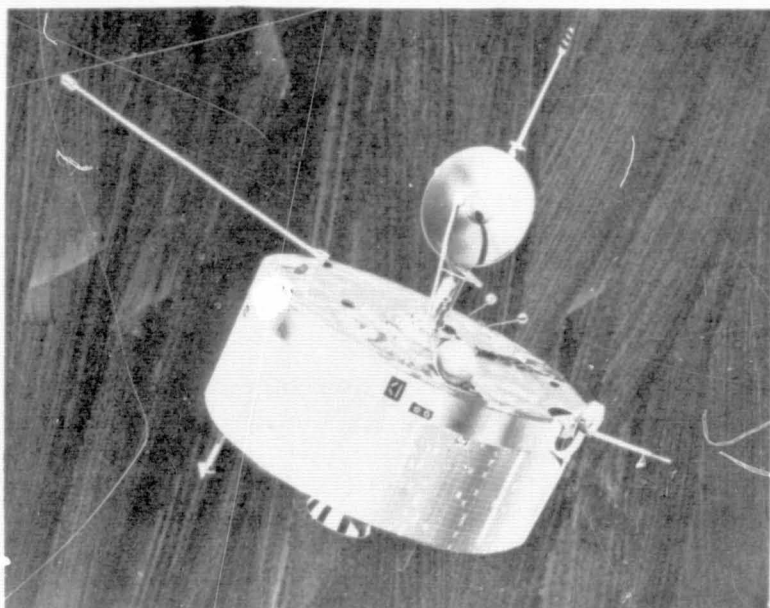
Figure 1. Pioneer Venus
Orbiter

Figure 2. Magnetometer
Deployment Mechanism
with Thermal Control
Finishes
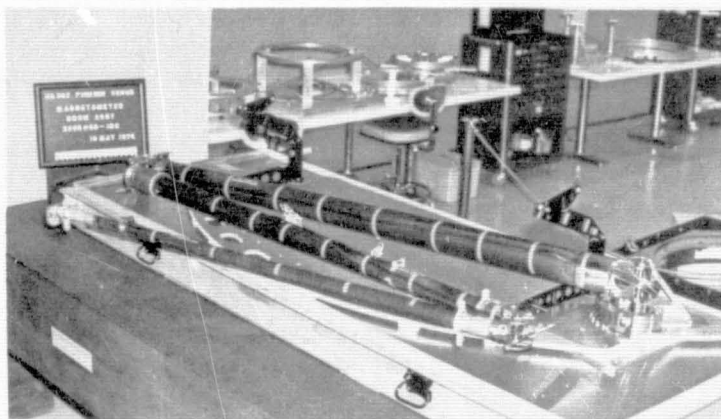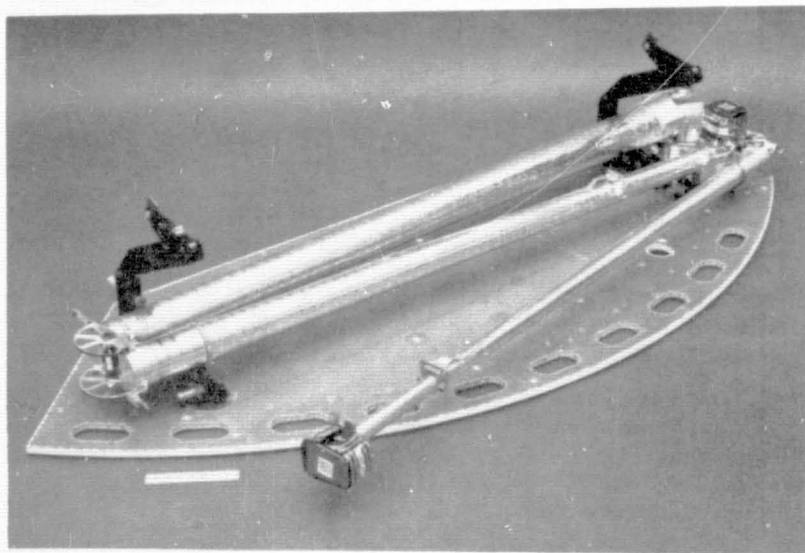
Figure 3. Magnetometer
Deployment Mechanisms
without Thermal Control
Wraps
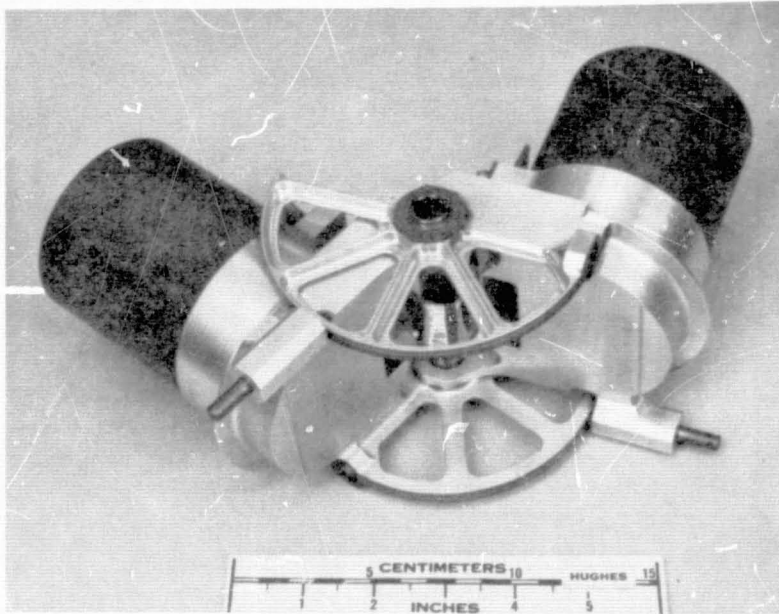
Figure 4. Hinge and Latch
Assembly, Engineering
Model with Partial Boom
Segments
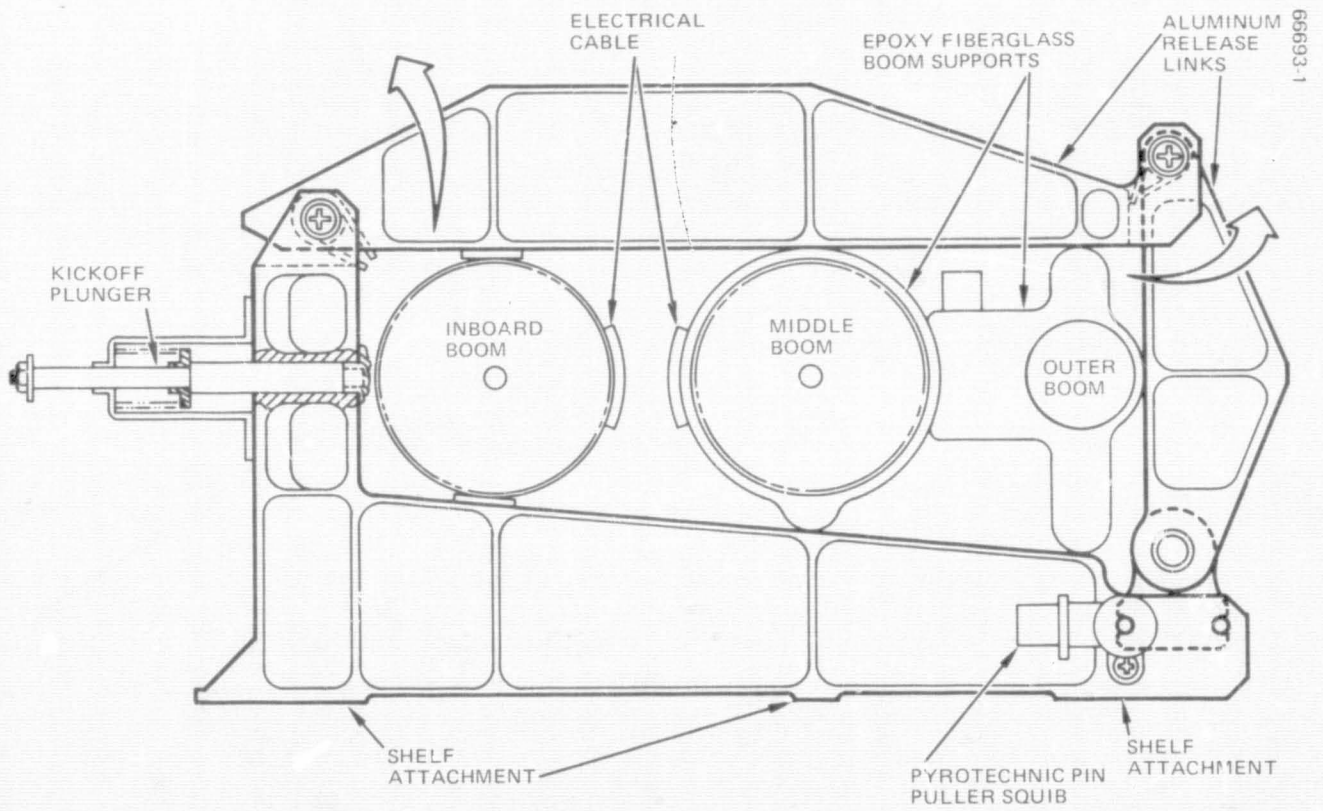
FIGURE 5. OUTBOARD BOOM SUPPORT

31

FRONT VIEW

66693-2

RELEASE
DIRECTION

PIVOT AND
TORSION
SPRING

BOOM SEGMENT

INTERMEDIATE
LINK

FREE PIVOT

REDUNDANT
PINS

REDUNDANT
PYROTECHNIC
PIN PULLERS

FIGURE 6. REDUNDANT PIN PULLERS

4
4.0 sec

3
2.75 sec

5
6.0 sec

0.0 sec

1.5 sec

2

6   7.0 sec

1

ROOT
HINGE

SPACECRAFT SHELF
SPIN DIRECTION

MIDDLE
HINGE

9.75 sec   8

1 — STOWED POSITION

8 — DEPLOYED POSITION

OUTBOARD
HINGE

9.0 sec

7

FIGURE 7. TYPICAL DEPLOYMENT SEQUENCE

FIGURE 8. SIMULATION OF 9.0 RPM DEPLOYMENT IN 95% HELIUM

33

FLY-AWAY RESTRAINT PIN MECHANISM
FOR THE ARMY'S PATRIOT MISSILE SYSTEM

By Frederick W. Knight

ABSTRACT

The development of the longitudinal restraint mechanism for the Army's PATRIOT missile system is reviewed. The initial design was an ordnance pin puller with a shear plane. Because of reliability problems and a desire to reduce cost, a "fly-away" restraint mechanism was chosen. After being manually unlocked, the restraint pin disengages the missile during launch by missile motion.

INTRODUCTION

The PATRIOT missile system concept incorporates a combination shipping-launching canister for maximum missile protection. The canister is designed to withstand and prot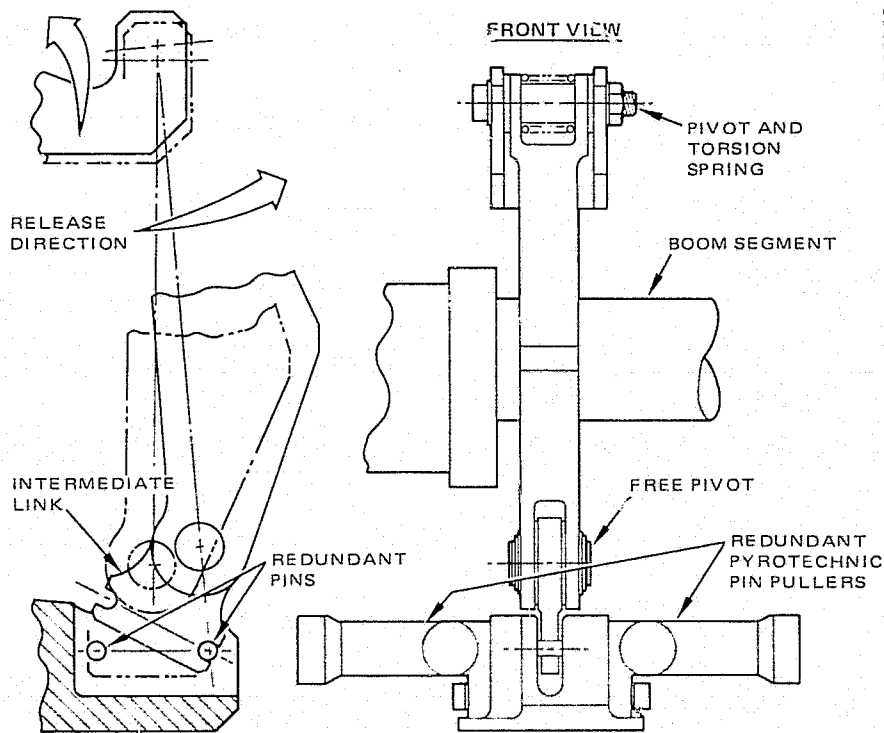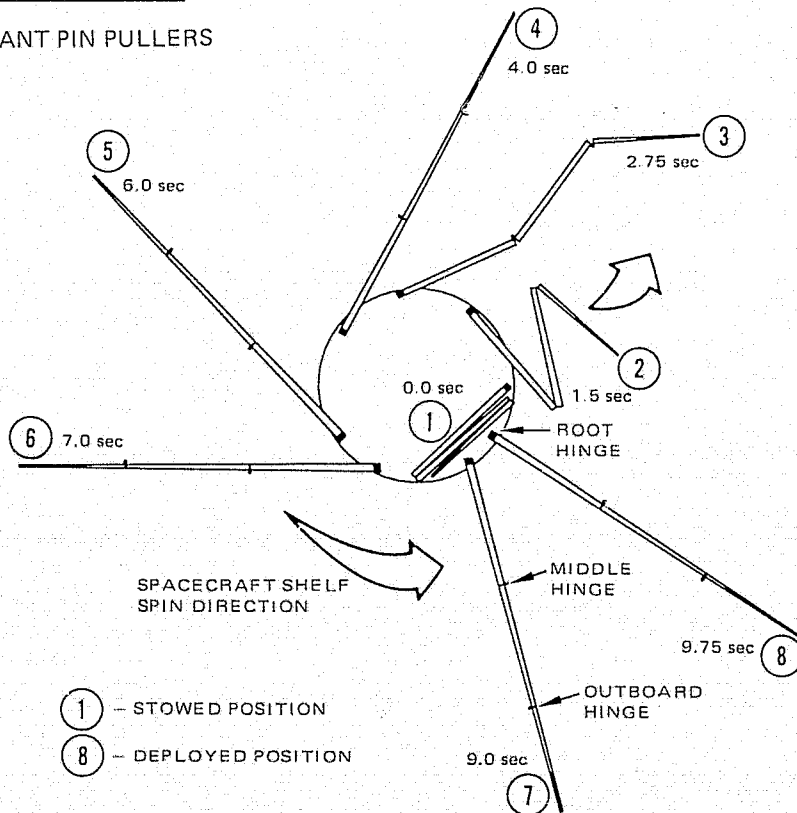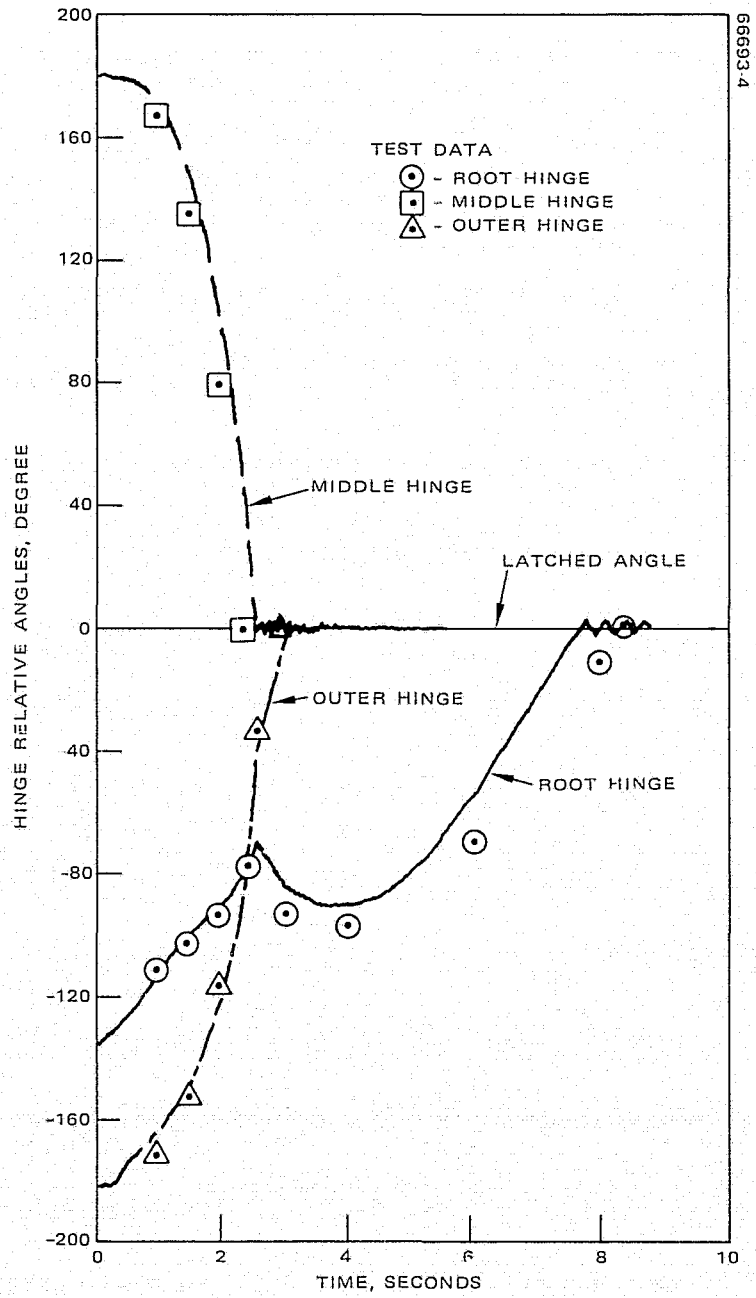ect the missile from a wide range of handling and transportation loads. The launch rail and side shoes support the missile vertically and laterally. The missile is held longitudinally inside the canister by a steel pin inserted into the missile just forward of the motor section. The maximum transportation load on this pin is approximately 34,000 pounds longitudinally.

The basic criterion for the restraint pin is holding the missile in place under all pre-launch conditions while not preventing missile exit from the canister at launch. A simple pin puller concept (one that completely pulls the pin out before launch) is inadequate because some degree of continuous restraint is always needed to prevent the missile from sliding backward at its 38 degree launch angle or under shock loads resulting from battlefield conditions. The restraint pin mechanism must be capable of returning to its transportation mode if a decision is made not to launch or in case of missile malfunction. There is also a requirement that the restraint pin not electrically ground the missile to the canister.

This paper discusses two approaches for restraint pin design: 1) an initial ordnance mechanism and 2) a passive fly-away mechanism.

SYMBOLS

A   Horizontal pivot length

B   Vertical pivot length

C   Depth of penetration of pin

D   Pin diameter

E   Horizontal distance for pin to clear socket

F   Socket diameter

R   Hypotenuse of A and B

X   Gap between pin and socket diameters for line to line contact

θ Pivot angle prior to launch

ϕ Pivot angle just as forward edge of pin clears the socket

α Pin rotation to clear socket ($\phi-\theta$)

ORDNANCE-DRIVEN RESTRAINT PIN DESIGN

Initially, an ordnance-driven restraint pin concept was selected for engineering development. This pin was located on the top portion of the canister, just forward of the motor section of the missile. The design consisted of an integral piston/pin arrangement that was driven upward by expanding gases released by an explosive power cartridge (Figure 1). Pin overtravel was attenuated by a return spring and crushable stop. The pin was retained in the retracted position by a spring-driven locking pin.

The pin did not completely come out of the missile, but far enough to expose a shear plane built into the pin. At launch, the missile thrust sheared the bottom portion of the pin and this portion was retained by the missile. This system was automatically activated a fraction of a second prior to launch as part of the launch sequence. In the event of missile malfunction, the locking pin holding the pin was manually retracted allowing the pin to return to its transportation position for safe missile handling. The electrical isolation requirement was accomplished at the interface of the housing and canister skin by hard coated aluminum shims, bushings, and washers.

Although this mechanism was successfully developed to meet system requirements, it had several undesirable features:

1   The locking pin had a tendency to hang up, thereby reducing system
      reliability.

2   A high degree of machining and close tolerances resulted in steep
      manufacturing costs.

3   The system required use of an ordnance device with its associated cost
      and reliability aspects.

FLY-AWAY RESTRAINT PIN DESIGN

The initial restraint pin mechanism was redesigned as part of a cost reduction effort in the PATRIOT engineering development program. Subsequent tradeoff studies comparing various design concepts selected the fly-away restraint pin design because of its simplicity, reliability, and cost. For convenience, the mechanism was relocated from the top to the bottom of the canister, while its longitudinal position remained the same.

A major feature of the new design is the elimination of an explosive device. The restraint pin is hinged to the housing aft of the centerline of the pin (Figure 2). The pin is restrained aft and laterally by a fixed housing and the forward direction is restrained for handling and transportation purposes by a movable steel bar. After the canister is elevated and prior to launch, the bar is manually moved out of the way through a mechanical linkage. When the missile moves forward after ignition, the pin rotates and drops out of the missile socket. In the event of a decision not to launch, the bar can be easily moved back to the locked position. The electrical isolation requirement was accomplished at the interface of housing and support channels (Figures 3 and 4) by hard coated aluminum bushings, and fiberglas shims and washers.

PIN TO SOCKET CLEARANCE ANALYSIS

Restraint pin to missile socket clearance is a critical part of this design. The movement of the pin to missile is a combination of rotational and translational motion. As the pin rotates out of the missile, sufficient clearance must be allowed between pin and socket to prevent binding and possible missile damage. The minimum clearance required is a function of pivot location, pin diameter, and depth of penetration. This relationship is derived in the following analysis.

Figure 5 shows the restraint pin-socket geometry prior to missile launch. Note that the socket contacts the forward side of the pin. This is because the missile and canister are elevated to a launch position of 38 degrees and the resultant weight of the missile is held by the pin.

Angle θ in Figure 5 can be defined as arc cos B/R where:

$$R = \sqrt{A^2 + B^2} \ .$$

Figure 6 shows the geometry at launch just as the forward edge of the pin clears the bottom edge of the socket. This is a minimum pin clearance condition. The forward edge of the pin has dropped distance C, so that the vertical height from the pivot point is now B-C. The angle ϕ is thus defined as:

$$\text{arc cos } \frac{B-C}{R}, \text{ where again } R = \sqrt{A^2 + B^2} \ .$$

The angle of tilt α equals,

$$\phi - \theta \text{ or } \alpha = \text{arc cos } \frac{B-C}{\sqrt{A^2 + B^2}} - \text{arc cos } \frac{B}{\sqrt{A^2 + B^2}} \ .$$

From Figure 6, the projected pin diameter $F = \dfrac{D}{\cos \alpha}$. If F equals socket diameter for worst case condition, then we can define the minimum gap X needed between pin diameter and socket diameter as:

$$F - D = \frac{D}{\cos \alpha} - D \text{ or } X = D \left(\frac{1}{\cos \alpha} - 1 \right).$$

37

Substituting the term derived for α, X can be defined as:

$$X = D \left[\cfrac{1}{\cos \left(\text{arc cos} \cfrac{B-C}{\sqrt{A^2 + B^2}} - \text{arc cos} \cfrac{B}{\sqrt{A^2 + B^2}} \right)} - 1 \right] \cdot$$

For the PATRIOT missile system the depth of pin C and the pin diameter D were frozen from the old design. Values for A and B were selected to be 1.97 inches (50.04 mm) and 4.40 inches (111.76 mm) respectively. These values were based partly on space limitation and structural convenience. Substituting these values for A, B, C and D in the above equation, the value of X is 0.0059 inch (0.150 mm) causing line to line contact between pin and socket (Figure 6). The existing difference between minimum socket diameter and maximum pin diameter is 0.0155 inch (0.394 mm). This is far mor. than the minimum required for system operation.

CONCLUDING REMARKS

The fly-away restraint pin mechanism has been functionally and structurally tested (including a short burn, full scale missile fly-out test) with complete success. This mechanism is very cost effective, representing an approximate 50 percent saving over the initial design.
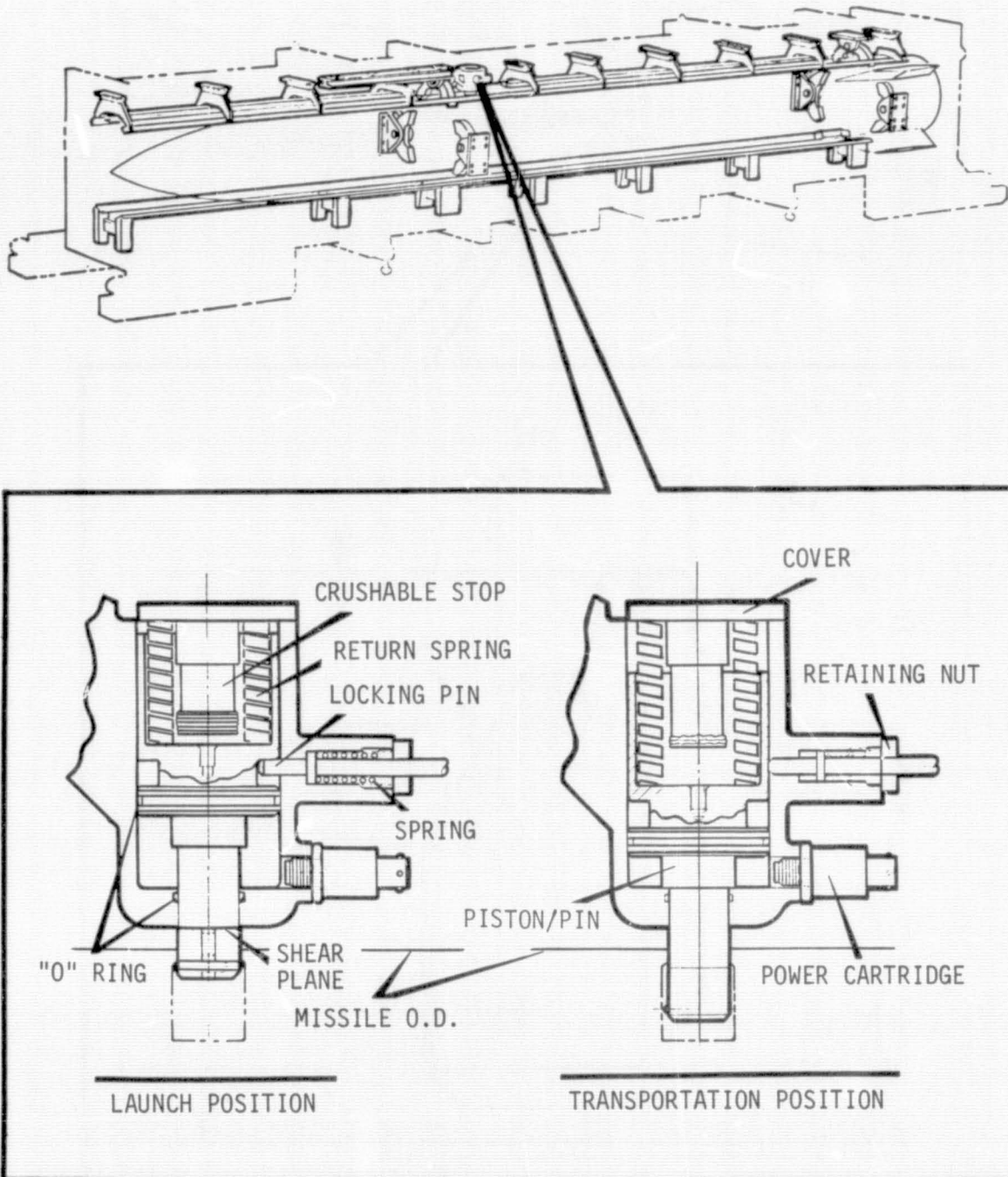
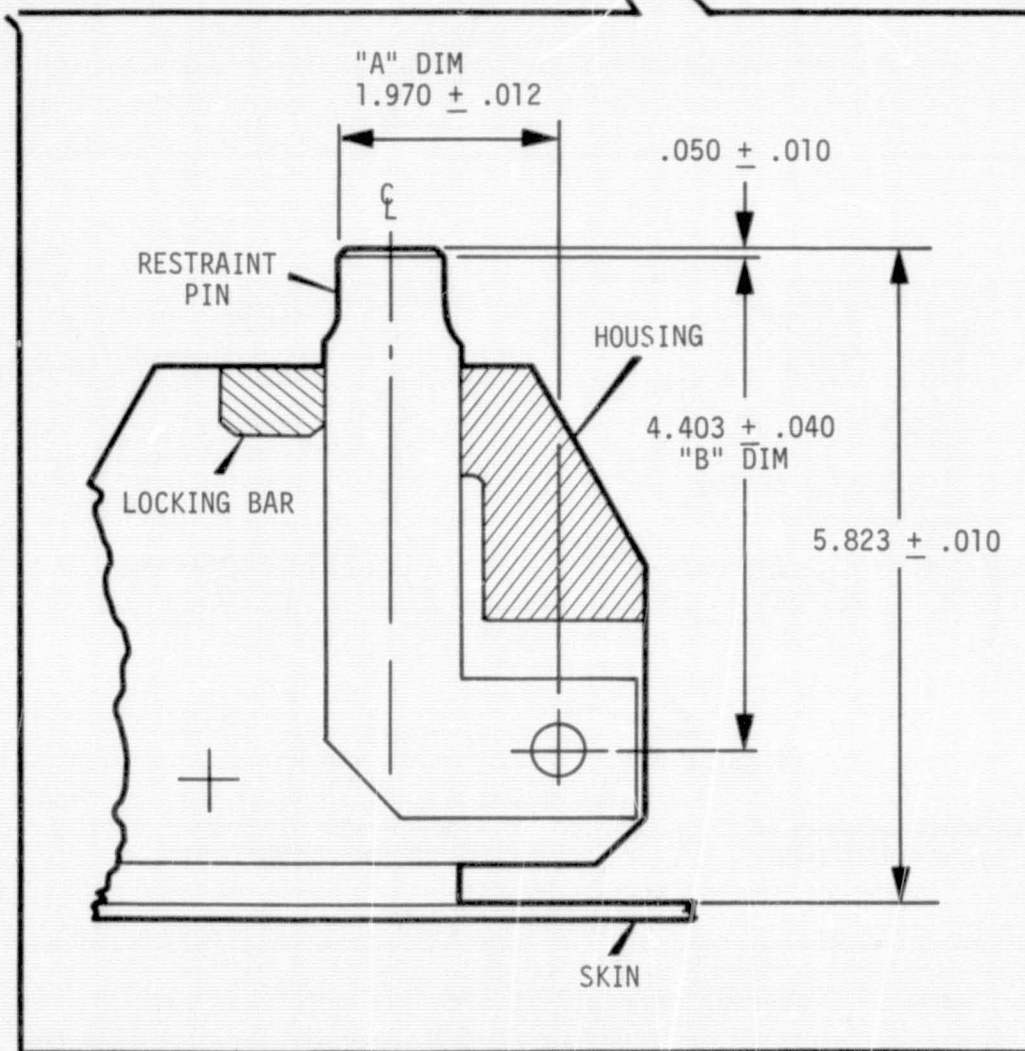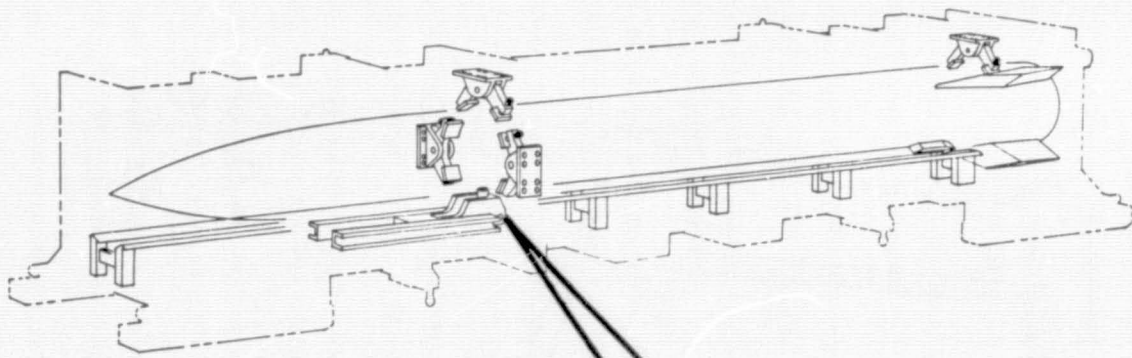Figure 1. Ordnance-Driven Restraint Pin - Initial Design

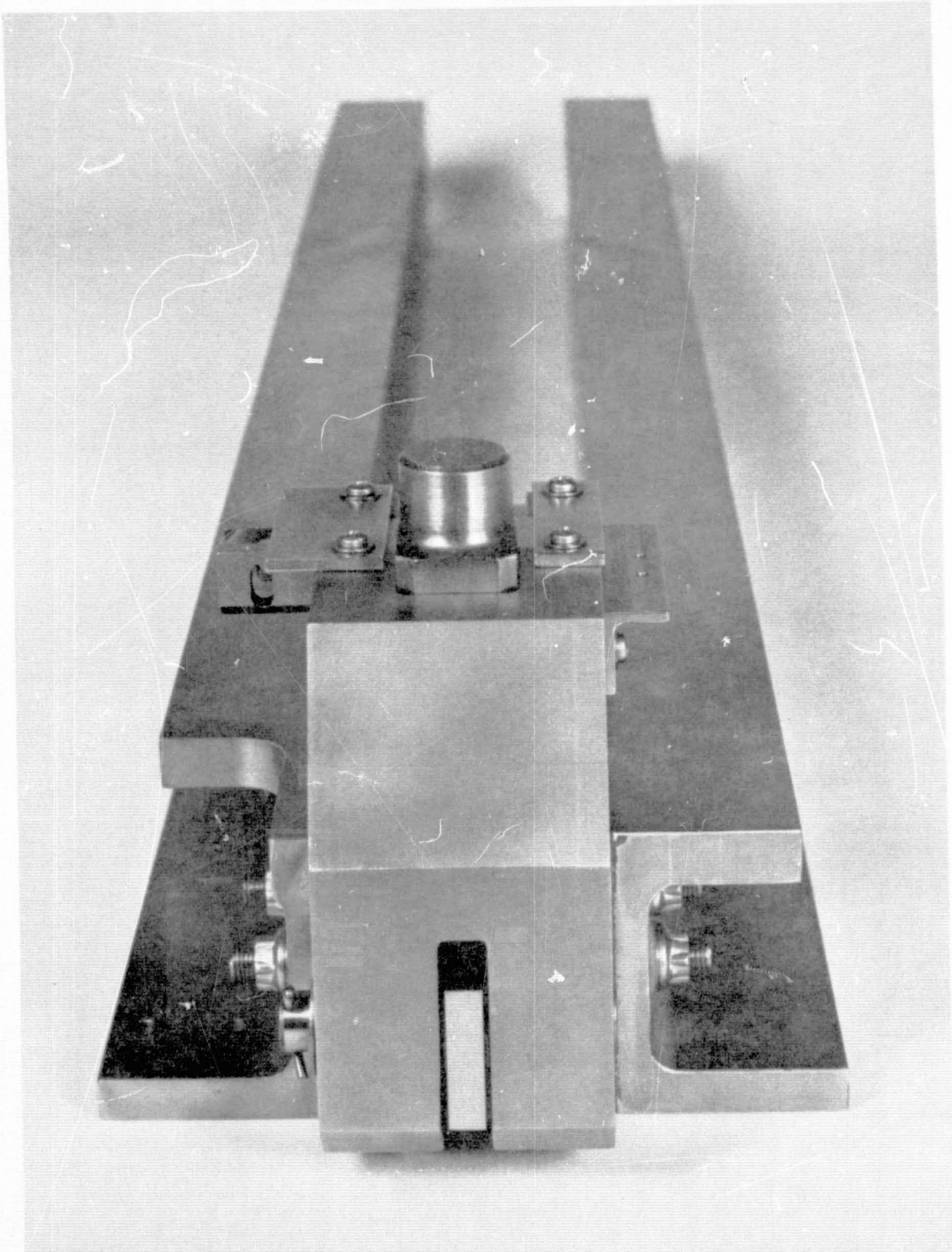Figure 2. Fly-Away Restraint Pin - New Design

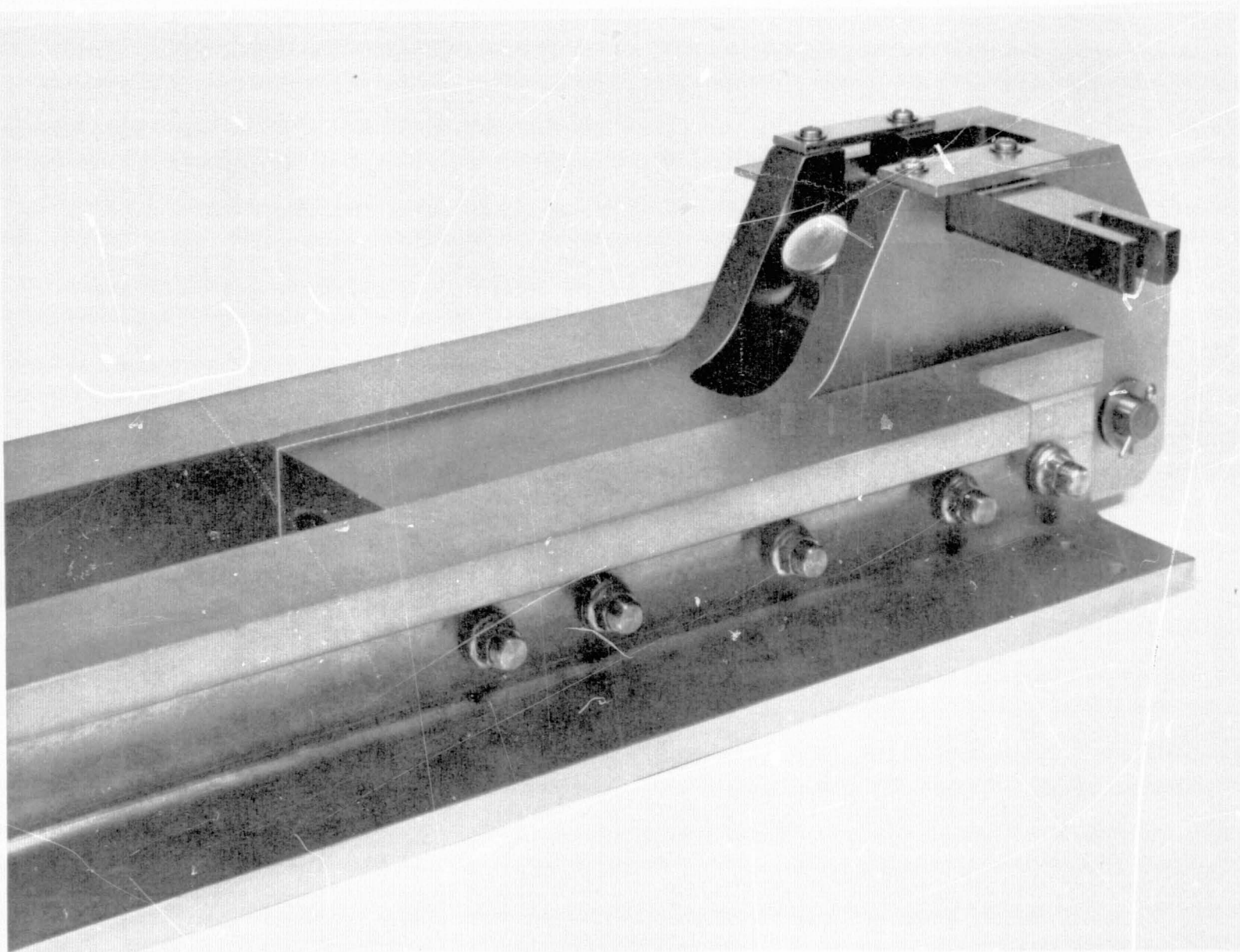Figure 3. Restraint Pin Position at Pre-Launch

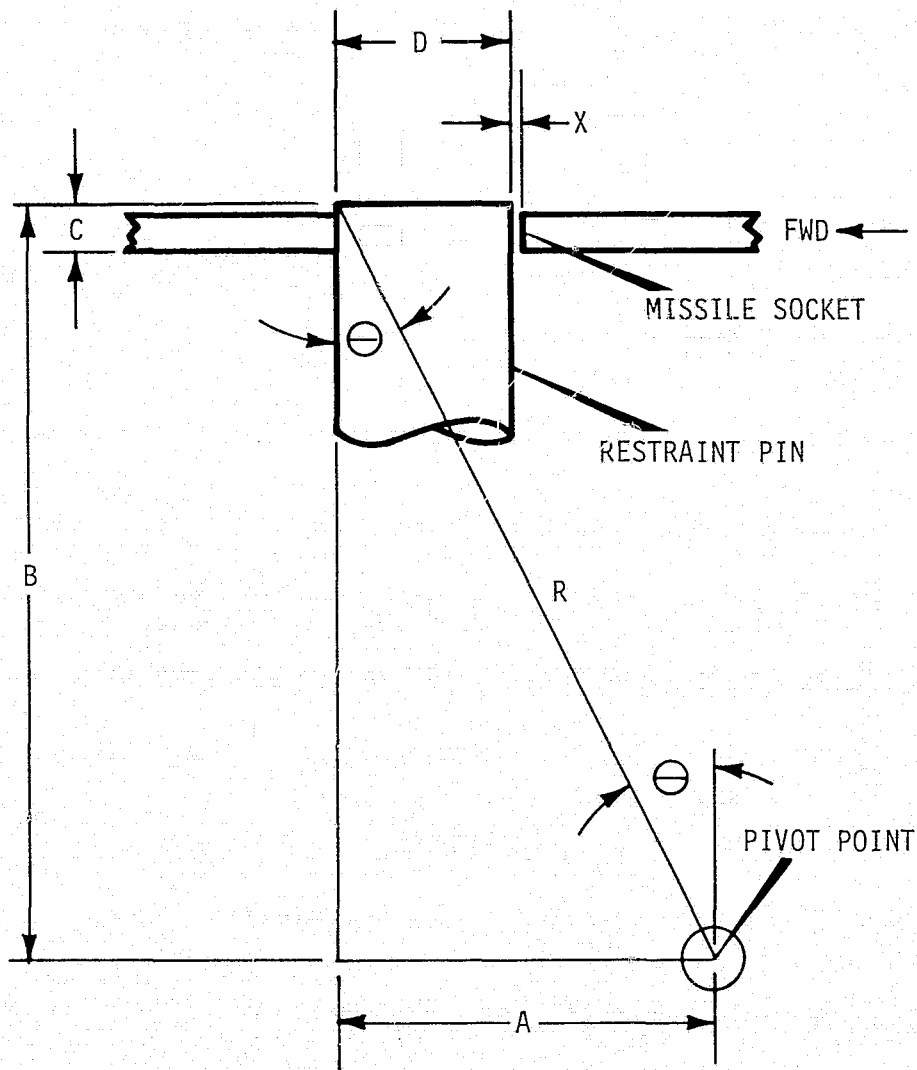Figure 4. Restraint Pin Position at Post-Launch
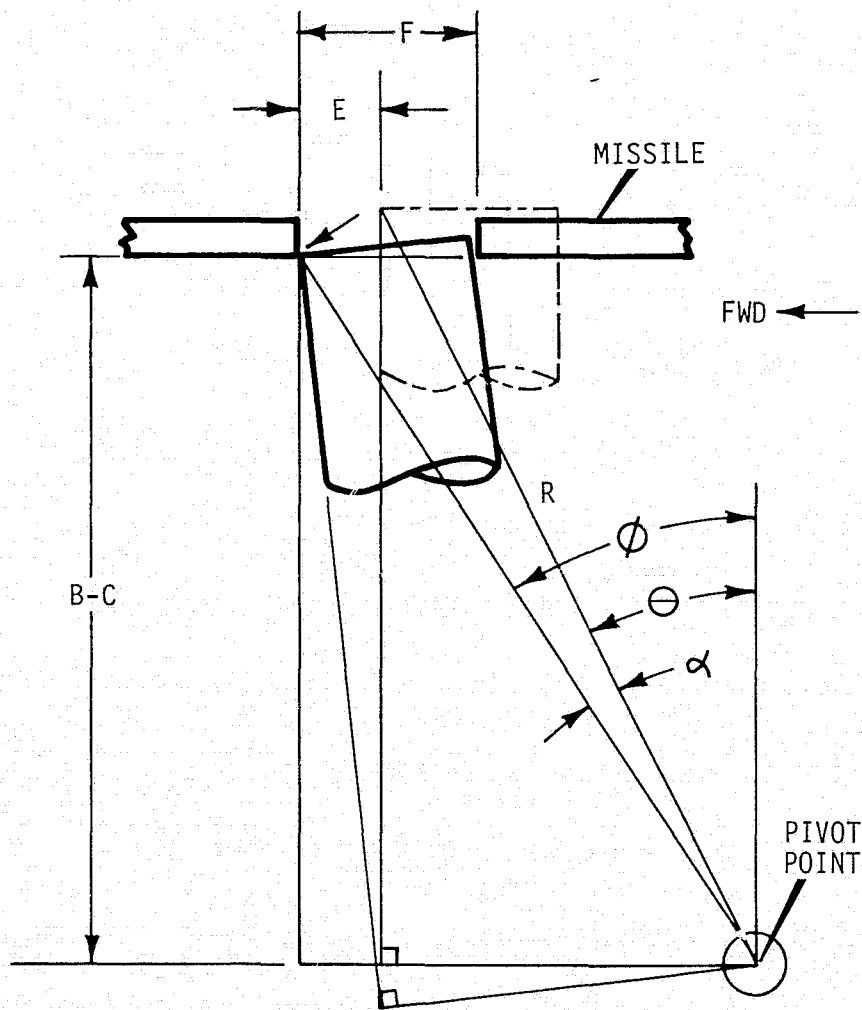
Figure 5. Position of Restraint Pin at Pre-Launch

43

Figure 6. Position of Restraint Pin Just as Forward Edge
Clears the Missile Socket at Post Launch

MAGNETIC BEARING MOMENTUM WHEELS
WITH MAGNETIC GIMBALLING CAPABILITY FOR
3-AXIS ACTIVE ATTITUDE CONTROL AND ENERGY STORAGE

by

Rainer S. Sindlinger

TELDIX GmbH, Heidelberg, Germany

ABSTRACT

Magnetic bearings used for the suspension of momentum wheels
provide conclusive advantages: the low friction torques and the
absence of abrasion allow the realization of lightweight high-
speed wheels with high angular momentum and energy storage capaci-
ty and virtually unlimited lifetime. The use of actively control-
led bearings provides a magnetic gimballing capability by ap-
plying external signals to the two servo loops controlling the
rotational degrees of freedom. Thus, an attitude control system
can be realized by using only one rotating mass for 3-axis active
satellite stabilization. In the future, an integrated energy
storage/attitude control system with one pair of counter-rotating
rotors could reduce considerably the mechanical complexity and
weight of conventional systems.

INTRODUCTION

The stringent attitude performance requirements of future
satellites can only be met by 3-axis body stabilization. Hereby,
the satellite's orientation is measured by the attitude control
system (ACS) with a set of optical, IR or RF sensors, and the
deviations from the desired attitude are transformed into ap-
propriate correction signals for the torque actuators. The most
common actuators are flywheels, i.e. reaction wheels or momentum
wheels.

For 3-axis active control, a set of three REACTION WHEELS
with mutually orthogonal axes can be used. Since external dis-
turbance torques are in the order of 10^{-4} to 10^{-5} Nm, an angular
momentum storage capacity of 0.2 to 5 Nms is sufficient.

With MOMENTUM WHEELS, active control is only possible in one
axis, and the remaining two axes are passively stabilized by gyro-
scopic effects. The angular momentum H required to maintain the
attitude to an accuracy of $\Delta\varphi$ at an external torque M over a time
interval T is

$$H \geqslant \int_0^T M \, dt \, / \, \Delta\varphi$$

45

Typical values are in the order of 20 to 100 Nms for an accuracy of $\Delta\varphi \leq 0.5°$.

If high angular accuracy is required, this passive stabilization is possible within short time intervals only, and frequent desaturations become necessary. Integration of the wheel into a double gimbal system (DGS) allows to overcome this disadvantage. At the same time, a DGS provides the capability of rotating the satellite, e.g. to correct the north-south error caused by inaccurate positioning or to turn the antenna pointing vector.

Conventional wheels with sliding or ball bearings are restricted to speeds below 5000 rpm due to their friction torque and limited life caused by fatigue effects of the bearings and aging of the lubricants. To prevent the lubricants from outgassing, a housing is needed maintaining an internal pressure of several hundred μbars.

MAGNETIC BEARING MOMENTUM WHEELS

During the last years, many efforts have been made to avoid the shortcomings of conventional flywheels by use of noncontacting bearings. Due to the absence of abrasion and their very low friction torque, magnetic bearings are prime candidates allowing the design of high-speed wheels with high angular momentum-to-mass and energy-to-mass ratios. Magnetic bearings are insensitive to hard vacuum and therefore need no housing. The lifetime is virtually unlimited and depends only on the reliability of the associated electronics which can be considerably increased by redundancy.

If appropriate materials are used, extreme velocities can be realized, providing an energy storage capability which is competitive to the best available batteries.

For the suspension of a rotating body, 5 degrees of freedom must be stabilized: three translational ones along the X,Y,Z axes, and the rotational ones about the X and Y axes (see Figure 1). Generally, each degree of freedom can either be stabilized passively, i.e. by means of permanent magnets, or actively with magnets controlled by a control loop. A complete passive suspension is not possible and at least one degree of freedom must be actively controlled [1].

PASSIVE SUSPENSION can be realized either with repulsive forces or with secondary forces yielded by attractive magnets. Since only one control loop is required, mainly passive bearings provide high reliability. Using the zero-power method [7] they can operate even in a 1 g environment with low power consumption, because the levitation of the rotor is done by forces generated by permanent magnets.

However, the magnets must be very homogeneous; otherwise considerable friction torque is generated by eddy currents and hysteresis losses. The stiffness is limited yielding a certain softness against external forces and torques. But the most severe disadvantage is the absence of any internal damping, requiring heavy and bulky dampers to prevent nutational and precessional oscillations. In many cases, these dampers are heavier and more voluminous than the bearings themselves. In the 1 g environment these dampers can generate considerable drag torque causing additional power consumption for the drive motor.

For ACTIVE SUSPENSION, two principles of operation can be considered: In an ELECTROMAGNETIC BEARING electromagnets on the stator generate attractive forces on ferromagnetic parts of the rotor. These forces are proportional to the square of the coil current, thus the control loops must include linearizing networks. Two magnets are required for each degree of freedom to yield positive and negative forces.

In the ELECTRODYNAMIC BEARING, the forces are generated by currents through electrical conductors on the stator, arranged perpendicular to the magnetic flux provided by permanent magnets fixed to the rotor. Since the forces are proportional to the current, positive as well as negative forces can be obtained, and the linearity facilitates the layout of the control loops. The forces can be either parallel or orthogonal to the gap between stator and rotor. Of course, the magnitude of the forces is much lower than for the electromagnetic approach.

MOMENTUM WHEEL WITH ELECTROMAGNETIC BEARINGS

In the following, a 5-axis active magnetic bearing momentum wheel (MBMW) is described. It was developed and built by Teldix in cooperation with SEP in France under a contract of the COMSAT and the German Space Organization DFVLR.

Two axial bearings AB, having the form of pot magnets, stabilize the rotor in axial direction. They are controlled by the axial sensors AS and a control electronics (see Figure 2).

The two radial bearings RB consist of four pairs of electromagnets each arranged in a plane and equally displaced by 90° as shown in Figure 3. Radial translations are generated by currents at the same side of the upper and lower bearing while torques about the radial axes are provided by activation of opposite sides. The control signals are obtained by addition or subtraction of the outputs of a number of radial sensors RS.

Figure 4 shows a block diagram of the translatory control loops. Since the mass of the rotor provides a double integration, proportional control would yield an oscillating system as it is true for passive bearings. Therefore, a phase-lead network is

necessary to damp oscillations. An integrating control is added to provide high statical stiffness. The frequency response of the control loop is depicted in Figure 5.

At zero speed, the same control loop design could be used for the rotatory degrees of freedom. At higher speeds, however, the two control loops are coupled due to gyroscopic effects. As shown in Figure 6, each variation of the input signal $\Delta\alpha$ of the X axis causes a disturbing torque $M_{H\alpha}$ on the Y axis via the differenciating block H·s. It results in a change of the angle β about the Y axis which, in turn, generates the desired angle α by a disturbing torque $M_{H\beta}$ about the X axis. Since H is proportional to the rotational speed, the parameters of the control loops vary in a very wide range, and a great bandwidth is required.

MAGNETIC GIMBALLING CAPABILITY

The use of active magnetic bearings for the rotatory degrees of freedom provides the unique possibility of controlling the attitude of the rotor. If the nominal values $\alpha_0 = 0$ and $\beta_0 = 0$ in Figure 5 are replaced by variable command signals α_c and β_c, the rotor can be tilted by a defined angle about any radial axis. By this tilting, the wheel is provided with a magnetic gimballing capability.

Such a Magnetically Gimballed Momentum Wheel (MGMW) was developed by Teldix on the basis of the MBMW described above (Figure 7).

A gimballing angle range of ± 10 mrad is obtained by increasing the gaps between stator and rotor from 0.3 to about 0.7 mm. At a nominal speed of n = 16,000 rpm, the wheel has an angular momentum of H = 100 Nms, so that the storage capacity about the perpendicular axes is ± 1 Nms. This is more than sufficient to balance the periodic disturbance torques on the satellite, and the attitude of the satellite can be controlled with an accuracy of better than 0.01°, depending only on the performance of the attitude sensors. Furthermore, the MGMW can be used as an active nutation damper, thus superseding separate nutation dampers for the satellite.

The magnetic gimballing needs practically no additional hardware. The wider gaps increase the magnetic resistance of the magnetic loops and, therefore, require a higher magnetic potential (i.e. a higher number of ampere-turns). Nevertheless, it was possible to reduce the weight from 14 kg to about 9 kg although effective emergency bearings and a caging mechanism, fixing the rotor during launch, were added.

The electronics package for magnetic suspension and gimballing and for the motor commutation is integrated in thin film hybrid technology and weighs about 3 kg. Thus, the total system

weight is about 12 kg. The power consumption at nominal operation in orbit is expected to be about 10 to 15 watts. The brushless and ironless d.c. motor/generator is able to provide the power for magnetic suspension in case of primary power failure for up to 20 minutes. Since the electronics is completely redundant, a reliability of about 98 %, based on a 10-year mission, is obtained.

ROTARY ENERGY STORAGE SYSTEMS

The rotor of the wheel described so far was composed of a momentum ring, a hub, and a disc connecting them. Of course, this is not the optimal shape for a momentum wheel rotor. In order to obtain the highest possible momentum-to-mass ratio H/m, the total mass should be arranged at the largest possible radius r, providing a thin-walled ring. The H/m ratio is then

$$\frac{H}{m} = r \sqrt{\frac{\sigma}{\rho}}$$

with σ being the allowed stresses, and ρ being the density of the material [4]. If such a ring is rotated at a speed fully utilizing the strength of the material, considerable kinetic energy can be stored providing the opportunity of realizing the dual functions of angular momentum and energy storage.

The energy-to-mass ratio of a thin-walled ring is

$$\frac{E}{m} = \frac{1}{2} \frac{\sigma}{\rho} = \frac{1}{2} v^2$$

with $v = \omega \cdot r$ being the circumferential velocity. The specific energy is, therefore, fully defined by the properties σ and ρ of the materials used for the rotor and independent of the ring diameter. High-strength materials of low density are best suited for energy storage systems, and since the stresses are mainly in circumferential direction, fibre reinforced composites are prime candidates for this application. In table 1 the energy density for different materials is listed. The static value is the theoretical limit for the fibres only, while the values given for dynamic loads take into account an energy storage cycling with the associated fatigue problems, and the weight for the matrix, which does not contribute to the strength.

Table 1
E/m Ratio for Various Ring Materials

Material	Energy-to-Mass Ratio [Ws/g]	
	Static	Dynamic (10^5 cycles)
Steel	250	200
Glass	670	370
Boron	610	425
Carbon	640	500
Kevlar	690	435

As can be seen, carbon fibre composites provide the highest ratio

$$\frac{E}{m} \approx 500 \ \frac{Ws}{g} \approx 140 \ \frac{Wh}{kg}$$

HIGH-SPEED RING WITH ELECTRODYNAMIC BEARINGS

For such a ring, the dimensions and the mass of an electro-magnetic bearing would be prohibitive, and the use of an electro-dynamic bearing is to be preferred. The large ring surface allows the use of comparatively large permanent magnets, and the stator coils can be arranged on a ring inside the rotor.

Figure 8 shows a cross section of the bearing: On the rotor, for instance, two permanent magnet rings with homogeneous radial magnetizing in opposite directions are mounted. A soft iron ring increases the flux density effective in the stator coils. The radial and axial coils are arranged in areas where the axial and radial component, respectively, of the magnetic field is predominant. Therefore, the axial coils generate mainly axial forces while radial forces are provided by the radial coils.

To form a complete bearing, the radial coils are divided into four 90° segments providing forces along two perpendicular radial axes. The tilting torques are yielded by segmented axial coils excited in opposite directions. Any deviation from the nominal rotor position is detected by a set of position sensors and – using five control loops – balanced by forces generated in the coils.

This bearing type provides high stiffness and excellent oscillation damping. Due to the absence of any iron on the stator and the uniform magnetizing on the rotor, the drag torque can be kept extremely low even at very high speeds. The only braking torques are caused by eddy currents in the magnets and the soft iron ring, generated by the weak field of the ironless stator coils. If the bearing must be able to support the rotor under 1g, however, about 15 to 25 % of the rotor mass is required for the magnets. Otherwise, the stator coil currents would become in-tolerably high.

Two counterrotating rings are necessary to realize an energy storage system which is free of distortion torques. A vernier magnetic gimballing of a few arc minutes is required to exactly align the momentum vectors under all operational conditions. This allows also to generate torques about all three satellite axes. Therefore, the functions of energy storage and attitude control can be combined in one system.

A first experimental model of a high-speed ring was de-veloped by Teldix under a DFVLR contract. Figure 9 shows the complete unit. Although it was mainly designed as a momentum

ring, it is able to store about 45 Wh corresponding to a rotor energy density of 16 Wh/kg.

The total rotor mass is 3.8 kg including 0.6 kg for the magnets. The bearings are able to provide forces of $F_a > 80$ newtons in axial, and $F_r > 70$ newtons in radial direction, allowing safe operation in each orientation under 1 g.

The maximum speed up to now was 15,000 rpm, corresponding to an angular momentum of 105 Nms. The total weight is 8.6 kg, and the dimensions are 290 mm diameter × 110 mm height. The volume is 7.2 l with 4 l available for the electronics in the interior of the stator.

The motor provides a torque of 0.1 Nm corresponding to a power of 150 watts. The angular freedom for magnetic gimballing is ± 0.1°, and the slew torque capacity is more than 2 Nm. The behaviour of the gimballing loop was tested with a square wave control signal input at a ring speed of 3000 rpm. In Figure 10 the resulting attitude angle of the ring is shown. As can be seen, the commanded angle for the X axis is obtained with a reaction time of less than 20 ms. In the orthogonal Y channel, only short distortions are produced with no steady-state error.

CONCLUSION

Magnetic bearing technology allows to realize a 3-axis active attitude control system with only one rotating part. This is possible by using a momentum wheel with magnetic gimballing capability as a torque actuator for all three body axes. Such a wheel has been developed and will be qualified for space applications within the next two years.

Based on this technology, an integrated energy storage/attitude control system with one pair of counterrotating rings could in the future considerably reduce the complexity and weight of conventional systems.

REFERENCES

1. Earnshaw, S.: On the Nature of Molecular Forces.
   Trans. Cabridge Phil. Soc. 7, 1842.

2. Sindlinger, R.S.: Magnetic Bearing Momentum Wheels with
   Vernier Gimballing Capability for 3-axis Active Attitude
   Control and Energy Storage.
   IFAC Symposium "Automatic Control in Space",
   Rottach-Egern/FRG, May 17-21, 1976

3. Wehde, H.P. and Sindlinger, R.S.: Rare Earth-Cobalt Magnets,
    Breakthrough to a new Generation of Drive Motors and Magnetic
    Bearings for High-Speed Rotors. Second International Workshop
    on Rare Earth-Cobalt Magnets, Dayton/Ohio, 1976.

4. Stellbrink, K.: Anwendung faserverstärkter Verbundwerkstoffe
    für magnetisch gelagerte Schwungringe zur Satellitenstabili-
    sierung und als Energiespeicher. DFVLR Report IB 454 75/7,1975

5. Notti, J.E. et al.: Design and Testing of an Energy Flywheel
    for an Integrated Power/Attitude Control System.
    AIAA Paper No. 75 - 1107, 1975.

6. Anderson, W.W. et al.: The Annular Momentum Control Device
    and potential Applications. NASA TN-D-7866, 1975.

7. Sabnis, A.V. et al.: A Magnetically Suspended Large Momentum
    Wheel. J. Spacecraft, Vol. 12, No. 7, 1975.
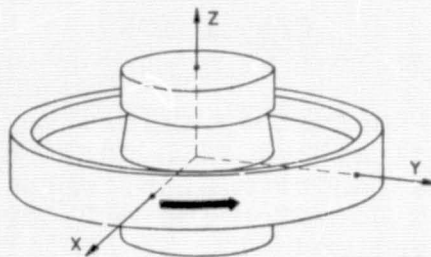
Figure 1: MBMW Coordinate System
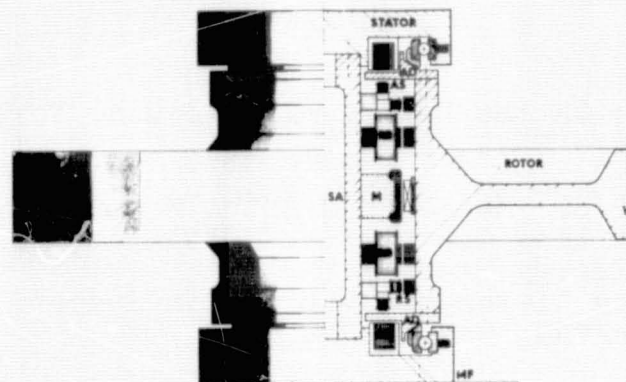
Figure 2: Cross Section of the Magnetic Bearing Momentum Wheel
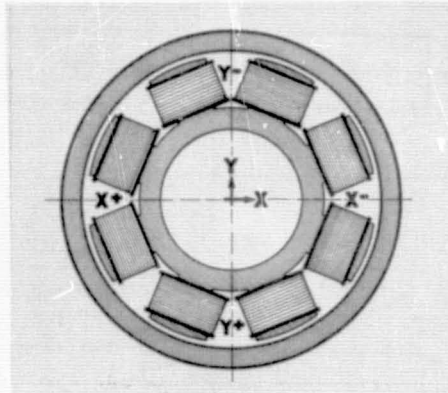
Figure 3:   Magnetic Radial Bearing
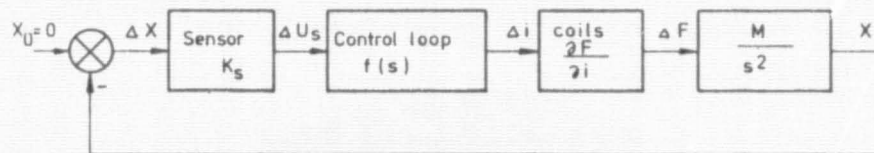
Figure 4:   Translational Control Loop
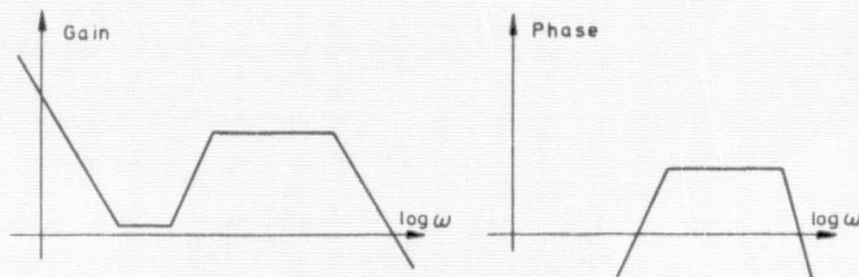
Figure 5:   Frequency Response of the Control Loop
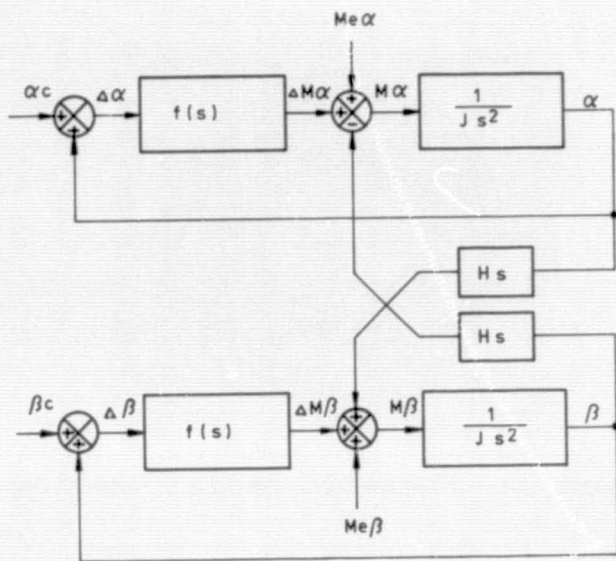
Figure 6: Rotational Control Loops
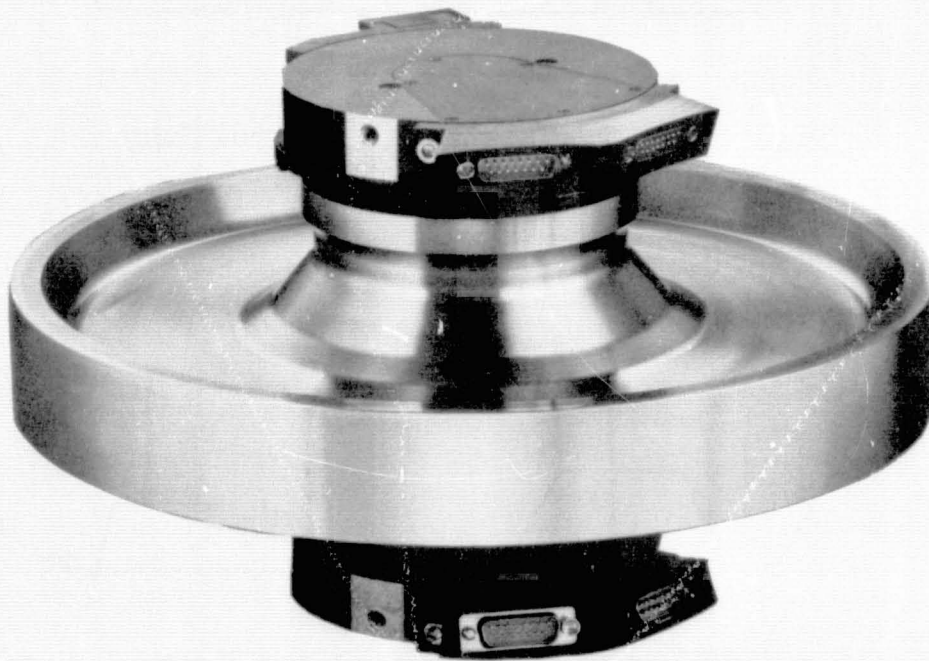
Figure 7: Magnetically Gimballed Momentum Wheel
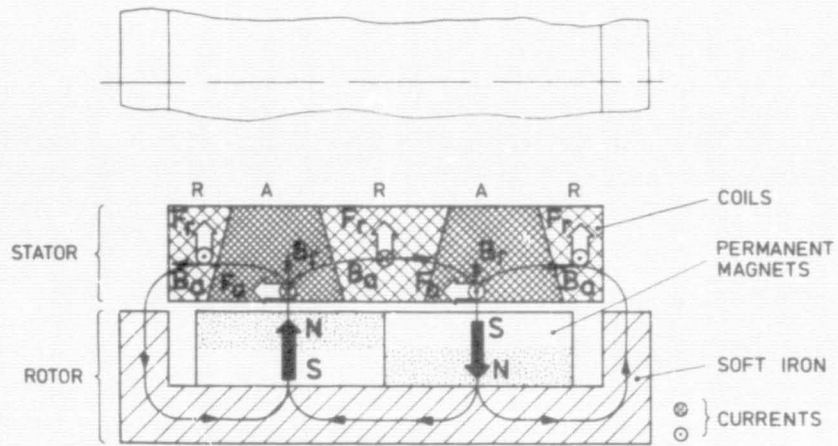
Figure 8: Basic Function of Electrodynamic Bearing
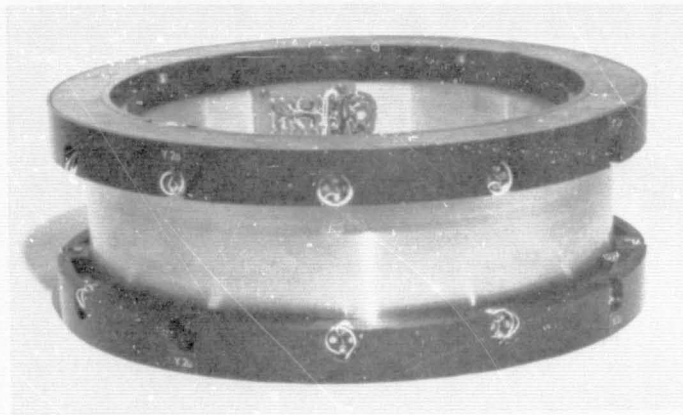
Figure 9: High-Speed Momentum Ring
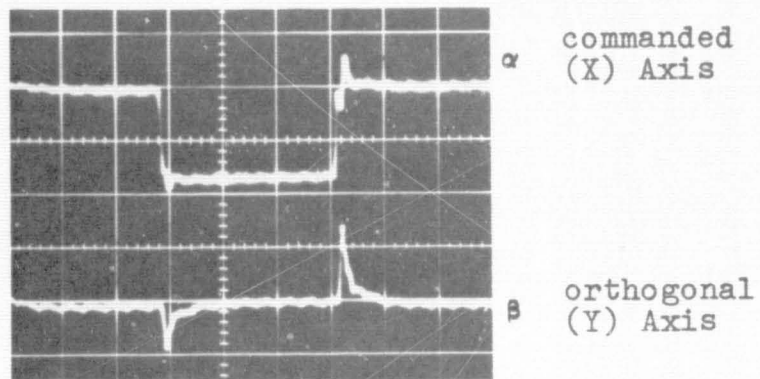
Figure 10: Magnetic Gimballing Angle
for Square Wave Command Signal
(vertical 0.4 mrad/Div.; horizontal 50 ms/Div.)

An Application of Interactive Computer
Graphics Technology to the Design
of Dispersal Mechanisms

by

B. J. Richter and B. H. Welch
Lockheed Missiles & Space Company, Inc.
Sunnyvale, California

ABSTRACT

Interactive computer graphics technology is combined with a general purpose
mechanisms computer code to study the operational behavior of three guided bomb
dispersal mechanism designs. These studies illustrate the use of computer graphics
techniques to discover operational anomalies, to assess the effectiveness of design
improvements, to reduce the time and cost of the modeling effort, and to provide the
mechanism designer with a visual understanding of the physical operation of such
systems.

INTRODUCTION

A general purpose mechanisms computer code has been developed that accurately
simulates complex interactive dynamic behavior between the various components,
which comprise mechanisms. Mechanism components that can readily be accommo-
dated with this new simulation technique are exemplified by rollers, nonlinear springs
and dampers, linkages, actuators, and arbitrary constraint guides. In addition,
mechanical components that collide, rebound, slide relative to one another, and which
are subjected to complex environmental loadings, can be modeled with this code.

Guided bomb systems for dispersing large numbers of submunitions belong to a class
of mechanisms for which the mutual interactions between components are geometri-
cally complex, numerous, and depend upon initial conditions and external environmental

loading. For these dispersal systems all of the possible interactions between the various components cannot be determined a priori and consequently must be calculated during the dynamic process. Adequate assessment of motions and reactions for this class of mechanisms is greatly facilitated by an interactive, visual, incremental-in-time solution technique. The problem is initiated on the computer using known conditions. By viewing the subsequent transient response via computer graphics, a previously unforseen interaction between mechanism components is detected. At such time the problem is stopped, the new interaction is incorporated into the model, and the problem is restarted. This incremental process continues for the desired time of interest.

The following sections discuss three guided bomb dispersal systems whose basic operation is similar. At a predetermined time, the vehicle is pyrotechnically severed into a nose section, a tail section, a payload section, and three cover panels. The dispersion of these components may be forced (e. g., internal pressurization of the vehicle simultaneous to the pyrotechnic cutting charge), or may be due solely to aerodynamic forces.

FIRST DISPERSAL SYSTEM

As a first step in analyzing the dynamics of a guided bomb dispersal system, the computer graphics technique can be used to visually locate specific areas of potential collisions between components. This is accomplished by performing an initial analysis in which no impacts are included in the model, thus allowing bodies to pass through one another. For the system depicted in Figure 1, operating with a given set of flight conditions, it is found that: (1) the aft surface of the nose section will impact/slide over the forward part of the payload section, (2) the aft tip of the winged, upper cover panel will impact/slide along the cylindrical surface of the tail section, and (3) one of the side cover panels initially moves radially away from the payload section but then returns to impact it. The areas that have been identified can then be modeled to simulate the forces generated by such impacts and the analysis can be rerun as shown in Figure 2. This approach results in a great savings of both man-time and computer time by eliminating the need to model the entire structure to account for all possible impacts.

Even though a side cover panel impacts the payload section in the example shown in Figure 2, the deployment of the payload is not seriously impaired. Under other flight conditions, however, the behavior of this system was found to be totally unacceptable. Figure 3 illustrates a case in which the winged, upper cover panel is aerodynamically 'trapped' against the payload section prohibiting successful deployment of the payload. To avoid this anomalous behavior, the only practical design fix was to restrict the operation of this system to certain vehicle angles of attack.

SECOND DISPERSAL SYSTEM

The example shown in Figure 4 is intended to illustrate two important aspects of using computer graphics techniques to study dispersal systems. The first thing to be noted is that two views of the dispersal sequence are necessary to comprehend the relative positions of the various components. In this particular case, the nose section happens to pass through the developing pattern of payload bodies untouched. Under slightly different flight conditions it can be expected that the nose section will impact several of these payload bodies. The design modification which was proposed to prevent this anomaly consisted of rigidly connecting the nose and tail sections of the vehicle via a center post. A combined nose/tail section was found to pitch much slower than the original separate nose section thus easily avoiding impacts with the payload bodies. This design solution was suggested by viewing the sequential pictures shown in Figure 4. Hence, the second thing to be noted is that the computer graphics technique can serve as a visual aid inspiring solutions to operational anomalies.

THIRD DISPERSAL SYSTEM

An example of a more complex dispersal system is illustrated in Figure 5. A side view of the entire system prior to deployment is shown in Figure 5a while in Figure 5b the three cover panels and the payload bodies have been removed to point out that the four tail fins are attached only to the tail cylinder and are cantilevered out over the

cover panels with a small radial clearance or gap.   Each of the tail fins is assembled to the tail cylinder by fitting a tab into a mating slot on the tail cylinder as illustrated in Figure 5c.   The tab is then secured in the slot by a single break bolt.

This system was originally intended to operate as follows:

- the nose section, tail section, and cover panels are pyrotechnically severed

- a simultaneous pressurization of the payload section drives the cover panels and the payload bodies outward

- the cover panels impact the cantilevered portion of the tail fins, prying them away from the tail cylinder and failing the break bolts (see Figures 5d and 5e)

- the four loose tail fins are then pushed out of the way by the cover panels allowing the payload pattern to develop

When this system was analyzed with the computer graphics technique as shown in Figure 6, it was found that the forces required to fail the break bolts retarded the deployment of the cover panels to such an extent that many impacts occurred between the payload bodies and the cover panels.   To correct this malfunction, a relatively simple design modification was proposed which consisted of substituting pyrotechnic bolts for the break bolts which attach the tail fins to the tail cylinder.   This allows the tail fins to be severed and aerodynamically carried away from the parent vehicle just prior to the dispersal event.   The deployment of the cover panels and payload bodies can then be conducted without anomalous impacts.

CONCLUSIONS

The merging of mechanisms technology with computer graphics technology has provided the designer of guided bomb dispersal systems with a valuable tool for use throughout the entire design process.   Specific examples have been discussed which illustrate the use of computer graphics techniques to discover potential design anomalies, to aid in making design improvements, to reduce the time and cost of the modeling effort, and to provide the mechanism designer with a visual understanding of the physical operation of such systems.
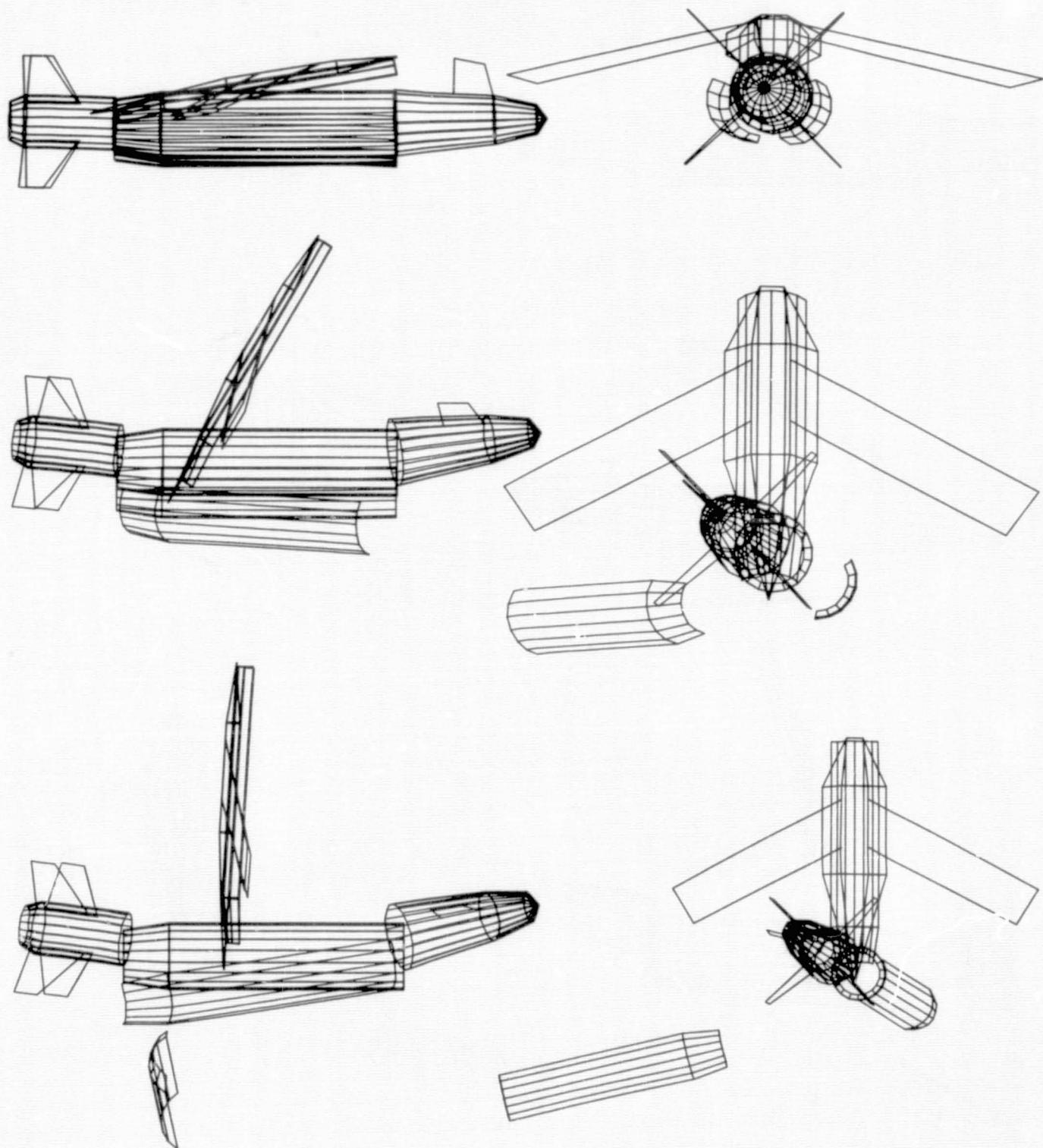
Figure 1.   First Separation System
Modeled With No Impacts
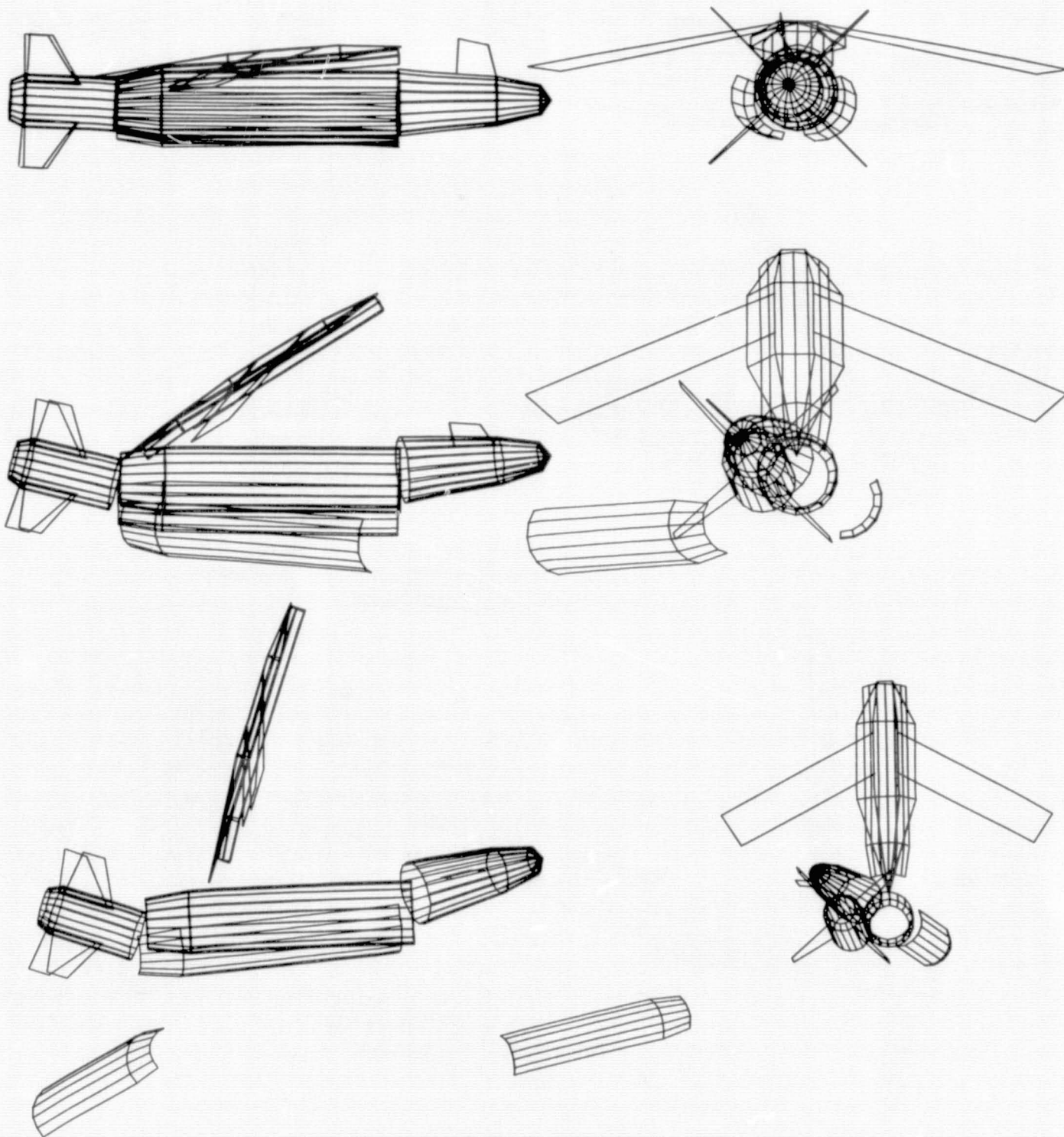
Figure 2. First Separation System
Modeled With Impacts
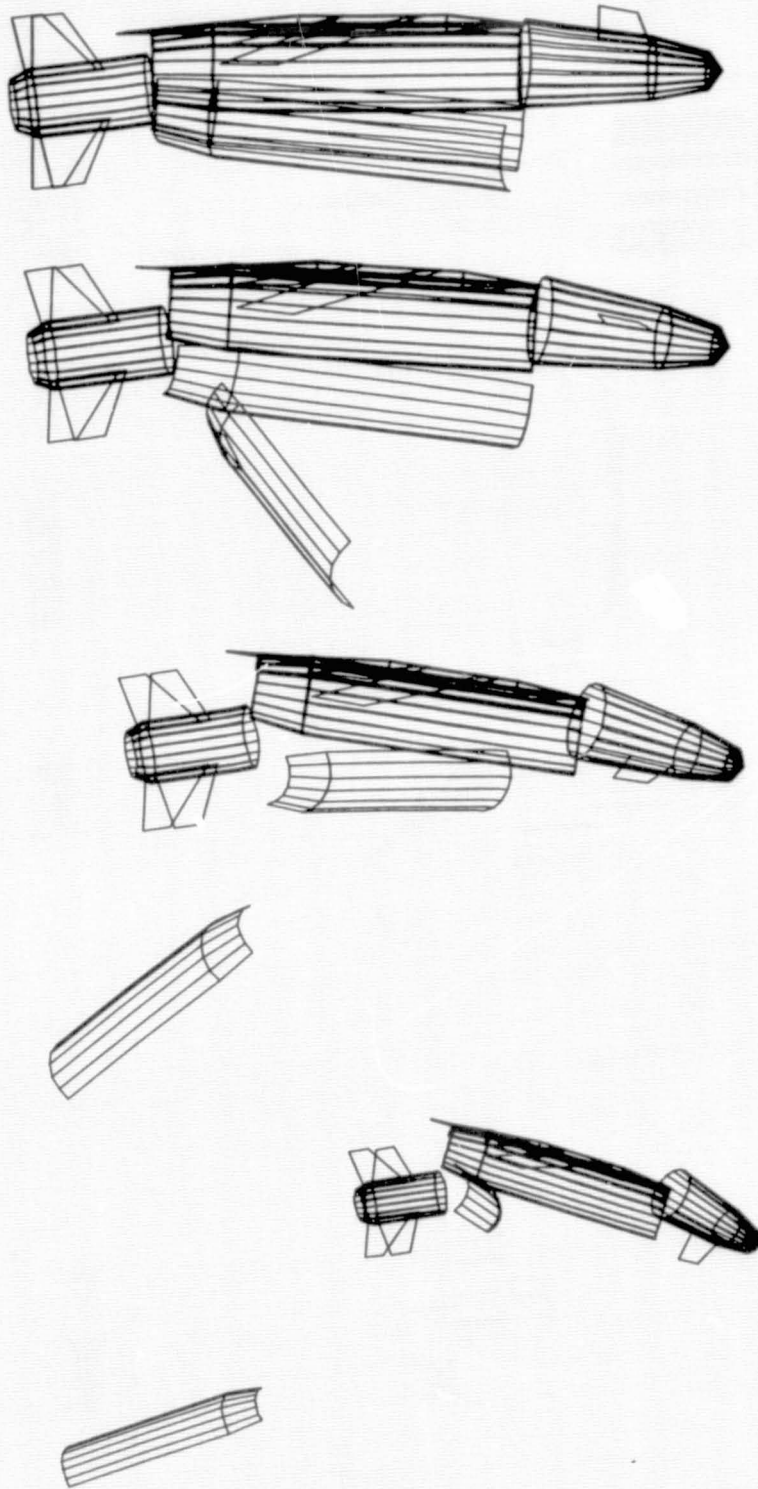
Figure 3. Anomalous Behavior
of First Separation System

63
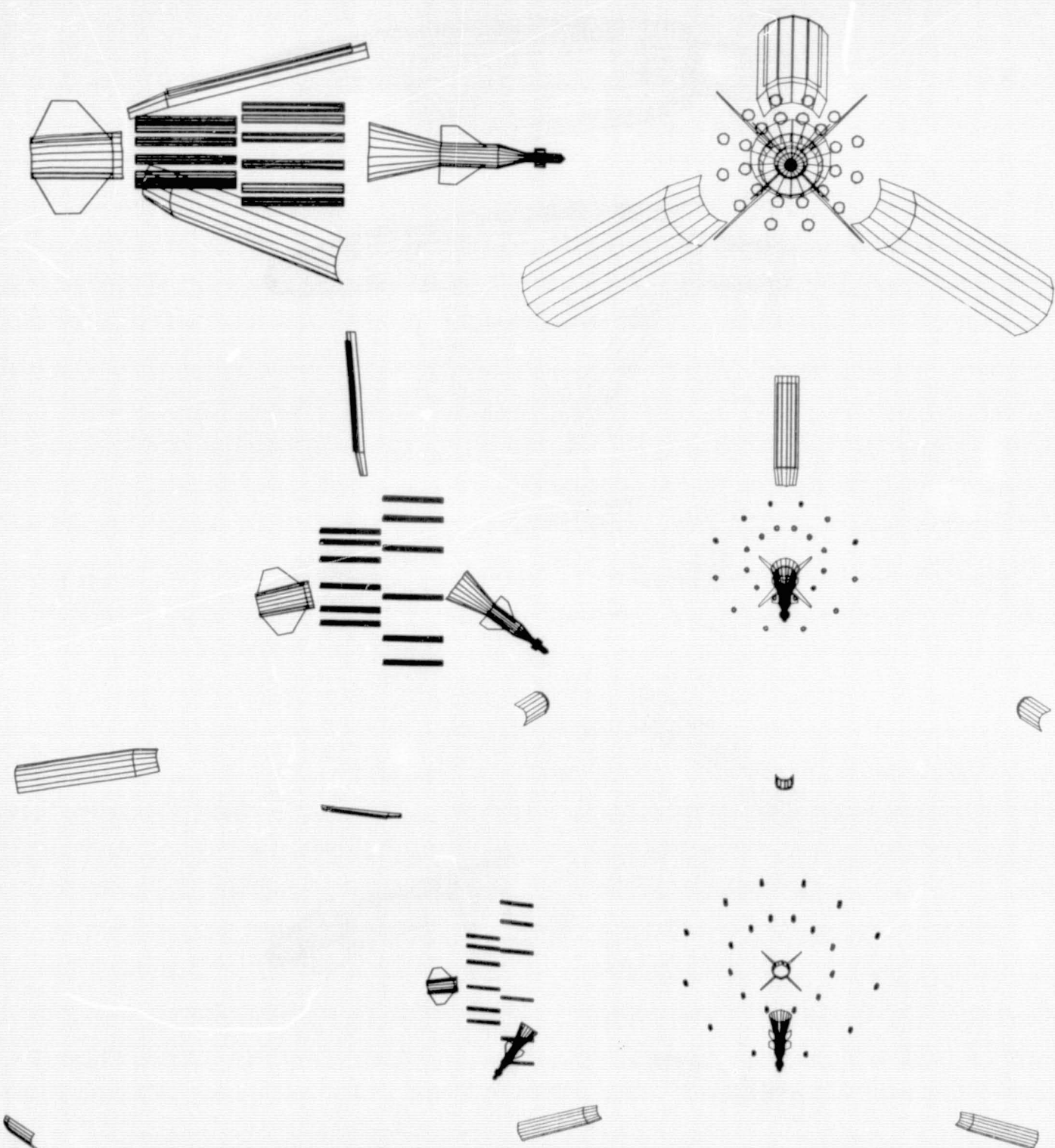
Figure 4.   Second Separation System

(a)

(b)

TAIL FIN

TAB

SLOT

TAIL CYLINDER

(c)

REACTION POINT

FORCE APPLIED BY COVER PANEL

F_P

F_B

F_B

d

BREAK BOLT SPRING

(d)

F_B

BOLT BREAK POINT

d

(e)
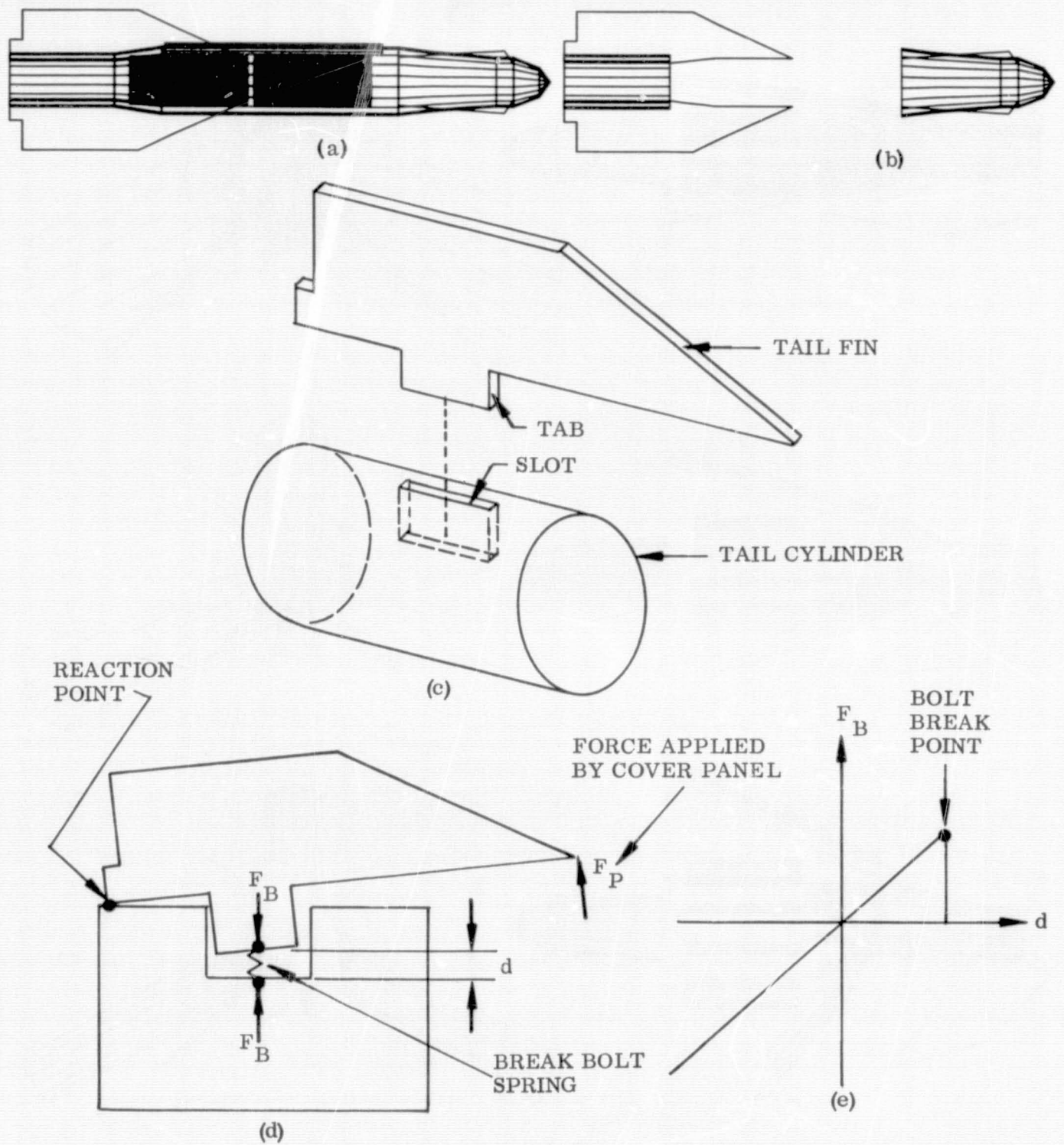
Figure 5. Details of Third Separation System
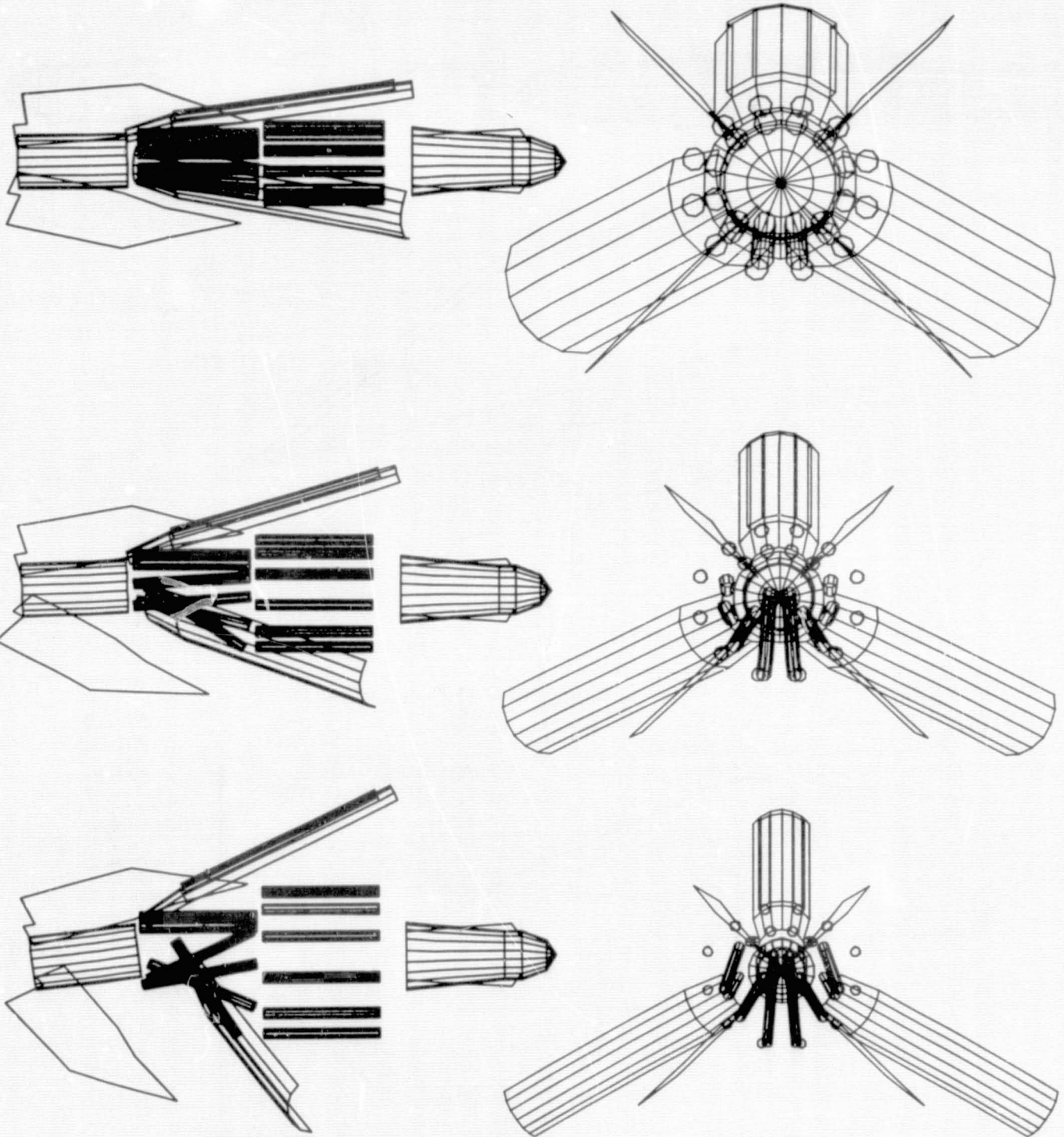
Figure 6.   Side View and End View of Deployment Sequence
for the Third Separation System

CARTRIDGE FIRING DEVICE DESIGNED FOR
ATTACHMENT, RELEASE AND EJECTION OF A SATELLITE

(Author : Lucien PIERRON - PYROTECHNIC's DEPARTMENT)
AVIONS MARCEL DASSAULT-BREGUET AVIATION
78 Quai Carnot - SAINT-CLOUD - France

1 - ABSTRACT

The under presented device has been manufactured by A.M.D.-B.A. for attachment , release and ejection of a small dimension satellite.

The device is of interest in that the above-mentioned functions are performed by a one-piece unit with resulting performances which are of interest regarding the satellite attachment and the accuracies of the path and velocity during separation and ejection.

A gain in weight may be obtained relative to the conventional device used, i.e. maintenance belt, belt unlocking device, pusher spring, cartridge fired pusher.

This expose specifies the tests conducted to demonstrate the device efficiency showing the development specific cases.

2 - GENERAL

The hereunder described device has been developed and manufactured by A.M.D.-B.A. as a contractor for CENTRE NATIONAL D'ETUDES SPATIALES (C.N.E.S.).

It was succesfully used by C.N.E.S. to orbit a 30 kilogram satellite.

The main C.N.E.S. requirements were :

- accurate path with a deviation along the various axis lower than $1°$/second

- ejection velocity 1.05 m/s ± 0.5

- correct tightness of the system during and after release.

3 - DESCRIPTION OF THE DEVICE

This assembly is shown on photograph N° 1.

Photograph N° 2 shows the device after release, with the upper part attached to the satellite and the lower part attached to the launcher.

Diagrams 1 through 5 show the device operation during flight, release and ejection phases.

Analysis of diagram N° 1 shows the main parts of the device, i.e. :

- an attachment plate (A) fitted to the launcher

- a comparatively light (B) main body

- a center assembly distributed between plate A and body B and ensuring attachment, release and ejection. This center assembly is briefly described hereunder.

3.1 - Diagram N° 1

The device is shown in its flight phase.

The satellite, through part B, is attached to plate A by means of the C ball-type lock.

This conventional ball-type lock is shown on diagram 4.

The D lock piston retains the balls within the E fixed part. Spring F inhibits ball unlocking.

Nut G applies a pre-stress to the locking unit. It eliminates all plays and, with spring F, ensures perfect strength when launching occurs (namely strength during vibrations generated during launching).

Let us specify that the whole device is installed and adjusted in the factory. It then only requires to attach B to the satellite and to attach A to the launcher.

68

3.2 - Diagram N° 2

The device is shown in its unlocking phase. The two small H gas generators have produced a comparatively high pressure (100 bars) in the I chamber. This pressure causes a comparatively high force which pushes the J unlocking piston (this force has to be important to overcome the ball locking force due to pre-stress of G nut).

The D locking piston plunges and allows balls withdrawal which free B part from A plate.

As soon as the balls are no longer maintained by piston D, an associated device causes pressure drop in chamber I. See diagram 5.

Once unlocking piston J has moved to allow action on piston D, an opening is caused on the piston face by the relative motion of pin K which discloses the L gas transfer part. The gases expand in the M annexed chamber.

3.3 - Diagram N° 3

The device is shown in its post-ejection phase.

The ejection velocity is obtained by the action of reduced gas pressure on piston J.

The piston tightness is obtained by conventional addition of O-rings to the piston head.

4 - DEVELOPMENT AND TESTING

As the specification requirements concerning the device should mainly be path accuracy and comparatively reduced ejection velocity, the hereunder mentioned tests specify the main steps cleared to prove correspondence with technical specifications.

4.1 - Checking the path accuracy

Because the satellite thrust during ejection is ensured by piston J centered relative to the satellite, and because the thrust axis passes through the gravity axis of the satellite, no specific difficulty was expected.

The path accuracy has been verified using the test set-up described hereunder and shown on diagram 6.

A model of the satellite was fitted to the device. The satellite axis of the device was horizontal. Plate A was attached to a rigid support. The satellite and its B plate was retained by a 5-meter long vertical wire. The hanging wire was attached to the satellite at a point such that the wire direction was passing through the gravity center of the B part satellite assembly.

The movement of the satellite was filmed by two cameras : one along the fore and aft center line and one for sideways filming.

The film analysis has shown on the basis of the first five tests that no parasite motion existed about he thrust axis over a distance of approximately 50 cm (later on, disturbances were found due to the presence of the gas generator supply wires).

4.2 - Adjustement and substantation of ejection velocity

This is the most interesting point to examine because the velocity required was very low (1.05 m/s ± 0.15) and because the various parametres summarized below affected this ejection velocity.

The test set-up used was identical to that specified in preceding paragraph, i.e. the satellite was hanged by means of a 5-meter long wire. The ejection velocity was measured by a test set-up shown on diagram 7.

4.2.1 - Test set-up for velocity measurement

Diagram 7 shows the test set-up for velocity measurement. The test set-up includes a graduated transparent scale including opaque lines spaced by two millimeters, with the width of each line being two millimeters. This scale is a conventional device which is called rake.

A punctual light source sends a light ray which goes through the rake and excites a photodiode whose reactions are recorded on a magnetic recorder.

The internal pressure in the I gas expansion chamber was also measured.

70

4.2.2 - Parameters affecting the ejection velocity

The following parameters had to be examined and adapted :

- gas pressure due to cartridge firing

- value of pre-stress caused by nut G

- tightness and friction of piston J

- gas pressure drop caused by pin K and M expansion chamber.

4.2.2.1 - Gas pressure of cartridge fired generators

- The generator powder charge was rapidly determined from the first tests (see table 1).

  To obtain the 1.05 m/s velocity, the main powder charge was 55 mg.

- Following this series of tests, the device has been operated using one gas generator. The test velocity has been 0.53 m/s, which has confirmed that the device was operating with a single squib.

4.2.2.2 - Value of the G nut pre-stress

Further checking tests have shown too high a variation in the ejection velocity. This velocity was increasing with the number of tests.

An analysis of the piston effect has shown that, due to the variation of the locking force, the gas pressure obtained in chamber I prior to motion of piston J was varying substantially with tightening of G nut.

It was necessary to determine accurately a method of application of the G nut tightening torque. This tightening has been lightly increased in order to decrease the force dispersion, which has caused a requirement for higher pressure in I chamber and the powder charge of the gas generators has been increased from 55 mg to 65 mg.

71

The velocity values recorded are shown
on table 2. . The results obtained were not
perfectly satisfactory. The dispersion was too
high and the velocity recorded was very often
lower than the average wanted.

4.2.2.3 - Tightness and friction of piston J

Following the additional tests, light
gas leakages between piston J and body B were
found to affect velocity substantially.

The requirements for installation of
the seal into the piston and for greasing in
piston B have been rapidly established and
a better regularity has been obtained in the
velocity recorded.

4.2.2.4 - Effect of pressure maintenance in
chamber M

The best accuracy was obtained after
establishment of the means to find the effect
of :

- the expansion volume in chamber M

- the diameter of pin K, i.e. gas through the
  L part (in actuel practise a variable pres-
  sion maintenance when the gas expand in cham-
  ber M)

- the setting of the known part of pin K which
  was adjusting, in the ejection first phase,
  the velocity of the gas expansion through
  part L.

After approximately thirty tests, all
these parameters have been perfectly determi-
ned and the results specified in table 3.
show that the velocity required was practi-
cally obtained very faithfully.

72

5 - CONCLUSION ON THE ADJUSTMENTS CARRIED OUT

The summary report of the tests specified here-above shows that the device used allows the performance required as for as accuracy is concerned for such a low ejection velocity.

By analysing systematically the records and various parameters, it was possible to define an assembly procedure likely to allow obtaining the velocity required : 1.05 m/s ±0.15.

It is clear that if the ejection velocity was higher, the various parameters specified here above would have a far more negligible effect and that, for instance, for a 3 m/s ejection velocity, the device could be much more easily adjusted.

Let us recall that the device is of interest in that all the devices required for carriage, release and ejection of a satellite are formed in the one-piece unit. The complete device as it is shown can be fitted to the satellite in the factory, which prevents any setting or specific operation later on.

Another interest can also be stressed : indeed no expandable part is used as compared with the problem of retaining the connection belt used in other devices.

Photograph N° 1

Photograph N° 2

DIAGRAM 1

DIAGRAM 4
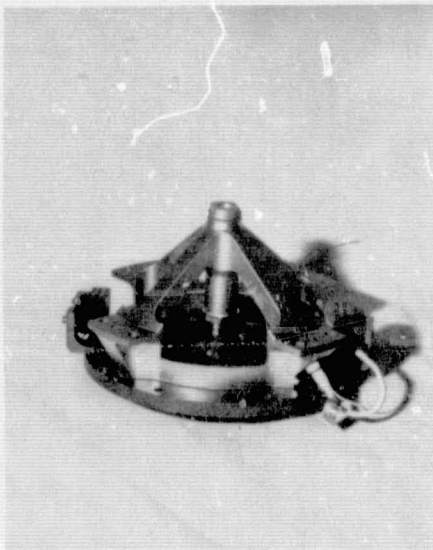
DIAGRAM 2
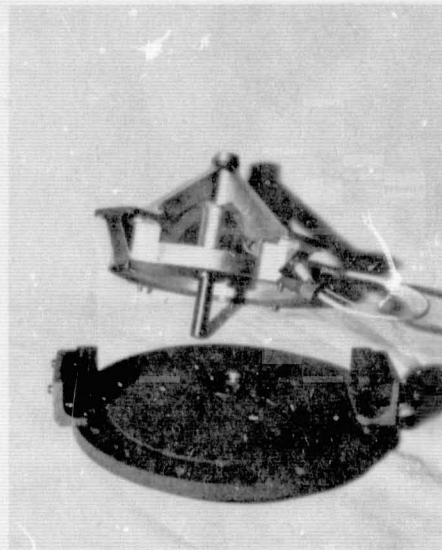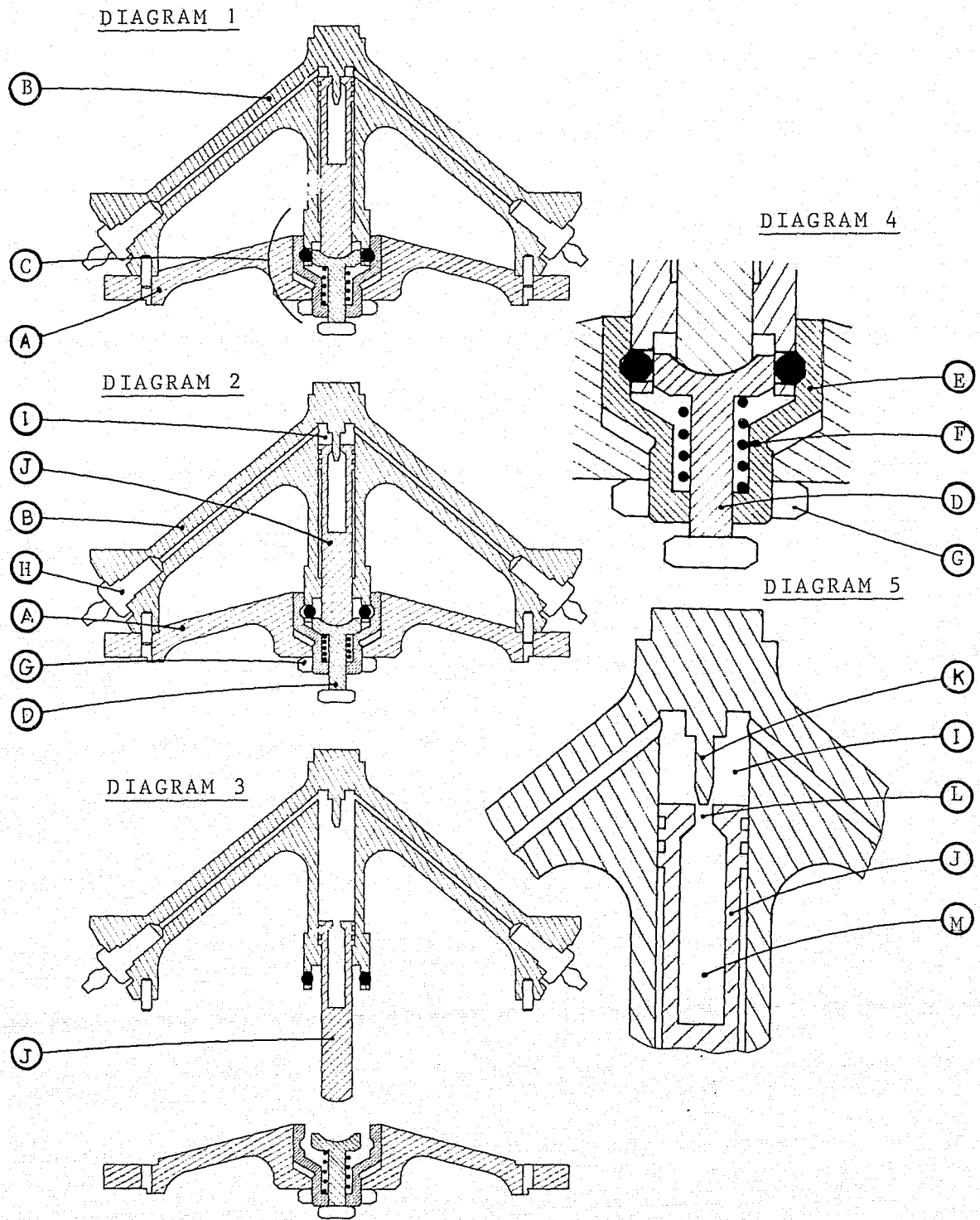
DIAGRAM 5

DIAGRAM 3

Figure 1.   Release and Ejection Phases During Flight

74

DIAGRAM 6

Checking the Path Accuracy

DOWNWARDS SIGHT

CAMERA 1

DIAGRAM 7

Velocity Measurement

Punctual
light
source

Rake

Photo diode

CAMERA 2

Tape recorder AMPEX

Pressure sensor

Recorder

Velocity

Pressure
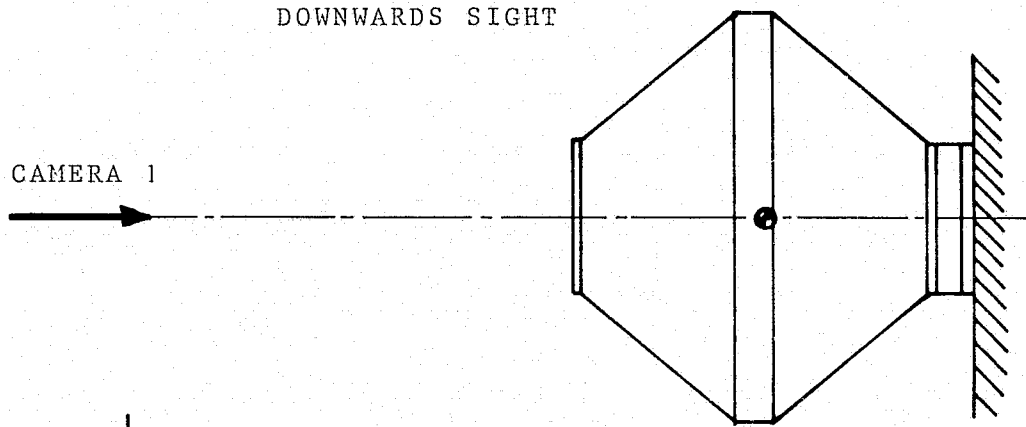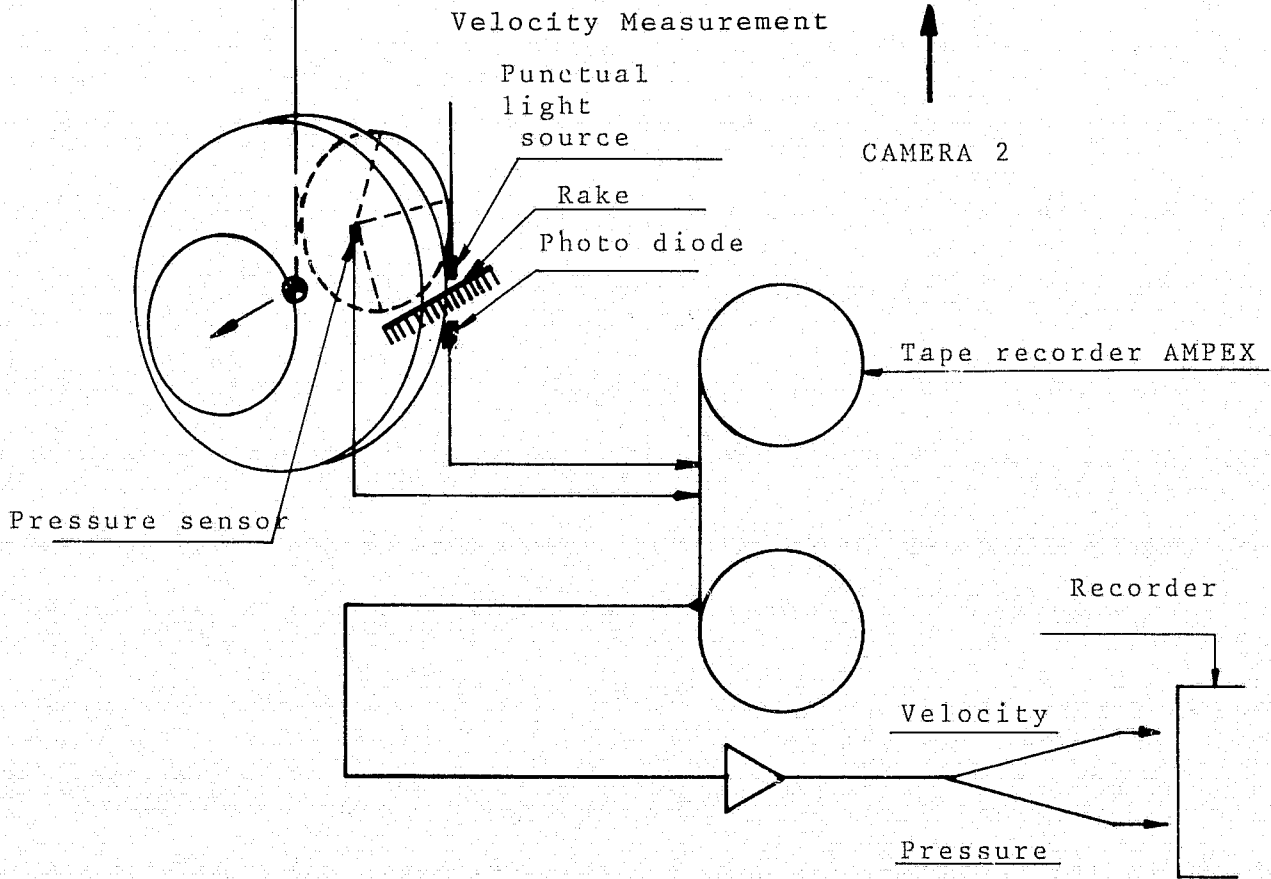
Figure 2. Test Set-up

TABLE 1

GBSe powder charge	Velocity
2 x 120 mg	2.15 m/s
2 x 100 "	1.7 "
2 x 60 "	1.15 "
2 x 50 "	1.00 "
2 x 55 "	1.05 "

TABLE 2

Firing	Velocity	Remarks
1	1.08 m/s	
2	1.02 "	
3	0.9 "	
4	1.03 "	
5	0.98 "	
6	0.836 "	)
7	0.815 "	) 3 firings made
8	0.815 "	) in presence of
9	0.768 "	) C.N.E.S.
10	0.795 "	
11	0.83 "	

TABLE 3

Firing	Velocity		Remarks
1	1.066)		
2	1.02)	Average :	Real gas
3	1.15)	1.07 m/s	generators.
4	1.04)		
5	1.087)		

THE MJS-77 MAGNETOMETER ACTUATOR

By William C. Stange

NASA Goddard Space Flight Center

SUMMARY

A two-position (0° and 180°) actuating mechanism (flipper) driven by alternately-heated wax motors (pellets) will be used to rotate the low field triaxial fluxgate magnetometer experiment on the 1977 Mariner Jupiter-Saturn spacecraft to its 0° and 180° positions. The magnetic field, power requirements, weight and volume of this device are very restrictive. The problems encountered in design and development of this mechanism are presented.

INTRODUCTION

The purpose of this experiment is to provide precise, accurate, and rapid vector measurements (from 0.01γ to 20 gauss, $1\gamma = 10^{-5}$ gauss) of the magnetic fields of Jupiter and Saturn in interplanetary space to them and beyond. These data extend in situ studies of the solar wind interaction with Jupiter and characteristics of its magnetic field and yield first studies of Saturn's field and its interactions if the solar wind extends to 10 AU.

Performing accurate measurements of magnetic fields on a spacecraft not fabricated magnetically clean is a major problem. A moderately long boom will be used to place two low-field ($\leq 6400\gamma$) triaxial fluxgate magnetometers at remote distances from the spacecraft. Simultaneous measurements will yield separate estimates of the spacecraft field and the ambient field.

The purpose of this essentially nonmagnetic actuator is in-flight calibration of the triaxial fluxgate magnetometers. This calibration, which determines the sensor zero point, is accomplished by periodically flipping the magnetometers by 180 degrees.

The advantages of this mechanism are that it satisfies more than any other known device, the constraints of volume, weight, nonmagnetic materials, and power in relation to the requirements of high torque, fast cycling and long life in the hard vacuum of space and exposure to intense radiation fields at Jupiter. These properties are derived solely from the unique mechanical qualities of the pellet. This actuator will provide cyclical bi-directional rotary motion under varying environmental temperatures (-45°C to +65°C) in a vacuum for periods up to five years.

This paper describes the mechanical and electrical functions of the design which evolved, as well as the problems encountered. The objectives achieved are evaluated and other possible applications are presented.

OBJECTIVE

The objective was to develop an actuator which would meet the following requirements.

1. Rotate 180 degrees ±15 minutes of arc.

2. Remain at the indexing stop until again actuated.

3. Have a permanent magnetic field (when not being powered) less than 0.1γ at 1.27 cm (1/2 in).

4. Have a minimum capability of 300 cycles during a period of five years.

5. Require not more than 11 watts of power.

6. Weigh less than 0.227 kg (0.5 lb).

7. Fail-safe indexing, i.e., the actuator must not stop in any position other than 0 or 180 degrees.

8. Operate within the temperature range of -45°C to +65°C.

9. Operate in a vacuum.

10. Complete the rotational indexing within 4 minutes of initiation.

DESIGN

The selection of a design approach required the consideration of other feasible concepts. Among those reviewed were bimorph piezoelectric devices, opposing coil solenoids (without cores), nonmagnetic electric motors, Freon state conversion bellows, and NITINOL actuators.

A concept utilizing pellets was adopted because it appears to most reliably meet the above design requirements.

PELLET

In 1965, McCarthy, et al., of Goddard Space Flight Center developed an oscillating magnetometer actuator which initiated the utilization of the wax pellet as its power element (see Reference 1). The pellet is a standard production line component* which is used in thermostats produced by the Harrison Radiator Division, General Motors Corp. It consists of a brass case with a rubber boot, an expansion material, and a piston. Figure 1 represents the basic configuration. The expansion material is Epolene and paraffin wax to which a fine copper powder has been added to improve the heat conduction. The

---

*Part No. 3005031, Harrison Radiator Division, General Motors Corporation

Epolene and paraffin proportions are adjusted to obtain the desired melting point. The solid to liquid transition of this material yields a 14% volumetric increase. Thus when the applied heat raises the material's temperature to the melting point, the material expands and presses the rubber boot against the conical tip of the piston, forcing it outward.

The magnetic requirements of the MJS-77 magnetometer experiment necessitated some modifications to the basic production line pellet. A survey of pellet production line components with a magnetometer allowed selective use of all components except the piston, flange seal and expansion material. A simple substitution of different materials eliminated the magnetic problem with the production line piston and flange seal; namely, titanium for the stainless steel piston and beryllium copper for the brass flange seal. The magnetic problem with the expansion material was found to be in the copper powder. The production line copper powder is processed with steel balls which contaminated the resulting product. After an exhaustive search and many trials, a magnetically clean copper powder was obtained which was processed with ceramic balls.

The developmental nature of these extremely magnetically clean pellets required that they be hand assembled and tested in a clean room environment with all components being checked with a magnetometer during all stages of fabrication. The Harrison Radiator Division of General Motors Corporation at Lockport, N.Y. in conjunction with NASA personnel successfully produced enough magnetically clean pellets to insure the ultimate success of this effort.

The pellet which was finally developed weighs 26 grams with 750 milligrams of expansion material and will produce a maximum force of 15.88 kilograms (35 lbs) with a stroke of 1.14 cm (0.450 inches). A summary of the pellet characteristics is presented in Table 1.

MECHANICAL OPERATION

The flight mechanism as shown in Figure 2 is simply an experiment container (triaxial fluxgate magnetometer) which can be bi-directionally rotated by heating either of two opposing pellets, whose indexing is biased by two over-center Flexator springs. When commanded, the function of the flipper is to rotate the triaxial fluxgate magnetometer 180° counter-clockwise from the position shown and then, when later commanded, to rotate the magnetometer back 180° clockwise to the original position.

As shown in Figures 2 and 3 the crank arm holds the contact against the left position stop, thus completing an electrical circuit. To rotate the magnetometer 180° counter-clockwise, the right pellet (Fig. 4) is heated to 100°C by a heater which is bonded to its cylindrical surface. The pellet is filled with a special wax and copper powder mixture, which undergoes a 14% volumetric increase in changing from its initial solid state to a liquid state. The internal pressure thus created squeezes a rubber boot (Fig. 4) which forces the piston out of the rubber boot. The shoulder of this piston bears against the right beam (Fig. 4) and causes the toggle to rotate counter-clockwise. The toggle is tied

to the shaft through a pin which travels in the toggle slot. As the toggle starts to rotate, it bears against the pin (Figs. 4 and 5A) and rotates the shaft and all members attached to it. When the crank arm rotates counter-clockwise about 100° (Fig. 5B) the two Flexator springs flip the shaft (magnetometer) the remaining 80° (Fig. 5C), which the slotted toggle allows, thus completing the 180° flip (Fig. 5D). This flip is sensed by the opening of the left contact to position stop (Fig. 3) opening the miniature switch (Fig. 3) and the closing of the right contact to position stop (Fig. 3). When the right piston extended from the pellet it compressed a spring which, as the liquid wax again solidifies forces the piston back into its pellet. The magnetometer can now be flipped 180° clockwise back to the position as shown in Figures 2, 3 and 4 by heating the left pellet and repeating the above process.

MATERIALS

The prime considerations in the selection of materials for this mechanism were low magnetic permeability (<1.001), volume and weight. The Flexator springs were made of Elgiloy, the bushings, housing and experiment container from Delrin, and the shafts and other hardware from titanium alloy, beryllium copper, aluminum and brass.

CONCLUSION

The mechanism described in this paper provides positive, cyclical indexing for a sensor rotating 180 degrees ±15 minutes; the permanent magnetic field is less than 0.1γ at 1.27 cm (1/2 in), the power consumed is less than 33 watt-minutes, the weight is less than 0.227 kg (8 oz), and the volume (less the experiment container) is less than 577 cubic centimeters (35.2 cubic inches).

Eight mechanisms have been fabricated: four flight models, two prototype models, and two engineering test units. These units have been environmentally qualified at temperatures ranging from -35°C to +40°C in vacuum. The flip times varied from 225 seconds at -35°C to 110 seconds at +40°C. The flight and prototype models have been shipped to the Jet Propulsion Laboratory for integration aboard the two MJS-77 spacecraft to be launched between August and October 1977. The two engineering test units have been life tested for up to 750 flips each through the temperature ranges of -35°C to +40°C in vacuum with no apparent change in operating characteristics.

REFERENCE

1. McCarthy, Dennis K., "Nonmagnetic, Lightweight Oscillating Actuator." NASA/ GSFC X-723-70-166.

Table 1

Pellet Characteristics

Start to open temperature	72°C
Start to open tolerance	±1°C
Piston travel	1.14 cm (0.450 in)
	0.95 cm (0.375 in) minimum travel after 10,000 cycles
Linear rate	0.023 cm/°C (0.005 in/°F)
Piston force	15.88 kilograms maximum (35 lbs)
Force required to return piston	3.62 to 4.54 kilograms (8 to 10 lbs)
Temperature fully open	92°C to 105°C depending on return spring force
Time to open	3 to 4 minutes, depending on initial temperature
Time to close	1 to 1.5 minutes
Life	10,000 cycles minimum
Advantages	Compact, lightweight and forceful
Disadvantages	Must allow for over travel. Requires a heat source.

Figure 1. Wax Pellet

TRIAXIAL FLUXGATE MAGNETOMETER

EXPERIMENT CONTAINER

SPOOL

SHAFT

PISTON (2)

SPRING (PISTON) (2)

POSITION STOP (2)

CABLE (MAGNETOMETER)

CONTACT (2)

BASEPLATE

CRANK ARM

MINIATURE SWITCH (POSITION)

END SUPPORT

THERMAL TRANSDUCER

TOGGLE

BEAM (2)

FLEXATOR SPRING (2)

PIVOT ARM (2)

HOUSING

PELLET & HEATER ASSEMBLY (2)

TRUNNION (2)

R.H.U. HOUSING

CABLE (FLIPPER)

INCHES

83
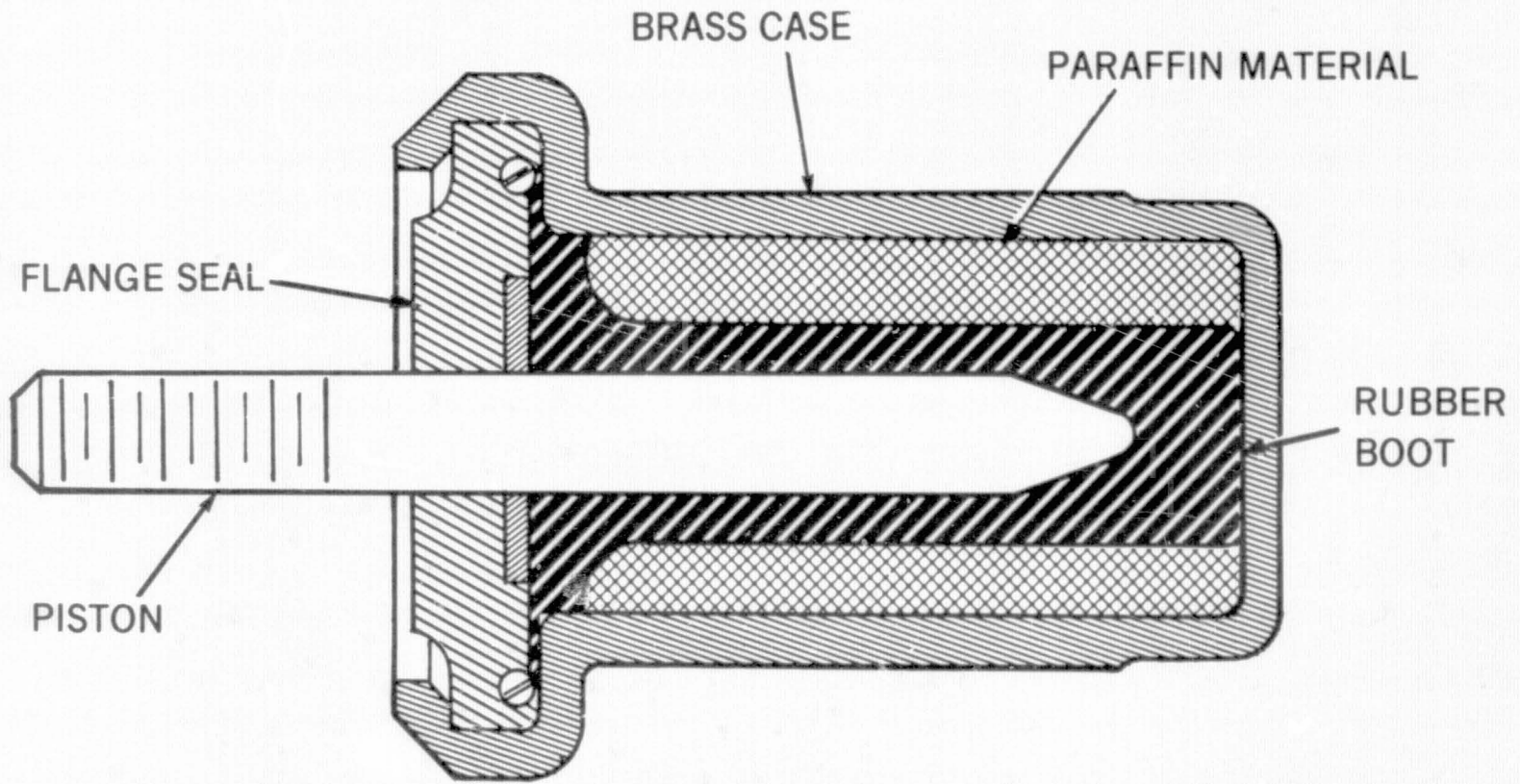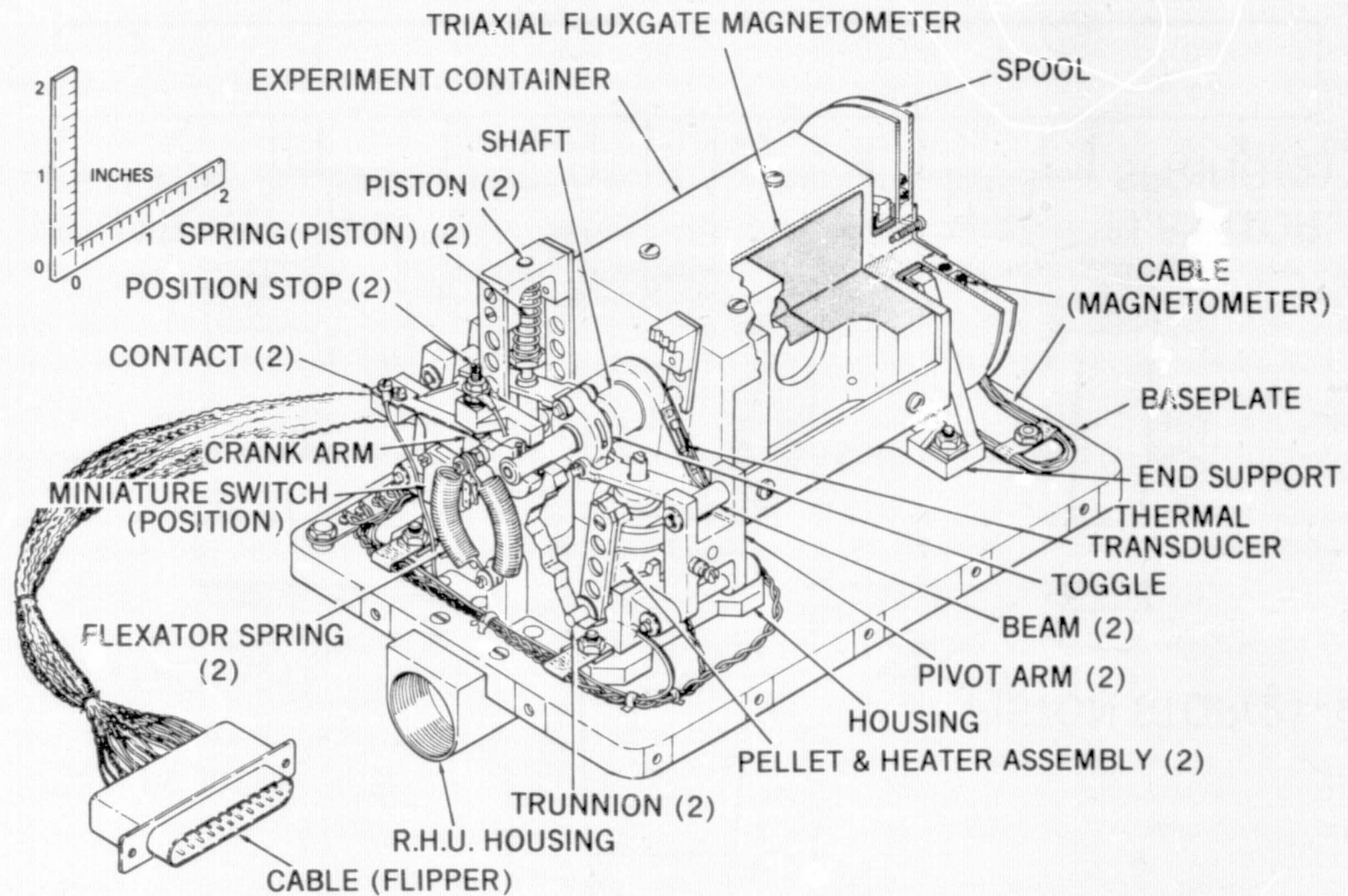
Figure 2. MJS-77 Magnetometer Flipper Assembly

PISTON(2)

CRANK ARM

CONTACT(2)

PISTON STOP(2)

MINIATURE
SWITCH

FLEXATOR
SPRING(2)
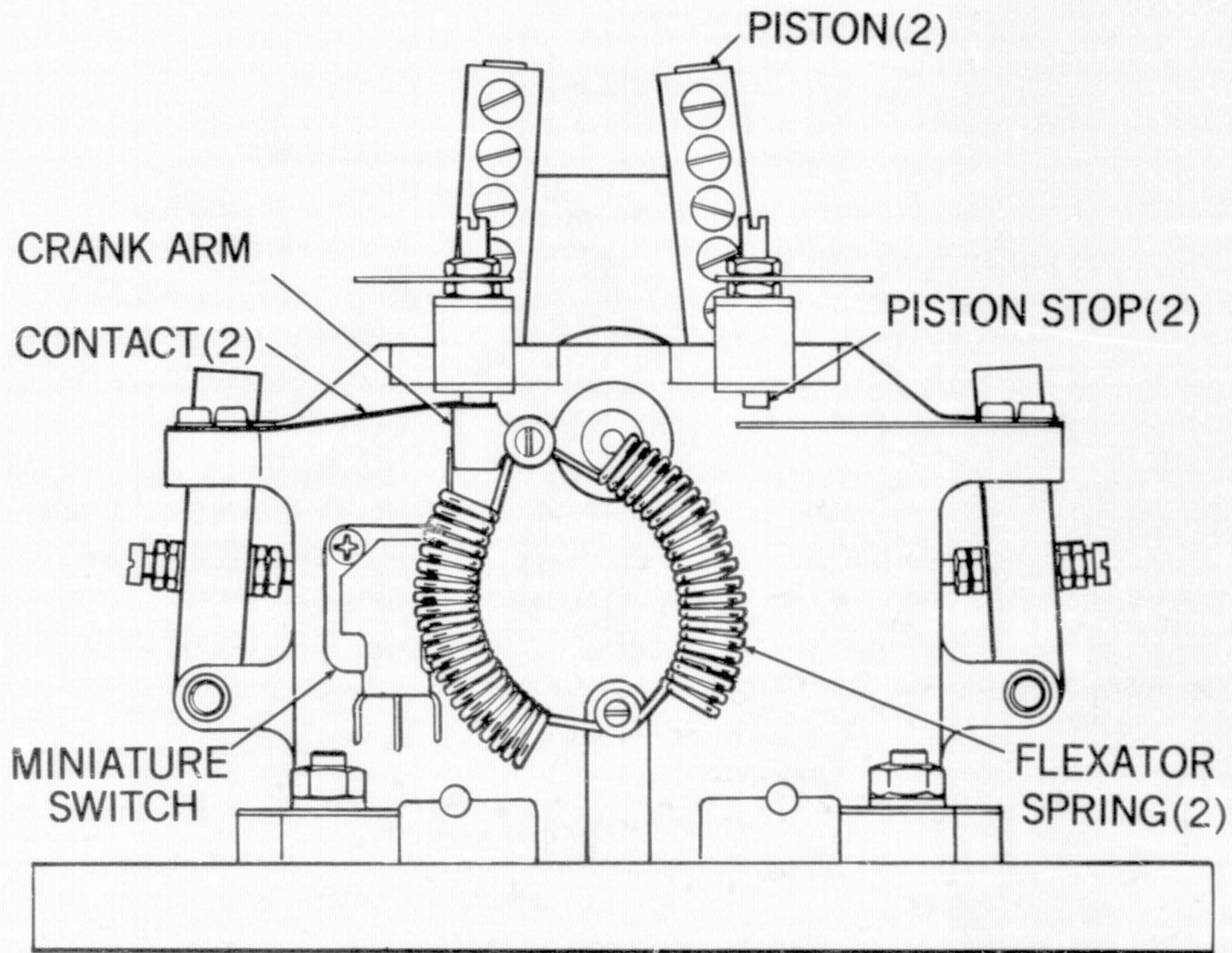
Figure 3. End View
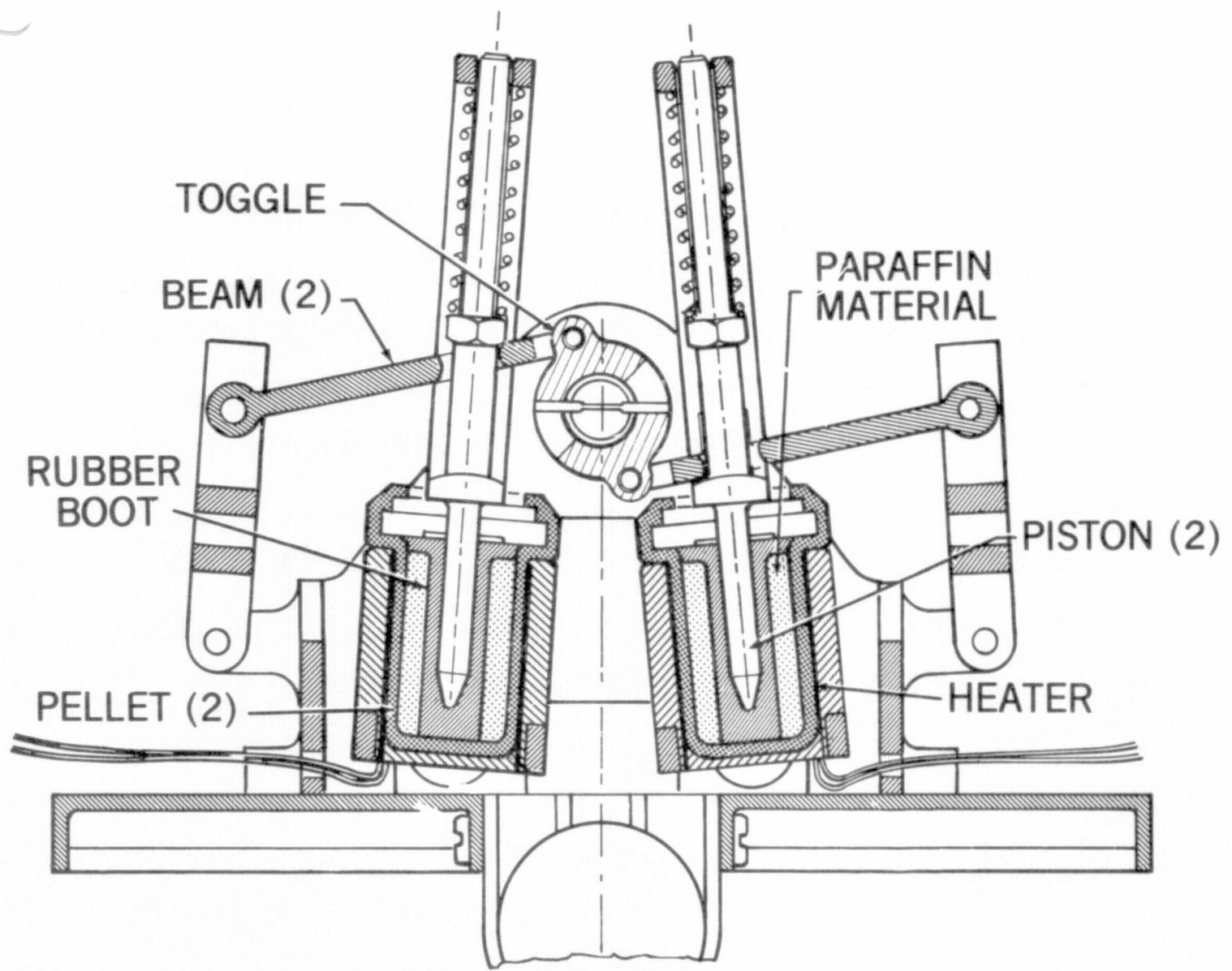
Figure 4. Flipper Section View

TOGGLE

SLOT

PIN

SHAFT

Fig. 5A

Fig. 5C

TOGGLE

SHAFT

SLOT

PIN

Fig. 5B

Fig. 5D

Figure 5. Toggle Section Views

POSITIVE COMMANDABLE OILER FOR SATELLITE BEARING LUBRICATION

By Gordon E. James

TRW Defense & Space Systems Group

ABSTRACT

The results of a feasibility study show that on-orbit commandable lubrication of ball bearings can be accomplished by direct oil application to the moving ball surfaces. Test results for the lubricant applicator portion of the system are presented in conjunction with a design approach for the reservoir and metering components.

INTRODUCTION

Oil lubricated ball bearings are key elements in satellite rotary systems. Reaction wheels, scanning devices, and communication satellite despin mechanical assemblies are examples where long life and uniform low torque performance are dependent on rolling element bearings.

Maintenance of a thin, clean, and uniform lubricant film at and near the bearing EHD ball-to-race contact zones and ball-to-retainer pocket interfaces is essential to performance. Lubricant for this purpose can be provided by passive means during the design life as long as on-orbit conditions do not vary from the design predictions. Thus oil loss from the bearing cavity by surface creep and molecular flow can be balanced by t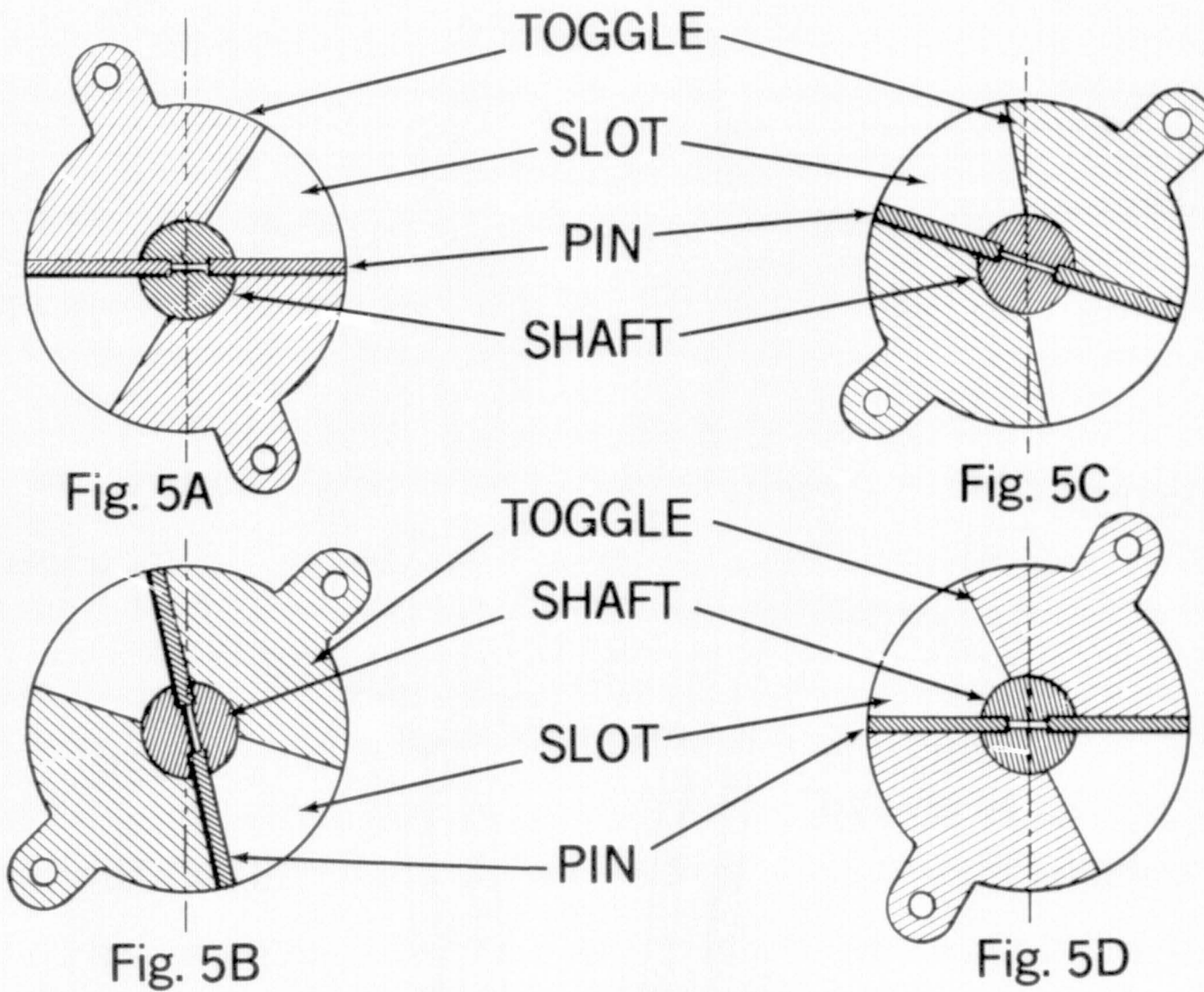he same phenomena using porous retainers and reservoir sources. Experience indicates that this passive equilibrium can be maintained for at least five years to provide a reliable film thickness (references 1 and 2).

For longer life requirements, it becomes increasingly desirable to have available a commandable oiler to replenish the lubricant when necessary. Positive control of the lubricant quantity can provide a safeguard against premature depletion and avoid the ensuing bearing degradation.

A basic design constraint in active oiling is to deliver all of the lubricant in a small metered charge uniformly to the ball pockets and to the contact zones of both inner and outer races. These regions are not easily accessed. Preferably, the relubrication should be done slowly by a device which is compatible with unmodified bearings and does not introduce contamination.

In a recently reported oiler for space applications, the lubricant charge is ejected onto one raceway by a single stroke pump immersed in a vented oil reservoir (reference 2). The present system uses an entirely different approach. Here the reservoir is sealed to prevent contamination and the lubricant is

applied slowly and evenly to reduce torque transients and assure uniform distribution.

The oiling technique described below slowly transfers a metered quantity of lubricant upon command directly to the bearing balls by means of a pressure-fed applicator. The applicator design is important and will be discussed in detail. Several reservoir/metering system approaches can be used for applicator feed, one of which is outlined to indicate feasibility.

SYSTEM DESCRIPTION

Operation

The oiler is designed for high surface energy oil such as Apiezon C. The high surface energy of hydrocarbon oils provides the stabilizing force for the lubricant droplet on the applicator tip. The system is best suited for large bearings where there is sufficient space between the retainer dynamic envelope and raceway to accept the applicator.

Figure 1 illustrates the applicator location with respect to the bearing and includes a representative reservoir/metering system.

The degassed lubricant supply is stored in a flexible metal bellows. Pressure is maintained by an external spring pack. Opening the release valve permits oil to inflate an adjustable-stroke metering bellows. Subsequent closing of the valve and opening of the metering valve starts the flow to the applicator. Metering pressure is sufficient to overcome the characteristic back pressure of the applicator and to provide the desired flow rate. A metering orifice provides a flow rate adjustment capability.

The applicator is supported rigidly in the space between the outer race and inner race guided retainer. In a 110 mm bore bearing with 1/2 inch ball diameters, the space is approximately .15 inches wide. A standoff distance separates the applicator tip from the ball path, typically by five times the expected launch-induced axial ball movement. A combination of toroidal tip shape and Teflon coating enables the applicator to support an oil droplet which spans the standoff distance. In the operating bearing, the passing balls wipe off a portion of the distended hemispherical droplet. In this manner, oil is slowly and uniformly transferred from the balls to the retainer ball pockets and both raceways. The droplet is continuously replenished by flow from the metering system during the 2-4 minute relubrication cycle.

Applicator Design

Figure 2 indicates the dimensions of the breadboard applicator. A 0.032 inch diameter steel tube supports a .07 inch Teflon toroid. The toroid was lathe-turned, using a form tool, and polished to reduce surface roughness.

A family of stable droplets at equilibrium with a downward gravity field is shown in Figure 3. Surface adhesion bonds the oil to the Teflon while the metering pressure maintains a balance against the oil surface tension. The resulting hemispherical droplet exhibits a characteristic surface contact angle with the Teflon toroid. This combines with the toroid shape to center the droplet on the toroidal axis. The centering force is appreciable and is effective over a wide range of droplet sizes and external forces.

Droplets larger than shown in Figure 3.4 flow back onto the outside of the applicator shank, and are drained to the outer raceway. The back of the toroid separates the overflow oil from the new droplet at the orifice. This important separation effect prevents a short circuit between the distended droplet and applicator shank. In practice, the droplet will only overflow if the bearing is not moving during delivery, or if the metering rate exceeds the design margin.

Figure 4 illustrates the droplet centering and stabilizing effect. Consider a centered droplet (A) to be laterally displaced to the right on the toroid without changing the droplet shape (B). The resulting contact angle Θ' on the left is larger than the characteristic or minimum energy angle (52.5° for Apiezon C on polished Teflon). Similarly, the angle Θ'' on the right is less than 52.5°. If the angles are corrected by changing the droplet shape (C), the oil surface curvature on the right will be greater than that on the left. Since the curvature is balanced by internal fluid pressure, a pressure gradient will form which tends to move the droplet back to a centered position. In the presence of a body force such as gravity, the displaced position is stable when the restoring pressure gradient balances the externally applied force.

It is interesting to note that this geometry was discovered while evaluating the failure of a previous applicator design. The first applicator was based on a "barrier" approach where the droplet was intended to be contained on a flat steel tube end by a surrounding barrier surface provided by a Teflon sleeve. By equating energies, it was shown that the droplet should grow in place on the iron. In reality, the oil easily flowed past the iron/Teflon barrier and accumulated on the sleeve end, held there by the slightly rounded outer Teflon edge. Microscopic examination showed that the iron/Teflon interface was minutely rough and irregular. This roughness was probably reducing the oil/Teflon surface energy difference and destroying the barrier effect for bulk oil. (See Reference 3 for a description of surface energy principles.) The present toroidal design does not rely on a metastable barrier.

Applicator Tests

The test apparatus shown in Figure 5 rotates a preloaded pair of 110 mm bore 440-C bearings which have 23 half-inch diameter balls per bearing and inner race riding phenolic retainers. A variable speed motor drives the inner races. Speed is monitored by an interrupter and electronic counter. A strobe light and stereo microscope, not shown, facilitate viewing the oil transfer process. The applicator location is shown in Figure 6.

Tests were conducted to determine oil transfer properties and droplet stability for a wide range of speed, flow rates, standoff distances, and gravity orientations.

It was found that for a given bearing speed and standoff distance, there was an upper limit to permissible flow rate. This occurred when the applicator was worst-case oriented (horizontal) with respect to gravity. Beyond the flow rate limit, the droplet would exceed its maximum stable .05 inch standoff size between ball passings. At 60 rpm, the flow rate limit occurred at approximately four times the normal operating rate of .1 cc in 2 minutes. For a stand-off distance of 0.02 inches, the applicator functioned properly for the speed range 60-700 rpm for various flow rates between 0.1 cc in 30 seconds to 10 minutes.

Oil is transferred without loss or splatter. During contact with the ball, a portion of the applicator droplet bonds to the ball surface, Figure 7. Separation of the ball and droplet carries a portion of the oil away on the ball and the remainder re-forms in a hemisphere on the applicator. The centering force of the applicator toroid stabilizes the droplet against the viscous ball shearing force. Oil on the ball surface is transferred to the retainer ball pockets, and from there to both raceways. Examination of ball-to-ball surface oil transfer patterns indicated that the lubrication was uniform.

A temperature sensitivity test was made using a heated ball and an inclined V-groove. The equivalent speed range tested was 0-420 rpm. Since the surface energy of hot oil is less than that on the cooler applicator droplet, the droplet might not have wetted and bonded to the ball surface. However, the transfer occurred properly for a 70°F-200°F ball rolled past the delivery head, thus indicating that the necessary wetting will occur for a broad range of bearing and reservoir temperatures.

CONCLUSIONS

The droplet transfer system was shown to be a viable approach to positive commandable oiling.

REFERENCES

1. Jacobson, P. E., "Long Life Ball Bearing Suspension System, A Present Possibility," AIAA Guidance and Flight Control, San Diego, Calif., August 1976.

2. Glassow, Frank A., "Assurance of Lubricant Supply in Wet-Lubricated Space Bearings," 10th Aerospace Mechanisms Symposium, 1976. JPL Tech. Memorandum 33-777, pp. 90-103.

3. Contact Angle, Wettability, and Adhesion. Advances in Chemistry Series, Vol. 43, American Chemical Society, 1964.
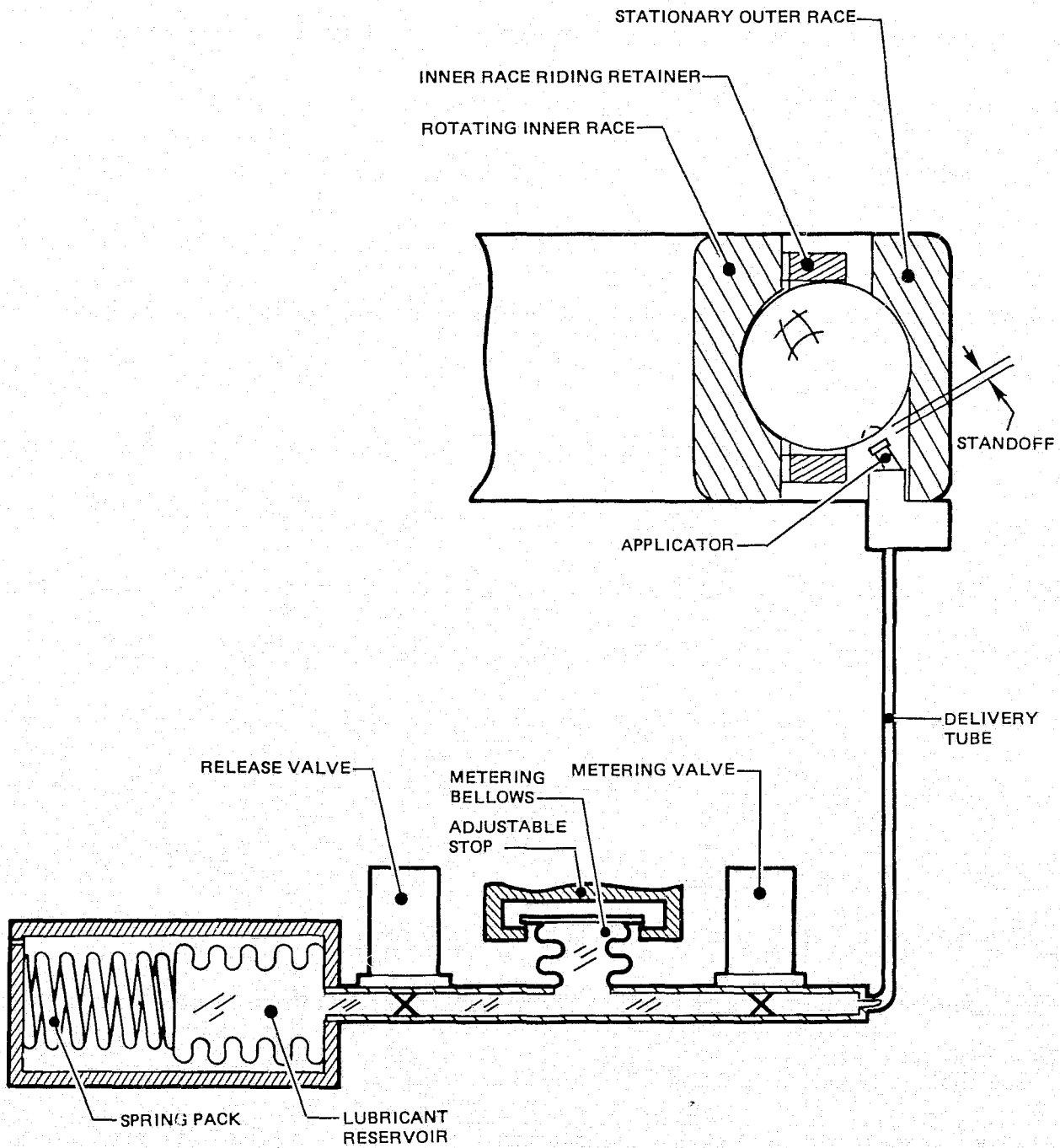
FIGURE 1. Oiling System Diagram

STAINLESS STEEL
DELIVERY TUBE

TEFLON TOROID

0.02

0.032

0.07
DIA

0.019

DIMENSIONS IN INCHES

0.128
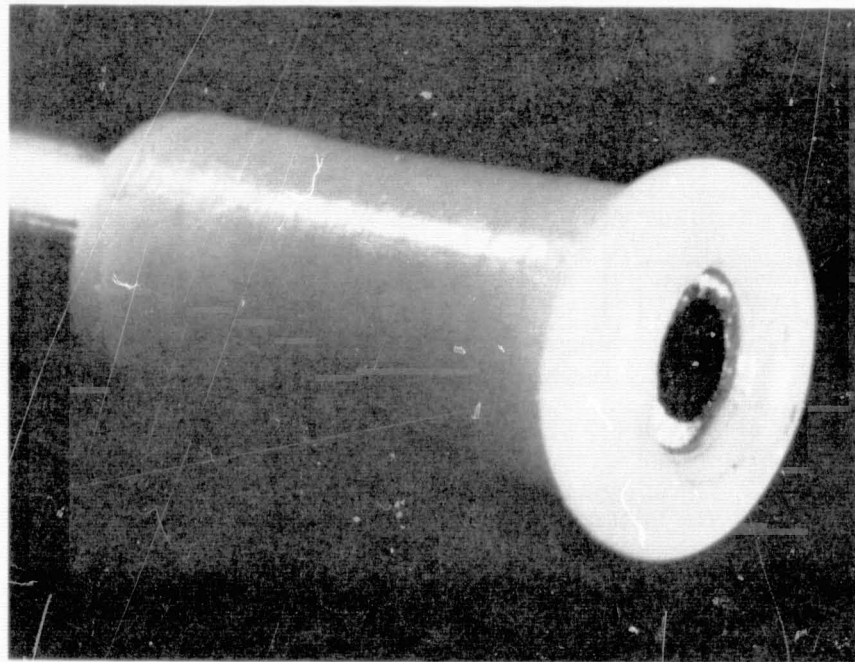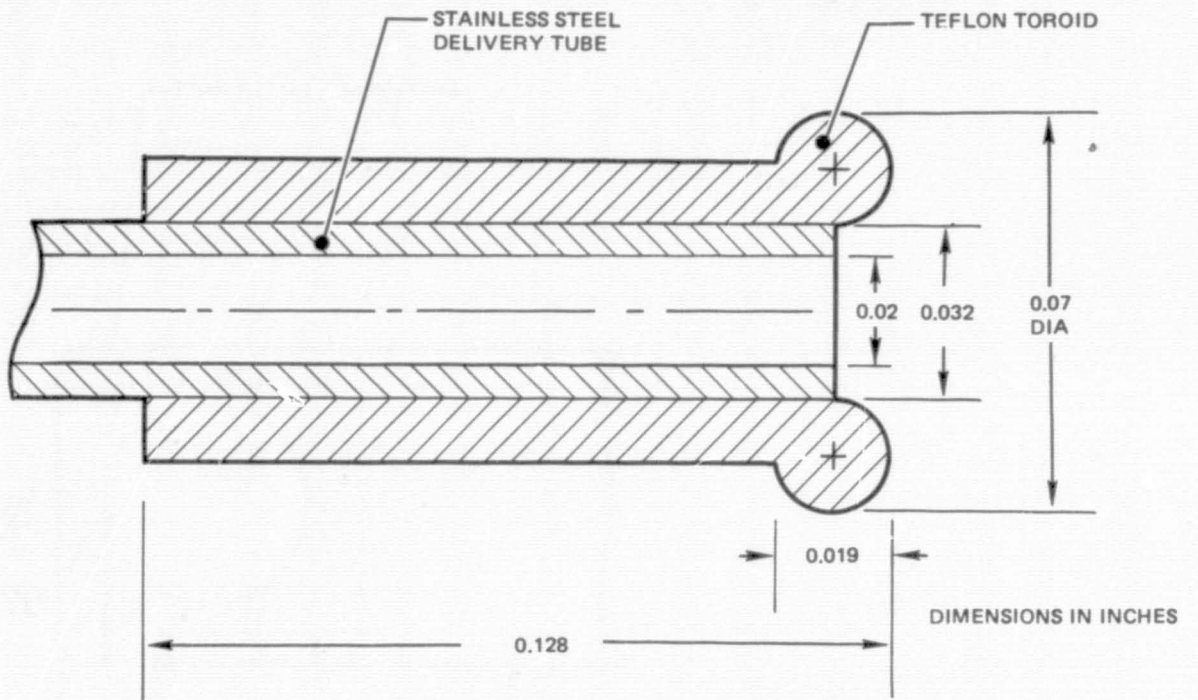
FIGURE 2.   Breadboard Applicator Dimensions

3.1.

GRAVITY

3.3.

3.2.

3.4.   MAXIMUM STABLE SIZE (0.05 STANDOFF)
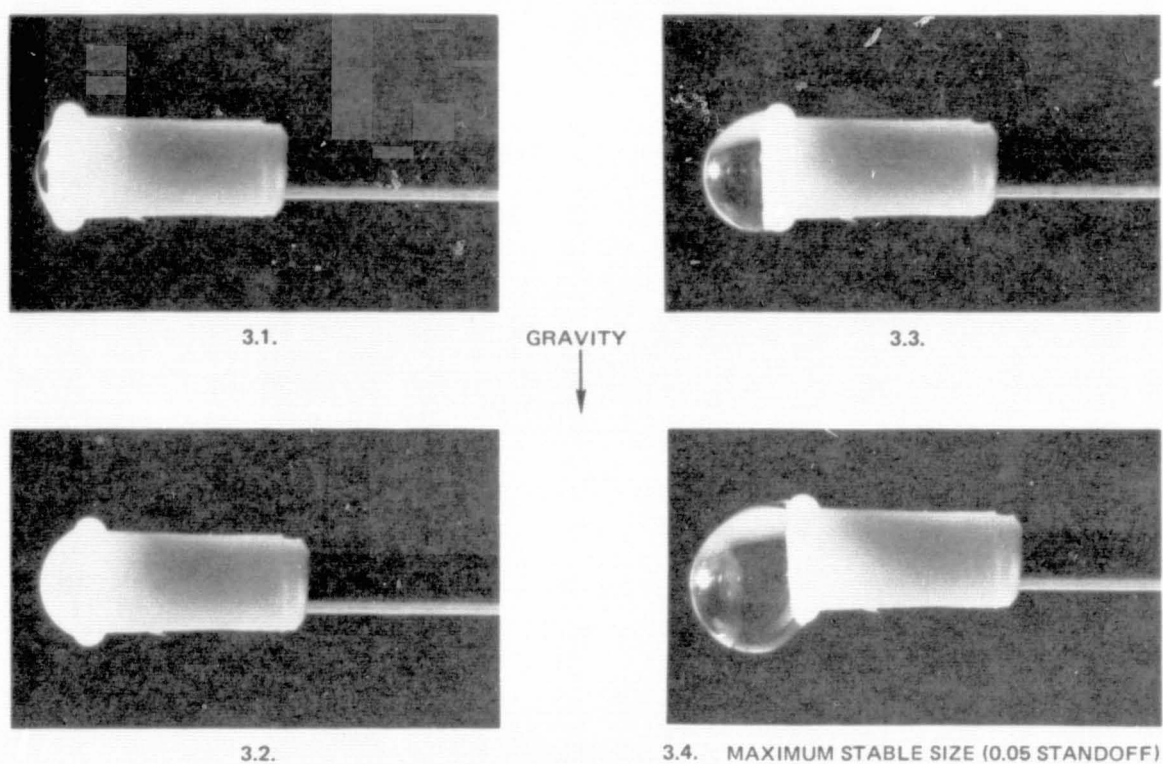
FIGURE 3.   Stable Oil Droplets at Equilibrium

STABLE DROPLET
INITIAL POSITION (A)

AXIS

CORRECTED SHAPE
52 DEG CONTACT
ANGLE (C)

ASSUMED LATERAL
DISPLACEMENT (B)

$\theta = 52°$

$\theta = 52°$

$\theta = 52°$

θ'

θ''

HIGH PRESSURE
REGION

LOW PRESSURE
REGION

FIGURE 4.   Oil Droplet Lateral Stability

FIGURE 5. Bearing Spindle Drive Test Setup

94
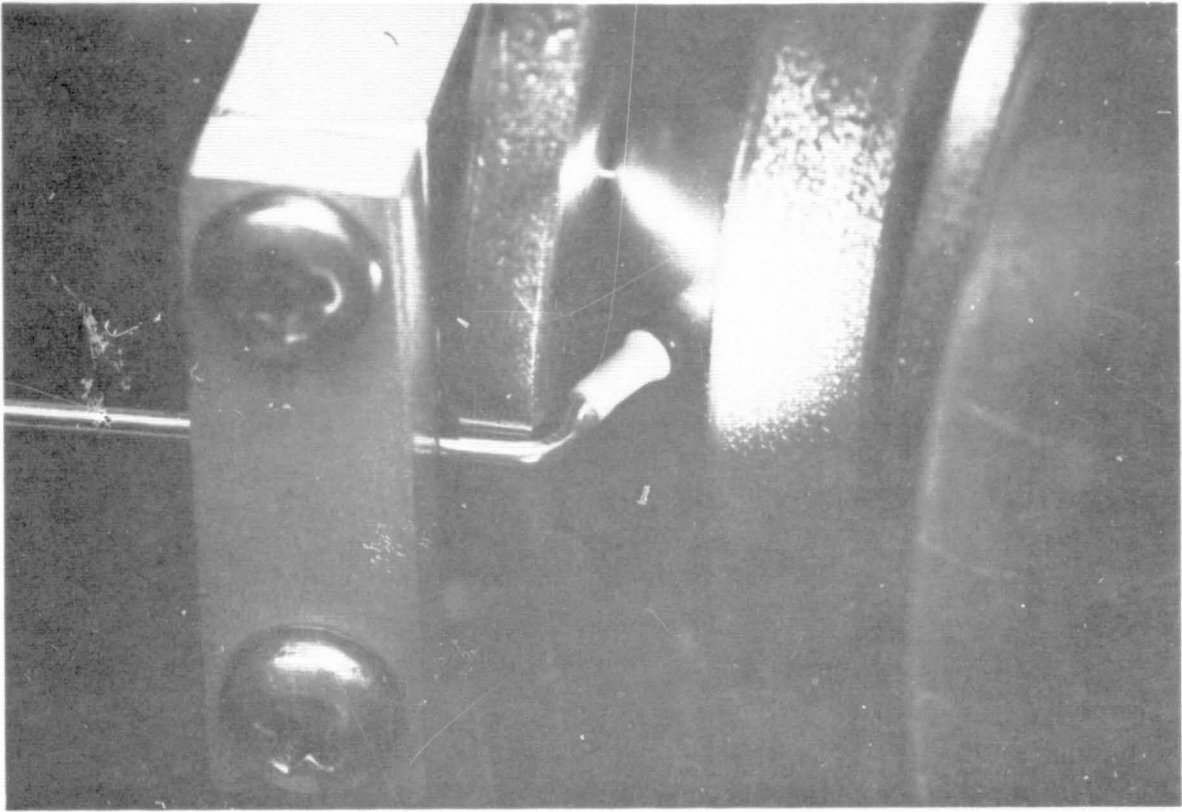
FIGURE 6. Breadboard Oil Applicator Location
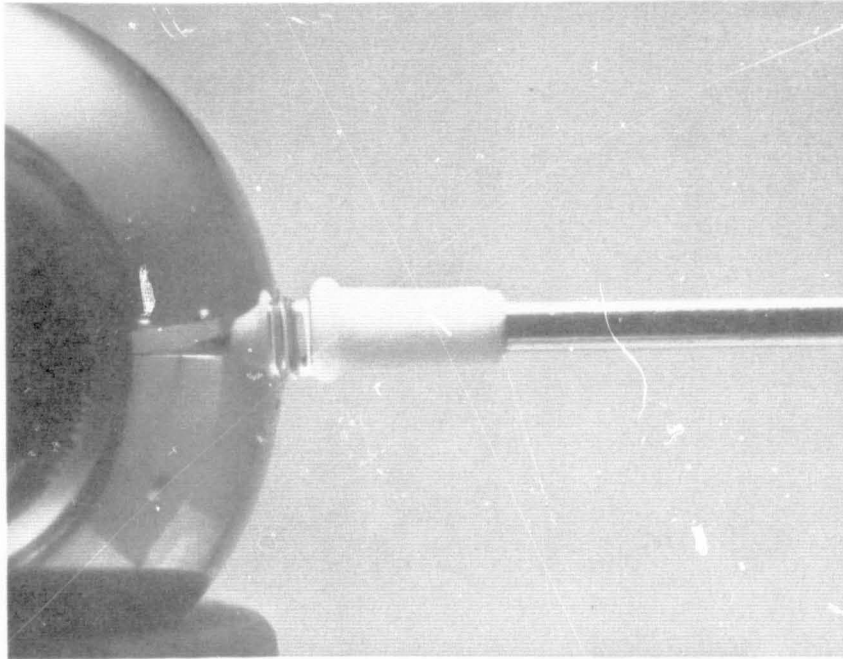
FIGURE 7. Oil Droplet Transfer to a Stationary Ball

95

AN EXTENDIBLE-HIGH STIFFNESS SOLAR ARRAY

D. E. Lindberg and D. T. Chung
Lockheed Missiles and Space Co., Inc.

ABSTRACT

The requirements for an array, 20 ft^2 in area, a natural frequency of approximately 3.5 Hz, started a development program at LMSC which would last three years from conceptual trade studies to the final qualification tests. The array wing is designed as a two panel add-on to the aft equipment rack of an Agena spacecraft. After release and deployment, a means of stiffening the panels was necessary. A hinge development program was initiated and conducted which resulted in selection of a 4 bar link locking hinge capable of transferring sufficient panel-to-panel stiffness to meet the natural frequency requirement. One significant feature of this array is that the panels are randomly deployed with no rate control, but only a balance between spring power and friction with sufficient energy and structural margins for deployment.
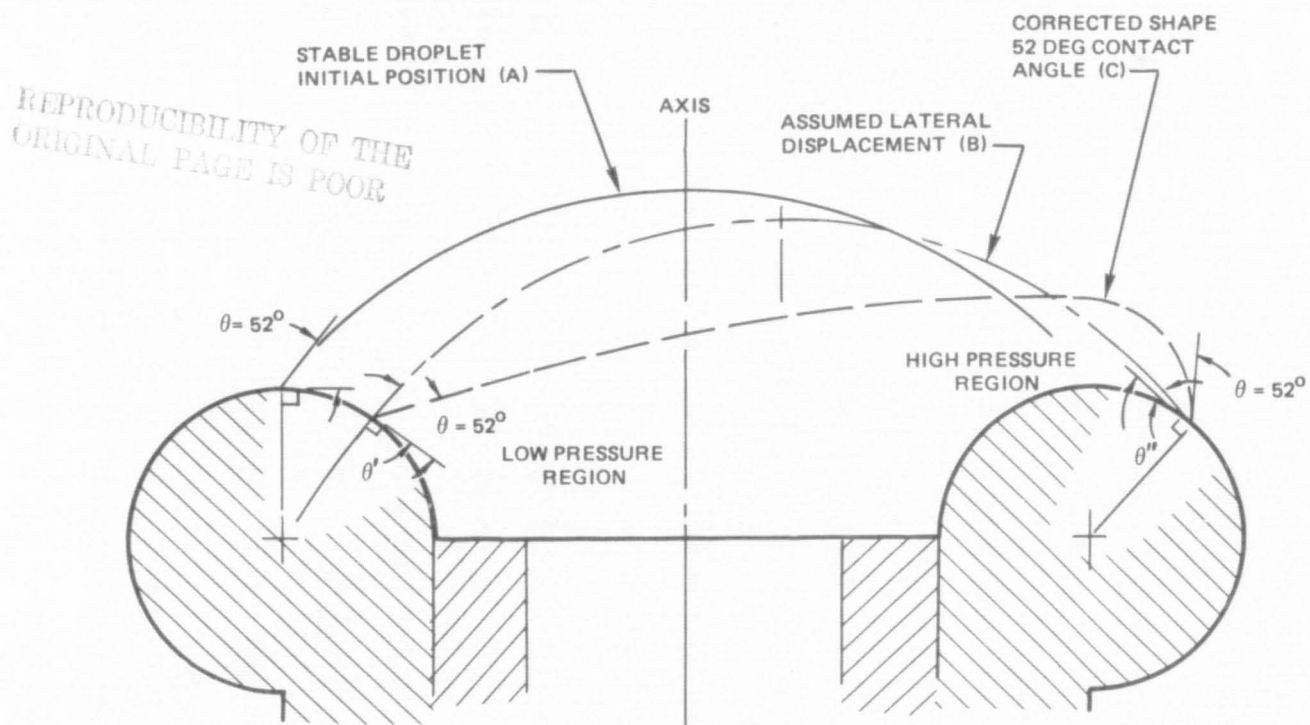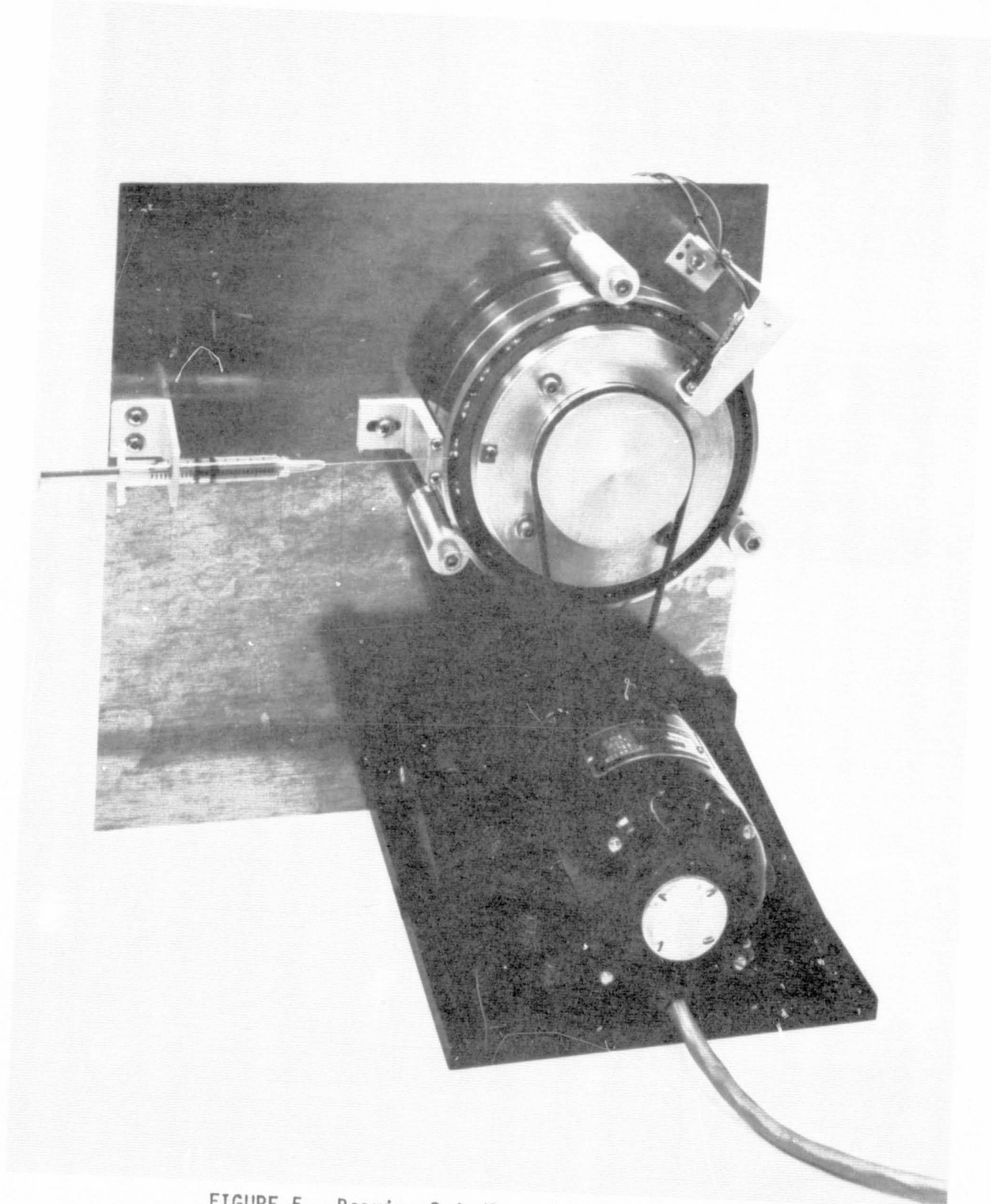
A mobile fixture was developed for zero-g simulated testing of the solar array wing. Deployment tests and natural frequency tests were conducted with satisfactory results (Figure 1).

As the spacecraft was developed, it was necessary to increase the stiffness and/or damping of the solar array wing from 0.5 percent at 3.5 Hz to 0.5 percent at 30 Hz or an increase in damping with a corresponding lower natural frequency. Three methods were considered: (1) Struts, (2) Tethers and (3) Squeeze Film damping. Struts seemed difficult to implement into the system, therefore, a tether system was pursued. After design, fabrication, and test of development hardware, modifications to the system were required which made this design very sensitive and difficult to practically control the damping characteristics.

The squeeze film damping hardware was designed, fabricated and tested in parallel with the tether system but appeared to require a comprehensive and long term test program to assure its satisfactory operation.

Another look at integrating struts into the array wing resulted in time delayed struts consisting of cables passing through close fitting tubular segments. Once the wing was deployed the cables were tensioned by viscous dampened spring actuators which aligned and compressed the tubular segments into stiffened struts. With the wing deployed, one end of the struts is fixed to the center of the outboard panel while the other is attached to the actuators which are dynamically isolated from the support frame with silicone rubber pads.

The array wing with the struts was successfully deployed in both air and vacuum for as many as 50 deployments on a single unit. The stowed wing has also successfully completed flight qualification testing.
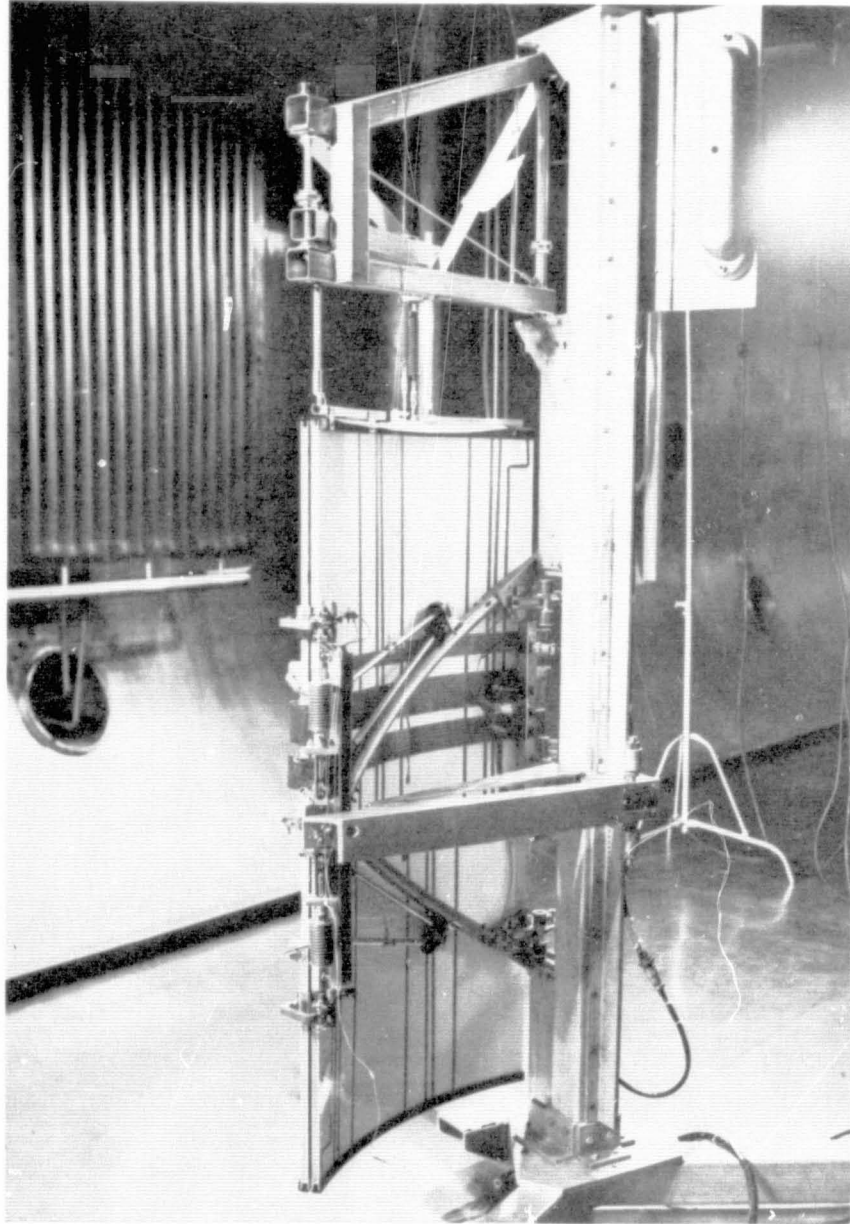
Figure 1. Stowed Solar Array Module in Ground Deployment Fixture

$\mathcal{D}_{i} \theta$

DOCKING AND RETRIEVAL MECHANISM

By J. Robert Tewell and Richard A. Spencer

Martin Marietta Corporation
Denver, Colorado

ABSTRACT

This paper describes an engineering prototype docking and retrieval mechanism (DRM) which enables two spacecraft to dock and be structurally joined on-orbit. The joining of two spacecraft or payloads on-orbit supports future planned space activities such as payload servicing, deployment and retrieval, and assembly of large space systems. The DRM, as developed,provides advantages over prior approaches because it is a nonimpact docking mechanism, does not require impact absorbing mechanisms or attitude stabilization on the target spacecraft, is capable of docking to a spinning spacecraft, and can spin up and deploy a spinning spacecraft or payload.

INTRODUCTION

The NASA is planning a Space Transportation System (STS) which will possess capabilities and flexibility far beyond that existing today. One of the first steps toward this STS is the Shuttle which is planned to become operational during the latter part of 1970's. The Shuttle will deliver and retrieve payloads and will be able to do a variety of space operations. Typical operations include checkout and deployment of satellites and space probes, servicing of satellites, satellite retrieval, and assembly demonstrations of large space systems.

Within the NASA, special consideration is being placed on the requirement to develop teleoperator technology and space teleoperator systems. The primary goal of this technology is to extend man's capability for doing useful work in a space environment. By allowing man, via teleoperator concepts, to have more control and flexibility over the proposed activities in space, substantial savings in program cost and other important benefits can be realized. Most of the savings occur because new approaches to low-cost payload design, satellite deployment, satellite retrieval, on-orbit experiment procedures, and on-orbit servicing of payloads can be seriously considered.

A teleoperator, as defined by NASA, is a remotely controlled, dexterous, cybernetic, man-machine system designed to enhance and extend man's manipulative, sensory, locomotive, and cognitive capabilities. The distinguishing aspects of a teleoperator are: (1) remote control by man; and (2) being capable of working at a location hazardous, inaccessible, or inconvenient for man.

The study, from which the DRM evolved, was an effort primarily directed towards the Earth Orbital Teleoperator System (EOTS) (Ref. 1). The EOTS provides a remote maneuverable unit controlled from the Shuttle, the earth, or both. Space applications investigated include on-orbit monitoring and inspection, support of EVA activities, servicing, deploying and retrieving satellites, handling of hazardous materials, assembling large structural systems in space, and overall support of earth orbital payloads.

Recent studies have recommended that a typical EOTS should have the functional capabilities of indirect viewing, remotely controlled maneuverability, rendezvous and docking to other spacecraft, and remote manipulation. The primary emphasis of this paper addresses the docking of the EOTS to other spacecraft and the associated docking hardware development and design.

DOCKING MECHANISM BACKGROUND

Three major space programs which required on-orbit docking have evolved the docking technology most often referenced in establishing future requirements. These include the Apollo, Skylab, and Apollo-Soyuz. The Skylab program continued the use of the Apollo probe and drogue concept, while the latter program used a peripheral type concept.

In summary, the docking concepts evaluated for Apollo were characterized by both impact and nonimpact designs (Ref. 2). The final selection was impact; however, the rationale behind this must be viewed using the requirements that were defined. The advantage of the impact type system is that the kinetic energy of the active vehicle can be transformed into forces to provide the alignment of the two halves of the docking interface. Complications arise because the remaining kinetic energy must be removed through an energy absorption system, typically springs and dampers. It was also noted that, for Apollo, the docking was between two stabilized vehicles. Thus, if the first impact did not effect capture (e.g., Apollo 14), the second attempt was not complicated by the tumbling of one of the vehicles. As the EOTS will be required to dock to passive payloads, the alternative is to provide the EOTS with a control system that enables the desired level of docking alignment and incorporates a nonimpact type docking system. It was also observed that, if the docking concepts can be categorized as either central or peripheral, all the proposed concepts for Apollo were of the central type since there was no requirement for the docking interface to transmit large structural loads. This docking characteristic is similar to the EOTS type of requirements. In addition, most of the docking operational sequences involve two basic activities: (1) aligning and capturing the payload, typically with a set of light latches; and (2) then drawing the two together so that a firm structural connection can be made by a second set of stronger latches.

The EOTS docking mechanism evolution was based on the "lessons learned" from the Apollo program as summarized in "Apollo Experience Report — The Docking System" (Ref. 3). In this report, Robert Langley concludes that one should:

1) Establish realistic design criteria so that simplicity of design can be achieved; remain flexible on arbitrarily established requirements.

2) Integrate the docking system with the initial design of the spacecraft rather than allocate an envelope for "scabbing on" the system at a later date.

3) Design a "forgiving" system by minimizing critical dimensions and sensitive components.

DRM GUIDELINES, ASSUMPTIONS, AND REQUIREMENTS

The review of past docking analyses and studies led to the incorporation of guidelines and assumptions for the EOTS docking mechanism.

These guidelines and assumptions evolved into a preliminary set of requirements as summarized in Table 1. The primary design drivers within this group turned out to be functional performance requirements associated with extend and retract, capture, latch and rotate.

DESIGN CONCEPTS AND ANALYSIS

The preliminary DRM conceptual design unit was separated into two main subassemblies: (1) the extendable mechanism and (2) the continuous rotation capture and latch probe mechanism.

Extendable Mechanism

The extension-retraction requirement baselined was a maximum extension length of 1.8 m (6 ft) with a 0.9 m (3 ft) retraction capability. To satisfy this capability, a three-segment telescoping device was required.

An initial evaluation of different telescoping techniques indicated that a simple sliding tube concept would not work because of the end loading, which causes bending and results in increased binding and friction loads. Therefore, a concept was developed which incorporated roller bearings between the telescopic segments. The next design area investigated was the method for powering the device through its extend and retract cycles. A number of different concepts were analyzed from a very heavy electro-mechanical linear actuator to a lightweight electric bistem unit.

The initial concept selected was a scissor-screw jack-type drive mechanism (see Fig. 1). A lab-type model of the scissor arrangement was built and evaluated. However, it was found that, while this type device would work well when under a continuous compressive load, it was not suitable for the docking application, which is in tension when docked.

Other approaches were considered (as discussed in Ref. 4) with the ball-screw drive technique (see Fig. 2) being selected as the best.

Probe Mechanism

A review of the various probe mechanism concepts developed during the EOTS docking device analysis led to the selection of a baseline probe. The guidelines used were: (1) minimize the probe diameter to maximize the relative probe-to-adapter ±5 cm (2 in.) radial misalignment requirement, and (2) provide continuous rotation of the latch mechanism without the use of electrical commutation across the rotating joint.

Numerous latch methods, ranging from complex to simple (Ref. 4), were evaluated. The approach selected was one in which the latches are initially deployed to effect capture and then drawn rearward an amount equal to the required longitudinal misalignment of approximately 10 cm (4 in.). A drawing of the probe assembly is shown in Figure 3.

DRM UNIT BUILD

The preliminary set of engineering drawings were delivered to the model shop for estimates on fabrication and assembly costs. The resulting cost estimate was greater than the funds available. A design review was initiated at this time to see if costs could be reduced to a level more in line with the initial proposal estimate. The areas addressed first included those subsystems having the greatest cost discrepancy. The greatest cost discrepancy was traced to the extendable assembly unit. Furthermore, the high cost elements were screened down to two primary subassemblies: (1) the machining and assembly of the hardened steel ball race assemblies mounted between the telescopic segments, and (2) the machining and welding of the triangular telescopic sections (Fig. 2).

Different solutions to reducing these high-cost problem items were investigated. The result of this investigation was a cost reduction plan using a step approach ranging from a major redesign to a minimal redesign. The initial step in the major redesign was to investigate the feasibility of using off-the-shelf hardware.

Therefore, several vendors of extendable devices were contacted. A pair of mechanisms were procured, evaluated, and found acceptable for incorporation into the DRM design. The design was then modified (see Fig. 4) to incorporate the off-the-shelf extendable mechanism. Part of this modification included replacement of the outer triangular section with a commercial cylindrical tube. An inherent design feature of the extendable mechanism allowed for the elimination of the middle triangular section. With these major modifications incorporated into the design, fabrication and assembly costs were reduced significantly to a level more in-line with the initial proposal cost estimate.

Fabrication and assembly of the unit proceeded smoothly with only minor problems being encountered due to fit and slip checks associated with some of the tight tolerances.

DRM OPERATION

The prototype DRM design requirements and drawings which make up the extendable assembly, the probe assembly, and the docking receptacle are contained in Reference 4. With reference also to Figure 5, which shows photos illustrating a typical operational sequence: the extendable assembly provides up to a 1.8-m (3-ft) extension and is housed in a 20-cm (8-in.) tubular section. The assembly is actuated by a ball screw drive directly coupled to a dc torquer motor. A brake is mounted near the motor housing to enable holding the extendable assembly in any position without requiring any torquer power. The position of the extendable assembly is provided by a potentiometer attached to the rear of the probe assembly and operating off a small gear rack.

The probe assembly consists of a forward capture/latch mechnism and a spin-despin drive. The forward capture/latch mechanism incorporates three latching prongs attached to a traveling carriage. The latch drive unit (located to the rear of the spin-despin drive unit) consists of a dc torquer motor, a brake, a potentiometer, and a ball screw assembly. The motor rotates the ball nut which moves the ball-screw forward and backward. This action results in the translation of the forward capture latch mechnism. As illustrated in the photo sequence, during the initial portion of travel, the latches are deployed to an angle of approximately 45 degrees. Subsequent travel results in translation of the fully deployed latches rearward drawing the docking receptacle on the spacecraft and an interface ring on the probe into contact, resulting in a rigid mating. The position of the latch mechanism is indicated by a potentiometer riding on a gear rack. The brake provides the ability to permit the full latching force to be in effect without requiring any motor power.

The spin-despin drive unit consists of a motor and a tachometer. The motor rotates the complete forward portion of the docking probe including the capture latch mechanism. The tachometer provides an output proportional to the probe spin rate up to 100 rpm. In addition to providing the satellite spin-despin capability, this drive is also used for relative positioning of the two spacecraft once docking is effected. A probe spin-lock, mounted on the extreme forward portion of the 20-cm (8-in.) tube, has six locking guides at 60 degree increments. Through use of the spin drive, any one of the locking guides can be selected which will change the relative position between the two spacecraft. This is a requirement for satellite servicing missions and eliminates the necessity of more than one docking maneuver.

The docking receptacle shown is that portion of the DRM assembly mounted on satellites to provide a docking interface for the DRM probe-extension assemblies. The receptacle consists of a flat plate with a centrally located hole which accommodates insertion of the probe. The receptacle hole diameter

is significantly greater than the probe diameter to enable probe insertion, including angular offsets, and space capture without contact.

The DRM assembly weighs: (1) extendable assembly 30.6 kg (67.5 lb), (2) probe assembly 15.0 kg (35.3) lb), (3) probe indexing ring 1.45 kg (3.2 lb), (4) spin lock ring 0.68 kg (1.5 lb) for a total of 48.6 kg (107.5 lb).

DISCUSSIONS AND CONCLUSIONS

The concept developed provided considerable operational flexibility and adequate visual coverage during the different operational sequences. However, the testing period at Martin Marietta was short and allowed only for performance requirement checks from a fixed base.

Additional testing will be initiated by NASA-MSFC to evaluate the docking and retrieval mechanism (DRM) before finalization of the EOTS docking design requirements. This test will be conducted at Huntsville, Alabama in the NASA free-flying mobility unit simulation facility.

The primary areas requiring evaluation are those in which man plays a significant role in its control and operation. These include: (1) EOTS thrust levels/controllability, (2) maneuvering with large c.g. offsets, (3) operation with limited illumination, (4) docking/manipulator/camera boom/ module stowage mechanism interactive control, (5) operator workloads/timelines, (6) control and display requirements/layout.

The results of the simulation will provide the preliminary baseline for the EOTS, primarily in all the areas of man-machine control and their interrelationships and interactions.

The design and fabrication of the concept verification DRM resulted in some unique design criteria. The following conclusions can be formulated from these criteria.

1) Designers need to continually be aware of the application of off-the-shelf components and hardware.

2) The probe assembly design enables the transfer of linear motion through a rotating joint without the use of slip ring assemblies to accommodate the electrical wires of the linear motion drive motors. Elimination of the slip ring assemblies results in a simpler design with a reduction in cost and weight. In addition, longer operational life and increased reliability, based on lubrication, wear and failures is available and one source of electromagnetic interference (EMI) is eliminated.

3) The device has an extremely high probability of successful capture on the first attempt without any physical contact between the two spacecraft before capture. One area of interest noted during the

performance verification test was related to angular misalignment during the probe-to-drogue insertion step. Actual angular misalignments of up to ±20 degrees were demonstrated. This is better than the design requirement of ±5 degrees.

4) The constraint that the docking interface on the target vehicle be passive, simple, and lightweight was demonstrated during the performance verification test to be feasible. This could prove to be economically beneficial for future planning.

5) Other possible applications for the DRM are proposed in which the attachment of two objects is desired. One specific application is for use as a satellite docking and retrieval device (i.e., as an end-effector on the Orbiter remote manipulator system). Another application is for use with industrial manipulator system or cargo handling devices. Other applications include ground-based coupler systems (trains, trailers, etc), remotely operated connectors (fluid, electrical), and as a mechanism for use in support of antenna deployment or large space structure assembly.

REFERENCES

1. "Earth Orbital Teleoperator Systems Concepts and Analysis", MCR-76-17 Technical Report, Vol. II, NAS8-31290. Martin Marietta Corporation, Denver, Colorado, May 1976.

2. Nishizaka, T. J., "Survey of Docking Mechanisms Applicable to Logistic Spacecraft Systems", AIAA Paper No. 67-908, AIAA 4th Annual Meeting and Technical Display Proceedings. Anaheim, California, October 1967.

3. Langley, Robert D., "The Apollo Experience Report: The Docking System, JSC, NASA".

4. "Earth Orbital Teleoperator Systems Concepts and Analysis, MCR-76-17 Docking Retrieval Mechanism", Vol. V, NAS8-31290. Martin Marietta Corporation, Denver, Colorado, May 1976.

Table 1 EOTS Docking/Retrieval Mechanism Requirements Summary

FUNCTION	REQUIREMENT	BASIS
• Deliver/retrieve passive three axis stabilized, or spin stabilized, spacecraft.	Spin: ≤ 100 rpm Torque: 2 N-m (1.5 ft-lb)	Section 3.5.9.5 Torque must be less than EOTS thruster capability; time to despin or spinup less than 10 minutes

• Dock under the following conditions:
 	
  Radial Misalignment:
  Angular Misalignment:
  Longitudinal Misalignment:
 	
  Angular Rate:
  Lateral Velocity:
  Longitudinal Velocity:
	
	± 5 cm (± 2 in.)
	± 5 deg
	< 10 cm (4 in.)
	
	± 0.1 deg/sec
	0.6 cm/sec (0.02 ft/sec)
	3.0 cm/sec (0.1 ft/sec)
		
		Within manual control capabilities based on man-in-the-loop simulation data (Reference P-34).
		
		Within the EOTS attitude control capability (Ref. Section 4.2.1).

• Sufficient strength and stiffness to support a spacecraft at all times during the servicing, transport, delivery and retrieval maneuvers.
 	
  Maximum Torques:
 	
  Longitudinal Force:
	
	Yaw: 200 N-m (150 ft-lb)
	
	Pitch: 200 N-m (150 ft-lb)
	Roll: 200 N-m (150 ft-lb)
	
	220 N (50 lb)
		
		Maximum anticipated external torque is 75-ft-lb developed by the manipulator system (i.e., 10 lb at 7.5 ft).
		
		Maximum anticipated external source is 10 lb developed by the manipulator system.

• Provide spacecraft capture and latch within the following time constraints
 	
  Capture:
  Latch:
  Total:
	
	≤ 5 sec
	≤ 15 sec
	≈ 20 sec
		
		Estimated based on reasonable time constraints

• Capable of docking to wide range of payloads Maximum payload mass:	 12,250 kg (27,000 lb)	 Maximum payload mass applicable from the SSPD (Section 3.4).

• Index to reposition, once docked (e.g. relative "roll" relationship between the EOTS and the payload).
 	
  Rotational Rate:
  Positional Accuracy:
	
	≈ 1 rpm
	± 5 deg
		
		Enables complete (360 deg) coverage by the manipulator system for servicing activity.
		
		Requirements not critical.

Note: The EOTS auto-stabilization mode should be inactivated once the capture and latch phases are initiated; after docking, the auto-stabilization mode may be re-activated.
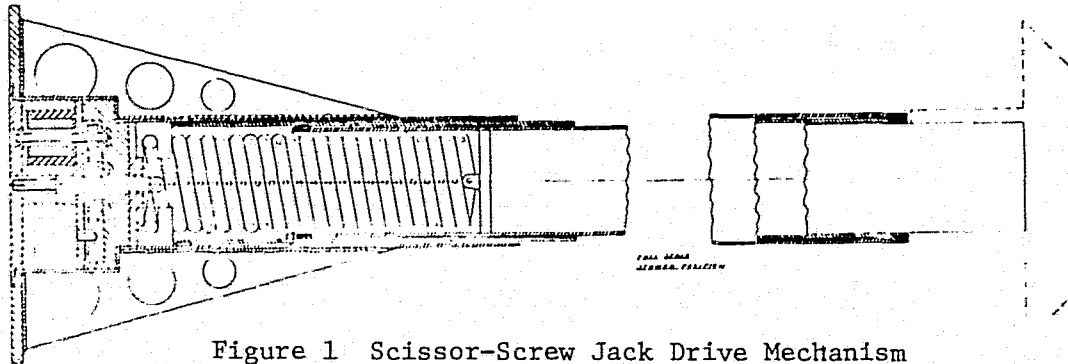
Figure 1 Scissor-Screw Jack Drive Mechanism
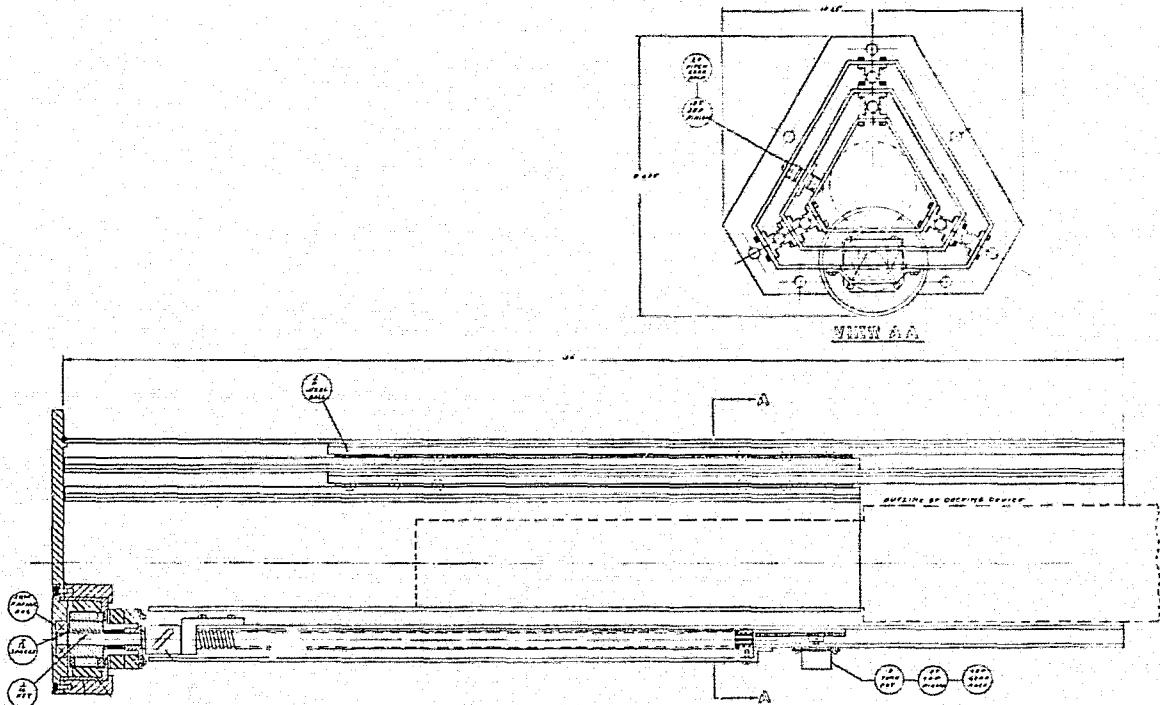
Figure 2   Ball Screw Drive and Extendable Mechanism Assembly
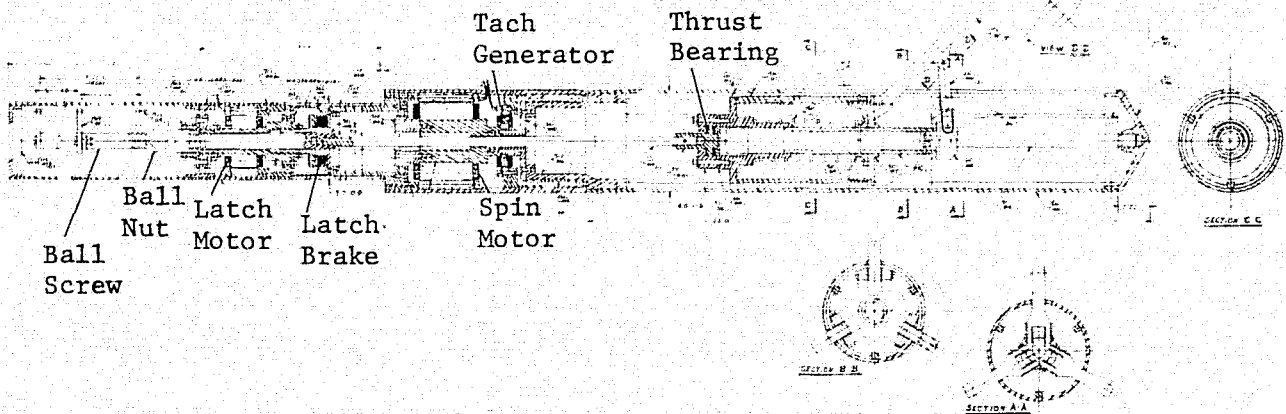
Figure 3 DRM Probe Assembly

109
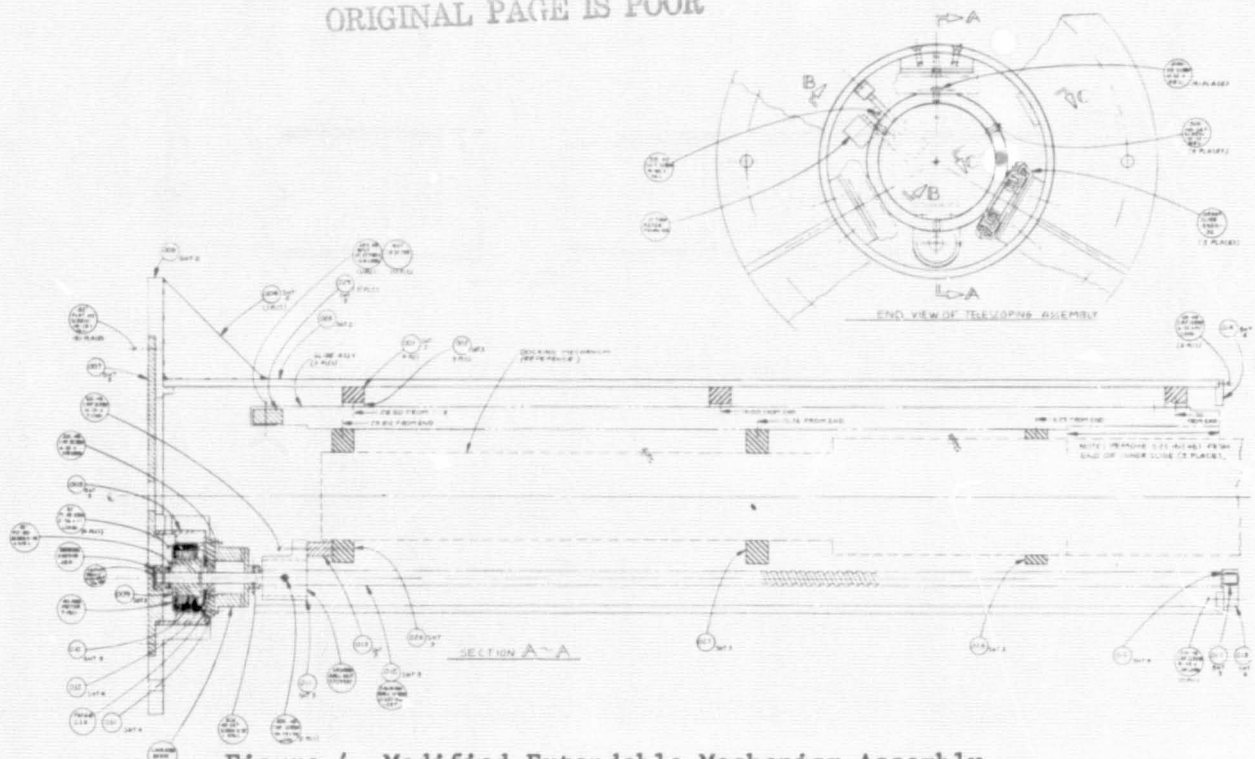
Figure 4   Modified Extendable Mechanism Assembly

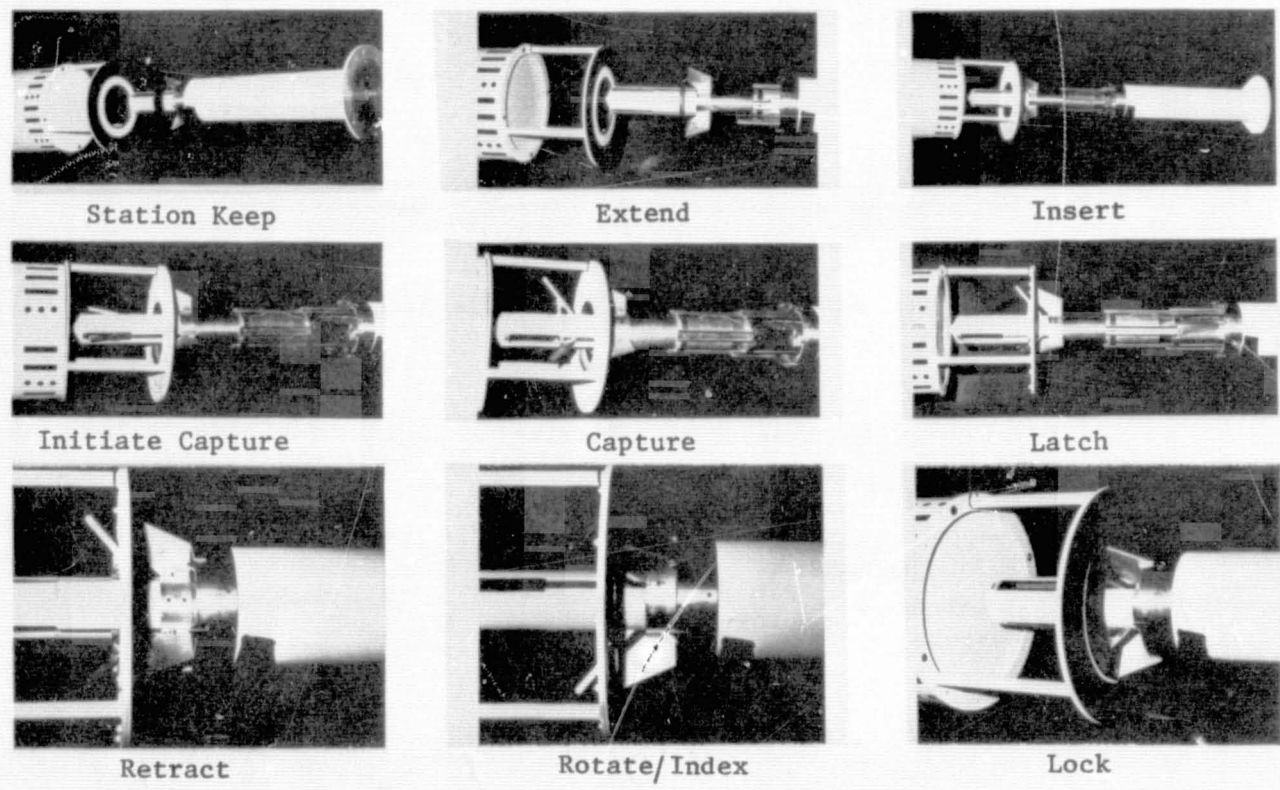|		
Station Keep	Extend	Insert
Initiate Capture	Capture	Latch
Retract	Rotate/Index	Lock

Figure 5   DRM Operation Sequence

TORQUE-WHILE-TURNAROUND SCAN MIRROR ASSEMBLY

By Charles John Starkus

Hughes Aircraft Company

ABSTRACT

This paper reviews mechanical aspects in the development of an oscillating scan mirror mechanism that featured a remarkably low level of structural vibration for the impact energies involved in mirror oscillation. Another feature was that energy lost during impact was returned to the mirror by applying torque only during the instant of impact. Because the duration of impact was only about 0.010 second, it was critical that energy losses be minimal because there was not much time to restore them.

INTRODUCTION

Early in the space program, NASA recognized the importance of remote sensing for management of the earth's resources and human environment. This recognition led to the formation of a program, under the management of the Goddard Space Flight Center of NASA, with a purpose of sensing data for such diverse applications as agriculture and forestry inventories, hydrology, geology, and land use inventory. One versatile sensor that emerged for these purposes was the Hughes multispectral scanner, which was first launched July 23, 1972 and is still operating successfully. A breadboard study contract for a next generation system, called thematic mapper (TM), has been completed. This paper discusses mechanical aspects of the scan mirror assembly portion of the breadboard study contract.

DESCRIPTION OF MECHANISM

The scan mirror assembly is part of a TM system. This scanning system can give complete optical coverage of the earth from an altitude of 705 km. As a spacecraft progresses southbound in a near polar orbit, scanning is accomplished by a mechanical oscillating flat mirror that sweeps the optical line of sight (LOS) from side to side as illustrated in Figure 1. This enables a 185-km-wide swath of the earth to be viewed during each orbit. Since successive orbits cover adjacent swaths, a series of orbits can completely map the entire earth.

The sketch in Figure 2 shows the elements of a TM scanner in relation to the orbit. Reflective optics focuses infrared energy from the earth upon detectors that are sensitive to designated spectral bands. Earth is downward, and the spacecraft velocity vector, which is nominally southbound, is moving away from the reader. Oscillating the scan mirror ±3.72° causes the optical LOS to sweep back and forth across the 185-km swath of earth. The scan mirror will sweep first in one direction, then back in the other, imaging data during both passes.

Earlier systems imaged data during only one pass and were inactive during the retrace. Scanning bidirectionally improves scan efficiency.

The scan mirror assembly is a key element of this conceptual TM system (see Figure 3). It is an object space scanner, which scans the earth in a direction orthogonal to spacecraft motion and thereby enables the sensor to view a swath of the earth with each orbit. The scan mirror assembly illustrated in Figures 4 and 5 consists of a 16 x 20 inch flat elliptical scan mirror mounted by Bendix flexural pivots on a fixed frame, an electromagnetic torquer, leaf spring bumper assemblies, and a position sensor. The scan mirror oscillates by rebounding between springs in a bang-bang manner and scanning between rebounds at nearly constant angular velocity. During the 0.010-second duration of impact, the torquer adds the energy necessary to maintain a constant 7-Hz oscillation. Mapping accuracy as well as data transmission and processing dictate the need for a nearly constant scan rate. Since the effect of torque is to change scan rate, torque can be applied only during those moments of turnaround when data is not being taken. In earlier systems, energy was restored by torquing during the entire return pass; hence, bidirectional scan was not possible. Each bumper is a leaf spring preloaded against a rubber stop. When the mirror impacts the bumpers at turnaround, the spring is deflected away from the stop; after turnaround, the stop damps out spring vibration before the next turnaround.

DESIGN REQUIREMENTS

The driving mechanical design requirements were minimization of structural vibration and of energy loss during turnaround. Specifically, it was required that:

- The total angular vibration of the mirror be less than 2 μrad peak-to-peak during operation at 7 Hz. This was a relatively small level of vibration for the impact energies involved in the mechanism. By comparison, angular vibration of the previous generation system, multispectral scanner, was 40 μrad peak-to-peak. The most significant mode of vibration was that of the mirror vibrating as mass suspended on two springs, each spring representing the shear stiffness of the flexural pivots.

- The coefficient of restitution of the bumper springs be sufficiently high that energy losses could be restored by operating an electromagnetic torquer only during a portion of the 0.010-second duration of turnaround.

The angular vibration requirement arose from the rather exacting pointing and timing specifications. Unlike angular vibration, translational vibration did not cause significant pointing errors. However, it was important to reduce translational vibration for the following reasons:

- Translational vibration has a tendency to excite angular vibration of adjacent components.

- The angular vibration of a given component would be expected to increase as translational vibration increases.

- Both angular and translational vibration represented energy absorbed from the scan mirror and hence lost from the scanner.

Vibrational damage of delicate components was not an overriding concern because the level of vibration was very low.

Angular vibration was measured by a laser beam reflected off the scan mirror and onto a position sensitive diode 50 inches in front of the mirror. Angular vibration of the mirror caused the reflected laser beam to shift position while the position sensitive diode provided a signal proportional to the shift. Coefficient of restitution was measured by a variation of this technique in which two diodes and a clock were used to measure velocity into and out of a bumper.

DISCUSSION

Structural Vibration

Bumpers were located at each end of the scan mirror in order to cause the force on the flexural pivots during turnaround to be, in the ideal case, zero. Actually, of course, pivot forces could not be made perfectly zero. Nevertheless, it was important that pivot forces be minimized because they tended to excite vibrations of the mirror on the pivots; this meant that bumper stiffnesses and impact locations had to be carefully adjusted. The adjustments were monitored by observing signals from magnetic pickoffs that measured bumper spring velocities.

The center of gravity was carefully adjusted so that it was located on the axis of rotation midway between flexural pivots. A moveable mass at the center of the mirror provided the means of adjustment. This positioning of the center of gravity had the effect of straightening the mode shape so that for a given level of vibration, the angular component was less than before; however, mode straightening alone did not bring angular vibration to within the required level. It was also necessary to reduce the general level of vibration. This problem was attacked (1) by adjusting bumper forces to be nearly symmetrical (as explained previously) and (2) by designing the bumpers in such a way that the frequencies of the impact forces were compatible with natural frequencies of the system. The second method afforded by far the more significant results.

The vibration of a structure is a strong function of the frequencies of the excitation forces; the excitation frequencies in this mechanism were the result of the impact of the mirror with the bumper springs. Consequently, reducing the general level of vibration involved thoroughly understanding the impact dynamics and evolving a bumper spring design such that impact frequencies were safely distinct from all natural frequencies of the system.

Figure 6 shows a schematic of the scan mirror assembly along with a simplified mathematical model that is very useful for understanding the dynamics

of the impact forces. Measurements of spring velocity indicated that the approximation was very realistic to the first order.

At turnaround, the mirror impacted bumper springs, which possessed some small mass. Therefore, in addition to the fundamental turnaround frequency ω_t that would have existed had the springs been ideal and massless, a higher frequency, due to the two colliding masses, was introduced at the moment of impact. Before the collision, the spring mass was at rest, and the mirror was approaching at its scan velocity. After the collision, the spring tip rebounded off the mirror, floated away from the mirror, then floated back toward the mirror and collided again. The process repeated itself until after a series of collisions, the process was damped out by surface friction. The natural frequency of the collision ω_c was approximately equal to $\sqrt{K/m}$, which states that in the collision, the spring tip mass m rebounds off the mirror and relies upon deformation of the contacting surface stiffness K to store energy during the collision. This type of collision is similar to that of a plastic sphere dropped on a steel plate. The frequency at which the spring tip mass floats away from the mirror is the first natural frequency of the bumper spring. In the simplified model, this is $\omega_f = \sqrt{k/m}$ as indicated in Figure 6.

The net result of the impact dynamics was that during turnaround, a force as illustrated in Figure 7 was produced at each end of the mirror. This force was made up of essentially two kinds of components, viz., a low frequency component, which was due to the stiffness of the bumper springs, and a high frequency component, which was due to spring tip mass and which occurred at the start of turnaround. Although the high frequency component had the appearance of noise, it was extremely repeatable from impact to impact. The high frequency forces were at a frequency similar to the collision frequency ω_c and were a known and modeled function of ω_c although they were not generally equal to ω_c.

A basic conclusion drawn from the model was that impact frequencies were the result primarily of bumper spring properties, viz., leaf spring mass, leaf spring stiffness, and surface contact stiffness. Therefore, all those properties were varied during the program by testing several bumper designs until eventually one was developed in which all of the impact frequencies were distinct from the natural frequencies of the system. Table 1 lists the frequencies of the final breadboard design. Testing was very useful since the collision forces depended somewhat on some very sensitive microscopic surface phenomena such as friction, stiction, and wear.

Energy Losses

Energy was lost during turnaround in three ways, and it was critical that each loss be minimized. First, energy dissipated in structural vibration represented one energy loss. Second, energy was left in the bumper mass after turnaround because spring velocity was equal to mirror velocity at the completion of turnaround (since the spring and mirror had been in contact and had been moving together), and the velocity spring mass product constituted a momentum that the spring received during turnaround. Consequently, this energy was lost from the mirror. The third loss was caused by friction at the point of contact between the mirror and the spring. Minimizing energy lost to structural vibration was a function of frequencies and stiffnesses. Two means were used to

114

reduce momentum lost to the spring mass. First, the leaf spring bumpers were designed to operate at a safe but high stress level in order to store maximum energy in minimum spring mass. Second, the leaf springs were tapered to distribute stress more evenly over their length.

Friction losses were minimized by designing a contact surface having a particular radial shape. The tip of the leaf spring bumper had a tendency to rotate as it was deflected, and that rotation constituted a sliding motion between the contacting surfaces. The purpose of the radial shape was to cause the distance that the contact point traveled along one contacting surface during turnaround to equal the distance traveled along the other contacting surface. The result of this design was to minimize sliding and maximize rolling friction. Since rolling friction is generally less than sliding friction, it was expected that energy losses from friction would be reduced. It was also expected that structural vibrations excited by friction force frequencies would be reduced. The contacting surfaces consisted of a flat polished metal surface on the mirror and a Delrin AF (several other materials were also tested) radially shaped button bonded to the tip of the leaf spring.

CONCLUDING REMARKS

Two major mechanical problems were solved during the breadboard program.

- Structural vibration was reduced to a remarkably low level for the impact energies inherent in the mechanism (to less than 2 μrad at 7 Hz, the primary mode of vibration occurring when pivots on the mirror deformed in shear).

- Mirror energy was conserved at each turnaround to ease the requirements of the torquer and control system, which input energy only during a portion of the 0.010-second bumper impact time.

The first problem was solved by understanding the collision frequencies that occurred when the mirror mass impacted the bumper mass and then designing the bumpers to have impact frequencies distinct from all natural frequencies of the system. The second problem was solved by using tapered leaf springs of very low mass and by making the contacting surface a rolling radius to maximize rolling and minimize sliding friction. The result was a high, 97% coefficient of restitution.

These very significant developments in scan mirror technology advanced the capability of optical scanning systems to provide high resolution and high scan efficiency.
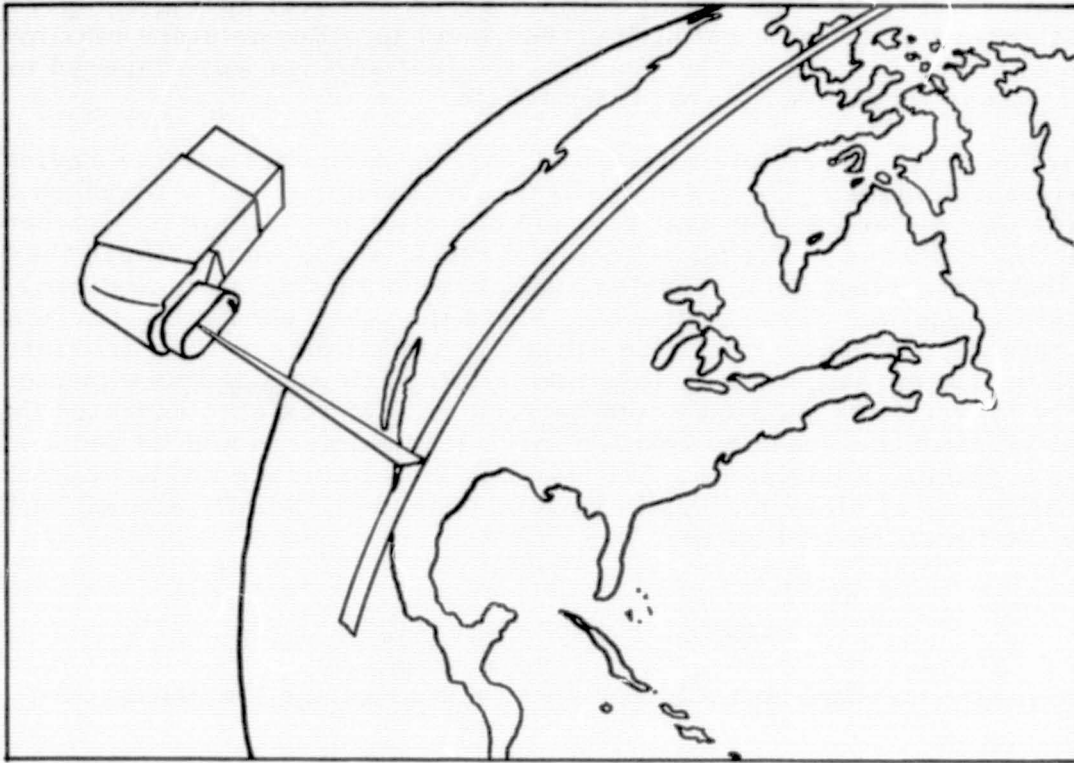
Figure 1. Conceptual TM in orbit showing scan pattern
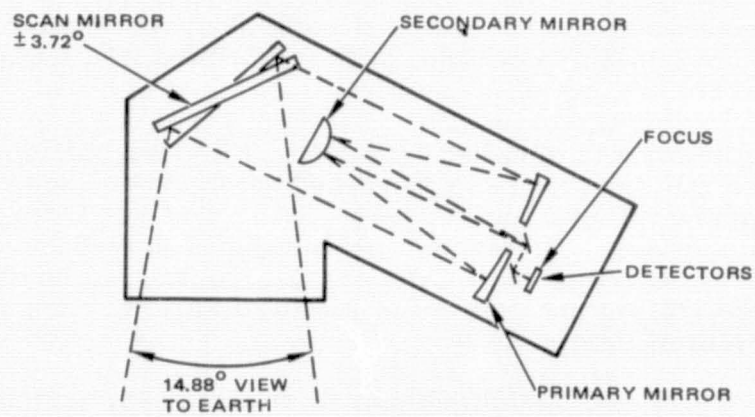

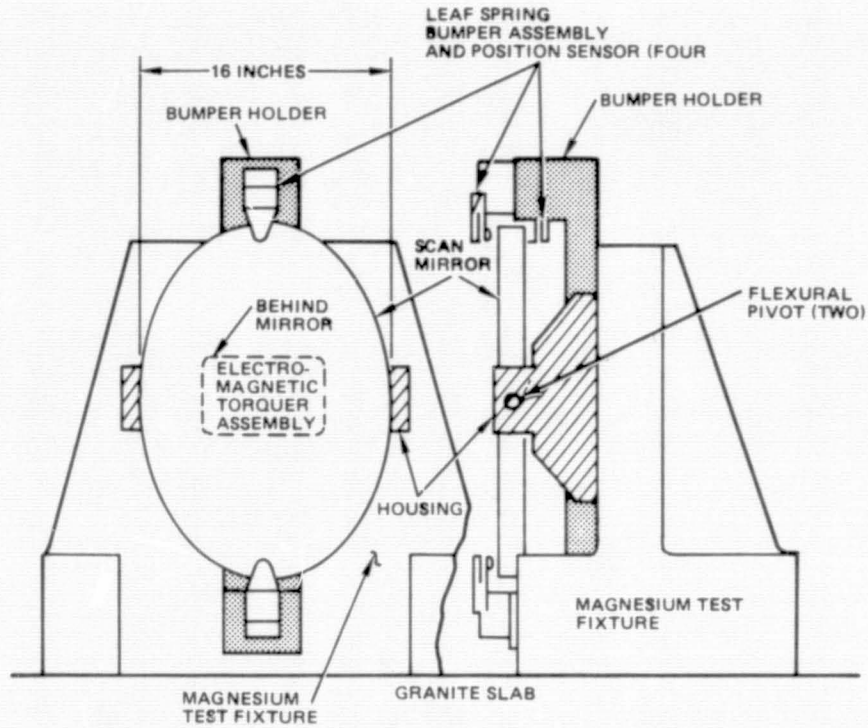Figure 2. Configuration of conceptual TM scanner

Figure 3. Cutaway view of conceptual TM system showing torque-
while-turnaround scan mirror assembly
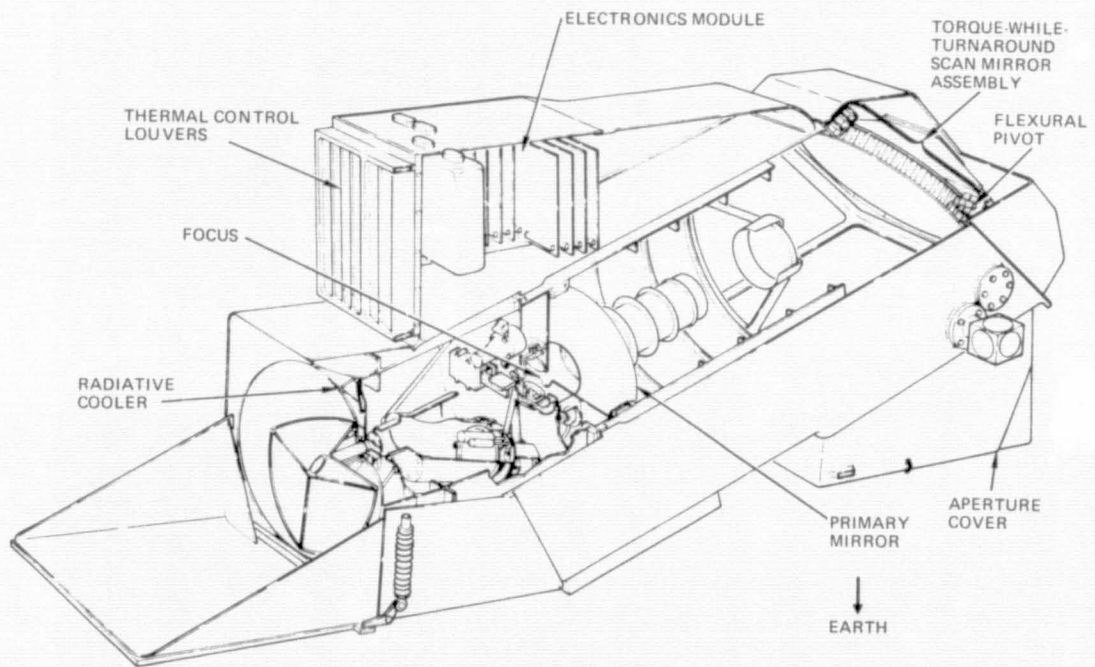
Figure 4. Sketch of breadboard scan mirror assembly showing
major subassemblies and supports of torque-while-turnaround
scan mirror assembly

117

75-38841
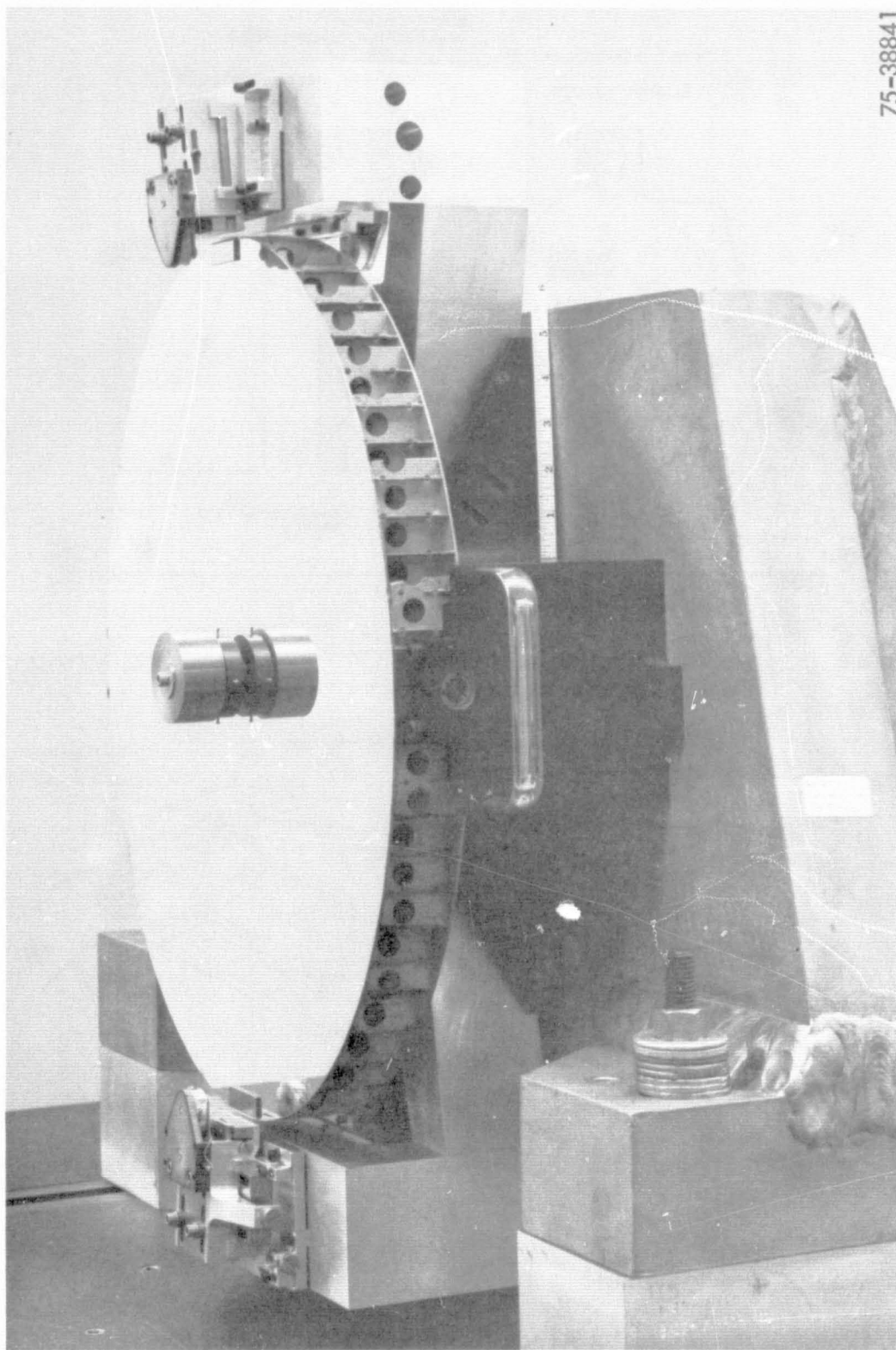
Figure 5. Breadboard scan mirror assembly mounted
on test fixture

118

BUMPERLEAF SPRING

SHAPED RADIUS
TO MINIMIZE FRICTION

SCAN
MIRROR
SURFACE

ELECTROMAGNETIC
TORQUER

FLEXURAL
PIVOT

RUBBER PRELOAD STOP TO
DAMP OUT SPRING VIBRATION
AFTER TURNAROUND

SCHEMATIC OF SCAN
MIRROR ASSEMBLY

SIMPLIFIED MATHEMATICAL MODEL
OF SCAN MIRROR ASSEMBLY
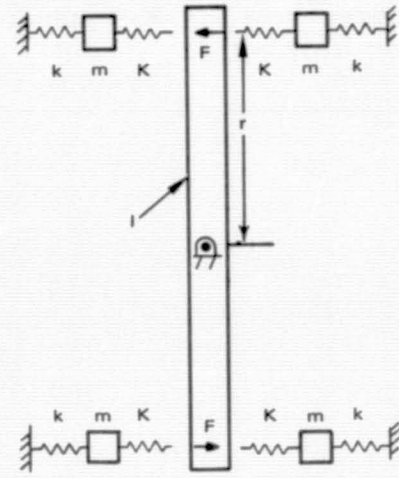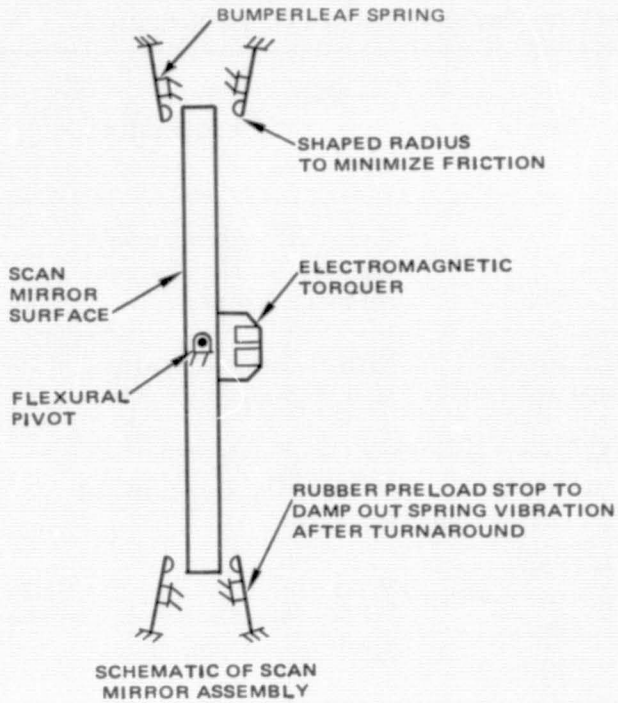
ω_t = TURNAROUND NATURAL FREQUENCY $\approx \sqrt{\dfrac{2kr^2}{I}}$

ω_c = COLLISION NATURAL FREQUENCY $\approx \sqrt{\dfrac{K}{m}}$

ω_f = FLOATING FREQUENCY $\approx \sqrt{\dfrac{k}{m}}$
(FIRST NATURAL
FREQUENCY OF BUMPER
LEAF SPRING)

I = MIRROR INERTIA

k = STIFFNESS OF LEAF SPRING

m = EFFECTIVE MASS OF LEAF SPRING
(m VERY SMALL COMPARED TO I)

K = STIFFNESS OF CONTACTING SURFACES
(K VERY LARGE COMPARED TO k)

r = DISTANCE FROM AXIS OF ROTATION TO
BUMPER SPRINGS

F = IMPACT FORCE ON MIRROR

Figure 6. Impact dynamics

HIGH FREQUENCY COLLISION FORCES
(FUNCTIONS OF ω_c AND ω_f)

IMPACT FORCE F
RELATIVE UNITS

FUNDAMENTAL TURNAROUND
FREQUENCY ω_t

$\omega_t = \dfrac{1/2 \text{ CYCLE}}{0.010 \text{ SEC}} = 50 \text{ Hz}$

TIME, SECONDS

0.010
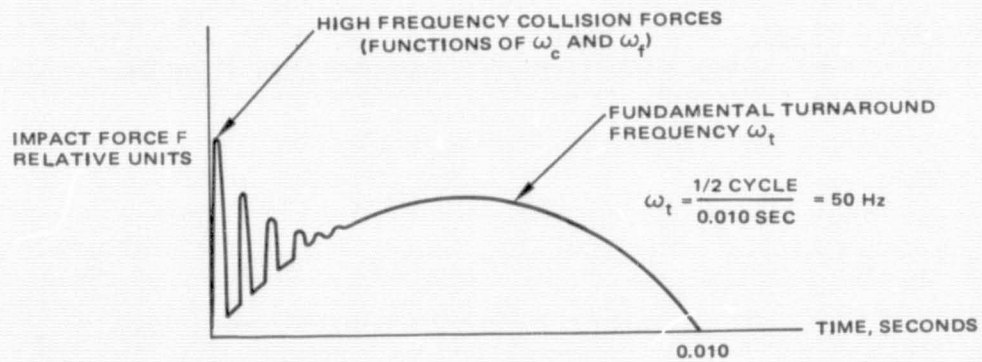
Figure 7. Impact force

119

Table 1. Impact Frequencies Versus Natural Frequencies

Impact Frequencies (Frequency of Half-Sine Impulse), Hz	Natural Frequencies of System, Hz	Mode	Comments
$\omega_t = 50$			Function of bumper spring stiffness and mirror inertia
	125	Support structure	Minimum excitation if $\geq 2.5\,\omega_t$
	330	Mirror on pivots (first mode)	<2 μrad excited primarily by contact friction
	1000	Mirror on pivots (second mode)	$\ll 1$ μrad with $\omega_c = 4$ kHz; 10 to 20 μrad with bumper springs in which $\omega_c = 1$ kHz
	2200 & Up	Plate frequencies of scan mirror	Strong functions of ω_c but always <1 μrad
$\omega_c = 4000$			Function primarily of spring tip mass and material

REFERENCES

1. Harris, C. M., and Crede, C. E., Shock and Vibration Handbook, Vol. 1, Chapter 8, McGraw-Hill Book., Inc., New York (1961).

2. Chou, P. C. and Flis, W. J., Design Curves for Structural Response Due to Impact Loading, Proceedings AIAA/ASME/SAE 17th Structure, Structural Dynamics, and Materials Conference, King of Prussia, Pennsylvania, (May 5-7, 1976).

WEAR-RESISTANT BALL BEARINGS FOR SPACE APPLICATIONS

By Boving, H., Hintermann, H.E., Hänni, W.,
*LSRH, Neuchâtel (Switzerland)

and

Bondivenne, E., *ESA-MPO, Boeto, M., Condé, E.,*CNES,
Toulouse (France)

ABSTRACT

Ball bearings for hostile environments have been developed. They consist of normal ball bearing steel parts of which the rings are coated with hard, wear-resistant, chemical vapor deposited (C.V.D.) TiC. Experiments in ultra-high vacuum, using cages of various materials with "self-lubricating" properties, have shown that such bearings are suitable for space applications.

ESA has considered using such treated ball bearings.

The results of different laboratory tests undergone by the ESA Meteosat Radiometer Focalising mechanism, which contains 6 coated bearings, are promising, and are summarised.

INTRODUCTION

Ball bearings are required for operation in hostile environments, for example, in corrosive media, under radioactive radiation, at elevated temperatures, in space, etc... They must be perfectly reliable as in most of these environments few or no parts can be replaced.

This paper deals with the development of ball bearings for space applications. Several solutions have been proposed; the use of bearings made of special high speed steels, cemented carbides, or various hard, wear-resistant materials other than steel have brought some improvements. We, at the LSRH, have tried to resolve the problem by coating standard commercial steel ball bearings with hard, wear-resistant TiC layers by C.V.D. (Chemical Vapor Deposition),

---

*LSRH = Laboratoire Suisse de Recherches Horlogères
ESA-MPO = European Space Agency - Meteorological Programme Office
CNES = Centre National d'Etudes Spatiales

and by using cages of various materials with "self-lubricating" properties (1,2). The ESA considered these bearings of interest for space applications, e.g., in its Meteosat programme.

In the following the characteristics of the bearings are described and the procedure for obtaining them is given in brief. Finally, some of the planned space applications are mentioned; some tests undergone by the various mechanisms in which such treated ball bearings have been used are also given.

CHARACTERISTICS OF THE BEARINGS

For rolling and sliding contacts during continuous and interrupted operation it is important that the materials of the partners are of a different nature. In vacuum particularly it is preferable to have metal - ceramic rather than metal - metal contacts in order to avoid microwelds and diffusion. Only one of the partners need therefore be treated with TiC, i.e., the balls or the rings. The combination "uncoated balls - coated rings" is preferable for small diameter bearings. For larger diameter bearings the contrary is true. In fact, the rings undergo distortion and/or deformation during C.V.D. For larger diameter rings the deformation can be so important that correction by mechanical means becomes impossible without removing the TiC layer (5 - 10 μm). At the moment development work is being done for the application of hard, wear-resistant TiC coatings to larger diameter ball bearings.

For most applications hard coatings are only of value if the supporting substrate material is also hard. Hence, only hardenable steel, cemented carbides or ceramic materials are suitable. For the ball bearings described here, a hardenable stainless steel (AISI 440 C) was chosen because:

- the rings and spheres can be machined from this steel, thus the existing ball bearing production know-how can be applied and the overall costs reduced;

- this steel is suitable for the C.V.D. of TiC; its composition (∿1%C; ∿17%Cr) enables air quenching to a hardness of about 62 Rc; its deformation and/or distortion during thermal treatment can be kept within reasonable limits.

During the last years the know-how for the C.V.D. of TiC on C and Cr containing steels has become well established (3). Such coatings are very friction- and wear-resistant and show no measurable wear from adhesion during friction against metals (4). The composition of TiC can vary greatly between $TiC_{0.3}$ and almost the stoichiometric composition TiC (5). The mechanical properties of single crystals and of sintered hot pressed TiC are given in (6). An important property of TiC for its application to bearings is its hard-

ness. In Table 1 the comparative hardnesses of several ceramic materials are given on a schematic scale.

PROCEDURE FOR OBTAINING TiC COATED BEARINGS

The TiC coatings are applied to polished, finished bearing rings. This is important since the surface roughness increases during C.V.D., and due to the hardness of TiC it is difficult and delicate to polish the races.

The C.V.D. of TiC is performed at the LSRH. The machining, thermal treating, polishing and assembling of the ball bearings are carried out by experienced manufacturers. In the case of the small diameter bearings which are discussed here, the manufacturing work, and some testing of the finished products, was done by RMB (Roulements Miniatures; Bienne, Switzerland).

The C.V.D. of TiC is achieved by the interaction of a volatile Ti halide with H_2 and CH_4 at a high temperature (2,7):

$$TiCl_4 \text{ (g)} + CH_4 \text{ (g)} \xrightarrow{H_2; \ 800 - 1000^{\circ}C} TiC \text{ (s)} + 4HCl \text{ (g)}$$
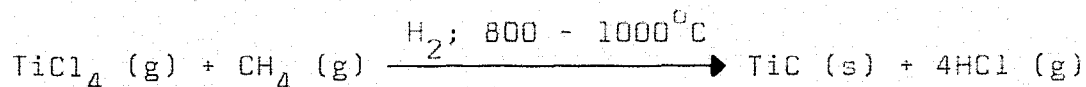
The deposition rate depends on several parameters and can vary from 1 to 5 micrometers per hour. Figure 1 shows a scanning electron microscope picture and the microprobe analysis results of a section through a TiC coating and its AISI 440 C steel substrate. The steel is in the quenched state, i.e., the mixed Cr-Fe carbide grains are dispersed in a martensitic matrix.

A very important aspect in the manufacture of high precision bearings is the fact that in the steel the phase changes "pearlite → austenite" and "austenite → martensite" are accompanied by volume changes. If the heating and cooling is not done according to the cycles prescribed (8), disastrous distortion might occur (9).

The C.V.D. process is characterised by the fact that the quality of its products is influenced by many parameters of which some important ones are: the pressure, total gas flow, gas composition, temperature and its profile and cycle, load density and its arrangement in the reactor. A slight change in one of these operating conditions can have a drastic influence on the characteristics of the TiC coating. For the bearings used in the Meteosat Programme, a vertical C.V.D. reactor of 120 mm I.D. was used; for each treatment a total of 36 pairs of bearing rings were evenly spaced upon 6 different levels. Despite the difficulties encountered in keeping the many parameters constant, the reproducibility of the coatings was more than acceptable. Due to the thermal treatment a certain number of rings underwent too large a distortion and had to be

rejected. Five reactor loads were necessary to produce the total amount of ball bearings for the Meteosat programme.

The TiC coating thicknesses averaged over the 6 levels are indicated in Table 2 for the 5 C.V.D. treatments. These results were obtained by sectioning a pair of rings from each level after each treatment, and by examining them in an optical microscope. These results show that by taking normal precautions, it is possible to obtain results which are sufficiently reproducible for the production of TiC coated rings for small diameter ball bearings.

APPLICATIONS

1. Solar Wind Composition Experiment (Apollo)

With its Solar Wind Composition Experiment the University of Bern, Switzerland, participated in Apollo experiments on the moon. A metal foil was unrolled manually by the astronauts of the first five Apollo landings, exposed to solar radiation and rolled up again. For these manual operations a device with standard bearings was used. For Apollo 17, however, an automatic foil roller was developed. At the start of the experiment the foil was to be un- rolled manually, then by means of a timer the foil was to be rolled up in a stepwise manner, at fixed time intervals. In order to en- sure a reliable operation, TiC coated bearings were considered, the characteristics of which are as follows:

    Types: two O.D. 13 mm, I.D. 6 mm, and one O.D. 13 mm, I.D. 4 mm
    Rings: AISI 440 C steel/ 3 μm TiC
    Balls: AISI 440 C steel
    Cage : AISI 440 C steel/ PTFE coated (photopolymerization)

The device which was provided with the bearings described above was submitted to the European Space Research and Technology Centre for operational and vibration tests. The operation of the mechanism was checked in ultra-high vacuum thermal and solar simulation con- ditions. In another testing programme the Solar Wind Experiment package was subjected to sinusoidal and random vibrations in 3 mutu- ally perpendicular axes, according to NASA specifications. The per- formance proved to be extremely satisfactory (10,11). This modi- fied Solar Wind Composition Experiment, could not, however, be flown as part of the heavy Apollo 17 programme.

2. Meteosat Radiometer Focalisation Mechanism

The Meteosat telescope will be used to take pictures of the Earth and clouds from a geostationary satellite. In order to obtain good quality images the focus of the telescope has to coincide at all temperatures with the detector. This is assured by a mechanism which causes the translation of a reflecting dihedron. The focusing device is manufactured by MATRA ENGINS, France. Figure 2 shows a

124

schematic view of the mechanism which consists of a step-by-step motor, 5 to 1 reducing gears and a screw-bolt system. The rotor, intermediate pignon and screw are mounted on ball bearings (Type O.D. 13) manufactured by RMB; the rings are coated with TiC. The bearings are prestressed to such an extent that there is no risk of shocks during the lift-off. The mechanism has been tested by MATRA ENGINS and CNES

2.1. Tests by MATRA ENGINS (12)

A mechanism was activated periodically in ultra-high vacuum. Each test cycle consisted of a complete focalisation range plus return. It was impossible to measure the torques induced by the bearings; variations in the total resistance were, therefore, followed by measuring the starting voltage of the step-by-step motor.

In Table 3 the programme followed for this series of tests is given. The number of revolutions achieved during the programme exceeds that which the mechanism is required to perform in space. These lifetime tests have not yet been completed, no visual examination of the bearings has therefore been done up till now.

During the first 20 focusing cycles in ultra-high vacuum there was a slight increase in the resistant torque, to a level close to that measured in the laboratory atmosphere. This increase never reached 30% of the low values obtained at the start of the U.H.V. testing. The safety margin of the mechanism was about 6, since the nominal voltage available was 10 V. In order to see if the torque increased after one lifetime, the tests were continued until twice the expected lifetime of the mechanism had been attained. The important conclusions of these tests are that the resistant torque in U.H.V. is not greater than that in normal atmosphere, and that it does not increase after an immobility of 30 days.

2.2. Tests by CNES

These tests are complementary to those done by MATRA ENGINS and are aimed at quantifying the resistant torques of the bearings, the behavior of the torque and the deterioration of the bearings, under the conditions in which the mechanism will be required to operate.

The resistant torque of the preloaded bearings was continuously measured by means of a microbalance (13). In order to take into account the different stresses the motor and screw bearings will be required to withstand, two types of tests were carried out:

- screw bearing type: characterised by continuous rotation at low speed (90 rph), and by a very high preload (7daN);

125

- motor bearing type: characterised by intermittent very high angular
  acceleration (typical for a step-by-step motor) and a high preload.

In order to take into account the integration, qualification
and acceptance tests of the mechanism, and its use during flight,
both types of tests were performed in two uninterrupted stages; one
in air and the other in U.H.V. The rotation direction was alternated
periodically. In Table 4 the conditions under which the tests were
performed are given. The length of the tests was determined by
taking into account the worst configuration and by multiplying by a
safety margin of 2.

Three types of information were obtained from each test:

- the behavior of the torque measured continuously with the micro-
  balance; every 15 minutes the average and maximum torques were
  recorded and plotted against time;

- the comparison between the individual bearing torques, before and
  after the tests, according to the U.S. standard MIL.STD.206;

- SEM analysis of the bearings after the tests; identification of
  the deposits on the races by means of X-ray spectrometry.

The results obtained with the screw bearings are as follows:

- In air, after a short running-in during which the torque increased,
  the latter stabilised between 40-50 g.cm; the average torque was
  relatively stable and the maxima were about 50% above the average.
  In vacuum, after a sudden increase of the torque there was a
  running-in corresponding to a decrease in the torque which became
  stable between 25-30 g.cm. The torque was noisy and the maxima
  were about 100% above the average. This can be seen in Figure 3.

- The ratio of the averages of the individual torques of the bear-
  ings, before and after the tests, was between 1 and 2.

- SEM analysis showed that despite the very high preload the TiC
  coating did not deteriorate, but that a double transfer (cage →
  ball → rings) of the Ag-In lubricant occurred. The Ag-In coating
  on the surfaces of the balls was uniform, but only particles of
  this material were present on the races.

The results obtained with the motor bearings are as follows:

- In air, the torque increased continuously throughout the tests,
  from 4.5 to 24 g.cm. The torque presented the same type of noise
  as the screw bearings in vacuum. The maxima were about 40% above
  the average. There was no running-in. In vacuum, the torque de-
  creased slowly from 24 g.cm and became stable at about 3-6 g.cm.
  The torque presented the same noise as in air and the maxima
  reached 150% of the average torque. This can be seen in Figure 4.

- The ratio of the averages of the individual torques of the bear-
  ings, before and after the tests, varied between 15 and 48, signi-

126

fying an important deterioration of the bearings.

- The SEM analysis showed that the TiC coating did not deteriorate, but that there was an excess of lubricating material on the races due to double transfer (cage → ball → rings). The deterioration of the performance of the bearings was significant. Nevertheless, the very severe conditions did not totally destroy them as the TiC coating remained perfectly in place and the cages resisted.

The TiC coated bearings tested satisfied the operational conditions required for the Meteosat Radiometer Focalising Mechanism as the behavior of the wear-resistant coating was good. The Ag-In lubricant should, however, be replaced by one based on MoS_2 or a similar material.

CONCLUSIONS

Hard, wear-resistant TiC coatings obtained by C.V.D. are sufficiently uniform and reproducible for use on rings of small high precision ball bearings. Several space applications for such treated bearings have been proposed. Both bearings and mechanisms using them have been tested in laboratory environment and in actual space simulations, and the results have shown that TiC coated ball bearings are suitable for such applications; no deterioration of the TiC layers was observed.

REFERENCES

(1) Gass, H., Hintermann, H.E., Stehlé, G., Briscoe, H.M., "Bearings for Extreme Environments", Paper presented at the European Space Tribology Symposium, Frascati, Italy, April 9-11, 1975.

(2) Gass, H., Hintermann, H.E., "Chemical Vapor Deposited TiC for Bearings", Chemical Vapor Deposition, Fourth International Conference, The Electrochemical Society, 563-576, 1973.

(3) Ruppert, W., "Die Abscheidung von Titankarbidüberzügen auf Stahloberflächen", Metalloberfläche, 14, 193 (1960).

(4) Hintermann, H.E., Aubert, F., "Friction and wear properties of TiC coatings", Proceedings of Eurotrib., London, 207, 1973.

(5) Pearson, W.B., "Handbook of lattice spacings and structures of metals", Vol II, Pergamon Press, 1967.

(6) Engineering Properties of Selected Ceramic Materials, The American Ceramic Society, Columbus, Ohio, USA, 1966.

(7) Ruppert, W., "Deposition and application of TiC coatings onto tools consisting of steels and sintered hard carbides", Chemical Vapor Deposition, Second International Conference, The Electrochemical Society, 443-459, 1970.

(8) Metals Handbook, 8th Edition, Vol 2, Heat Treating, Cleaning and Finishing, 245-250, 1964.

(9) Lement, B.S., Distortions in Tool Steels, American Society For Metals, 1959.

(10) European Space Agency, Testing Division, Solar Wind Experiment, Test No. 733, Ref. HBF-VTC, 1970.

(11) European Space Agency, Testing Division, Solar Wind Experiment, Test No. 0732, Ref. DDT/TD/JGR, 1972.

(12) Jouan, J., Pautret, M., "Utilisation des Roulements RMB sur le Mécanisme de Refocalisation du Radiomètre", Matra Engins, No. 60/194, August 1976.

(13) Condé, E., "Méthode de Contrôle en continu de Roulements secs miniatures", Paper presented at the European Space Tribology Symposium, Frascati, Italy, April 9-11, 1975.

Table 1. COMPARATIVE HARDNESSES OF TiC AND OTHER COMMONLY USED CERAMIC MATERIALS.

Microhardness Kg/mm^2

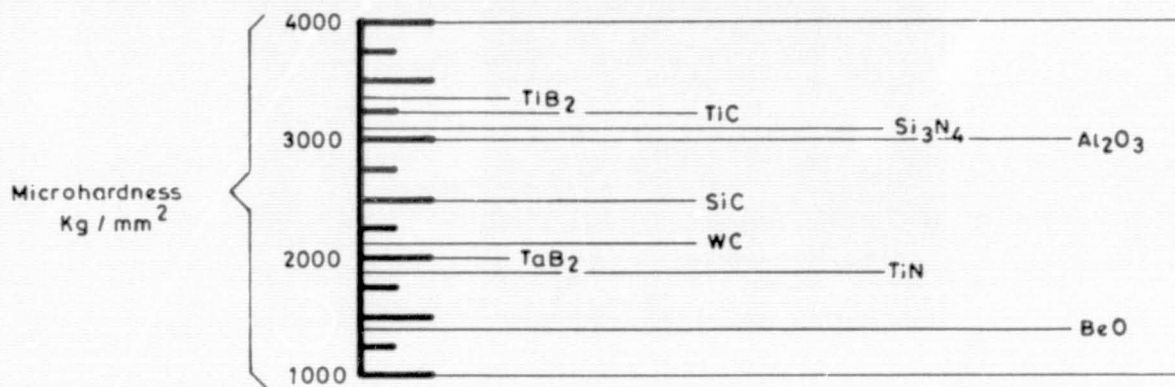Table 2. AVERAGE TiC-COATING THICKNESSES ACHIEVED DURING THE 5 C.V.D TREATMENTS

TREATED PART	COATING THICKNESSES IN μm				
	C.V.D TREATMENT NUMBER				
	1	2	3	4	5
OUTER RING	6.5 ± 0.5	5.0 ± 0.5	4.5 ± 0.5	4.5 ± 0.5	4.5 ± 0.5
INNER RING	6.2 ± 0.2	4.5 ± 0.5	4.5 ± 0.5	4.7 ± 0.2	4.5 ± 0.5

Table 3. CONDITIONS OF TESTS PERFORMED BY MATRA ENGINS ON THE RADIOMETER FOCALISING MECHANISM.

DURATION (days)	PRESSURE (Torr)	RHYTHM (cycles/days)	NUMBER OF TOURS	
			SCREW	MOTOR
44	$2 \cdot 10^{-6} - 9 \cdot 10^{-9}$	variable	1832	9268
68	$7 \cdot 10^{-9}$	4	1665	8425
30	$7 \cdot 10^{-9}$	1	366	1830
30	$7 \cdot 10^{-9}$	NO	0	0
27	$7 \cdot 10^{-9}$	1	312	1559
TOTAL			4175	21082

Table 4. CONDITIONS OF TESTS PERFORMED BY CNES ON MOTOR AND SCREW BEARINGS

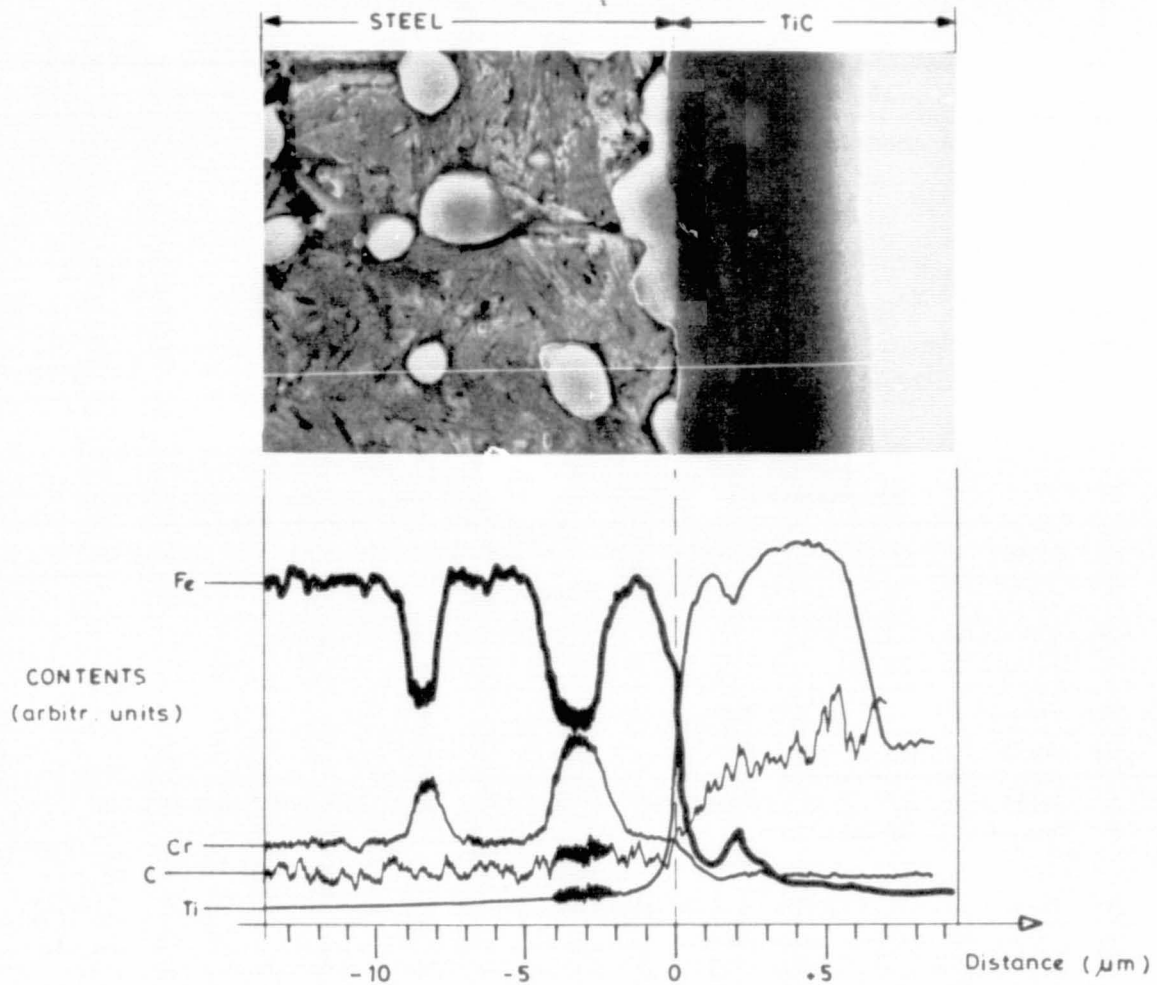| BEARINGS TESTED	QUANTITY	PRELOAD (daN)	MOVEMENT		UNITS	QUANTITY	
			angular accelerat.	speed		AIR $25\pm3°C$ $45\pm15\%$ RH	VACUUM 10^{-9} Torr
MOTOR	6	4.5	very large	$1.8°/<4msec$	motor steps	$6.2 \cdot 10^6$	$7.2 \cdot 10^6$
SCREW	6	7.0	0	90 rph	number of tours	6150	7074

Fig.1 MICROPROBE ANALYSIS ON SECTION THROUGH TiC COATING AND AISI 440 C STEEL SUBSTRATE.
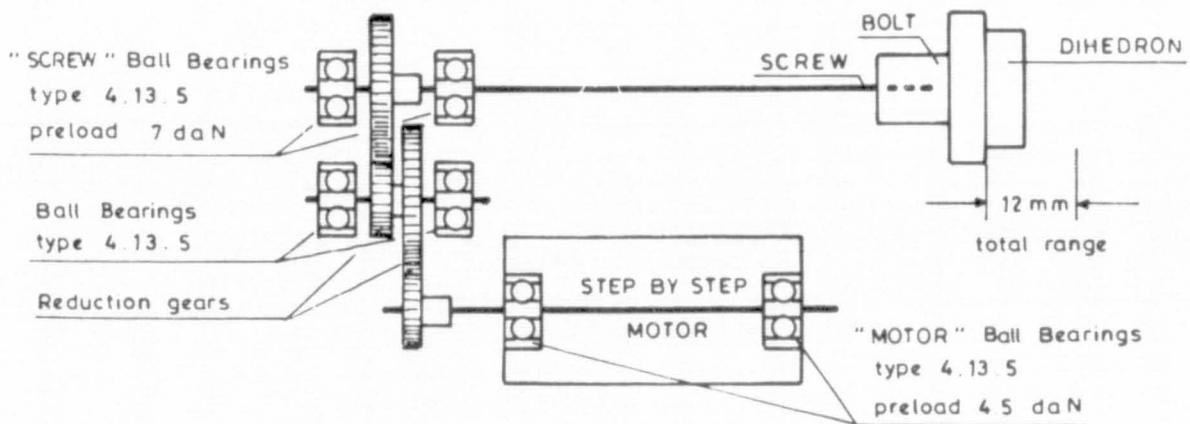

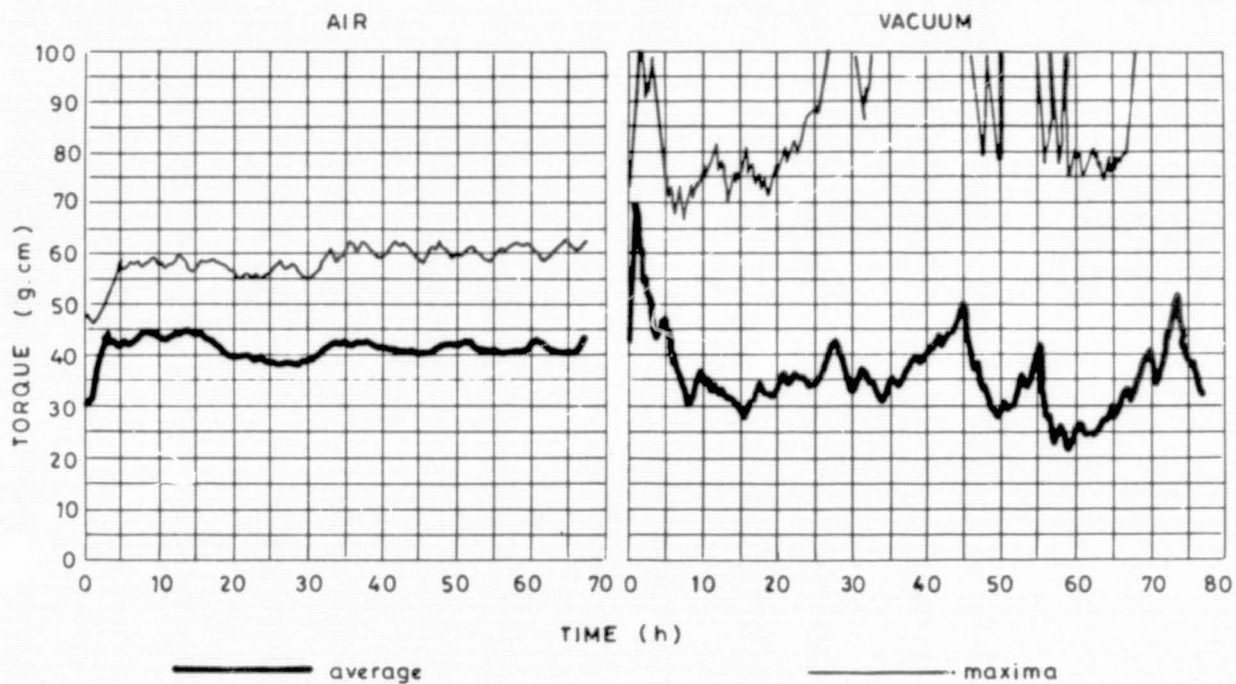Fig. 2 SCHEMATIC PRESENTATION OF THE RADIOMETER FOCALISING MECHANISM.

Fig. 3 BEHAVIOR OF TORQUE OF THE BEARING DURING THE SCREW TYPE TEST.
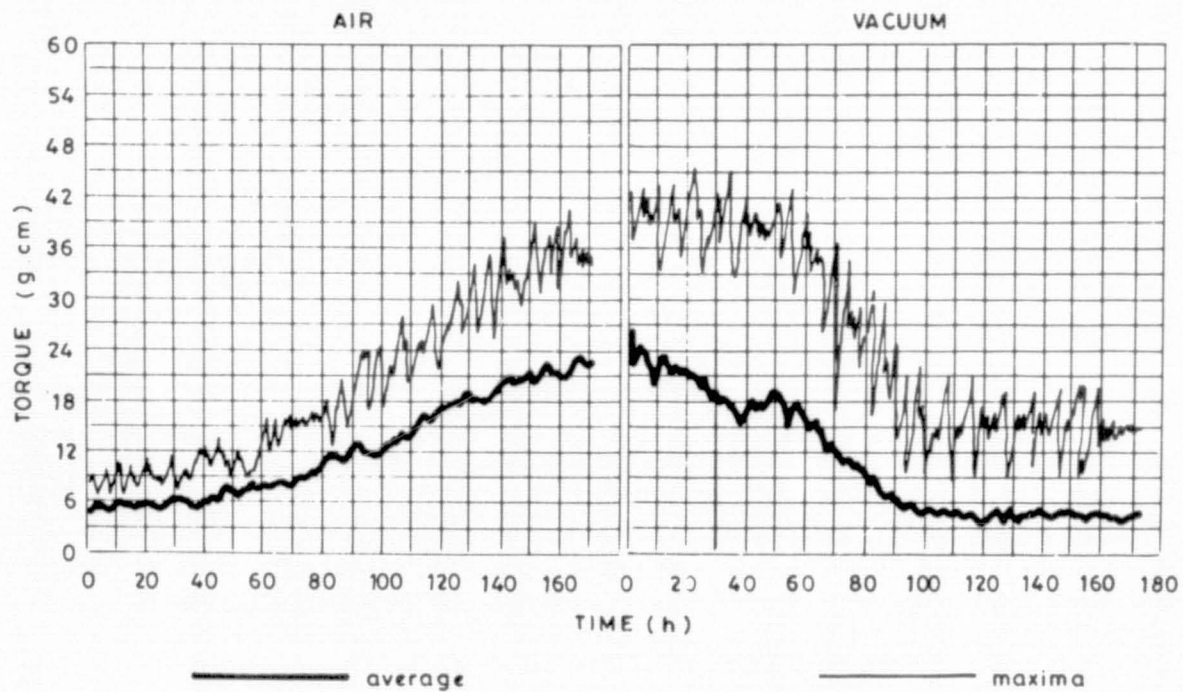

Fig. 4 BEHAVIOR OF TORQUE OF THE BEARING DURING THE MOTOR TYPE TEST.

131

AN ACTIVE NUTATION DAMPER

FOR SPACECRAFT

by

Richard A. Abercrombie

and

Dr. Thomas W. Flatley

Goddard Space Flight Center

ABSTRACT

An active nutation damping device, consisting of an angular accelerometer, a dc-motor-driven flywheel, and associated electronics, has been developed for spacecraft use. This damping system was used on the LAGEOS spacecraft, launched May 4, 1976, to control nutation buildup during the long coast period (approximately 75 minutes) after the third stage separation.

Of the many electrical and mechanical design choices involved, the use of an angular rather than linear accelerometer offers some advantages. There are, however, some problems of adapting the angular accelerometer to spacecraft use.

The damper package was evaluated and proven on a three-axis gas-bearing simulator that duplicated the LAGEOS spacecraft critical flight dynamics. In addition, a failure analysis of the damper assembly was performed.

Performance of the damper during the LAGEOS flight has confirmed the pre-flight evaluation and analysis.

INTRODUCTION

The Active Nutation Damper was developed to combat nutational instability of spinning spacecraft, particularly for spacecraft using long coast periods during a transfer orbit prior to firing an apogee kick motor (AKM).

This active damper was first used with the Laser Geodynamic Satellite (LAGEOS) which is a 906 lb. 2 foot diameter sphere

launched into a near-circular, near polar orbit on May 4, 1976. The purpose of the satellite is to demonstrate relevant space techniques that will contribute to the development and validation of predictive models for earthquake hazard alleviation, ocean surface conditions, and ocean circulation. The satellite is tracked by measuring laser beam reflections from a set of 426 corner reflectors which cover its surface.

The LAGEOS had an unfavorable moment of inertia in its transfer orbit and was thus nutationally unstable. Uncertainties in the estimation of the energy dissipation characteristic of the LAGEOS assembly during the long transfer orbit, particularly within the rubbery solid propellant of the AKM, dictated the use of a device to reduce any nutational coning that might occur because of this instability. Thus, the LAGEOS Active Nutation Damper (LAND) was developed for this specific purpose.

SYSTEM DESCRIPTION

The active nutation damper system consists primarily of an angular accelerometer, a dc motor driven flywheel and associated electronics. All components are mounted in a single cubical box with the accelerometer input axis perpendicular to the motor/flywheel axis of rotation. On the spacecraft, these axes must also be perpendicular to the nominal spin axis (Figure 1). Since the angular accelerometer is insensitive to translational motion and the relative orientation of the accelerometer and motor in the box are fixed, no other position or alignment requirements exist. That is, the damper unit may be mounted in any position provided the plane of the accelerometer/motor is normal to the spacecraft spin axis and, for phasing, the proper end of the housing is up. Thus, the angular accelerometer has an alignment advantage compared to the precise alignment requirements necessary when using linear accelerometers or gyros. It should be noted that the availability of angular accelerometers, space qualified or not, is very limited. This lead to problems in the test program which will be discussed later.

Digital electronic circuitry was used to divide the nutation period into 8 parts. Using positive-going zero crossings of the accelerometer signal as a reference, it drove the motor positive for one fourth of a nutation cycle starting at one eighth of the period, then off for a quarter of a cycle. Figure 2 shows this logic schematically and illustrates the actual flywheel speed achieved relative to the optimum.

GENERAL DESIGN DETAILS

Figure 3 illustrates the overall dimensions and locates the components that make up the damper assembly. The assembly includes the power converter, accelerometer, reaction wheel, and associated electronics. The dc-to-dc regulated converter is designed to put out $\pm$ 15 volts with inputs ranging from 24 to 32 volts. The converter output will power the accelerometer and the control electronics. The angular accelerometer is operated with the $\pm$ 15 volts and will give a $\pm$ 5 volt functional output. Full scale output represents an input acceleration of 0.5 rad/sec^2.

The control electronics measure the period of the nutation signal and uses this information to properly phase the reaction wheel drive to reduce the spacecraft nutation. The reaction wheel is made up of a 28 V dc torque motor rotor and a stainless steel flywheel. This unit is mounted on pre-loaded, duplex, back to back, paired bearings directly to the housing at right angles to the accelerometer. The motor is energized by suppressed contact relays driven by the control electronics. A wiring diagram of the LAND system is shown in Figure 4. A relay is provided to enable the system to be operated either internally or externally. Power is furnished through this relay to the 28 volt bus which, in turn, furnishes power to the converter, the accelerometer, and the electronics. Power is not furnished to the relays that operate the motor until an additional relay is activated by a spacecraft timing or separation switch. Thus, the system, with the exception of the reaction wheel, may be turned on prior to launch. This allows accelerometer and power telemetry to be received throughout launch, while holding off reaction wheel operation until needed.

MECHANICAL CONFIGURATION

The damper package is basically a 20.3 cm (8 inch) cubical box, weighing approximately 7.5 kilograms (16.6 lbs.). Flanges, that are an integral part of the housing, are provided for mounting. The active nutation damper assembly interfaces mechanically with the spacecraft through a mounting bracket which rigidly attaches and transfers the torque loads from the damper assembly to the spacecraft and positions the assembly to a specified orientation.

The reaction wheel incorporates a flywheel driven by a frameless dc, permanent magnet torque motor (Figure 5) with the rotor mounted to the flywheel and the stator mounted to the housing. The reaction wheel bearings are pre-loaded and lubricated with Krytox to reduce friction and wear between moving parts, to dissipate heat, and to prevent corrosion of critical surfaces. The bearing and lubrication are protected from contamination by a labyrinth seal.

TEST PROGRAM

The LAND system was subjected to a test program to generate performance data and to prove its capability of meeting the LAGEOS flight requirements. Engineering tests were run on the breadboard unit proving the electronic design. Performance tests of the complete unit were conducted before and after vibration, EMI, and thermal vacuum tests. Two complete LAND units were constructed. One unit was environmentally qualified at Flight Prototype levels to be used as a flight spare. The other unit was tested at Flight Acceptance levels, and was the flight unit.

Mechanical Stimulation Test

All major components were subjected to pre-assembly performance checks. The accelerometers were mechanically stimulated using a single axis air bearing table mounted on a seismic block. Four large arms, equally spaced from each other, were secured to the floating portion of the air bearing assembly. Cables were attached to the ends of opposing arms, then passed over pulleys and attached to weights (Figure 6). Thus, if the whole floating arrangement were deflected a few degrees and then released, it would oscillate at varying frequencies depending on the quantity of equal weights applied to the opposing arms. Weights were added until a frequency of 1.3 Hz (the calculated LAGEOS nutation frequency) was reached. The large mass of this arrangement allowed the table to oscillate at a specific frequency fairly constantly for a short period of time. The complete system was placed on a seismic block to effectively isolate the sensitive accelerometer from various building vibrations. With the LAND unit mounted to the center of this arrangement and powered up through a connector, a functional test of the accelerometer, reaction wheel, threshold level, and phasing was conducted visually and recorded as the table was oscillated. This test revealed that movement of wires carrying a 10 MHz accelerometer oscillator signal produced a noise level that exceeded the threshold level of the system. This problem was solved by shortening the cable between the electronics and the sensing unit of the accelerometer, conformal coating all wires carrying this 10 MHz signal so they could not move, and filtering all accelerometer inputs and outputs with RC networks.

Gas Bearing Test

The active nutation damper package was evaluated and proven on a 3-axis gas-bearing simulator (Figure 7) that duplicated the LAGEOS critical flight dynamics. The spin rate and spin and transverse inertias of the simulator were made to be equal to that of the LAGEOS spacecraft in transfer orbit. Testing was conducted under vacuum in a dynamic test chamber. Nutation was induced in the simulator and both the flight and back-up LAND units were activated for full scale performance tests. These tests verified that the

LAND system would reduce nutation at the predicted rate of one degree per minute.

FLIGHT PERFORMANCE

The LAGEOS spacecraft was successfully launched May 4, 1976. The LAND system was turned on just prior to launch except for power to the motor driven flywheel. The angular accelerometer and electronics were powered up prior to launch as a functional check and to provide accelerometer telemetry data during the launch phase. The reaction wheel was furnished power through a timing switch closure which occurred shortly after third stage separation, at which point the long coast (4500 seconds) transfer orbit started. Telemetry indicated that the LAND system's motor/flywheel was activated as the timing switch closed. The nutation at the beginning of the long coast period was 0.6 degrees which was greater than the 0.38 degrees threshold of the logic circuitry. Thus, the LAND's motor turned on and it operated for a period of approximately 20 seconds, reducing nutation to 0.25 degrees. This performance verified the nominal pre-flight prediction of 1.0 degree per minute for the nutation control capability of the damper. The balance of the long coast period was completed without sufficient nutation growth to re-start the LAND system.

CONCLUDING REMARKS

The most significant features of this development program may be summarized as follows:

(1) This was the first time an angular accelerometer has been used for sensing spacecraft nutation.

(2) This was the first time an active nutation damper made use of internal torquing to control nutational coning.

(3) The flight capability of this active nutation damping system has been proven by the LAGEOS launch.

(4) This damper design is particularly suitable to those spacecraft without gas control systems that require long coast transfer orbits.

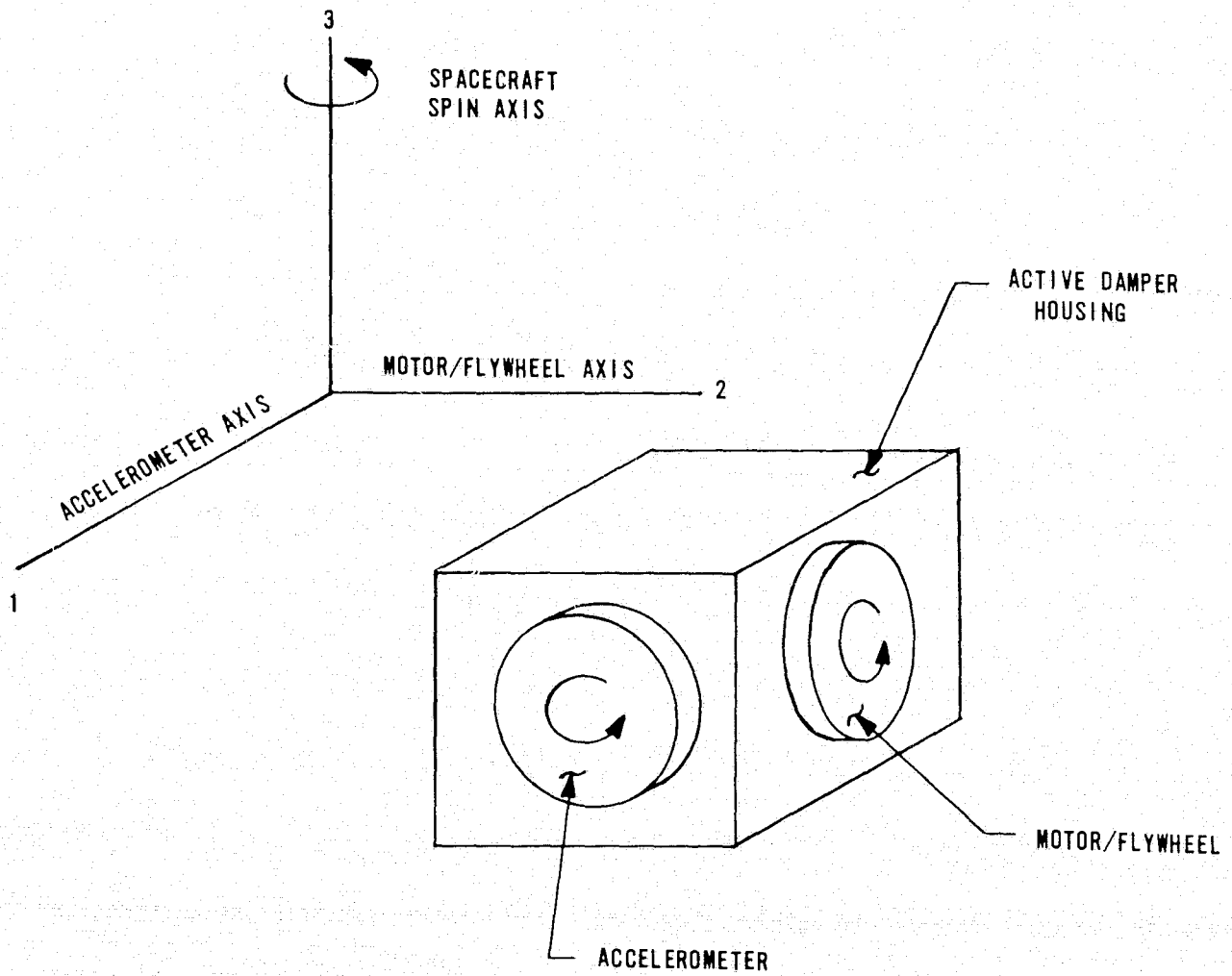(5) This system can easily be adapted to fire jets for gas control of nutational coning.

ACKNOWLEDGMENTS

Figure 1. Active Nutation Damper Configuration
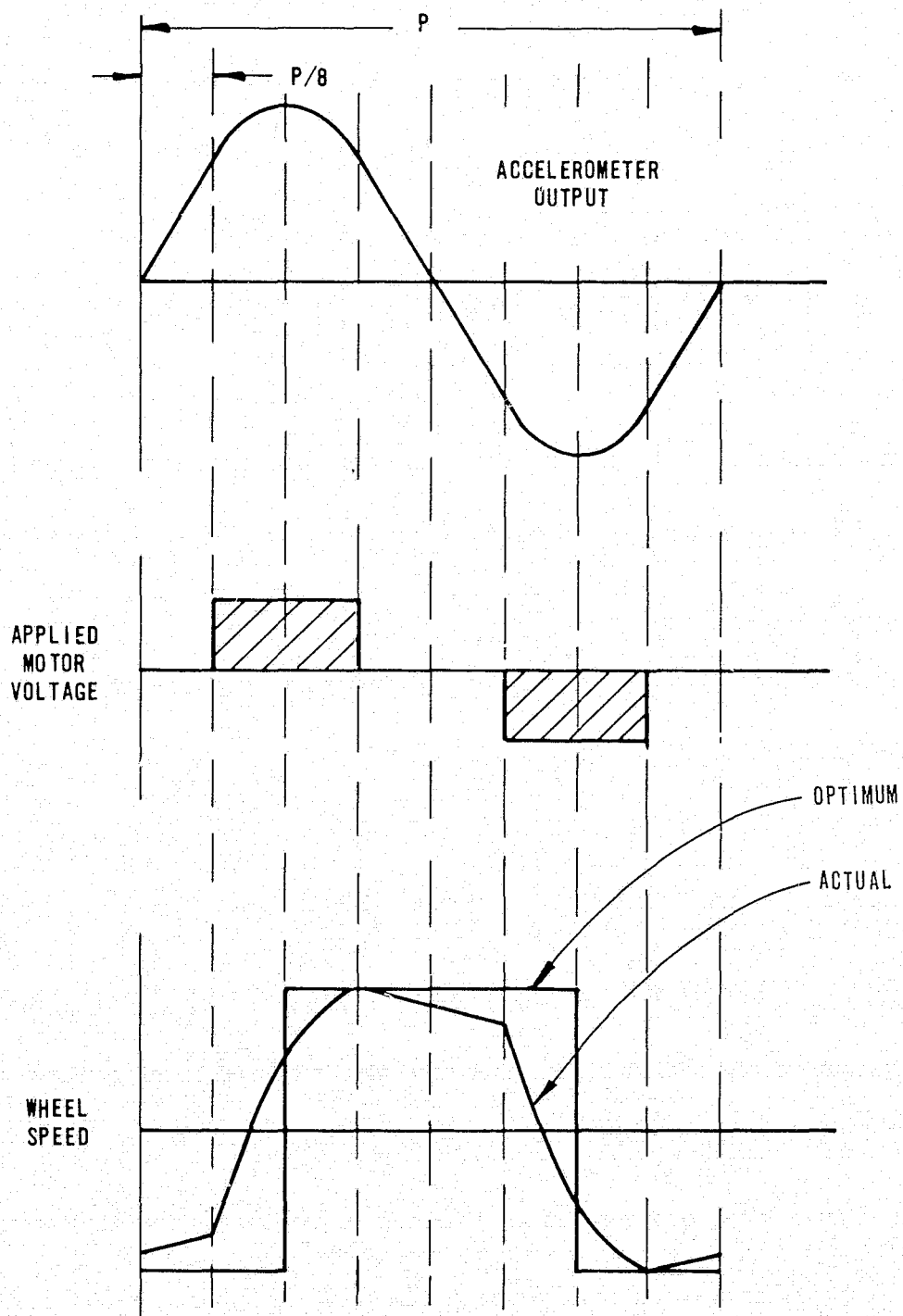
Figure 2. Actual Flywheel Speed Achieved Relative to the Optimum

LATCHING RELAY
(NO LOAD)

ANGULAR
ACCELEROMETER
(0.5 WATT)

ELECTRONIC CARDS
(0.5 WATT MAX.
CONTINOUS)

COVER
PARTIALLY REMOVED
FOR CLARITY

TIMER RELAY
(1.2 WATT CONTINOUS)

9.00

8.04

REACTION WHEEL
(60 WATT AVERAGE - PROBABLE
OPERATING TIME - 10 MIN.)

8.00

MOTOR RELAYS
(1.2 WATT - 50%
DUTY CYCLE)

BATTERY DIODES
(1 WATT EACH - 50%
DUTY CYCLE)

UMBILICAL CONNECTOR

TEST CONNECTOR

8.13

POWER CONVERTER
(2.0 WATT)

Figure 3. Active Nutation Damper Package
LAGEOS

141
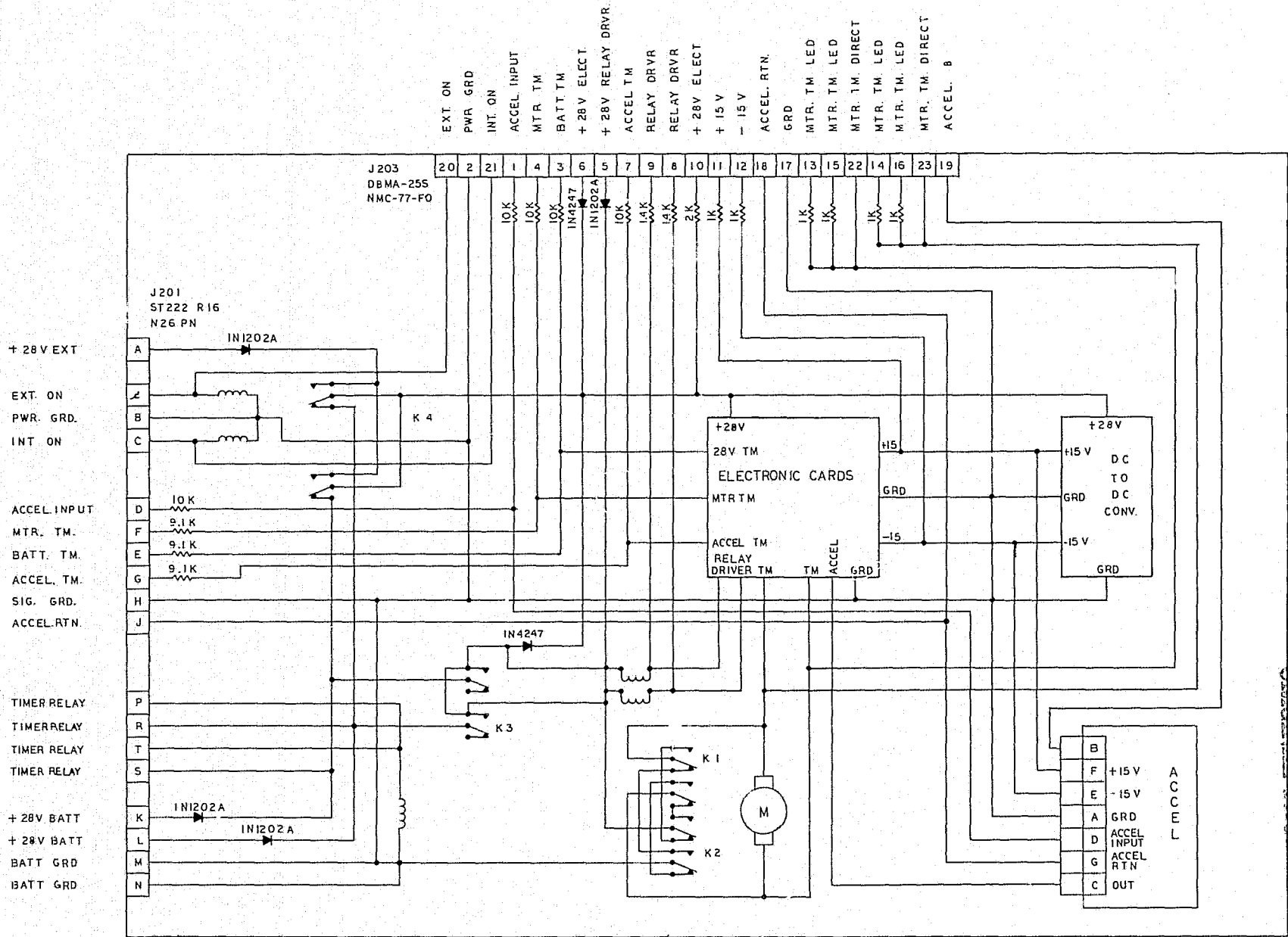
Figure 4. Wiring Diagram of the LAND System

142

PRE-LOAD ASS'Y

ROTOR CLAMP

BEARINGS

BEARING SHAFT

ROTOR

FLYWHEEL

STATOR/BRUSH ASS'Y

Figure 5. Motor/Bearing Assembly
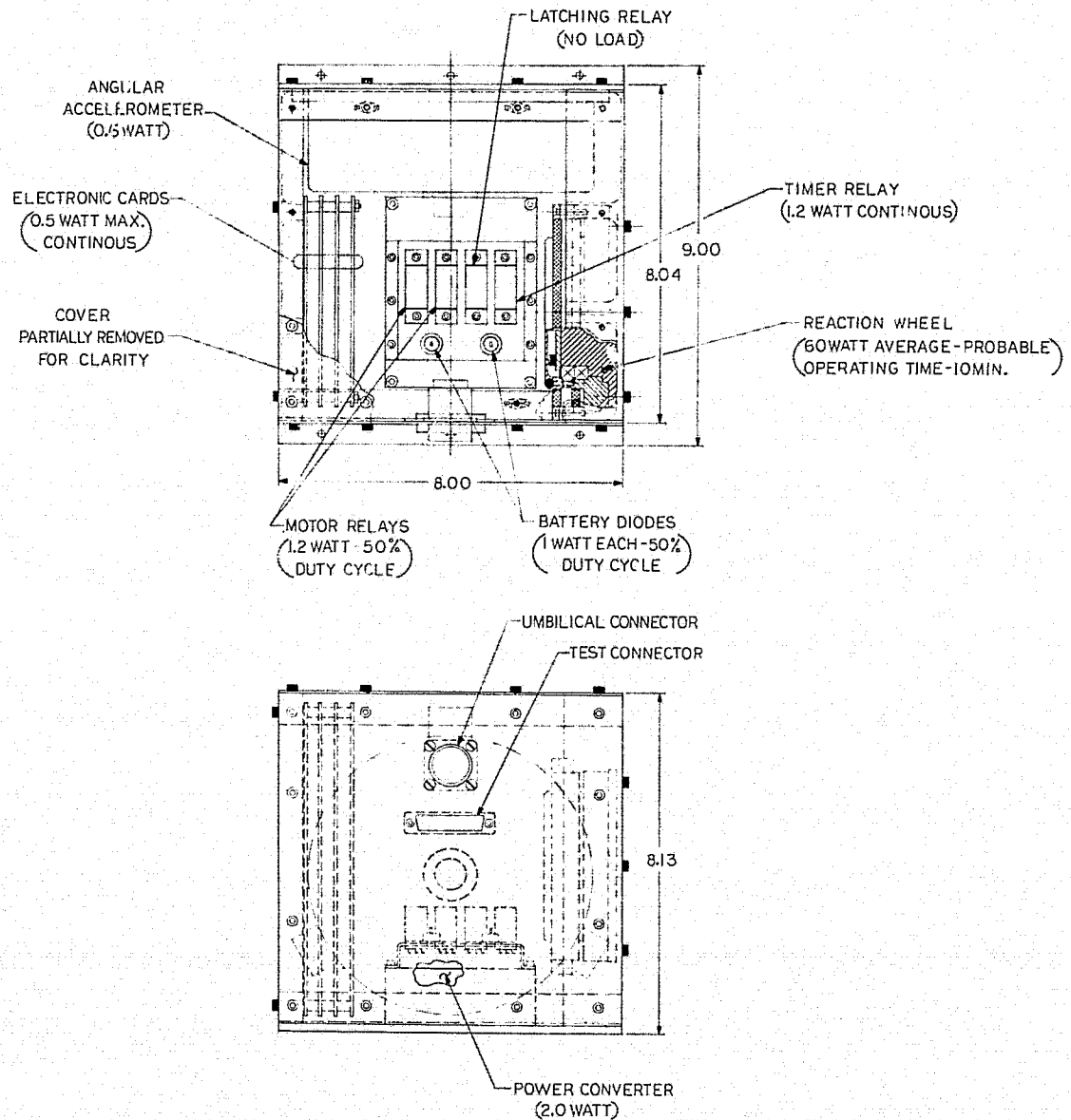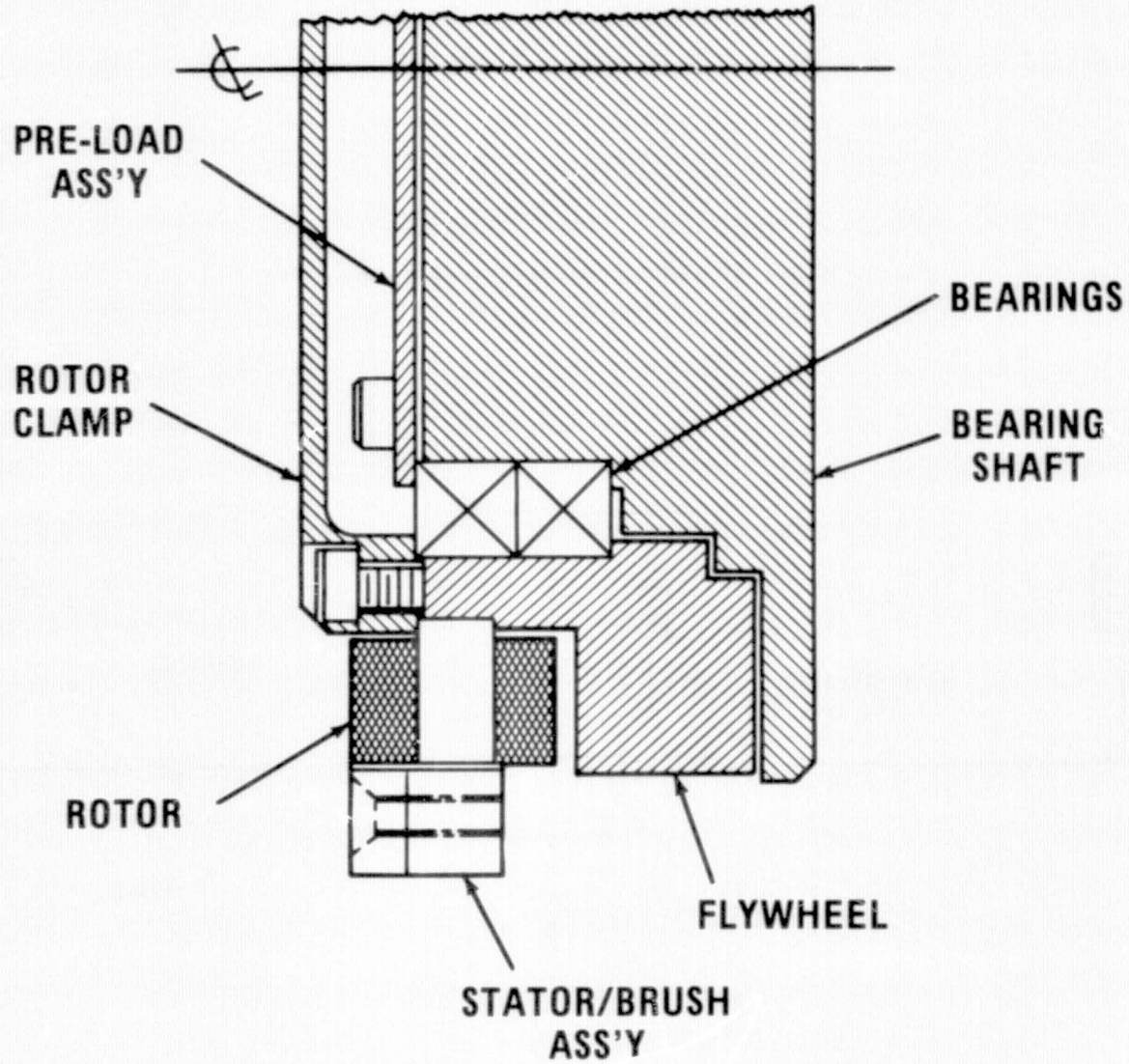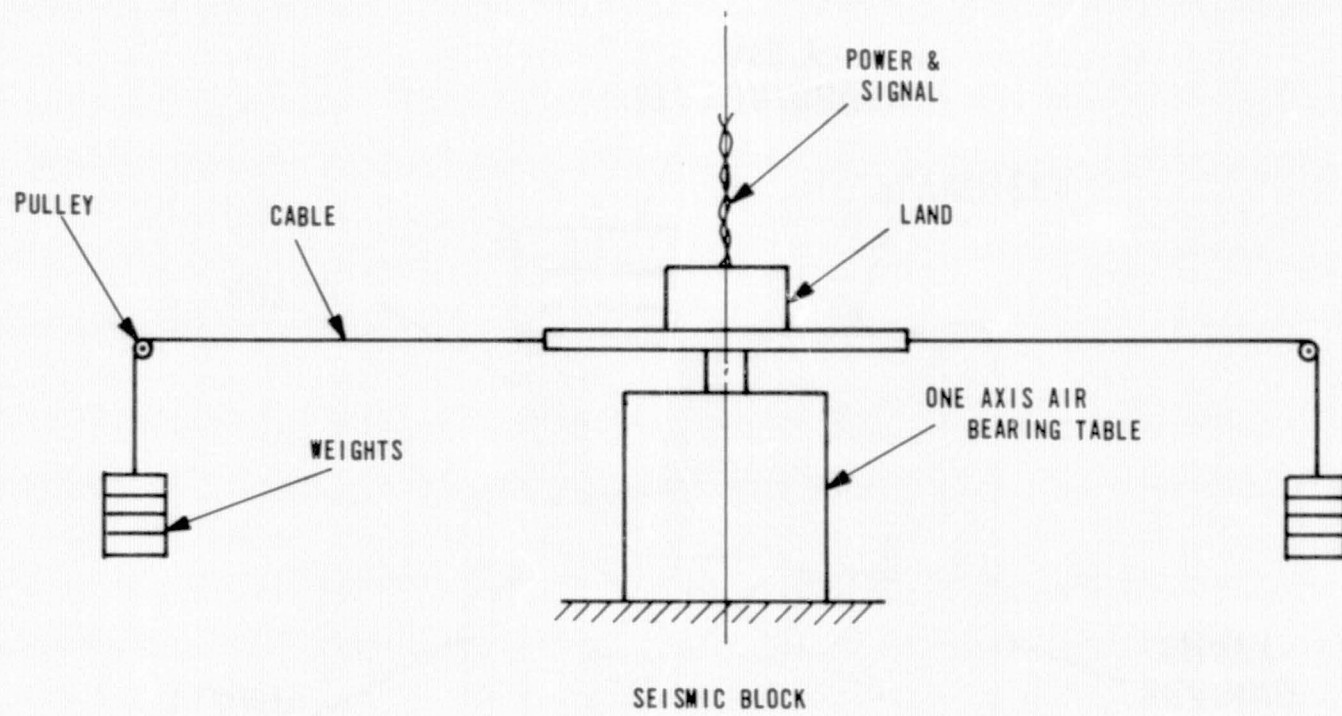
143

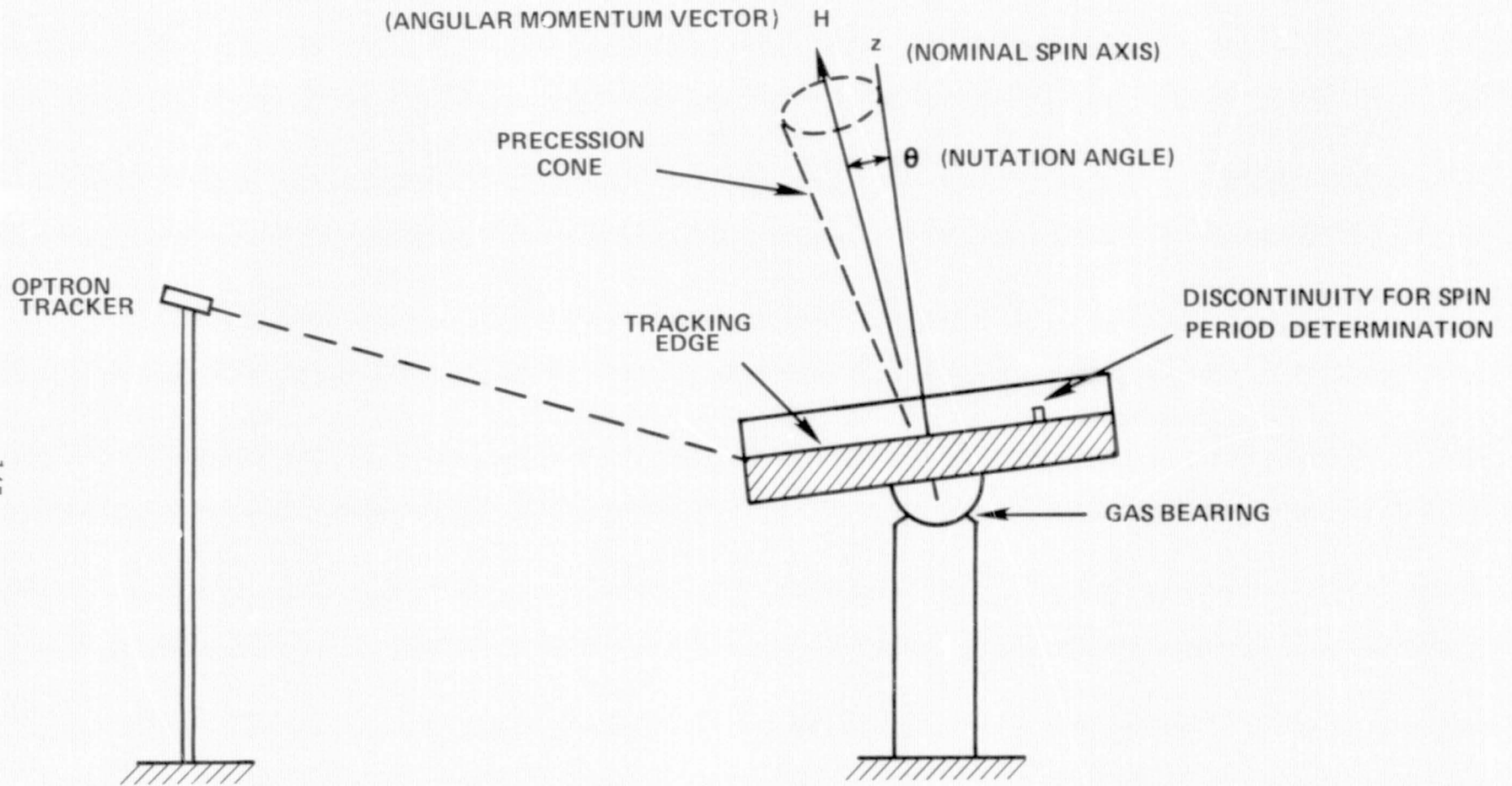Figure 6. Physical Stimulation Test Setup

Figure 7. OPTRON Attitude Sensing

GEOS — 20 m Cable Boom Mechanism
By Günter K. Schmidt and Klaus Suttner
Dornier System GmbH — Germany

ABSTRACT

The GEOS Cable Boom Mechanism allows the controlled deployment of a 20 m long cable in a centrifugal force field. In launch configuration the flat cable is reeled on a 240 mm diameter drum. The electrical connection between the rotating drum and the stationary housing is accomplished via a Flexlead positioned inside the drum. Active motion control of this drum is achieved by a self locking worm gear, driven by a stepper motor. The deployment length of the cable is monitored by an optical length indicator, sensing black bars engraved on the cable surface.

This paper describes the design, development, and testing of the operational modules.

    Drum with Cable and Flexlead
    Worm gear drive with stepper motor
    and
    Deployment length indicator

1. INTRODUCTION

GEOS is a scientific geostationary satellite spinning at 10 rpm in orbit. The payload consists of seven experiments with approximately 30 modular units. Most of the experiment probes and sensors had to be positioned at specific distances from the S/C surface to reduce body interference. The location and orientation requirements of these probes led to the design of a Boom and Mechanism Subsystem comprising of 8 different booms and 5 mechanisms. Two of the booms are 20 m long Cable Booms serving two active electronic sensors at their tips. During launch these sensors are stowed tangentially on the spacecraft surface in experiment containers. When released, these containers are opened to allow the sensors to swing out. The swinging motion is damped by a release system and a tubular damper. This release system is called the "Experiment Release Mechanism" and was presented by Mr. G. Bring from ESA at the May 76 Symposium in Frascati, Italy. (Ref. 1). After the release motion is damped out, the two boom cables are radially deployed by their "Cable Boom Mechanisms", which are positioned inside the Spacecraft below the lower equipment shelf.

2. BASIC DESIGN REQUIREMENT

    Deployment length is 20 m.
    Deployment accuracy is ± 5 cm.
    Intermittant synchronous deployment in 10 cm steps and general start-stop mode.
    Test retractability and limited retractability in orbit.
    All bearings are dry lubricated.
    Maximum power consumption is 35 W.
    Maximum height is 270 mm.
    Magnetic cleanliness has to be achieved.
    1 Dipole and 10 connection lines for signals and power between tip sensor and S/C.
    Operation in vacuum between -20 and +55°C.

3. FUNCTIONAL DESIGN CHARACTERISTICS

A brief description of the Cable Boom Mechanism design is shown in Fig. 1. Additional details are provided in a Design Study Report. (Ref. 2). The following will highlight the more interesting functional groups: —

    Cable and Flexlead
    Worm gear drive
    Stepper motor
    Optical deployment sensor.

4. CABLE AND FLEXLEAD

For GEOS a flat cable of 1,5 x 7,3 mm cross section, consisting of five pairs of signal- and power leads AWG 36 and one AWG 24 central load wire with 60 pf/m lead capacitance was used. (Fig. 2). The cable was braided with twelve AWG 42 conductors and covered with gold plated Kapton tape. One side was painted with 2 x 6 mm black bars spaced at 10 mm intervals for the optical length indications. The cable was manufactured by HABIA, Sweden. Further details and dynamics of this cable are provided in Ref. 3.

Major problems were created by use of the Kapton tape. Due to poor gold adhesion of the standard tape, the gold had to be vapor deposited in an ultra high vaccuum chamber. Following this process, a double sided self adhesive scotch tape was applied to the inner surface of the gold plated Kapton tape. The tape was then wrapped around the braided cable body.

The Flexlead which is attached to the stationary housing is positioned within the cable drum. It is reeled on the centre hub in the stowed configuration and unreeled onto the inner surface of the worm wheel fixation ring in the deployed configuration.

The Flexlead cable which electrically connects the rotating drum and the stationary housing, is a flat teflon cable of 0,5 x 14 mm cross section with sixteen AWG 30 leads. The cable complied with specified capacitance and impedance values. This cable was also developed and manufactured by HABIA, Sweden.

To assure reliable performance, one side of the Flexlead cable is required to be as flat as possible to reduce lateral forces between the layers during unreeling. The results of tests and post test analyses led to a design shown in Fig. 3.

The geometrical lay-out of the Flexlead is based on the following equations.
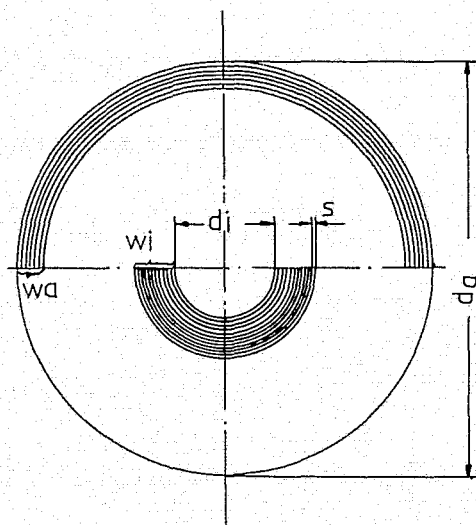
1. $L = d_m \cdot w \cdot \pi$

2. $d_{mi} = d_i + W_i \cdot S$
      $d_{ma} = d_a + W_a \cdot S$

3. $n = W_i - W_a$

L = Flexlead length
W_i = number of inner windings
W_a = number of outer windings
n = number of revolutions
S = Flexlead cable thickness
d_i = inner diameter
d_a = outer diameter

using the dimensionless Factors

$$\frac{d_i}{s} = \sigma \qquad \frac{d_a}{s} = \delta \qquad \frac{L}{s} = \lambda$$

the following Flexlead equation can be derived:

a) Range of definition: $d_i \leqslant d \leqslant d_a$

$$\frac{n}{\sigma} = \sqrt{\frac{1}{4} + \frac{\lambda}{\sigma^2 \pi}} + \sqrt{\frac{\delta^2}{4} - \frac{\lambda}{\sigma^2 \pi}} - \frac{1}{2}(1 + \delta)$$

b) differentiated for maxima:

$$\frac{n_{max}}{\sigma} = \sqrt{\frac{4\lambda_{max}}{\sigma^2 \pi} + 1} - \sqrt{\frac{2\lambda_{max}}{\sigma^2 \pi} + \frac{1}{4}} - \frac{1}{2}$$

The Flexlead Diagram, see Fig. 4, includes equations (a) and (b). For GEOS the following parameters were used:

$$\delta = 6 \qquad \sigma = 58 \qquad \frac{n}{\sigma} = 0{,}64 \qquad \frac{\lambda}{\sigma^2} = 6{,}4$$

A Flexlead cable length of 12 m for 37 reel revolutions was derived from this diagram. A coiling factor of 0,9 was used.
The Flexlead was built and tested according to these parameters and performed successfully.

5. WORM GEAR DRIVE

For a cable boom system, a worm gear drive has fundamental advantages. Since cable booms deploy by the action of centrifugal force induced by the spinning satellite, deployment forces need not be provided. The task of the gear in this case is to prevent uncontrolled deployment. This can be obtained in a very efficient way with a self locking worm gear. The lower the self locking efficiency, the lower the torque requirement at the worm shaft necessary to control deployment motion. Thus, deployment control can be accomplished with a very small motor.
However, these operational conditions with the use of dry lubrication require a very careful design of the worm gear configuration and material selection. Of considerable importance are stable friction conditions between worm and worm wheel.
Several material combinations were tested in a special test to determine their frictional behaviour as a function of operation time. Excellent results were obtained with a titanium worm and a HOSTAFLON worm wheel. In actuality, the initial friction of this combination is rather high. However, the friction reduces after a run-in period to a very constant value. A friction value of about $\mu = 0{,}16$ to $0{,}18$ was determined as the result of these friction investigations. Considering this value and the configuration data the gear data was thereby chosen:

    pitch 2 mm
    gear ratio 100
    pitch angle 6,33°

With this gear design and the available torque of the stepper motor, an operational range of $\mu = 0{,}11$ to $0{,}25$ was achieved, providing a sufficient safety margin. The design parameters for the worm gear can be obtained from the worm gear Nomogram (Fig. 5) which was specifically developed for this drive assembly.
Full conformity between design and actual hardware was demonstrated during qualification testing.

6. THE MOTOR

A size 11, 4 phase variable reluctance stepper motor was chosen to drive the Cable Boom Mechanism.
Even considering the poor efficiency of these motors, they provide several important advantages:

    Small rotational speed without gear head and speed variation capability
    High calculated reliability due to minimal amount of mechanical parts
    Low residual magnetism following switch off
    Digital servo electronics
    Simple electronic synchronisation of several motors.

The motors, used for the GEOS Cable Boom Mechanisms, were specially developed by SAGEM, France. These stepper motors can provide a starting torque of more than 25 Nmm. The length of the housing is 52 mm and its mass 125 g. The motor has a step angle of 15° and runs with 12 Hz (speed A) and 48 Hz (speed B).
The motor is operated by a Motor Control Electronic (MCE), which functions in several deployment modes, with a synchronous four phase driver signal for two stepper motors.

7. DEPLOYMENT LENGTH INDICATOR

The purpose of the deployment length indicator is to measure the deployed length of the boom cable. It consists of the following:

    the optical head and
    the processing electronics.

The optical elements of the optical head consist of a matched pair of light emitting diode and photo transistor. The geometrical arrangement of both of these devices assure that the maximum possible amount of emitted light is reflected into the photo transistor. Reflectance is achieved by a gold plated cover tape on the Boom Cable, which passes under the optical head. Maximum reflection occurs when the optical axes of the light emitting diode and the photo transistor intersect in the plane of the cover tapes. The gold plated cover tape is marked with a periodic pattern of non-reflecting black bars, that are spaced 10 mm apart and are 2 mm wide. (Fig. 6).

The processing electronics generate a counting pulse when a bar has passed the optical head in either direction. However, no counting will occur if the bars are oscillating back and forth in the cable axis direction at amplitudes of less than 5 mm. To achieve this count deletion, a second optical element in the optical head is displaced from the first by 5 mm in the cable axis direction. Using the outputs of both optical elements, the counting pulses due to cable longitudinal oscillations are automatically suppressed by the processing electronics. For reliability purposes, the arrangement of the two optical elements is duplicated in the optical head, the outputs of the redundant photo transistors being OR-gated.

8. TESTING

The Cable Boom Mechanism as a unit was successfully tested at development, qualification and acceptance levels. The following environmental tests were carried out at unit level:

Vibration tests - sinus and random
Thermal - Vacuum test between -30° and +60°C at a pressure less than 10^{-7} Torr
Electromagnetic Cleanliness Tests

The environmental tests were accompanied by unit performance tests. The most significant and comprehensive performance test was accomplished by means of a special Unit Test Rig.
This Unit Test Rig consists of an electronic Unittester simulating the electrical interfaces to the Satellite, and a test fixture simulating the mechanical orbit conditions. It also allows the simulation of any required orbital deployment load characteristic.
The deploying cable is stored on a drum which simulates the cable load by means of a controllable torque motor. The torque profile is provided and monitored via the Unittester. The Cable Boom Mechanism itself is mounted on a base plate supported by bar springs. Strain gauges positioned at the bar springs measure the cable loads, applied to the drum.
The test fixture is very compact and enables simulated Cable Boom deployments also in small test chambers. In addition to these unit tests, comprehensive component tests were carried out with the Boom cable, and cable marks, Flexlead cable, stepper motor, worm gear, optical head and control electronics.

9. CONCLUSIONS

For the GEOS satellite a 20 m Cable Boom Mechanism was designed, developed and qualified. This effort was sponsored by the EUROPEAN SPACE AGENCY as part of the GEOS Development Contract.
The layout of the Flexlead and the worm gear required rather careful consideration. Problems associated with the adhesion of the gold layer and the black marks on the gold surface as well as with the optical head had to be solved.
However, due to the modular configuration and the availability of a parametric design lay-out and computer programs, the application of this mechanism is not limited to a 20 m cable, but can be easily adapted to other configurational requirements and applications. Longer and heavier cables can be deployed and retracted with a stronger motor for instance.
The application range of this mechanism covers 100 and more metres deployment lenght. If necessary, a deployment accuracy of less than 1 cm can be achieved.

10. REFERENCES

1) ESA SP 117, Presentation held in Frascati, Italy 24-26 May 1976 by G.L.Bring: Design Features and Zero Gravity Simulation of the GEOS Satellite Long Radial Boom Release.

2) ESTEC Publication Nr. 1511/71 AA by Dornier System GmbH, Günter K. Schmidt: Cable Boom System for Spin-Stabilized Satellites — Design, Development, and Testing.

3) ESTEC Presentation at the 8th Aerospace Mechanisms Symposium, October 1973 by G.L. Bring: Development of and Dynamic Studies Concerning a Cable Boom System Prototype.

CBM Scheme

A   Boom Cable with optical marks

B   Cable Drum

C   Flexlead

D   Central Hub

E   Housing

F   Worm Wheel

G   Worm

H   Motor

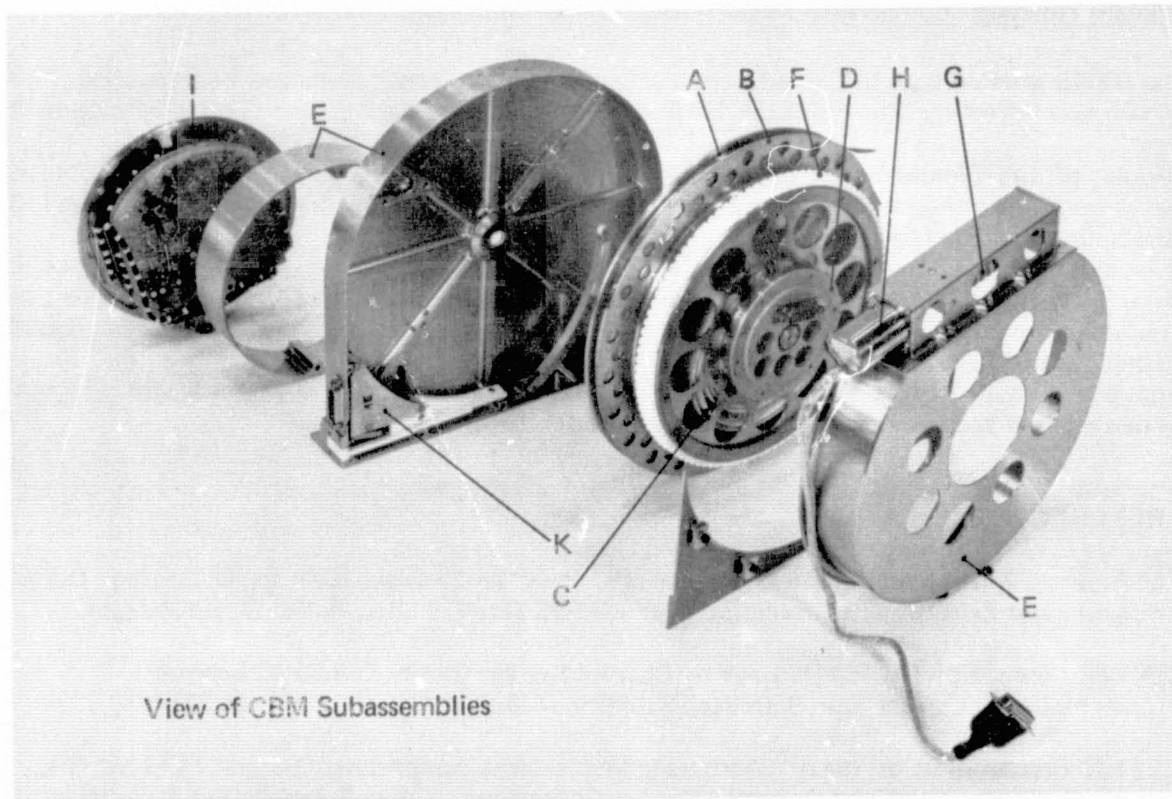I   Motor Electronics

K   Optical Head and
     processing Electronics

View of CBM Subassemblies

Fig. 1   GEOS – Cable Boom Mechanism

152

Fig. 2   LRB Cable Cross Section

SCALE |—— 1 mm ——|

Fig. 3   Flexlead Cable Cross Section

153
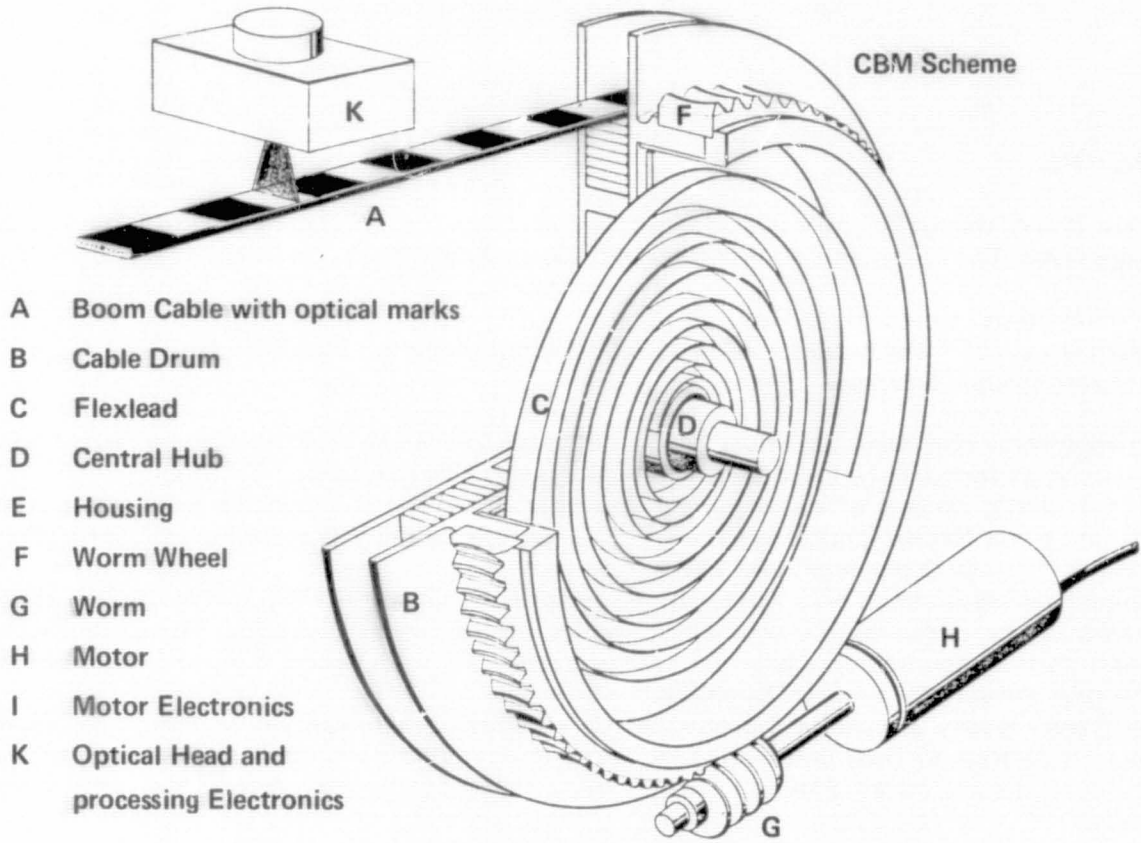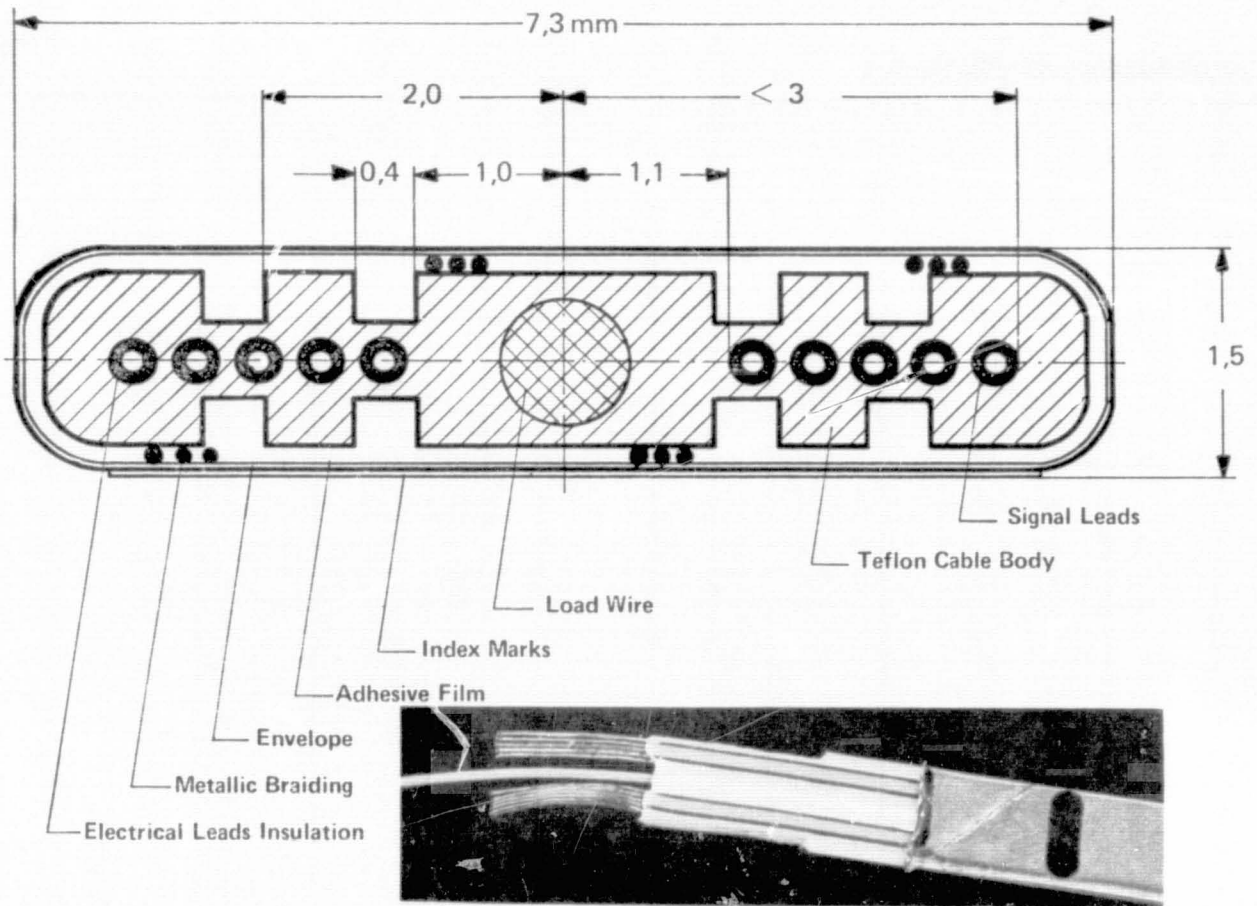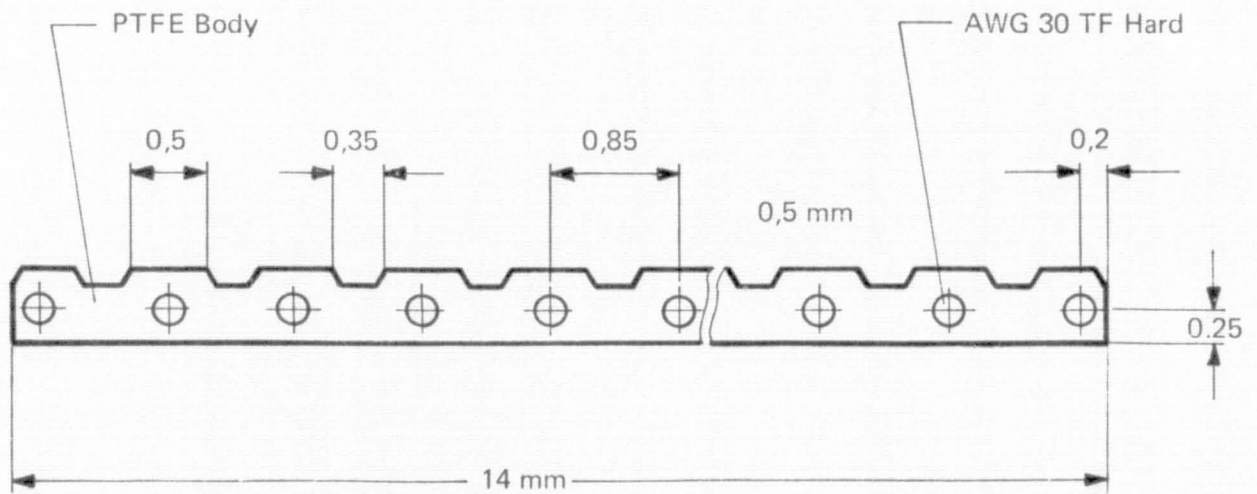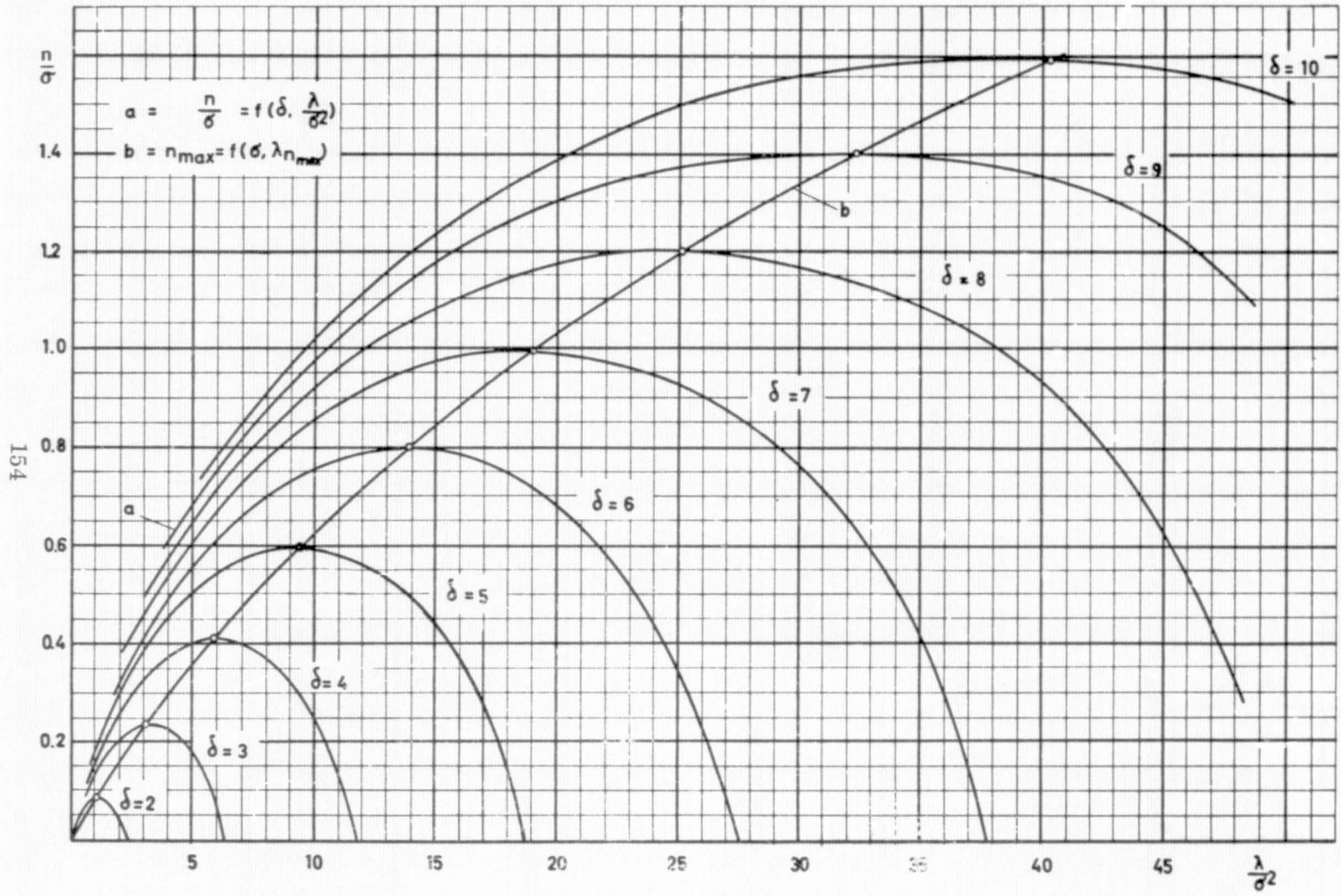
Fig. 4   Flexlead Diagram

Fig. 5   Worm Gear Nomogram

LIGHT SOURCE
GA–AS–DIODE
TIL 23/24

COUNTER
PHOTO TRANSISTOR
TIL 601/604

REFERENCE
PHOTO TRANSISTOR
TIL 601/604
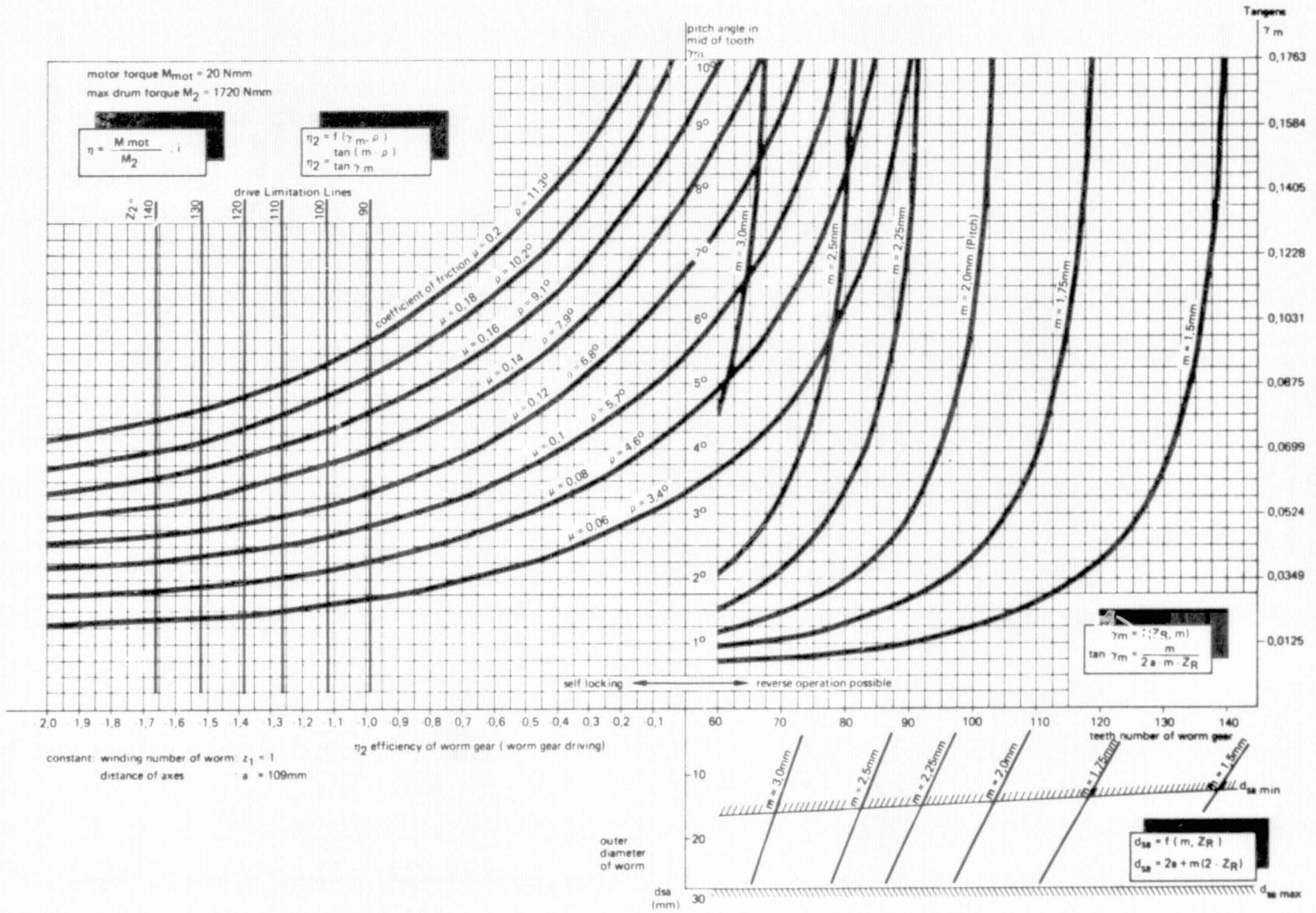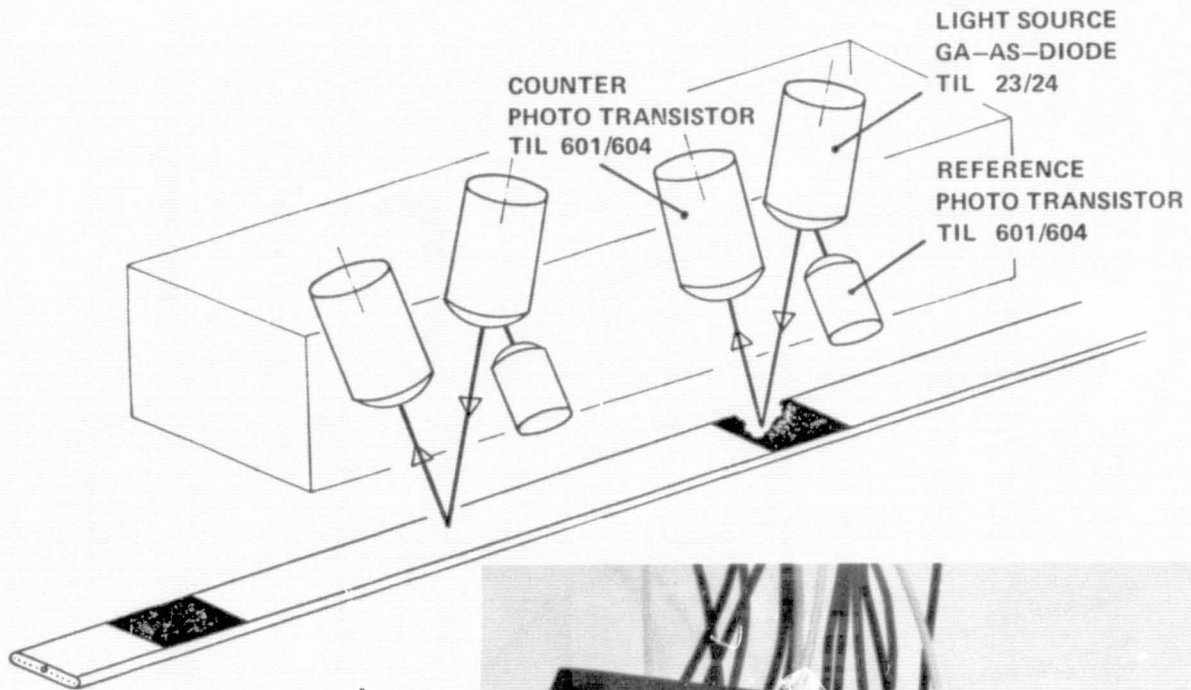
OPTICAL HEAD:

Scheme
and
Hardware

Block Diagram of Processing Electronics

OPTICAL HEAD

SQUARER

SQUARER

VIBRATION
SUPPRESS.

Fig. 6   Deployment Length Indication

A LOW COST HIGH TEMPERATURE SUN TRACKING

SOLAR ENERGY COLLECTOR

By Gerald S. Perkins

Jet Propulsion Laboratory
Pasadena, California

ABSTRACT

This paper will describe the design and economic evaluation of a low-cost
high-temperature two-axis sun tracking solar energy collector. The collector
design is specifically intended for solar energy use with the freedom of motion
about its two control axes being limited only to the amplitude required to track
the sun. An examination of the performance criteria required in order to track
the sun and perform the desired solar energy conversion is used as the starting
point and guide to the design. This factor, along with its general configuration
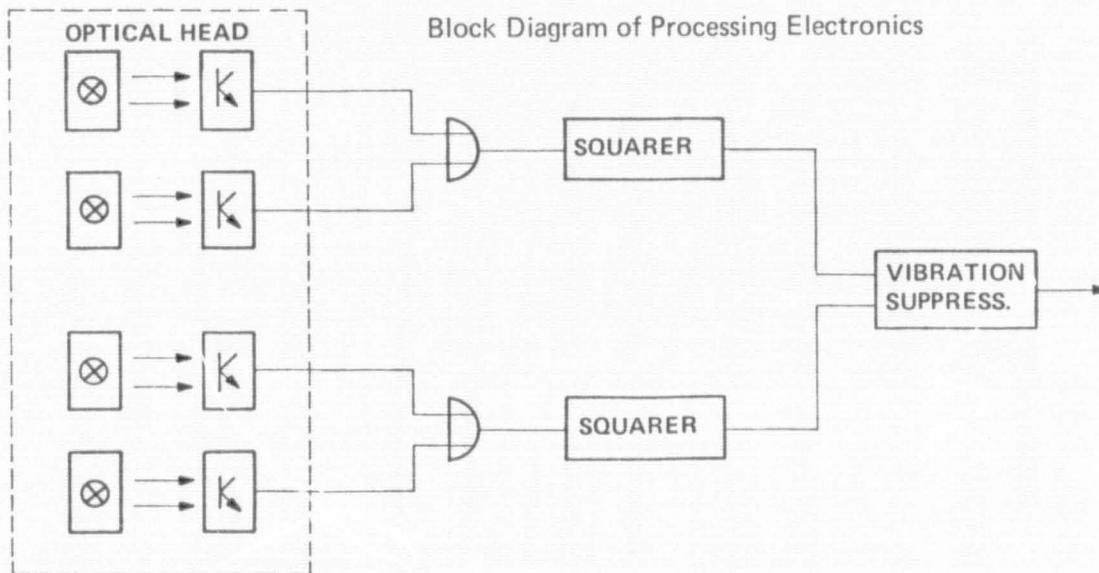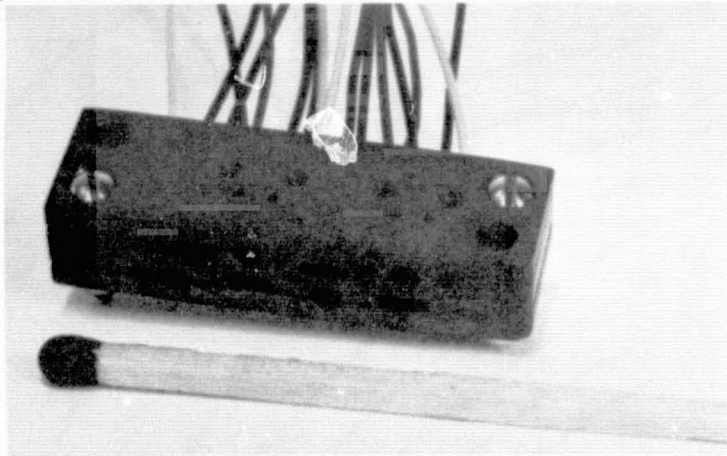and structural aspect ratios, is the significant contributor to achieving low
cost. The unique mechanical design allows the control system to counter wide
tolerances that will be specified for the fabrication of the azimuth frame and
perform within a small tracking error.

INTRODUCTION

In answer to the question "Why is the solar concentrating two-axis tracker
preferred?", two of the key factors in evaluating the relative performance of
various collection systems are:

    (a) How much of the available solar energy is "harvested" each year?
    (b) What is the net overall plant conversion efficiency?

A comparison of solar energy collected by typical non-tracking, single-axis
and two-axis tracking collector designs for a fall day at Albuquerque, N.M., is
shown in Fig. 1. The approximate seasonal variation for the same three designs
at the same locations is shown in Fig. 2.

The ability of the two-axis system to harvest 78-80% of the available
direct normal insolation, whereas the single-axis collects 30-35% and the
non-tracking 17-20%, holds for most locales of interest to potential users.

It should also be noted that the temperature of collection is usually
limited to 300-400°F for the non-trackers and 500-600°F for single-axis tracking;

but temperatures in the 1000-2000°F range may easily be attained by two-axis tracking. Thus, for both questions (a) and (b) above, the two-axis system is clearly superior. The bottom line, of course, is not determined solely by (a) and (b), but must also consider such items as initial cost, operating costs, etc. The key to taking advantage of the much higher potential performance of the two-axis system is to achieve initial cost and operating expense levels which will be less in proportion than the factor of 3-10 advantage in relative perform- ance. Figure 3 shows a comparison of the costs per kWe for the three collector designs studied previously, when realistic cost figures were added to the performance calculations. As may be seen, the two-axis performance was better by a factor of two, even though a collection temperature of only 1000°F was assumed.

The major conclusion here is that two-axis tracking is clearly superior in potential thermal performance; so, if initial cost and operating expenses can be held to a level, which will not offset this advantage, two-axis tracking is the appropriate choice. The key will be to achieve low cost ($16/ft^2). The $16/ft^2 cost figure is for a complete solar conversion system with electrical output from solar energy input.

<center>DESIGN DESCRIPTION</center>

The control axes, azimuth, and elevation are arranged to intersect at the focal point of the parabola. Figure 4 illustrates the design configuration of the sun tracking solar energy collector. The structure which will support the reflecting surface rides on wheels captured in curved channel rails on top of the azimuth structure. The azimuth structure is supported and restrained at the center by a pivot anchored in concrete and by two wheels on a peripheral circular track near its outer end. The parabola structure is counterbalanced about its elevation axis by a pendulum cable system.

Figures 5, 6, and 7 also illustrate the design configuration of the 50 ft solar tracking collector. The parabolic reflector has a focal length to diameter ratio of 0.5. The structure that will support the reflecting surface rides on wheels captured by curved rails on top of the azimuth frame. This pro- vides the elevation axis motion. The structural relationship between the reflector support structure and the azimuth frame is a triangular (3 point) load transfer configuration. This kinematic relationship will prevent a deflection of either structure from imposing a strain on the other. This kine- matic feature will also allow large tolerances on the order of ± one inch radial deviation to be used in the fabrication of the azimuth frame curved rails. The elevation drive is provided by a tensioned chain looped around the drive sprocket of the elevation actuator.

The azimuth frame is supported and restrained at the center by a pivot anchored in concrete and by a system of wheels on a peripheral track near its outer end. This allows the azimuth motion. One of the wheels is driven by the azimuth actuator in order to provide the azimuth drive motion. Both the eleva- tion and azimuth actuators are coupled to their respective drive systems with effectively antibacklash linkages. This will allow the use of standard commer- cial gearboxes for the makeup of the drive actuators since they will be placed ahead of the output coupling of ratio η. The output drive ratio η is friction

<center>158</center>

coupled in the azimuth drive and torque biased in the elevation drive. This
condition will eliminate output ratio backlash from either axis. The output
drives can be described as antibacklash drives. The backlash from the gearboxes
will now be reduced by $1/\eta$.

The expected resultant backlash as seen by the control system is now in the
higher speed regimes of the actuator mechanisms and is shown to be reduced by the
following relationship:

$$\text{output backlash} = \frac{\text{gear train backlash}}{\text{output ratio}}$$

$$\text{output ratio } A_z = \frac{\text{support track dia}}{\text{drive wheel dia}} > 30$$

$$\text{output ratio El} = \frac{\text{drive chain trough radius}}{\text{elevation actuator drive sprocket radius}} > 50$$

$$\text{output backlash} \leq 0.05°$$

The fixed focal point concept provided by the intersection of the elevation
and azimuth axes at the focal point of the parabolic reflector will allow the
heat engine or receiver to be mounted independently of the parabolic reflector
and its structure. The heat engine or solar flux receiver is mounted separately
on a small tower. It may be mounted in a gimbal and tethered to the parabola
structure by a system of cables. This will keep the receiver pointed along the
axis of the parabola. The cables will be equipped with spring damping systems
in order to minimize dynamic interaction between the separate structures that
might be caused by wind induced vibration.

The mirror surface is made by mounting second surface glass mirror segments
to a series of monocoque panels that will cover the parabolic structure. The
glass will be attached to the panels by discrete fasteners in order to be free of
strain that is caused by thermal expansion.

A scale model of the low cost solar tracker is shown by Figs. 5, 6, and 7.
The features that make this device a low cost system are discussed and listed as
follows.

1. The sun will be tracked only for the purpose of energy collection, not
    navigation. This will allow a larger tracking error (0.1°) than is
    conventionally used for space navigation with resultant economies
    throughout the design of the mechanism and control system. A 0.1°
    tracking error is acceptable; this is several orders of magnitude
    greater than allowed for space navigation tracking. The prior
    technology for two-axis parabolic tracking systems is in space naviga-
    tion and communication systems. This is the primary point of reference
    for the cost reduction.

159

2. The unique design configuration transfers the load from the azimuth frame to the parabolic support structure at or near the optimal restraint points of its radial trusses where the effects of the load distribution moments are minimized. This will reduce the steel usage in the parabolic structure with regard to its required loading.

3. The large tolerances allowed for the fabrication of the curved rails on the azimuth frame by the kinematic relationship between it and the parabolic reflector support structure will minimize the construction costs. The sun tracking deviations ±0.4° occurring at 0.03°/hr that might be caused by these tolerance-induced errors will be countered by the control systems with no increase in complexity or cost. The desired tracking accuracy of 0.1° will be achieved. The control sun tracking rate capability is 2000 times the rate occurrence of the error rate being corrected. The dynamic response demanded for this correction is negligible.

CONTROL SYSTEM

The actuators and drive motors will be sized to drive the tracker in the wind load condition and to drive the elevation axis without benefit of counterbalance aid. This can be as large as 500,000 ft lb in a 100 mph wind. The largest wind load the tracker is required to operate in (30 mph) should not cause torques greater than 80,000 ft lb for a 50 ft diameter parabola. The larger torque is about the azimuth axis. The actuators will not back drive because of the inclusion of a worm gear drive on the gearbox output stage. This feature will cause the tracker to be held in any shutdown position and will eliminate the need for a brake or latching device.

In order to reduce the wind strain while in the stow position (see Fig. 7) near the ground, a wind deflector fence will surround it. This fence will enhance the boundary layer properties and cause desirable lift and drag reducing turbulent flow over the parabola. The mechanical design of the tracker control system is such that it will never be overloaded in any condition of operation or stowage in winds up to 100 mph. The output stage of the azimuth drive is friction coupled. Slippage should occur at about 300,000 ft lb torque load. The actuator will tolerate greater than 800,000 ft lb torque in a static condition. A large safety margin is realized.

The control system functional parameters for operation are as listed.

1. The tracker will track the sun within 0.1° (tenth degree) accuracy in the presence of 30 mph wind loads and 39 mph gusts.

2. The tracking rate capability for either axis will range from 0 to 50° per hour.

3. The rapid slewing rate will be 550° per hour minimum for the "panic mode" (used to stow the tracker in a high wind) and eastward return.

The tracker control system consists of the following basic elements:

- o microprocessor
- o wide angle sun sensor
- o motors
- o gearboxes and related hardware
- o chain and sprockets
- o wire rope
- o assorted electronics

The dynamic model of the solar energy collector is shown in Fig. 8. The basic philosophy of the control system is: a predetermined desired rate is modified or trimmed by actual position errors determined by a sun sensor. The controller residing within the microprocessor ensures that the tracking collector is pointed generally toward the sun in the morning and sends "start track" command. The controller constantly calculates the sun's rate for both azimuth and elevation during the day. The maximum rate for any time of the year is 50° per hour. The controller uses this "open loop" sun's rate and sun sensor information as inputs to generate proper motor commands to slew the collector. If the average wind exceeds 30 mph the collector is commanded by an operator or automated input from a wind sensor (not shown in Fig. 8) to a safe position, 90° elevation, azimuth stopped, see Fig. 7, using a fast slew ("panic mode") rate of 550°/hr. To restart, the operator turns on the system, the collector reacquires the sun and resumes tracking. If clouds mask the collector sun sensor the open loop rate command stored in the microprocessor will drive the system. Upon unmasking the sun sensor will trim the collector position. The control system will assume the closed loop method of control.

ECONOMIC EVALUATION AND COSTS

From the introduction it is seen that a two-axis sun tracking system is the most economic of the three types compared. The cost goal of $16/ft^2 for a two-axis system is derived from a series of studies relating to the economic use solar energy. All seem to converge on the $16/ft^2 cost figure as an upper limit.

In order to estimate the costs the assembly is broken into its component parts with each part being separately costed out. Tooling and process planning is included in the cost figures. The cost of all materials and hardware parts were discussed with sales managers of representative companies. All companies contacted have sales, price, and delivery experience relating to this type hardware. Tooling and process planning was reviewed with representative manufacturing companies. The cost estimation is made for prototype and pilot production, through limited and finally large scale production. Figure 9 is a tabulation of these cost data.

The labor/materials ratio tends to approach a lower limit of one with adequate tooling and coordinated production procedures. Figure 10 is a graphic presentation of the cost versus production quantity and shows that the low cost goal of $16 per square foot previously mentioned in the economic analysis and cost section can be achieved with modest production quantity. A comparison of

collector size versus cost is displayed by Fig. 11. The indication is that a 60-foot diameter parabolic tracking collector appears to be a cost optimum.

SUMMARY

Based on the study and analysis performed for the design of two-axis solar concentrating tracker, the following observations can be made.

o The low cost goal <$16 per ft^2 appears to be achievable.

o Two-axis sun tracking produces more power than any of the other systems compared for less cost.

o The tracking assembly can be constructed using standard parts and conventional materials.

ACKNOWLEDGMENT

Mr. John C. Becker of JPL provided the sun tracking system comparative data used in the introduction.

Dr. Robert O. Hughes of JPL performed the control system design.

Dr. Roy Levy and Mr. Smoot Kato, both of JPL, performed the structural design analysis that was required in order to evaluate the design.
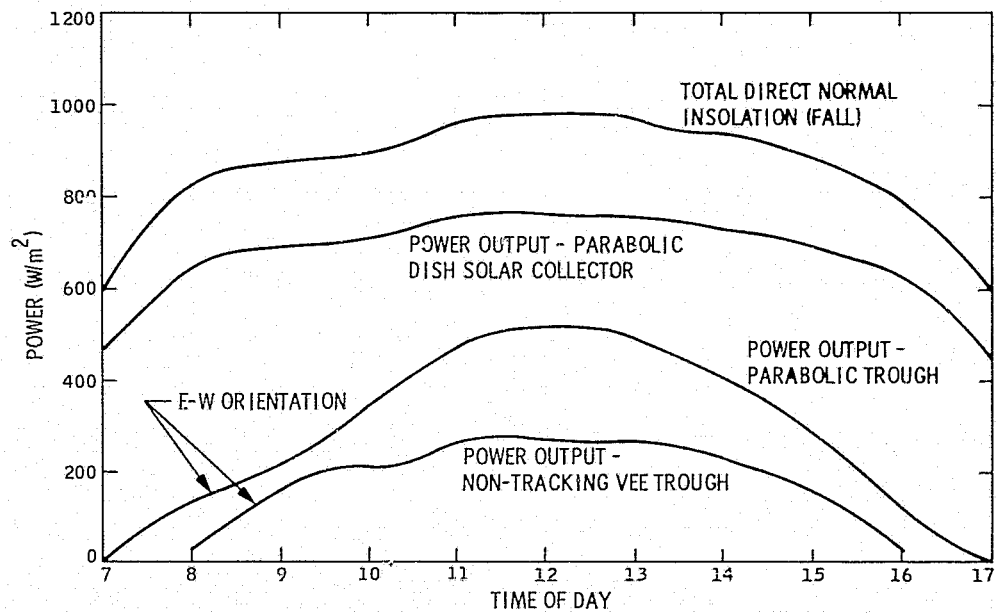
Fig. 1. Comparison of solar power collected by
different collector designs (Albuquerque, N.M.)

WATT-HOURS/m^2

COLLECTOR	SPRING	SUMMER	FALL	WINTER
PARABOLIC DISH (2 AXIS TRACKING)	7408	8113	7298	6049
PARABOLIC TROUGH (E-W; 1 AXIS TRACKING)	2978	3443	3002	2945
VEE-TROUGH (NON-TRACKING)	1633	2002	1645	1876

Fig. 2. Total energy collected by three collector
designs (per day – Albuquerque, N.M.)

	COST	TOTAL ENERGY COLLECTED PER DAY	AVERAGE POWER COLLECTED PER DAY	COST PER KILOWATT THERMAL	TEMPERATURE OF COLLECTION	COST PER KILOWATT ELECTRIC**
	$/ft^2	wh/m^2	w/ft^2	$/kwt$_{avg}$	deg F	$/kWe$_{avg}$
PARABOLIC DISH (2 AXIS TRACKING)	13.49	7298 (78%)	61.6	217	1000 F	505
PARABOLIC TROUGH (1 AXIS TRACKING)	8.97	3002 (32%)	25.4	353	600	1080
VEE TROUGH CONCENTRATOR (NO TRACKING)	4.10	1645 (17.6%)	13.9	295	450	1090

TOTAL ENERGY AVAILABLE PER DAY (FALL-AVERAGE) = 9350 wh/m^2

** THERMAL ENERGY CONVERSION TO ELECTRIC AT 70% CARNOT EFFICIENCY USING 100°F REJECTION TEMPERATURE

Fig. 3.   Calculated Fall (season) performance
of collector types at Albuquerque, N.M.

COUNTER
BALANCE

COUNTERBALANCE
PULLEY ASSY

DISH SUPPORT
WHEEL (TYP)

AZIMUTH
FRAME

ELEVATION
ACTUATOR

AZIMUTH
ACTUATOR

AZIMUTH
TRACK

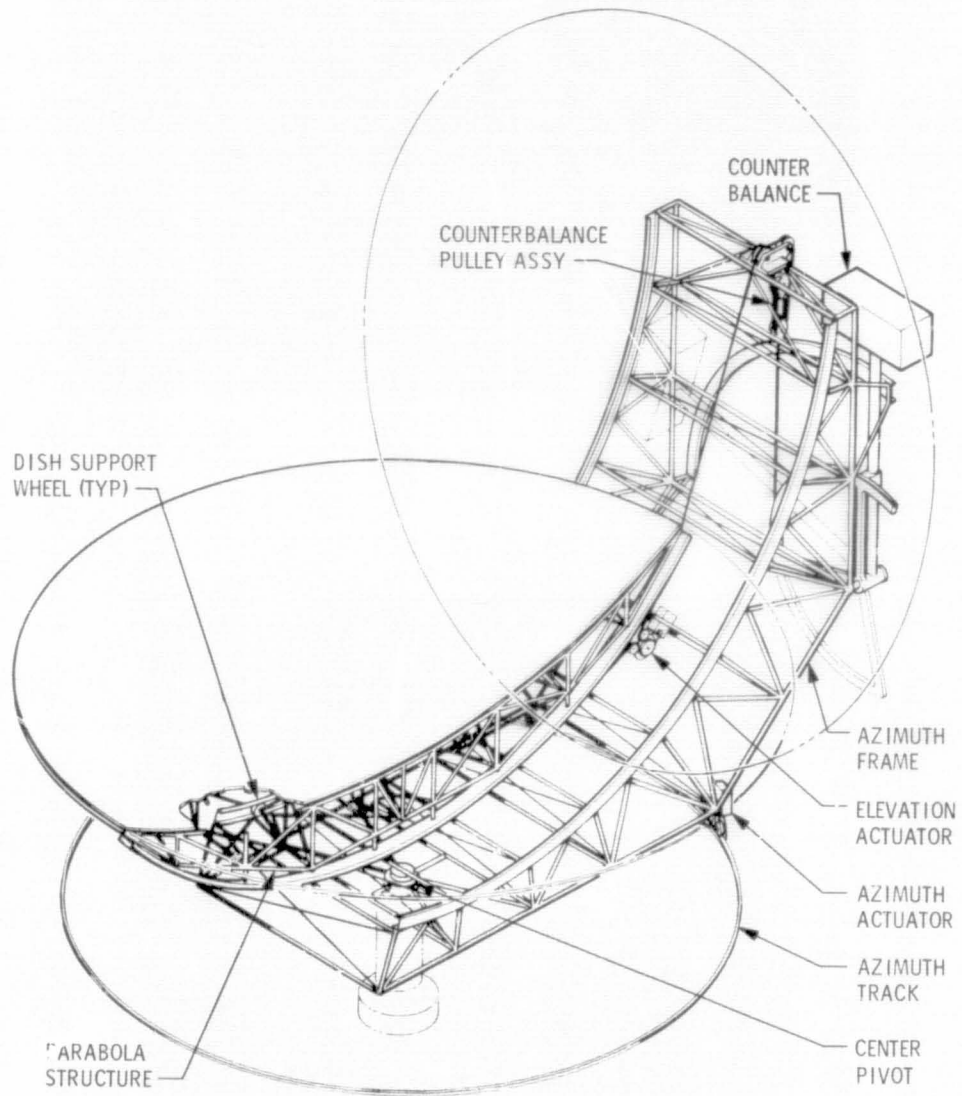PARABOLA
STRUCTURE

CENTER
PIVOT

Fig. 4.   Solar tracker assembly
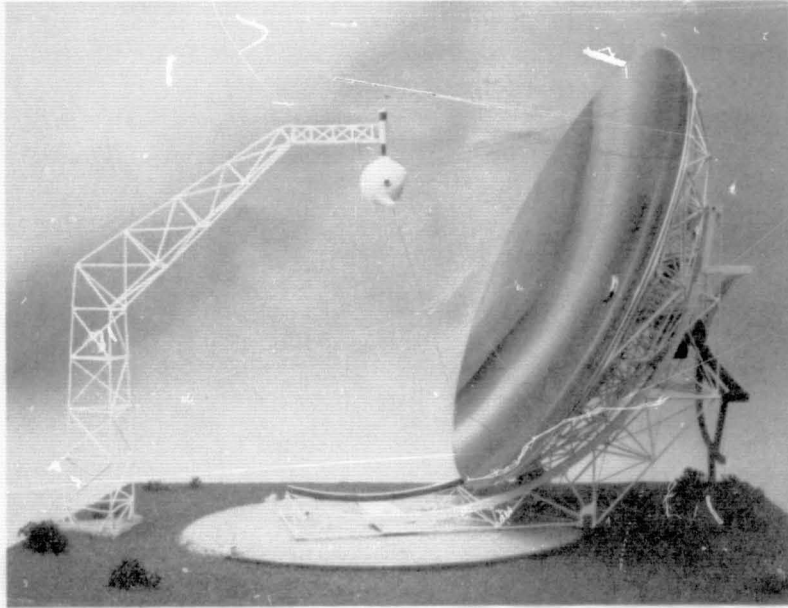
Fig. 5.   Solar tracker assembly, side view
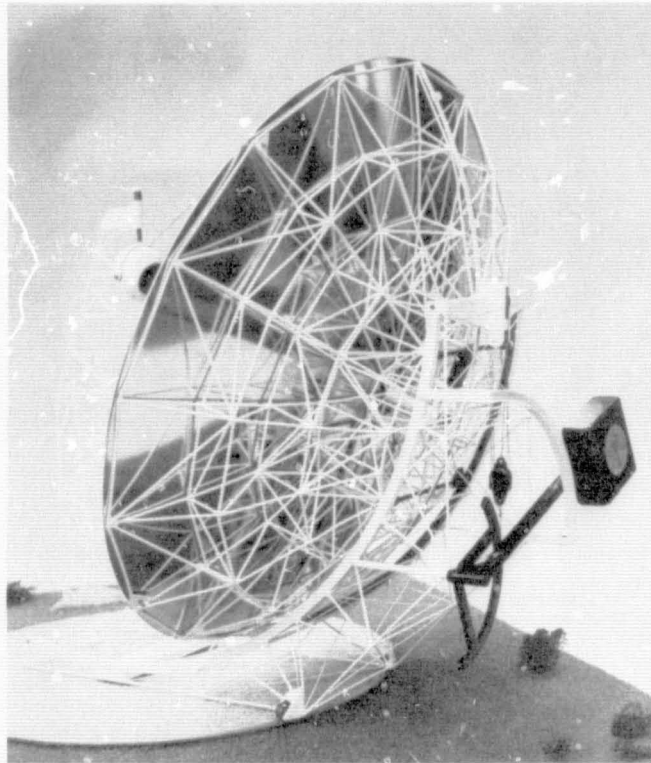
Fig. 6.   Solar tracker assembly, rear view

166
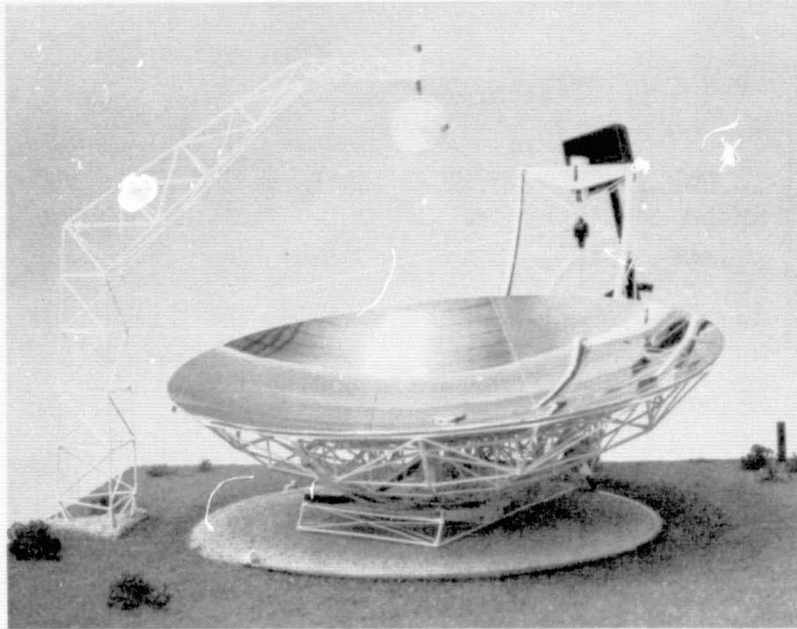
Fig. 7. Solar tracker assembly, stow position
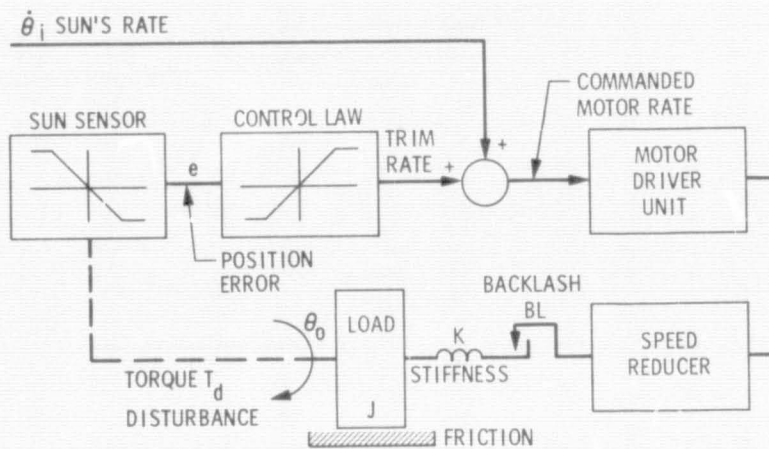
Fig. 8. Collector control system, typical
for either axis

167

COST	PROTOTYPE	3-10 UNITS	10-100 UNITS	100-1000 UNITS	50 000 UNITS
COST PER FOOT^2	60	21.25	16.27	12.97	9.93
STEEL FABRICATION COST PER POUND	3.38	2.40	1.71	1.39	1.10
LABOR/MATERIALS RATIO	5.01	1.36	1.17	1.13	1.11

Fig. 9.   Economic and cost data
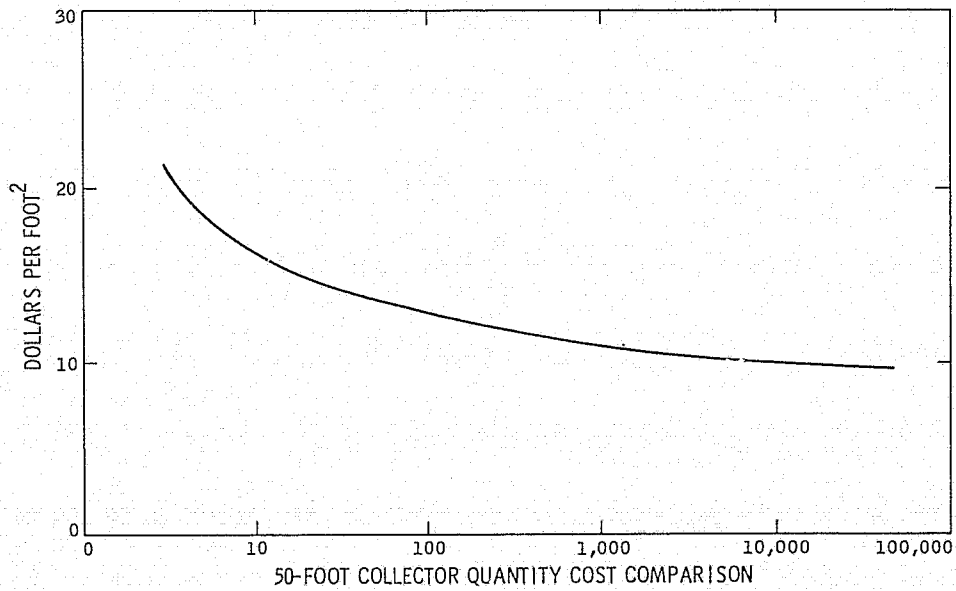
Fig. 10.   Collector manufacturing lots

168
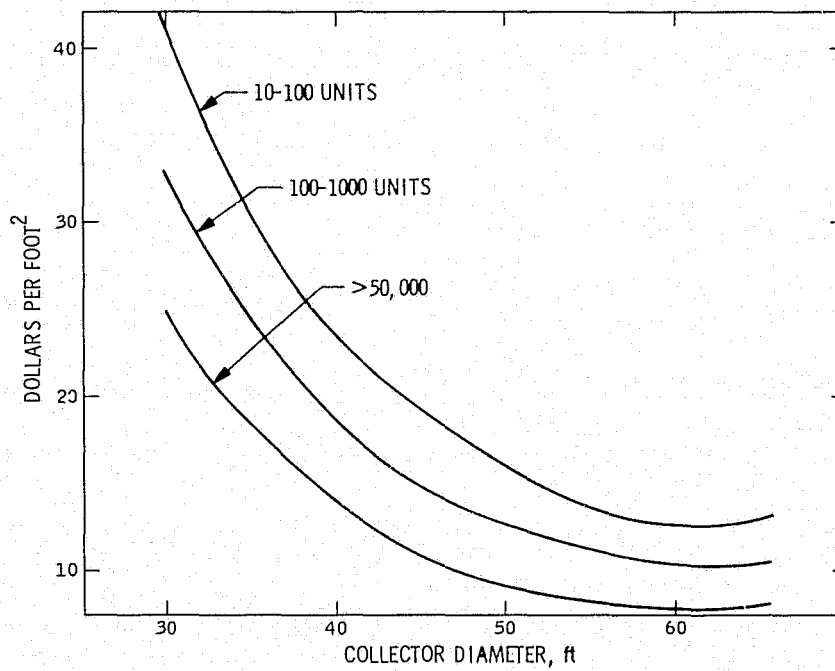
Fig. 11.   Collector size cost comparison

TWO-DIMENSIONAL OSCILLATING AIRFOIL TEST APPARATUS

By Frank L. Gibson, Andrew J. Hocker, Jr.,
and Dennis S. Matsuhiro

NASA Ames Research Center

ABSTRACT

A Two-Dimensional Oscillating Airfoil Test Apparatus is presented as a method of measuring unsteady aerodynamic forces on an airfoil or rotor blade section. The oscillating airfoil test rig, which is being built for use in NASA Ames Research Center's 11x11-foot Transonic Wind Tunnel (speed range M = 0.4 - 1.4), will allow determination of unsteady loadings and detailed pressure distributions on representative airfoil sections undergoing simulated pitching and flapping motions. This paper will present the design details of the motion generating system and supporting structure. This apparatus is now in the construction phase.

INTRODUCTION

Experimental unsteady aerodynamic data are urgently needed to validate and guide computational aerodynamics research in process at Ames, Langley, and the Air Force Flight Dynamics Laboratory. Data obtained with this apparatus will be compared with theoretical work concerning boundary layer effects on aileron flutter. Boundary layer effects are a major reason for the large uncertainty and consequent weight penalty associated with current predictions of control surface or flap flutter at transonic speeds.

A helicopter blade in forward flight is subjected to wide variety of unsteady loads due to aerodynamic effects. The effects of cyclic pitch, flapping motions, and the asymmetry caused by advancing and retreating blades all contribute to unsteady aerodynamic loads. The unsteady flow is extremely complex because the speed regime may change from subsonic through transonic to supersonic in one revolution. The importance of predicting these forces becomes especially important at high forward speed where transonic effects on stability and flutter margins degrade performance. A rational theoretical study for unsteady aerodynamics is extremely complex; therefore, a concerted effort was directed by Ames Research Center into the design of a Two-Dimensional Oscillating Airfoil Test Apparatus. The test apparatus was especially designed to apply programmed pitching and heaving motions to the test airfoil so that different simulated blade systems could be included in the test program.

BASIC OPERATION

The Two-Dimensional Oscillating Airfoil Test Apparatus (see Figure 1) will oscillate a 20-inch (0.51 meter) chord, 54-inch (1.37 meter) span airfoil in

Ames' 11x11-foot Transonic Wind Tunnel at frequencies from 0 to 60 HZ. The test objective will be to oscillate the airfoil at pitch angles to ± 2° of rotation about any point along the chord and also to vertically displace the airfoil up to ± 2-inches. The mean angle of attack of the airfoil will be variable over the range of -5° to +15°. Before each test, wedge blocks are manually installed between the top flexure and wing to obtain the desired angle of attack. See Figure 3.

The oscillating motions are produced by motion generators which are hydraulic actuators with push-pull rods connected to the airfoil. Two pairs of high performance servo-controlled linear-hydraulic actuators induce the motion. One pair of actuators is for driving the leading edge and the other pair for driving the trailing edge of the airfoil. Actuator cross-coupling is provided by the lightweight airfoil structure. The actuators contain two pistons on a common rod for the dynamic and static loads. Each actuator drives identical graphite-epoxy push rods and flexure bearings which attach to the four corners of the test airfoil.

TEST APPARATUS

Motion Generators

The servo-hydraulic actuator package was designed and built by M.T.S. System Corp. (Minneapolis, Minnesota) to Ames' specifications and will be driven by two 150 HP units rated at 65 GPM and 3000 PSI. Each actuator consists of two separate pistons on a single rod enclosed in a dual chamber cylinder as shown in Figure 2. The upper piston is used for generating dynamic forces. The lower section is for load biasing. The load bias system is used to support the constant aerodynamic load thereby reducing the size and power required for the dynamic cylinder. The load biasing circuit includes an accumulator to maintain a constant load bias force along with differential control. This load biasing section is controlled by a servo-valve system with a resonance frequency below 0.5 HZ. This system allows slow dynamic movement yet maintains static preload. As static bias requirements change, the servo-valve ports oil into the appropriate end of the cylinder. This essentially changes the accumulator (nitrogen precharge) and adjusts the static force output.

A velocity and position transducer are mounted in the center of the actuator. They combine into a single physical unit with coils and cores in line axially for placement within the hollow actuator rod.

The displacement or dynamic section is controlled by a high performance servo-valve coupled through a manifold into the cylinder. The valve spool lap is adjusted to achieve flow linearity of better than ± 2% to 35 GPM. The manifold houses adjustable cross-port relief valves. To keep the breakaway friction below 8 pounds force, controlled leakage clearance fits and labyrinth grooves are used on both piston and end caps.

A hydraulic service manifold between the power unit and servo-actuator provides hydraulic filtration and suppresses line pressure fluctuation in the

high electrohydraulic actuator supply and return lines. This service manifold also houses safety features which include provisions for automatic low pressure shutdown and solenoid valves to relieve all system pressure.

The wing is mounted to push-pull rods through flexure bearings. The airfoil is a lightweight graphite-epoxy structure designed to withstand a 230 G acceleration and a 10,000 pound aerodynamic load. See Figure 3. Extensive development in the fields of engineering, fabrication techniques, and testing was performed at the Ames Research Center in order to obtain an acceptable graphite-epoxy structure of various configurations. The first natural bending frequency is above 100 HZ and the first torsional mode is above 60 HZ. Forty (40) dynamic pressure transducers and forty (40) static pressure taps are imbedded in the skin of the airfoil. Samples laminated like the final airfoil design had the following properties: an ultimate tensile stress of 130 KSI (8.96×10^8 N/M^2), a modulus of elasticity of 14×10^6 PSI (9.65×10^{10} N/M^2), and a density of 0.6 LBM/IN^3 (1.66×10^4 KG/M^3).

Support Structure

Included in the test apparatus are splitter plates with trailing edge flaps and side struts. The splitter plates are a practical method of supporting the two-dimensional model wing in the test section without extensive modification to the wind tunnel test section. All instrumentation in the model wing is funneled down through the central part of the splitter plate. Approximately 130 static pressure orifices are imbedded in the surface of the splitter chordwise and exit through the top of the splitter plate. Also, the splitter plate serves as a mount for the drag link and stabilizes the model wing in the lateral direction.

Trailing edge flaps were incorporated to adjust the pressure gradient in the channel between the splitters. Adjustments of the flaps are continuous, as opposed to discrete, and are remotely controlled. Angles between ± 5 degrees can be obtained about the center line of the flap.

The side strut is a supporting member to stabilize the splitter plates and to eliminate excessive deflection in the lateral direction due to aerodynamic loads imposed on the splitter plates (See Figure 1). The side struts are fastened to the splitter plates and protrude through the tunnel wall to the exterior tunnel structure.

PRETEST SETUP

A dynamic test will be conducted on the motion generators before installation into the 11-foot wind tunnel. All of these component designs are pushing the state-of-the-art and no previous test information is available to judge their worthiness when used in combination. Figure 4 illustrates the test setup. The test will determine what performance levels can be expected from the hydraulic system, the push-pull rods, the flexures, and the wing. The model will be preloaded by an underside airbag. The model wing will be oscillated vertically, causing a fluctuation in surface loading. In addition, the effect of the cyclic loading on the flexures and push-pull rods will be determined.

CONCLUDING REMARKS

The Two-Dimensional Test Apparatus was designed to apply programmed pitching and heaving motions to the test airfoil so that various applications to blade systems can be included in the test program. The results of these tests will be used as input parameters for the dynamic analysis of existing rotorcraft and for checking numerical and analytical schemes for advanced rotors. This paper has described an oscillating mechanism for wind tunnel studies which should provide the motions necessary for generating this aerodynamic data.

TWO-DIMENSIONAL OSCILLATING AIRFOIL TEST APPARATUS

WIND TUNNEL TEST
SECTION OUTLINE

SPLITTER PLATES

SIDE STRUT

SPLITTER FLAP

SIDE STRUT

MODEL WING

AIRFLOW

HYDRAULIC ACTUATORS

DRIVE RODS

SUPPORT COLUMNS
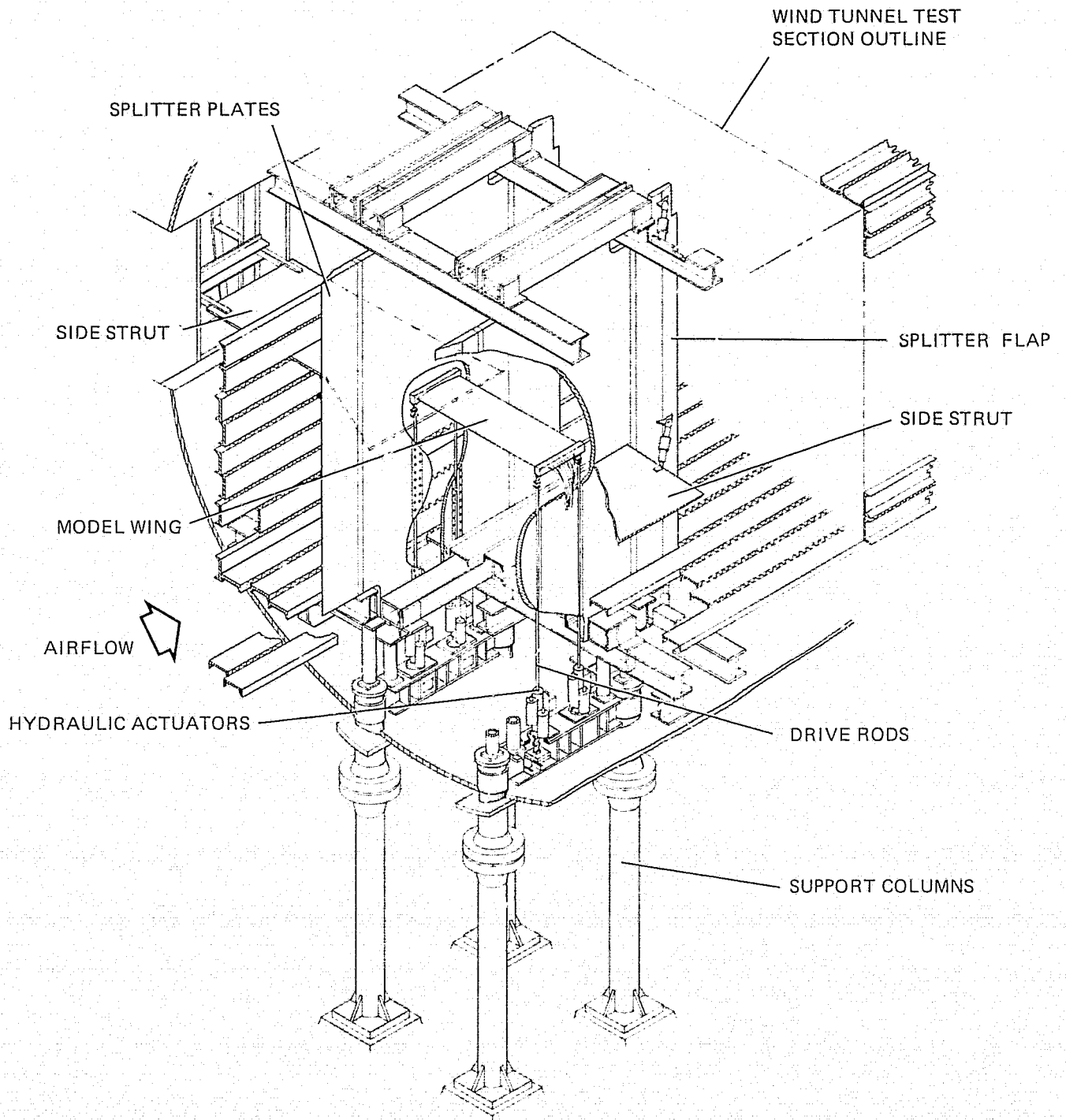
Figure 1 WIND TUNNEL INSTALLATION OF TWO DIMENSIONAL
OSCILLATING WING TEST APPARATUS

175

TWO-DIMENSIONAL OSCILLATING AIRFOIL TEST APPARATUS

CYLINDER ROD

CYLINDER

LOAD BIASING
ACCUMULATORS

DISPLACEMENT SERVO VALVE

ACCUMULATORS

LOADING BIASING
SERVO VALVE
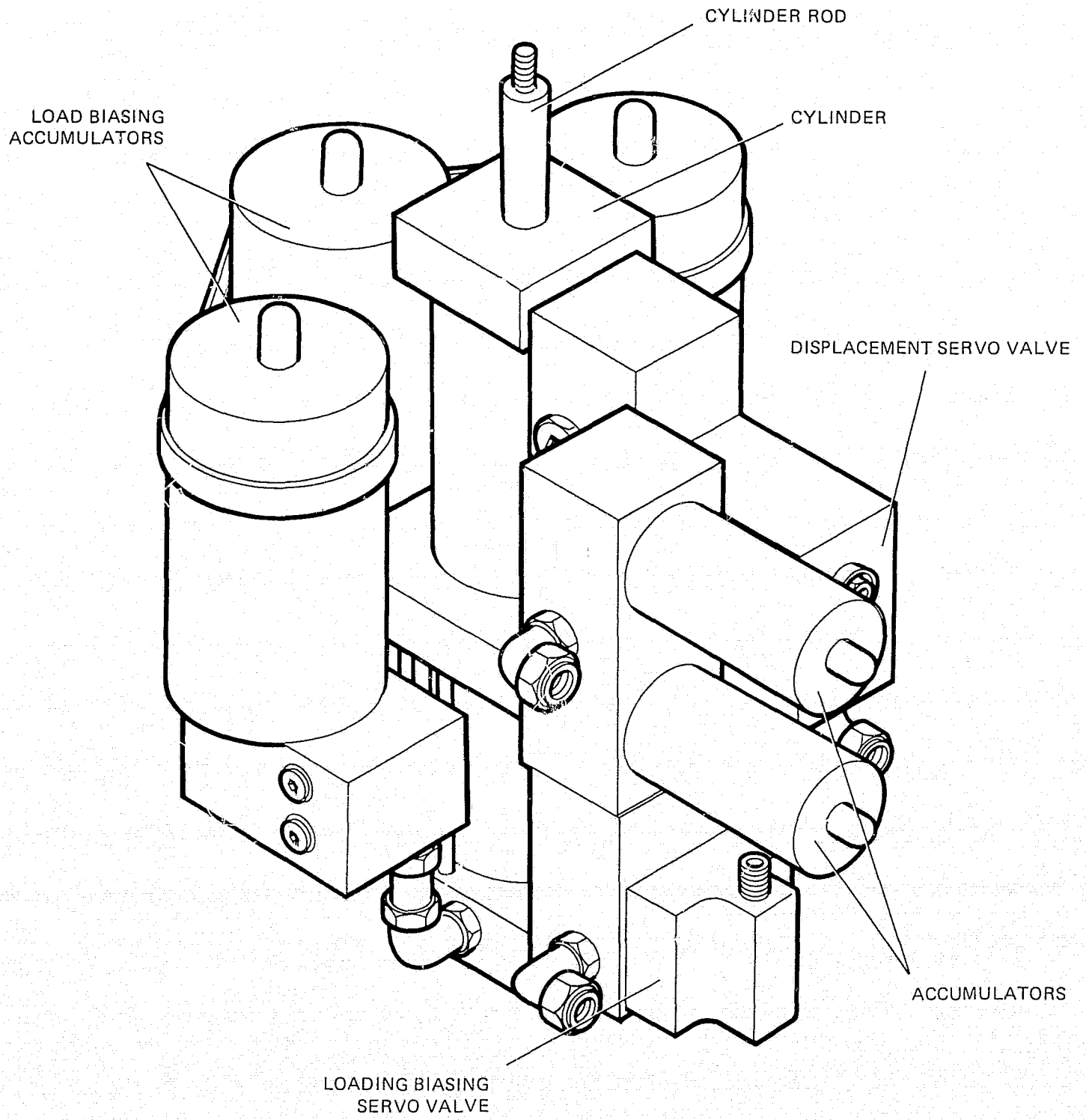
Figure 2 HYDRAULIC ACTUATOR

TWO-DIMENSIONAL OSCILLATING AIRFOIL TEST APPARATUS

CLAMP BOLTS

PRESSURE TRANSDUCER

ANGLE OF ATTACK WEDGE
BLOCKS FORE AND AFT

FLEXURE
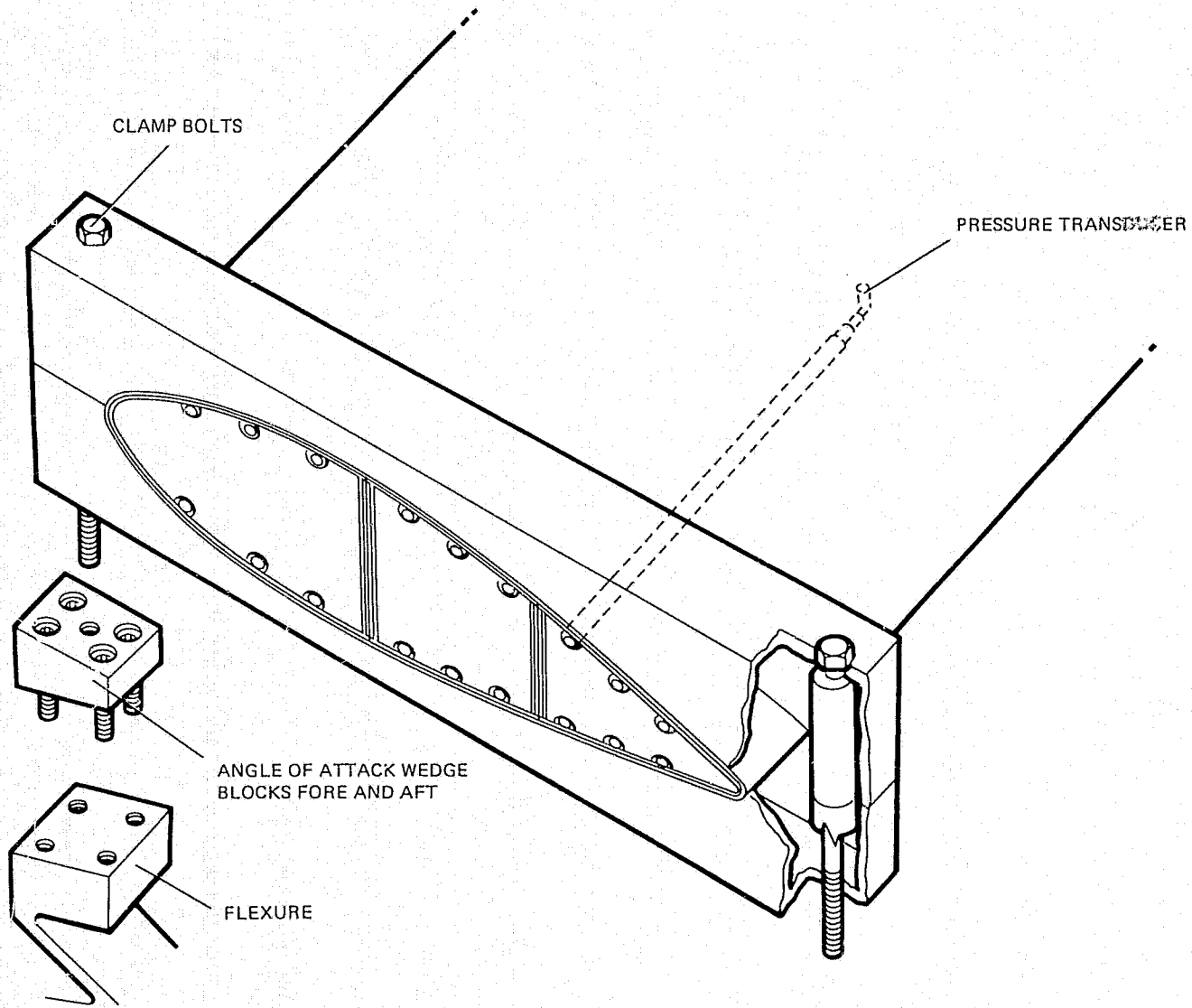
Figure 3 MODEL WING

TWO-DIMENSIONAL OSCILLATING AIRFOIL TEST APPARATUS

LATERAL STABLIZER

MODEL WING

DRAG LINK

DRAG LOAD SIMULATOR

FLEXURE

AFT DRIVE RODS

TEST STAND

HYDRAULIC ACTUATORS
FORE AND AFT

SUPPORT BASE
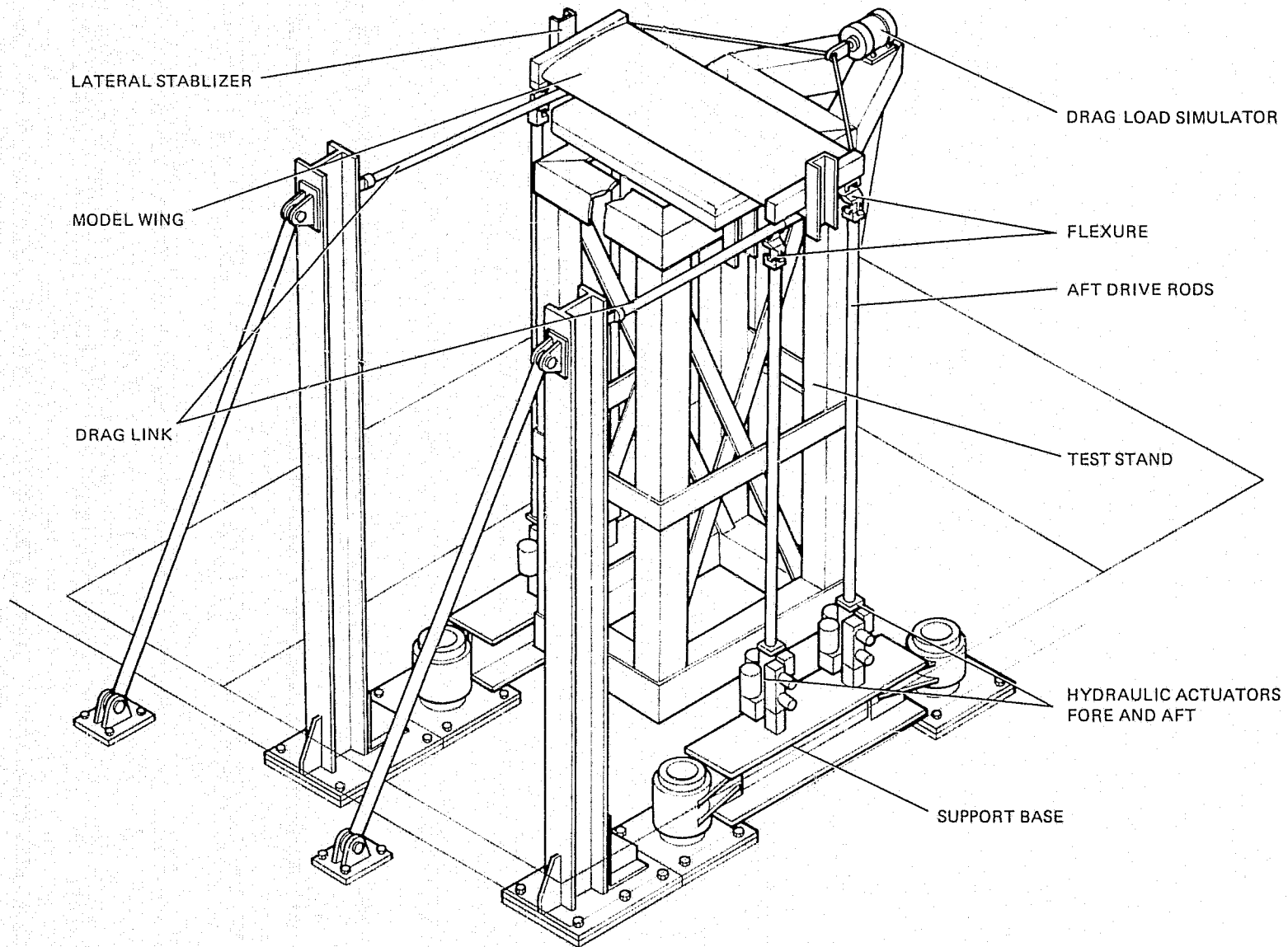
Figure 4 DYNAMIC TEST STAND

DEVELOPMENT OF A SATELLITE FLYWHEEL FAMILY

OPERATING ON

"ONE ACTIVE AXIS" MAGNETIC BEARINGS. [x]

By Pierre C. Poubeau

AEROSPATIALE
ETABLISSEMENT DES MUREAUX - FRANCE.

ABSTRACT

Since the Samarium-Cobalt magnets were available at industrial level, new possibilities appeared in the area of magnetic bearings with the radial passive centering and axial active control of the rotor position. This paper describes magnetic bearings of this type on which a wide effort was made towards the optimization for satellite flywheel applications. It describes also the momentum and reaction wheels already developed or presently under development and the extension of this work to the kinetic storage of energy for satellites.

I-ADVANTAGES OF THE "ONE ACTIVE AXIS" MAGNETIC BEARINGS FOR SATELLITE FLYWHEELS.

The interest of the magnetic bearings for satellite momentum and reaction wheels, allowing the operation of the equipment without any mechanical contact between rotor and stator, was often described ; therefore it is only useful to summarize the advantages of such a system.

- Elimination of the life limiting wear processes of ball bearings.

- Reduced mass ; it is possible to replace two or more conventional wheels by one magnetically suspended rotor wheel, with "no single point failure" the redundancy being implemented in the active part only.

- Improved performances concerning stiction and friction torques which are reduced by several orders of magnitude with elimination of the temperature effect ; consequently, the friction power is reduced.

- Higher speeds allowing a significative improvement in the momentum/mass ratio of the wheels.

- Higher reliability of the "one active axis" magnetic bearings compared to other types of magnetic suspension and to the ball bearings.

II- MAIN PARAMETERS OF SATELLITE FLYWHEEL MAGNETIC BEARINGS

The main parameters on which is based the design of satellite flywheel magnetic bearings are indicated here :

- The radial stiffness which defines the critical speed of the suspension together with the mass of the wheel rotor.

- The transverses stiffness (angular stiffness about an axis perpendicular to the axis of rotation of the rotor) ; for a given angular momentum it defines the maximum slew rate that the flywheel can accept taking into account the possible angular displacement of the axis of the rotor towards the axis of the stator.

- The damping of radial oscillations for critical speed crossing when the maximal speed exceeds the critical speed and the nutation damping.

- The mass of the overall device.

- The power necessary for the axial servoloop, and to compensate the overall losses in the range of useful torques and speeds.

- The reliability of the electronically controled axial servoloop and the possibility of redundancy with no single point failure in the overall equipment.

The design of a magnetic suspension oriented towards the optimization from the point of view of the above indicated parameters was undertaken ; models were fabricated and tested. The successful operation of the magnetic suspension gave birth to a family of satellite flywheel engineering and qualification models, the objectives consisting in covering the range of following applications (the numerical figures are given as order of magnitude) :

- Medium speed momentum wheels from 10 Nms up to some hundred Nms and 12.000 RPM.

- High speed momentum wheel angular momentum in the range of 100 Nms for 24.000 RPM ; this technology gives the possibility with further development, to provide kinetic energy storage capacity with mass improved characteristics and long life reliability compared to the chemical batteries.

- Reaction wheels up to 15 Nms and 3000 RPM.

- Reaction or momentum wheels with specific characteristics (low level of vibration, high angular momentum reaction wheels, etc..).

IV – DESCRIPTION OF THE MAGNETIC BEARINGS.

IV.1) Radial Centering

The radial centering of the rotor is provided by magnetic rings operating in attraction, the dimensions, disposition (side by side axially or radially) and number of which are defined according to the specific characteristics of each equipment. A centering ring on the rotor faces a centering ring on the stator. Each ring is constituted by two iron sleeves with an internal segmented ring of samarium-cobalt magnets. The axial magnetic field between the iron sleeves produces a restoring force as soon as the rotor magnetic ring axis is not exactly coincident with the stator one. The radial stiffness is currently in the range of 1.5 to 5.10^5 N/m (15 to 50 kg/mm) and can be extended to several times these values in increasing the number of centering rings. The choice of the different parameters of the centering rings (thickness and height of magnets and iron sleeves) gives a wide range of possible characteristics such as : radial to axial stiffness ratio, e.g. 2.1 to 3.5 and radial stiffness to mass ratio e.g. 6 to 8.10^5 N/m/kg.
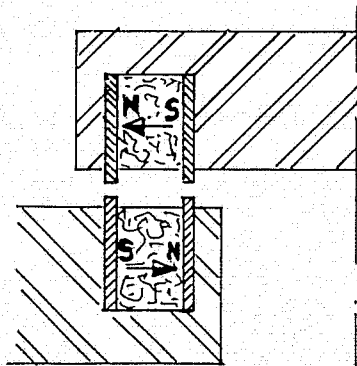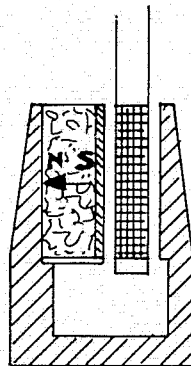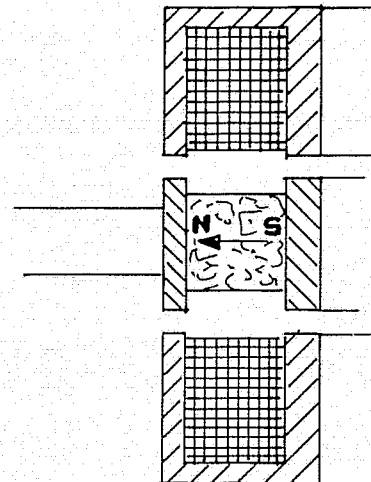

Figure 1

Figure 2

Figure 3

IV.2 Axial position control of the rotor.

The attraction between the iron sleeves providing the radial restoring force involves an axial negative stiffness and consequently an instable equilibrium position which is made stable by an electronically controlled servoloop. This servoloop includes :

- An axial rate electrodynamic sensor (Figure 2) .

- An axial actuator constituted by two electromagnets attached to the stationnary central shaft and a magnetic biaised circuit fixed to the rotor (Figure 3).

- An electronics circuit controlling the current in the coils of the electromagnets.

The input signals of the electronics are :

- A voltage signal proportional to the axial rate of the rotor.

- A voltage signal proportional to the current in the electromagnets.

A lift-off logic enables initial operation of the servoloop from the rest position when the power supply is switched on.

IV.3 Damping system

The damping system is necessary for the critical speed crossing. The system chosen is of the electrodynamic type. A magnetic circuit on the rotor, constituted by samarium cobalt segmented rings, provides a magnetic induction in a gap in which a copper disk is fixed to the stationary central shaft. The magnetic field has a revolution symetry without azimuthal variation of induction ; there is an energy dissipation only when the rotor translation or nutation oscillations occur.

The smoothing of the magnetic field variations in the gap is provided by iron (or ferromagnetic material) sleeves according to two configurations (Figures 4 and 5).

The damping ratio obtained for 50 to 100 Nms wheels, according to the radial stiffness and to the mass of damper material, is in the range of 0.02 to 0.08.

Instead of a copper disk, it is possible to adapt three coils at 120° or four coils at 90°. When these coils are electronically short-circuited, they provide the damping on the same bases as the copper disk ; but it is also possible to amplify the current induced in these coils and to provide a higher damping coefficient in this active damping configuration.

Another application of the damping system in which the copper disk is replaced by coils consists in modifying the orientation of the axis of rotation of the rotor by sending permanent currents in the coils. The electrodynamic

forces produced between these currents and the magnetic field, are vectorially added. (Figures 6 and 7).
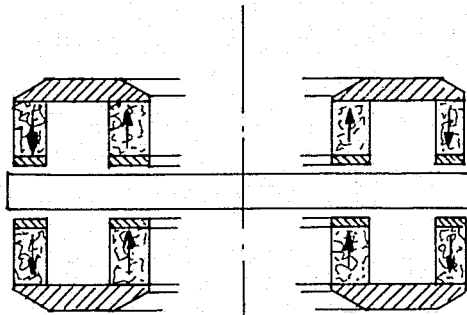
Figure 4
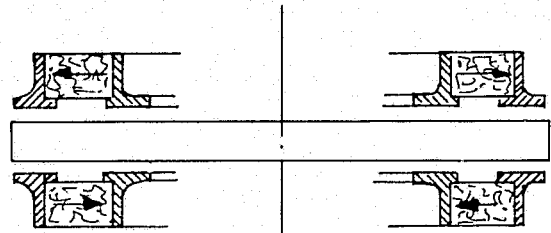
Figure 5
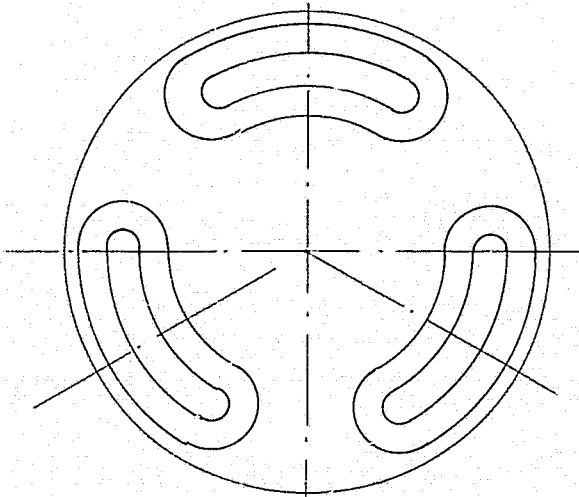
Figure 6
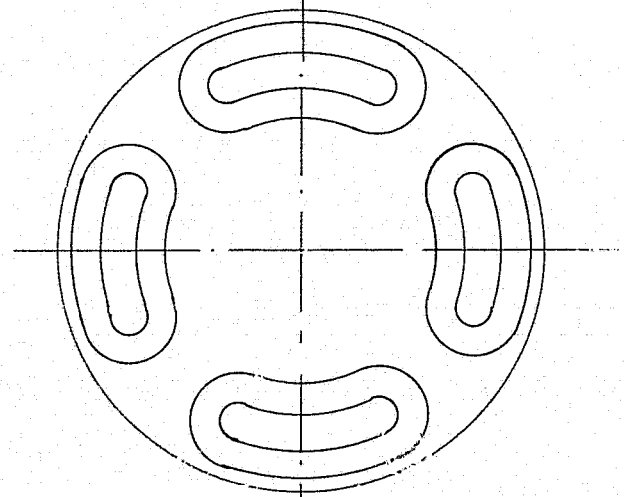
Figure 7

Combined with the restoring forces of the centering rings, these electro-dynamic forces allow a rotation around an axis different of the centering ring axis. This solution has a possible application in the energy storage system. It allows the compensation of mechanical misalignments between the axis of the two counter-rotating bodies and of the misalignment of the resulting angular momentum in relation to its nominal position.

V   ASSOCIATED SUBSYSTEMS IN A MAGNETIC BEARING SATELLITE FLYWHEEL

Motor

The acceleration and deceleration torques are provided by an electronics commutation iron-less DC motor-generator. According to each specific wheel design the number of poles was, till now, between 12 and 24. It can be adapted for each

case. In the case of a reaction wheel the rotating magnetic circuit of the motor is integrated in the rim of the wheel in order that the mass of the motor can participate to the inertia.

For the deceleration the motor operates as a generator. Several systems of commutation were developed and tested :

- Photo-diodes/ photos transistors commutation.

- Hall effect cells commutation.

- Electromagnetic sensor commutation, which is chosen for equipments presently under development ; a windowed sleeve on the rotor crosses the magnetic flux of stator ferrite coils fed with a high frequency signal. The Q factor of the coils is modified by the windowed sleeve, according to the relative angular position of the rotor in relation to the stator.

The resulting signals are utilized to open or close the gates controlling the current in the motor coils. Two types of windings were successively experimented with 3 and 4 circuits sequentialy commuted. The useful torques were either 0.05 or 0.1 Nm. Much higher torques can be produced. The efficiency of the motor itself without the control electronics is of 95 % at the maximum torque at nominal speed and higher for lower torques.

Rotor

The rotor is constituted of several functional parts :

- The central part which contains the elements of the magnetic bearings and, generally, for momentum wheels the magnetic circuit of the motor.

- The rim which produces the main part of the inertia and which includes the magnetic circuit of the motor in the case of reaction wheels.

- The connexion between the central part of the rotor and the rim.

Two main problems are in relation with the rotor rim and its connexion to the centering rings although the central part of the rotor.

- To accept the stresses due to centrifugal forces.

- To keep an accurate balancing : i.e. to maintain the coincidence between the axis of the rotor centering rings and the main axis of inertia with a high level of accuracy. This accuracy will have to remain stable in spite of launch vibrations, of elongation due to centrifugal forces, of temperature variations, of time effect associated to the above indicated parameters.

Several solutions were developed and tested :

- Aluminium alloys rim with two different centerings on the magnetic bearing : by spokes and by cônes.

- Composite filament material rim also with two different centerings : by spokes and by a special technique called "eyeloprofile".

The high speed rotors need filament material, and special techniques to achieve a stable balancing. The following one was selected for the 24.000 RPM. The rotor consists of three parts : an aluminium alloy hub that is used as interface between the filament rotor assembly and the rotor shaft, a circumferentially wound filament rim, and the cycloprofile envelope windings that attach the rim to the hub. The rim is wound about a mandrel. After curing, the mandrel and rim are finish machined. The envelope winding consists of two layers of filament tape. After the tape is cured, the mandrel is washed away. Three complete rotors have been fabricated, one in glass fiber, one in graphite fiber, and one in KEVLAR 49.

Emergency bearings.

Ball bearings specially treated for ultra vacuum are utilized for touch down operation of the rotor ; they are able to allow the deceleration of the rotor, in the case where the power supply or the axial servoloop are disrupted. In normal operation, there is not contact between the rotor and the emergency bearings.

Caging mechanism

The first solution which was designed and tested to lock the rotor on the fixation flange of the wheel was similar to the Marman clamp locking a satellite on the upper stage of its launcher. This solution is available when it is considered that the wheel can be locked after its tests and installed on the satellite without any further test before orbital operation. In many cases, it will appear necessary to have a test controling the operation of the wheel during the count down operation. A locking device which can be operated by remote control was developed and is now a part of the basic concept.

Housing

In the early model a light alloy ventilated housing was adopted. On the models presently in test and development, the housing is replaced by a very light carbon fiber structure with three arms. Its purpose is principaly to stiffen the upper part of the central fixed shaft by a mechanical connexion to the lower flange of the wheel.

Electronics

The electronics which is specific of a wheel provides two functions :

- The data processing of the input signals of the axial servoloop to control the current in the biaised electromagnets.

- The commutation of the motor.

The axial servoloop has to operate in stable conditions with sufficient phase and gain safety margins. This is obtained by adjusting the transfer function taking into account the negative axial stiffness of the magnetic centering

185

ring added to the axial stiffness of the axial actuator, the rotor mass and the mechanical resonances of the different parts of the rotor.

A lift-off logic provides the necessary signals for initial operation when rotor is resting on one of the emergency bearing and when the circuits are switched on. The electronics of the early models was based on the utilization of operational amplifiers. When the feasibility of the magnetic bearing was demonstrated, the electronics was completely redesigned. The new concept utilizes only conventional transistors which allows the operation exclusively on the 28 volts power supply. In the case of lack of the 28 volts power supply, the motor operating as a generator, is able to feed the electronics of the axial servoloop in the momentum wheel configuration during about half an hour before the rotor goes back to the emergency bearings.

The electronics is able to operate in "hot redundancy or cold redundancy" for the axial servoloop. In hot redundancy, the coils of the electromagnets are doubled and the two coils are energized simultaneously by two separate electronics circuits. If one of the circuit operation is wrong, it is detected by a surveying logic and the concerned circuit is switched off.

The electronics is presently existing in discrete components. The transposition in hybrid thick film circuit is presently under development. The operation of the discrete component electronics was tested in the range $- 30°$ C to $+ 70°$ C. The mass of the electronics with a redundancy of order 2 is the following :

$$\text{Cordwood technology} : 1.4 \text{ Kg}$$

$$\text{Hybrid thick film circuit} : 0.6 \text{ Kg}$$

In the cordwood technology the electronics package is outside of the wheel with interconnecting plug. The hybrid circuits are fixed inside the wheel on the lower flange with direct interconnexion. A wheel drive electronics was developed : it allows as well the control of the torque as the control of the speed.

VI – APPLICATION OF THE MAGNETIC SUSPENSION AND ASSOCIATED SUBSYSTEMS TO SATELLITE FLYWHEELS.

The above described subsystems were first applied on in-house laboratory models for verification of their validity. Later they gave birth to a complete family of satellite flywheels. Several models were developed and submitted to functional and environmental tests ; others are presently under development up to qualification tests and long duration operation.

VI.1 – In house momentum wheel engineering and prototype models.

Several models were successively developed since 1969 for the experimentation of the different subsystems and for the experimentation of the overall concepts.

- EM1 and EM2 models ; Period 1969-1971 :

These models were utilized for the initial application of peripheral ironless brushless DC motor to laboratory model of flywheels operating on self lubricated journal and pivot bearings.

- EM3 model ; Period 1971-1973 :

This model was utilized for comparison of different types of magnetic suspensions of the rotor :
. attraction compared with repulsion radial centering ;
. radial compared with axial polarisation of magnets for the centering rings operating in attraction ;
. axial control provided by separated centering rings and actuator compared with actuator integrated in the centering rings ;
. motor with iron in the stator contributing to the radial centering compared with motor without iron in the stator and producing no radial or axial stiffness.

In each case the subsystems were studied and tested separately and later they were tested in operation on the EM3 model.

- EM4 model ; Period 1973-1974 :

This laboratory model was a preliminary experimental configuration of a satellite flywheel leting appear all the experimental aspects of the assembly of the different subsystems already theoritically studied and experimented in the EM3 model. The EM4 model was a direct preparation of the medium speed and high speed engineering momentum wheel models, developed respectively since november 1973 and february 74 in the frame of the ESA and INTELSAT contracts.

- EM5 model ; Period 1975-1977 :

This model was utilized to prepare the final optimization of the magnetic bearing momentum wheel. The optimization of the centering rings, actuator dampers, motor was separately performed and the choices were tested in the EM5 model. This model will be delivered to CNES for tests or an air bearing.

- Medium Speed Qualification Prototype ; 1975-1977 :

This model was developed in order to have a prototype made on the bases of complete set of drawings and procedures at the level of satellite hardware quality. This model is realized on the same principles as the EM5 model. After the qualification tests performed in 1976, three sets of equipment will be utilized in long duration experimentation for demonstrating the operational validity of the system by long term systematic operation. The purposes of these tests are to demonstrate the operational validity of the system and particularly to confirm the stability of the axial servoloop.

The existence of this model will make possible the utilization of magnetic bearing momentum wheels for early program. The developed medium speed prototype covers the range of applications of geosynchronous telecommunications satellites of the Intelsat V class.

With a mass of 11 Kg5 all the active electric circuits of the wheel are redundants ; the possibility of remote control of the caging mechanism allows the complete verification of the axial servoloop and motor torque capability during the count down before launch.

VI.2 - Momentum wheels engineering models developed under contracts.

- ESA Medium Speed Momentum Wheel engineering model - Period 1973-1975 :

This model was developed on the ESTEC 2038/73 contract starting in november 1973. It was involving a 50 Nms $\pm$ 10 % wheel rotating at 7.700 RPM $\pm$ 10 % The characteristics are given in the annexed table and the concept in the annexed plate.

- INTELSAT High Speed Momentum Wheel engineering model - Period 1974-1976 :

This model was developed on the INTELSAT IS 555 contract (Fébruary 74). It was involving a 100 Nms wheel rotating at least at 24.000 RPM. The characteristics are given in the annexed table, the concept in the annexed plate. The experimentation of this model up to 24.000 RPM demonstrated several points :

. the validity of the "one active axis" magnetic suspension for high speed rotors ;
. the wide safety margin of the axial servoloop towards the excitations of the high rotation speed ;
. the validity of the damping system even at high speed without excessive eddy current losses ;
. the possibility of operating composite filament rotors at rotation speeds enabling to envision kinetic energy storage for long life satellite at the place of chemical batteries.

This model was successfully submitted to environmental tests (thermal between - 20° C and + 50° C;vibrations tests according to COMSAT specifications).

- ESA Medium Speed Momentum Wheel optimization prototype , Period 1975-1977

This model was developed in the frame of the ESTEC 2481/75 contract since november 1975. The purpose is to have an optimization of the "one active axis" magnetic bearing momentum wheel for the range of 50 Nms taking into account :

. the mass and dimensions ;
. the power ;
. the slew rate ;
. the caging mechanism ;
. the reliability and redundancies ;
. the hybrid thick film electronics.

The characteristics are given in the annexed table.

The realization is made in order to be able to adjust some characteristics according to each program equipment with or without remote control of clamping mechanism, slew rates from 0.01 to 0.1, level of redundancy of the axial actuator, level of torque in the range up to 0.1 Nms, without questionning the overall concept. From the minimal to the maximal capabilities, the range of mass is from 8 to 11 Kg.

VI.3 – In-house reaction wheel engineering model – Period 1976-1977

A 2 Nms reaction wheel engineering model utilizing the same principle of magnetic suspension as the momentum wheels was designed, fabricated and tested. It utilizes the rotating parts of the motor to contribute to the inertia of the rim. The rotating speed is 2.000 RPM and the radial stiffness of the centering rings added to the radial stiffness of the axial actuator is sufficient to avoid the crossing of the critical speed which is at 3.000 RPM. The concept can be extrapolated up to 15 Nms (Characteristics and view in annexed table and plate). This model will be delivered to CNES in 1977 for tests on an air-bearing table.

VI.4 Reaction Wheel engineering model under ESTEC contract – Period 1976-1977

This development, in the frame of the 2470/76 contract, covers the study of an optimized concept of magnetic bearing reaction wheel for the range of 1 to 5 Nms. An engineering model of 2 Nms is being realized. The characteristics are given in the annexed table. The concept can be extrapolated up to 15 Nms.

VI5 In-house studies and development in the field of kinetic energy storage for satellites.

The successfull operation of magnetically suspended high speed rotors performed in the INTELSAT IS 555 contract demonstrated the possibility of storing energy under kinetic form by two counter-rotating wheels. The range of stored energy is from 10 Watt/hour per kilogramme to 50 Watt/hour per kilogramme for peripheral speed of the rotor going from 500 m/sec. to 1000 m/sec. and for level of energy of 0.5 to several KW/hour. As well the magnetic bearing as the characteristic of composite filament material such as carbon fiber-epoxy or kevlar 49 (1) - epoxy let appear the validity of the research work in this field. Such a work is in progress: it utilizes 2 wheels of the High Speed Momentum Wheel type developed under INTELSAT contract (and one spare). The control of the operation is made by a microprocessor. The purpose is to verify the following points :

    - the capability of the system to provide the control of the torque on the two wheels in order to maintain the resulting angular momentum along the main axis of the wheel at the right value, in spite of input and output of power into and from the two wheels : correlatively, the system has to provide the control

(1) Dupont de Nemours trade mark.

of this resulting angular momentum by the attitud control signal of the satelli-
te for the concern axis.

     - to cancel the components of the angular momentum due to residual misali-
gnment of the two wheels even if they are very small, taking into account the
large angular momentum of each wheel.

     The first step in this long term development is the control of the torques
of the two wheels taking into account the maximal and minimal output of power
and the variation of moment of inertia due to elongations, variations of the
rotor when the speed is varying. This phase is foreseen to be completely covered
in 1977.

VII - CONCLUSION

     After a considerable development effort including functional and environ-
mental qualifications, satellite flywheels (momentum and reaction wheels) opera-
ting on "one active axis", magnetic bearings are now at the level of industrial
production. In the same time, a great need appears for this type of equipment.

     This development carried on largely with in-house effort, benefited from
wide international participation. We take this opportunity to mention and to
state our appreciations for part taken by the Representatives of international
organizations involved in this programm : C.J. PENTLICKI for INTELSAT/COMSAT
High Speed Momentum Wheel and A.A. ROBINSON for ESA Medium Speed Momentum and
Reaction Wheels. Their suggestions and advices were of the greatest interest,
particularly when difficult technical choices and trade offs were to be made.

	TYPE OF FLYWHEEL	DIAM. mm	HEIGHT mm	MASS Kg	TORQUE Nm	SLEW RATE rad/s	STEADY STATE POWER Watts	RELIABILITY
MEDIUM SPEED MOMENTUM WHEELS	ESA ENGINEERING MODEL 50 NMS – 7.700 RPM	350	220	10,5 ⊠	0.1	0.04	9	0.98 to 0.995 according to the type of electronics circuits for 2 redundant channels.
	ESA PROTOTYPE 50 NMS – 7.700 RPM	350	180	8.5 to 11.5	0.1	0.04 to 0.1	9	
	IN-HOUSE QUALIFICATION PROTOTYPE 50 NMS – 7.700 RPM	350	220	11.5	0.1	0.06		
HIGH SPEED	INTELSAT ENGINEERING MODEL 100 NMS – 24.000 RPM	350	220	11	0.05	0.02	9 W at 8000 RPM 25 W at 24000 RPM	
REACTION WHEELS	IN-HOUSE ENGINEERING MODEL 2 NMS – 2000 RPM	230	150	5	0.1	0.1	8	
	ESA ENGINEERING MODEL 1-5 NMS – 3000 RPM	250	120	3.7 to 4.5	0.1	0.1	3	

ELECTRONICS	
COORDWOOD TECHNOLOGY	0.7 dm^3 ; 0.7 Kg (1 channel) 1.3 dm^3 ; 1.4 Kg (2 redundant channels)
THICK FILM TECHNOLOGY	0.3 dm^3 ; 0.350 Kg (1 channel) 0.5 dm^3 ; 0.6 Kg (2 redundant channels)

⊠ Without caging device for launch restraint.

Figure 8. Magnetic Bearing Momentum and Reaction Wheel Characteristics
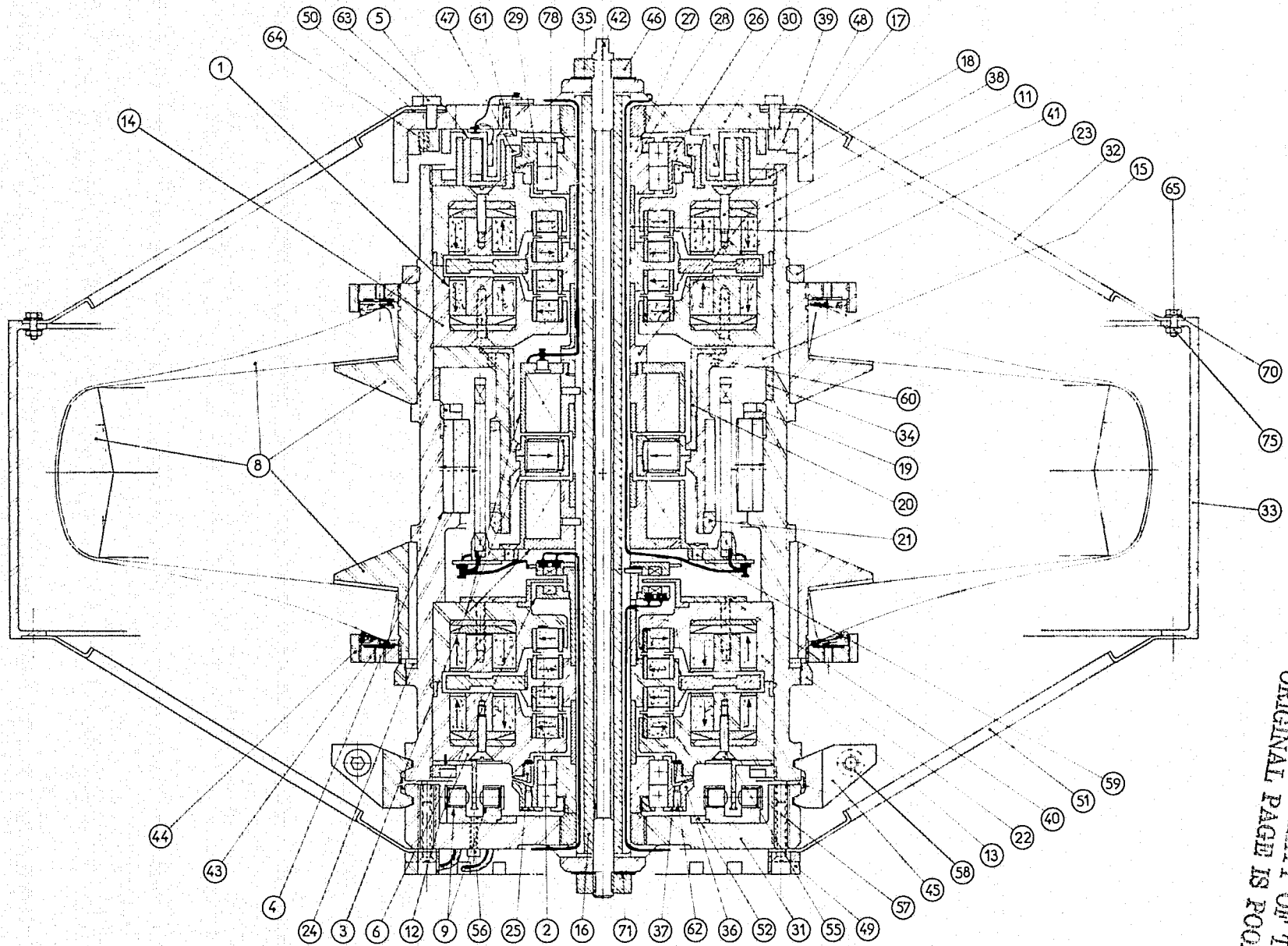
Figure 9. High Speed Momentum Wheel
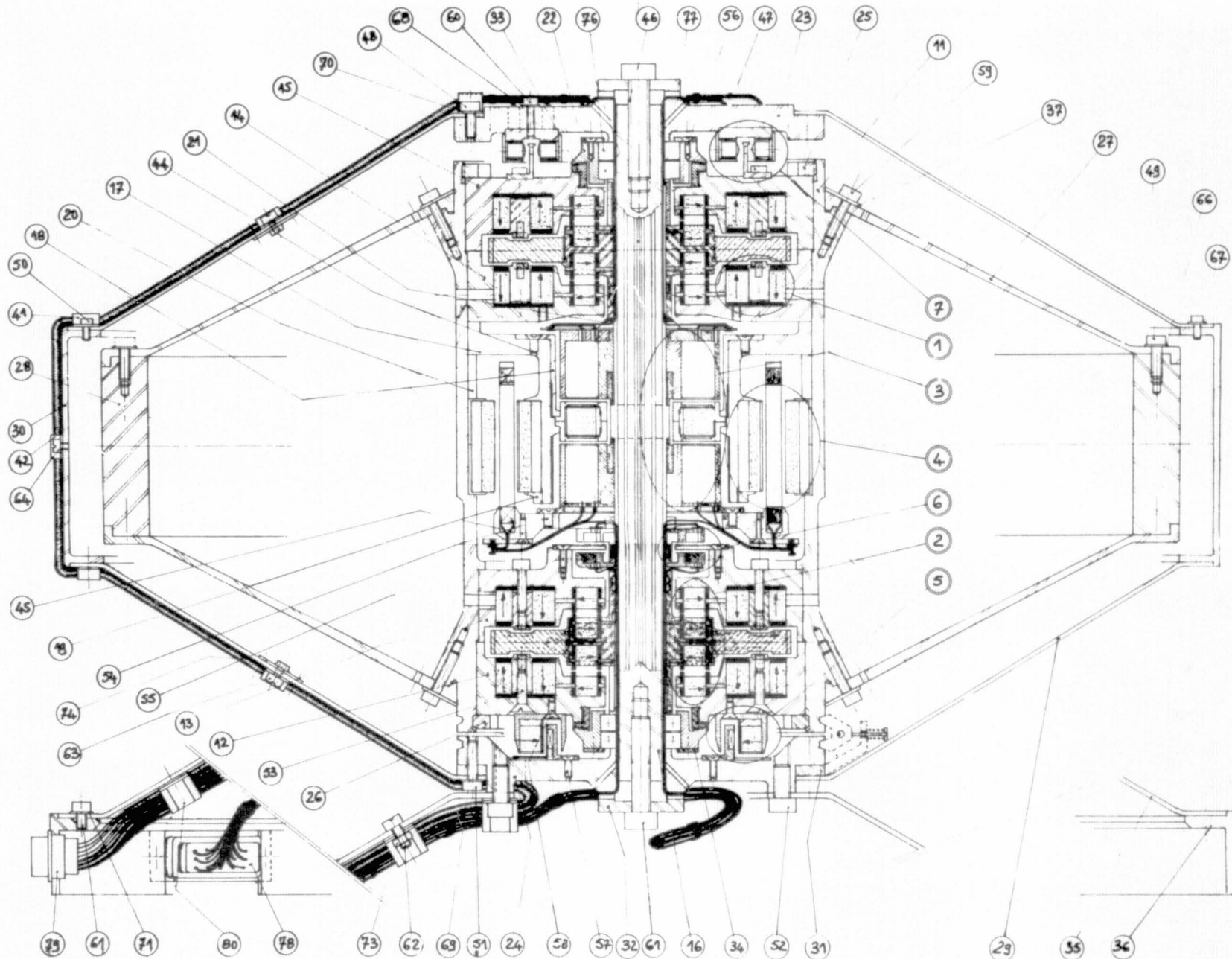
Figure 10. Medium Speed Momentum Wheel
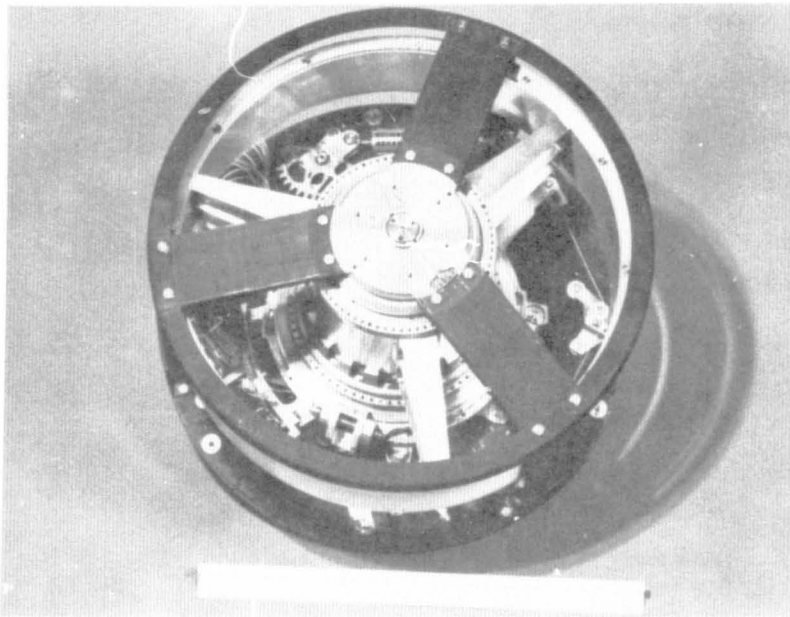
Figure 11. 50 Nms Momentum Wheel Qualification Model
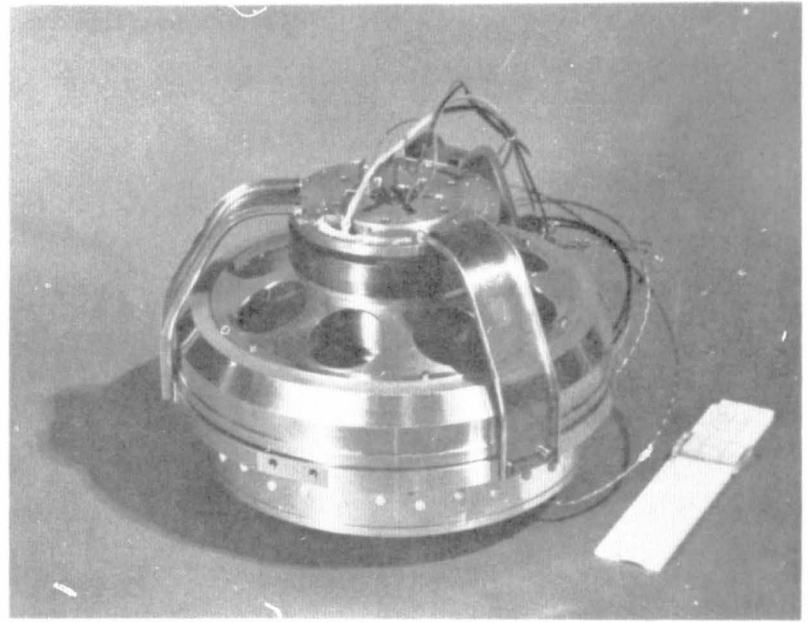
Figure 12. 2 Nms Reaction Wheel Engineering Model
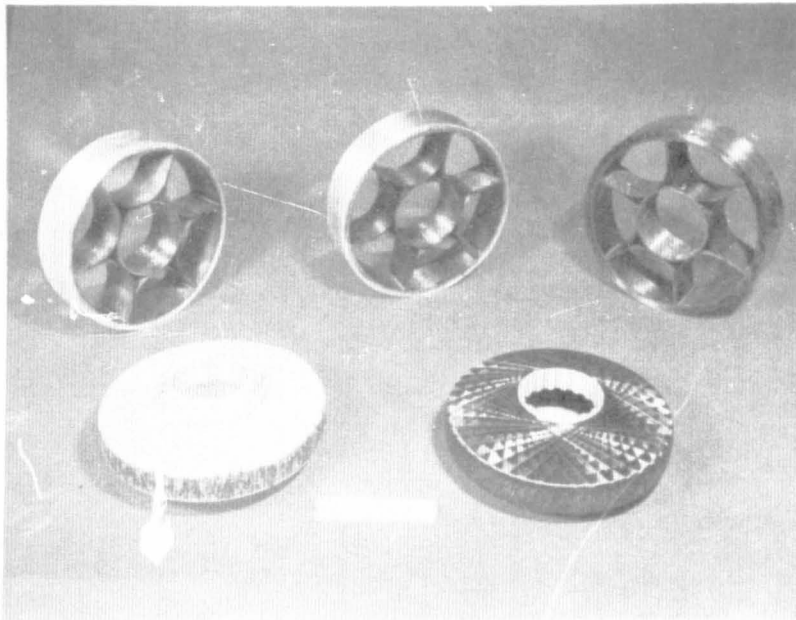
Figure 13. Composite Filament Rotors

Figure 14. High Speed Momentum Wheel in Vacuum Chamber
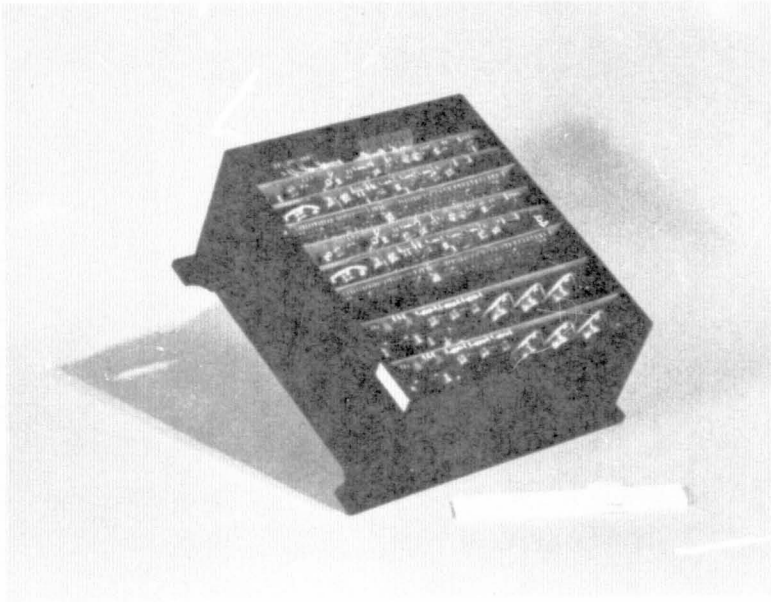
Figure 15. Control Electronics for Momentum and Reaction Wheels

Figure 16. Electronics Breadboard Model for Kinetic Energy Storage

THE CONCEPTION, BIRTH, AND GROWTH OF A MISSILE UMBILICAL SYSTEM

By Glenn W. Nordman

Martin Marietta Corporation

Orlando Division

ABSTRACT

This paper traces the design development of the SPRINT II and Improved SPRINT II Missile System (ISMS) umbilical system. It describes the unique system requirements, umbilical designs considered to meet the requirements, and the pr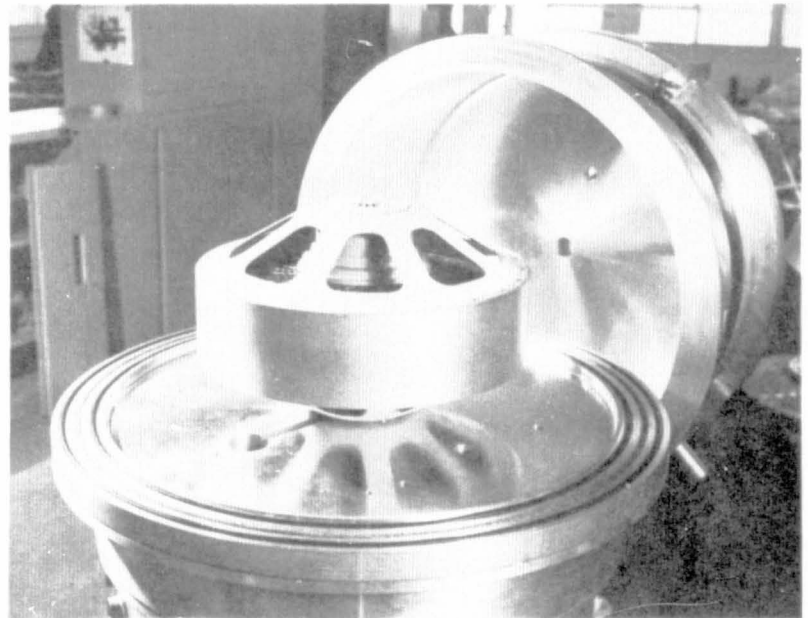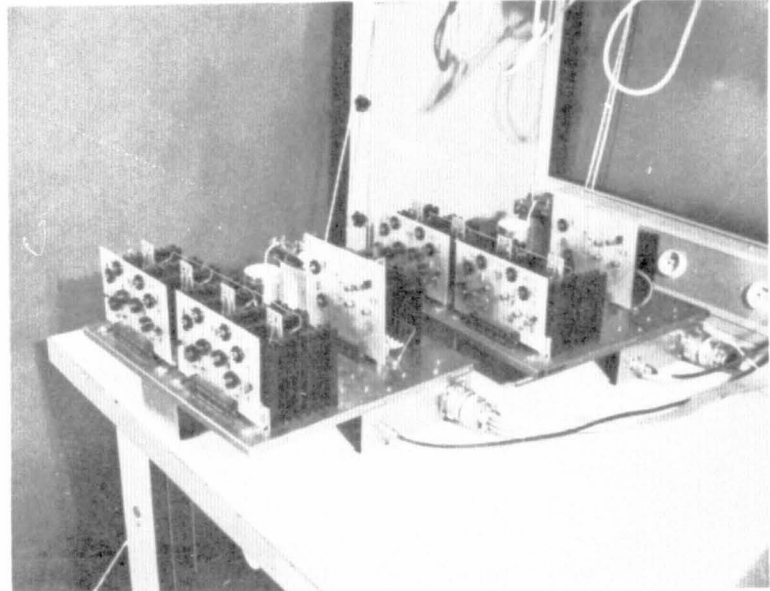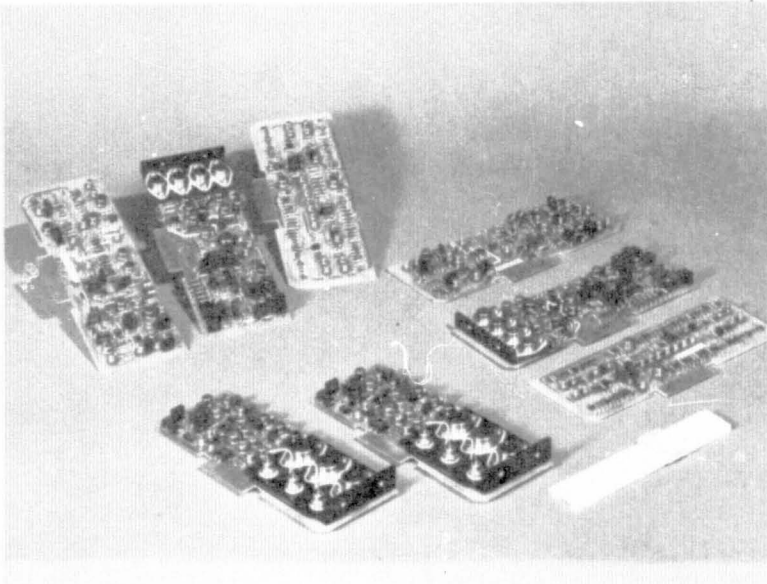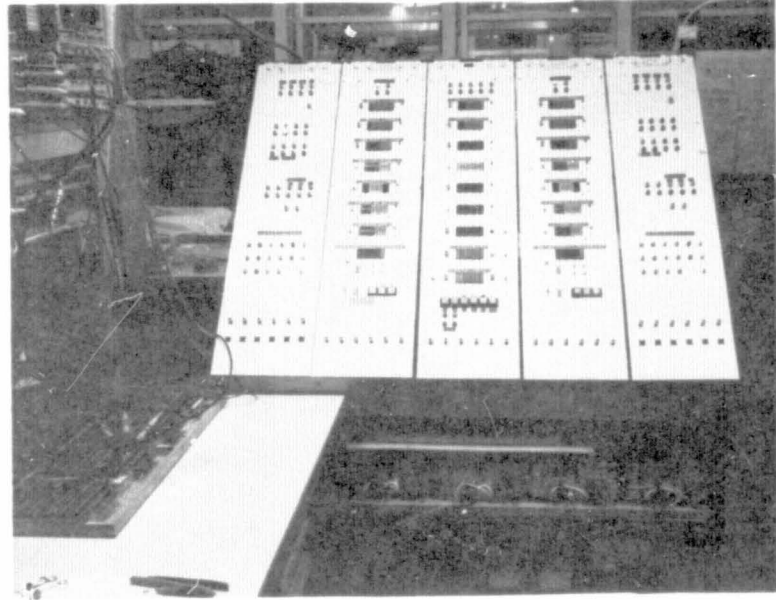oblems encountered and solutions derived during the design and development testing of the selected systems. The SPRINT II development effort consisted of design, analysis and testing activities. The ISMS effort involved the performance of an extensive trade study to determine the optimum design to meet the ISMS conditions.

INTRODUCTION

The task of the quick reaction, high velocity SPRINT missile is to intercept intercontinental ballistic missiles at relatively short range. The nature of the mission involves exposure to the nuclear environment, and increasingly severe operational requirements were imposed on the SPRINT missile systems as they evolved from the SAFEGUARD system to the SPRINT II system and the ISMS. These, in turn, required greater capabilities of the umbilical system. The task of the umbilical system is to transmit electrical signals and power between the missile and ground equipment prior to launch. The umbilical system must disengage and clear the launch envelope within system time constraints without adversely affecting the launch.

SPRINT II MISSILE LAUNCH STATION DESCRIPTION

The SPRINT II launch station with missile is shown in Figure 1. The station consists of a full-length steel launch tube with a circumferential compartment containing the umbilical system and related equipment. Two umbilical mechanisms are mounted within the Launch Preparation Equipment Compartment. The umbilical cables enter the launch cell through small holes in the cell wall and engage the missile near its tip. The missile contacts the launch

cell wall sufficiently to permit pressurization beneath the missile during launch. Thus, the umbilical must retract fully behind the launch cell wall during launch. The umbilical facilities must not create discontinuities that could affect the missile during launch. As the SPRINT II missile umbilical receptacle location on the missile was determined prior to the umbilical design effort, the umbilical considered the missile interface only at that location.

UMBILICAL SYSTEM REQUIREMENTS

The umbilical mechanism must meet the following requirements:

Be easily, safely, and quickly connected and disconnected by personnel during maintenance operations, and must transmit electrical signals and sensor signals between the missile, launch station equipment, and interfacing subsystems.

Remain electrically and mechanically connected to the missile during benign, ground shock and airblast conditions.

Electrically disconnect upon command within 30 milliseconds (MS) during benign and ground shock conditions.

Mechanically clear the launch envelope within 70 MS without impeding missile launch or creating debris affecting missile launch.

Attenuate magnetic and plane wave fields over a wide frequency range. It must not adversely affect missile heat shield integrity.

SPRINT II UMBILICAL MECHANISM DESCRIPTION

The final design of one of the two identical systems within the launch station is shown in Figure 2. The mechanism consists of two electrical cable assemblies, each with a flexible metal shield that is attached to the connector, an umbilical frame with a fixed pulley, a compression spring and attached traveling pulley, and snubber box with decelerating material, spring pack and split nut explosive cartridge, and two wire rope cables.

The electrical cables are connected to the missile umbilical receptacles, and the cable shields are secured to the spring pack. One wire rope is attached to the spring pack and to the clevis held by the split nut explosive cartridge. One end of the second wire rope is attached to the umbilical frame and rove through the pulleys. The spring is compressed and the free end of the wire rope is secured to the clevis at the split nut. Upon command, the explosive cartridge fires, causing separation of the split nut segments. The clevis is released and the spring force is exerted

on the wire ropes, which in turn pull on the electrical cable shields. Spring collets within the electrical connectors release when the disconnect load exceeds the connector spring load, thus disengaging the connectors from the missile receptacles. The force provided by the expanding spring pulls the connectors through the cell opening against the snubber material. A slight force is maintained on the cables, after retraction is completed, to assure their retention in the snubber box.

SPRINT II RETRACT MECHANISM DEVELOPMENT

During the SPRINT II retraction mechanism development program analyses were performed to determine the necessary umbilical capabilities required to meet system requirements. Engineering model equipment was fabricated and tests were conducted to verify the system's performance. The tests consisted of retraction in a benign, no ground shock, environment. Retraction tests with simulated ground shock conditions were also performed. Dynamic testing of the umbilical cable assemblies engaged with their missile receptacles evaluated connector retention capabilities.

The following major design problems were addressed during the design and development of the SPRINT II Umbilical system:

Missile-Cell Interface Compatibility

The conflicting requirements for a cell surface that would not affect missile launch and the desire for a large opening through which the umbilical cables and connectors could be retracted led to consideration of doors on the cell wall that would close after cable retraction. Structural, dynamic, and retract time considerations nullified that concept. A compromise solution involved the use of a 6.5 inch diameter hole through which the assemblies were retracted. The open hole introduced the possibility of excessive launch gas pressure loss. Computer analysis indicated that the design with the snubber box and decelerator material in position would reduce gas loss to acceptable levels.

Cable-Connector Motion During Retract

The umbilical system must accommodate, without disconnection, missile-cell relative motions approximately ±2.0 inches in the vertical direction and ±2.5 inches horizontally due to ground shock conditions. Successful retraction must be accomplished with relative motions approximately ±0.1 inch vertically and ±2.0 inches horizontally.

This requirement led to conduction of an extensive retraction test program to determine cable motions during retract. It was found that application of the retraction force to the connector at the

missile was satisfactory as long as the umbilical cable remained straight in the cell. However, the changing distance between the cell hole and the receptacle due to missile-cell motions would likely cause cable bending which would result in an excessive amount of cable within the cell. Tests were conducted to determine the effect on retract action of slack cable within the cell. It was found that the cables were not stiff enough to retract through the hole, and the connectors struck the wall rather than passing through the hole. The point of load application was moved from the connectors to a point on the cables behind the cell face. Tests verified that, contrary to expectations, this change did not improve cable action during retract. The connectors continued to strike the cell wall when slack cable was introduced in the cell. The system was redesigned, with the addition of the snubber box spring pack to maintain a tension on the cables at all times. Dynamic tests to 70g from 0 to 400 Hz verified connector retention. Retraction tests under static and dynamic conditions verified the ability to retract without damage.

Time Constraints

The SPRINT missile system countdown is understandably short. The countdown timeline requires transmission of a signal indicating that the umbilical is disconnected prior to missile first motion. Missile motion during eject, however, commences prior to complete retraction. A maximum of 30 milliseconds is allotted between retract command and electrical disconnection; an additional 70 milliseconds, maximum, is permitted for complete retraction. This limit is imposed to avoid umbilical contact with the rising missile. Tests verified consistent disconnection times within 25 milliseconds and retraction times within 60 milliseconds.

Loads

The missile-cell ground motions introduce high loads that tend to separate the connector and missile receptacles. Continuous electrical continuity is vital and care must be taken to assure that even intermittent signal losses are avoided. Thus, the connector-receptacle retention load must be high enough to assure retention. This load must be overcome by the retract mechanism and, in addition, enough force must be applied to accelerate the assemblies to the cell wall within the allotted time interval. Upon reaching the wall, they must be decelerated without damage. During tests, the disconnection loads were 1000 to 1200 pounds per cable pair, retraction loads were 1200 to 1600 pounds per cable pair, and deceleration loads were 700 to 1100 pounds per cable pair. Of interest is the fact that proper design of the decelerator permits arresting loads lower than the maximum loads imposed during retraction.

Cost

The cost of the resultant umbilical system is an important design
consideration, as the SPRINT program was engaged in a design-to-
cost effort. The selected system must be technically correct and,
in addition, must meet the design-to-cost target established for
the item. The selected system has been determined to be cost
effective.

SPRINT II CONNECTOR DESIGN EVALUATION

Three methods of connector retention were explored and tested
for the SPRINT II umbilical application, Figure 3.

The first, a conventional ball detent connector, was dis-
carded because the high concentrated loads applied to the shell
by the few balls resulted in rapid wear. Also, the retraction
force had to be applied at the connector to unlock the locking
collar. The application of force at the connector end of the
cable introduced the possibility of the cable bending within the
cell, thus preventing retraction through the umbilical hole.

In the second design, two fracture bolts retained each
connector to its receptacle. The bolts were captive on the
connector and screwed into the receptacle. The bolts had a necked
area that fractured as the retraction load was applied. This
design was an improvement over the ball detent method, as the
retraction force was applied to the cable outside the launch cell
and point wear was avoided. The small diameter (0.064 inch)
within the necked portion of the bolts was a major disadvantage,
as inadvertent overtightening and fracture of a bolt could occur
within the confined launch cell area. Inadvertent tool loss was
also a possibility.

In the third design, which is the one selected for implemen-
tation, the connector is screwed into the receptacle for initial
engagement. Thus, the engagement is initiated at no load. As the
thread collar is tightened, a collet spring is compressed to
achieve a 500-pound preload. When the disconnect load exceeds
preload during retraction operations, a collar is retracted, per-
mitting the peripheral collets to disengage within the shell and
release the connector from the receptacle. A braided wire shield
attached to the connector and extending through the cell hole
provides mechanical strength and electromagnetic (EM) protection.
The shield avoids application of force on the wire cable during
retraction.

IMPROVED SPRINT II MISSILE SYSTEM (ISMS)

The SPRINT II missile had the same umbilical interface point as used in the earlier SAFEGUARD SPRINT missile. The SPRINT II design evolved about that interface. However, for the ISMS the missile guidance control system was revised, also potential motor changes were evaluated. The guidance package configuration and increased system capabilities made a change to the umbilical interface desirable. The motor changes provided the opportunity to consider using a tailplug umbilical design on ISMS. Thus the interface could occur in a variety of radial and longitudinal locations. In addition to the above, the ISMS EM and ground shock levels exceeded the SPRINT II requirement. To assure adequate consideration of all aspects of the umbilical function to meet the ISMS requirement, a trade study was performed covering the mechanical and electrical portions of the system. All design and design support disciplines were represented. Five umbilical disconnection and retraction concepts were investigated as shown in Figure 4. Several alternative techniques were proposed under each concept. The electrical portion of the system was also evaluated. Eight types of connectors were reviewed. The compatible connector-mechanical systems were selected.

Mechanical Design

Retract Concept - Each technique explored within this concept requires that the umbilical cable be retracted through an opening in the launch cell wall in a manner similar to that of the SPRINT II system.

Several methods of providing the motive force were investigated: mechanical spring, stored gas pressure, missile exhaust gas pressure, and missile motion.

Flyaway Concept - In each of the techniques studied under this concept, the umbilical cable remains engaged with the missile as it begins its eject motion. When the umbilical is disconnected, it continues its upward motion until the end of the tether line is reached. The cable then moves outward from the missile to clear the launch envelope. As the cell end of the umbilical cable is secured at the upper end of the launch station, the cables do not have to be retracted to clear the envelope. This concept eliminates the requirement for retract mechanisms, spring pack mechanisms, and snubber devices. Increased cable shielding is required due to the higher EM levels above the launch station.

Tailplug Concept - This concept theoretically offers the advantage of a passive umbilical mechanism, as the umbilical remains fixed in position and the missile moves from it during eject. The problems associated with this concept include assurance of positive and accurate engagement of the blind mated connectors

during missile installation and the missile design impact of routing the additional electrical wires from the aft end of the missile to the guidance section.

Shear Concept - This concept eliminates the retraction mechanism by using other missile support items in a dual-purpose role. The umbilical cables and connectors are secured to one of the missile forward support wedges. As the wedges move with the missile during eject and fly free as they clear the launch cell, they also disengage the umbilical connector and carry it clear of the launch envelope. Several of the techniques investigated under this concept severed the umbilical cable during eject to obtain cell-missile separation.

Test-Only Concept - This concept questions the necessity of a continuous umbilical link between the missile and the launch station. Periodic testing of the missile to verify missile condition was investigated. Extensive missile changes were required to accommodate this concept.

Electrical Design

Concurrently with the mechanical system trade study, an electrical system trade study was also conducted. Six connector configurations, with several variations of each, were evaluated.

The first configuration uses the connector developed and tested for the SPRINT II system.

The second design was developed for the ISMS program where the increased EM level prohibits the exposure of the electrical contacts to the EM environment for even the brief period during and after separation in the launch cycle. The flush mounted umbilical design solved this problem.

This connector system (Reference 1) consists of a spring-loaded, shielded plug on the umbilical cable and a receptacle on the missile. The receptacle is a rear flange-mounted sealed unit with socket contacts. The face of the receptacle is mounted approximately tangent to the exterior conical surface of the missile flame shield.

Figure 5 shows the unmated plug and receptacle. A heat shield is incorporated on the face of the receptacle rotating shutter with minimum clearance through-holes for the mating plug electrical pins. The rotating shutter base has holes that are larger than the heat shield holes.

To engage the plug and receptacle two asymmetrical guide/alignment pins on the plug half are inserted into the shutter, and the plug and shutter are rotated counterclockwise 10 degrees.

The guide/alignment pins then engage the guide holes in the receptacle base and the plug electrical pins initially engage the electrical sockets in the receptacle. The ball detent quick-release pin is engaged into its socket in the center of the assembly. The coupler nut, which is restricted in the axial direction on the quick-release pin, is turned to fully engage the electrical pins through the shutter holes into the receptacle sockets, depress the deadface pin protector plate in the plug, and compress the eject-separation spring in the receptacle. The spring-loaded deadface plate protects the electrical pins during handling and initial mating steps. To separate the plug and receptacle an axial pull is applied to a wire rope lanyard attached to the ball detent quick-release pin. The pin is released. The eject-separation spring force and axial load disengage the units. After disengagement, the spring-loaded rotating shutter closes over the socket contacts in the receptacle.

A third configuration considers a commercially available connector design in which the connector is disengaged by spring force. The spring is released electrically.

Two additional connector concepts considered are special designs that are compatible with the tailplug concept and test-only concept previously noted. The sixth configuration is a special design for use with a receptacle mounted on a door within the missile. When the connector plug is disengaged, the door closes for flight.

The flush-mounted connector was selected for further evaluation.

CONCLUSIONS

The development of the SPRINT II and ISMS umbilical system design emphasizes again the necessity for a thorough understanding of requirements, consideration of a wide range of optional designs prior to establishment of the preferred design, analysis to determine equipment capabilities required to fulfill the requirements, and the desirability of test activities to substantiate the analytical effort and disclose anomalies.

REFERENCES

1. KERR, J. MORGAN, Flush Mounted Umbilical Connector,
    EMP & RFI Attenuating. Ninth Annual Connector Symposium
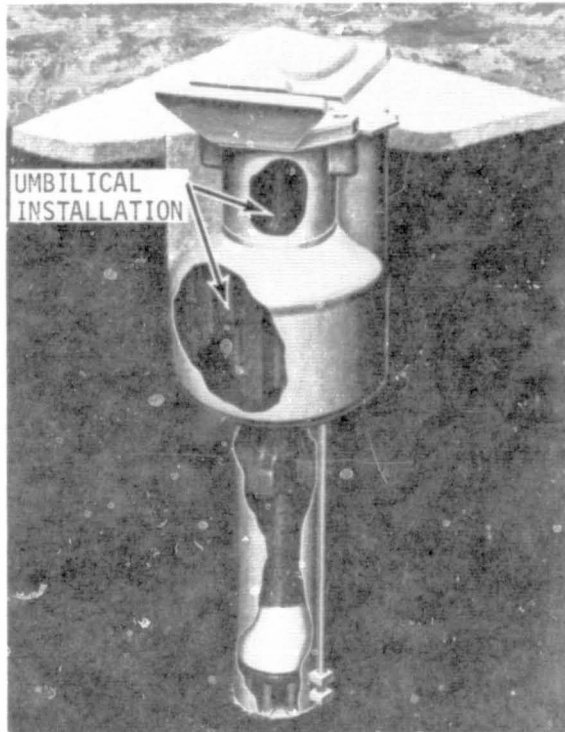
Figure 1. SPRINT II
Launch Station
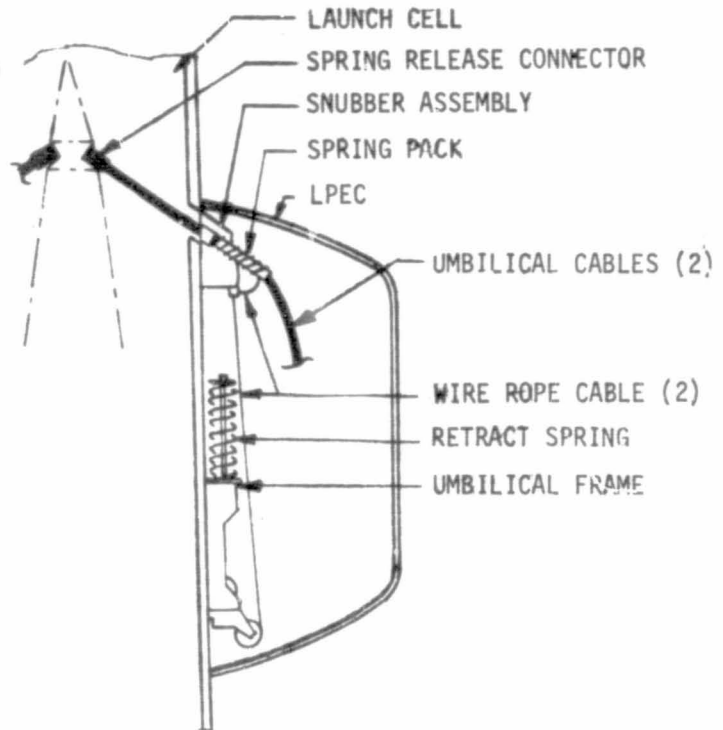
Figure 2. SPRINT II Umbilical
Retract Mechanism
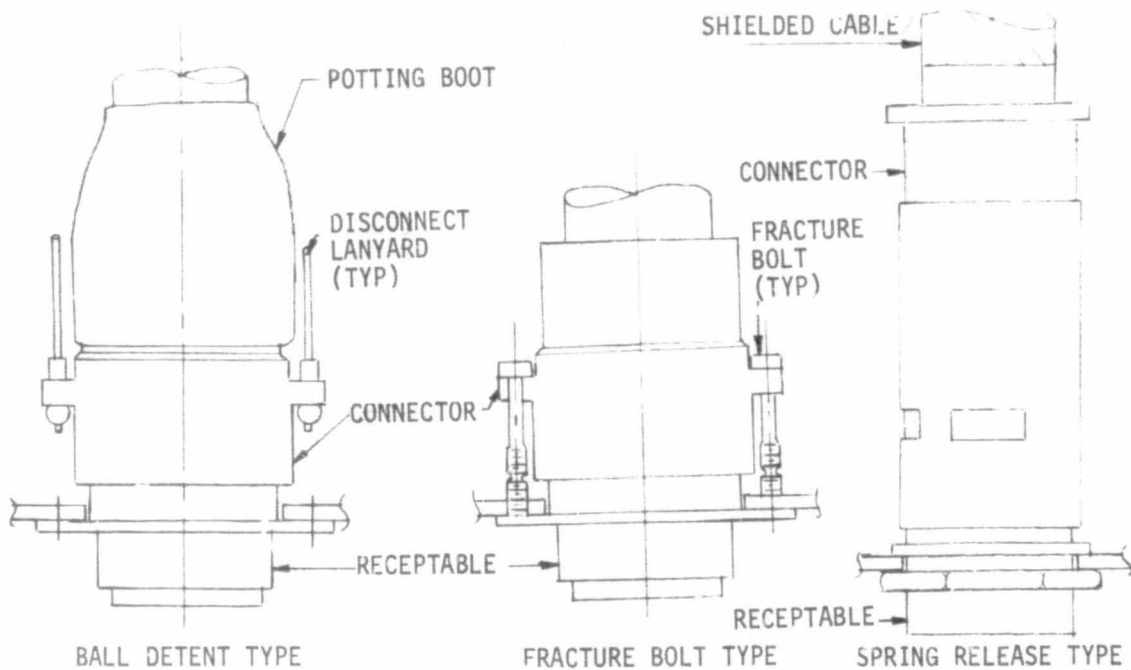
Figure 3. SPRINT II Connector Configurations

FLYAWAY CONCEPT

UMBILICAL CABLE

RETRACT CONCEPT

TEST ONLY CONCEPT

SHEAR CONCEPT

TAILPLUG CONCEPT

TAILPLUG CONCEPT

DISCONNECT POINT

UMBILICAL CABLE

FLYAWAY CONCEPT

DISCONNECT POINT

UMBILICAL CABLE

MISSILE WEDGES

SHEAR CONCEPT

UMBILICAL CABLE

RETRACT CONCEPT

UMBILICAL CABLE

TEST ONLY CONCEPT

Figure 4. ISMS Umbilical Concepts

RETRACT CABLE ATTACH POINT

COUPLER NUT

CONNECTOR PLUG (HOUSING REMOVED FOR CLARITY)

PIN RETAINING PLATE

DEADFACE PIN PROTECTOR PLATE

GUIDE/ALIGNMENT PIN

BALL DETENT QUICK RELEASE PIN

RECEPTABLE

Figure 5. Flush Umbilical Connector Assembly

206

FOCUS DRIVE MECHANISM

for the

IUE SCIENTIFIC INSTRUMENT

By Edward J. Devine and Thomas B. Dennis, Jr.

NASA Goddard Space Flight Center

ABSTRACT

A compact, lightweight mechanism was developed for in-orbit adjustment of the position of the secondary mirror (focusing) of the International Ultraviolet Explorer (IUE) telescope. This device is a linear drive with small (.0004") and highly repeatable step increments. Extremely close tolerances are also held in tilt and decentering. The unique mechanization is described with attention to the design details that contribute to positional accuracy. Lubrication, materials, thermal considerations, sealing, detenting against launch loads, and other features peculiar to fl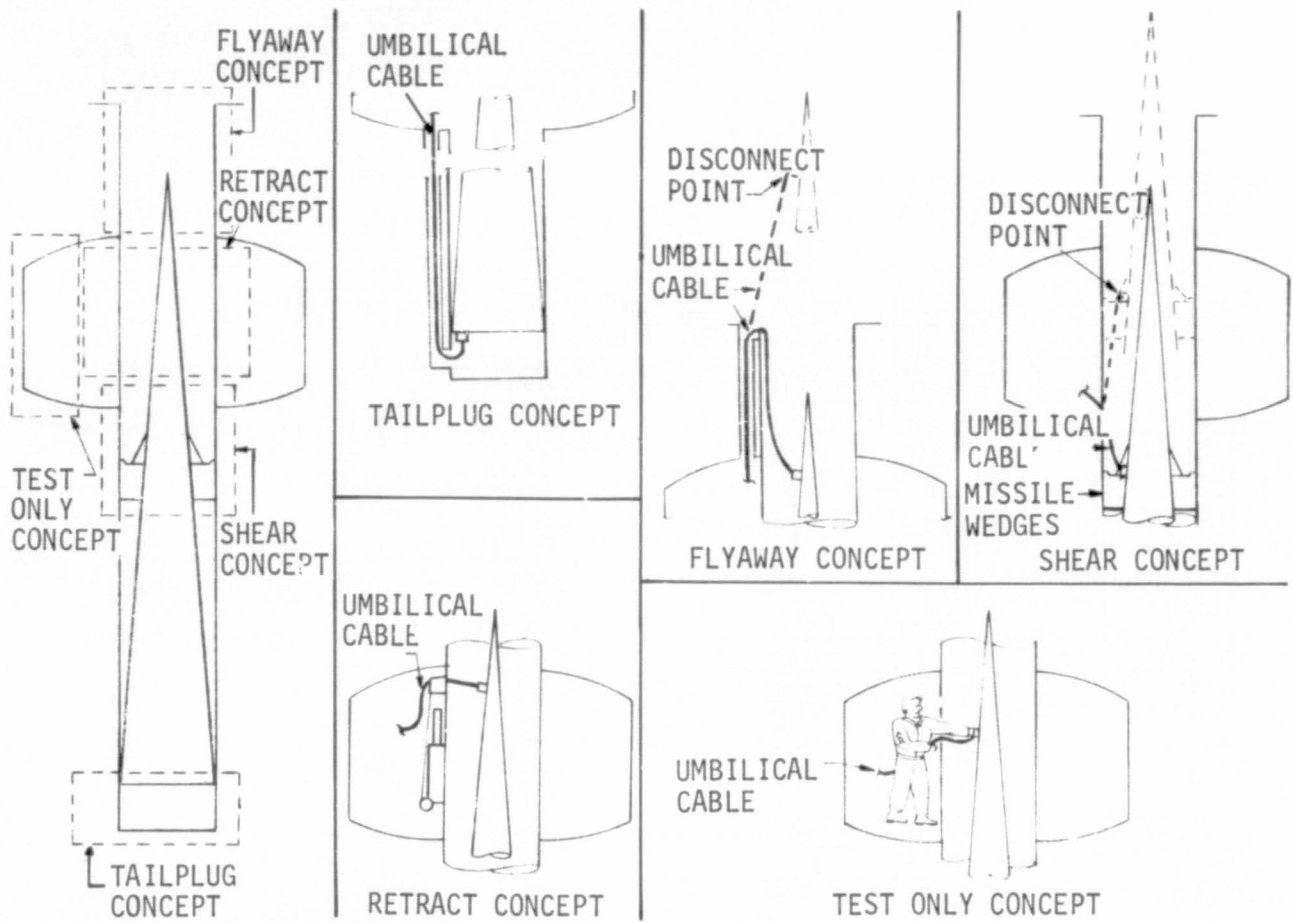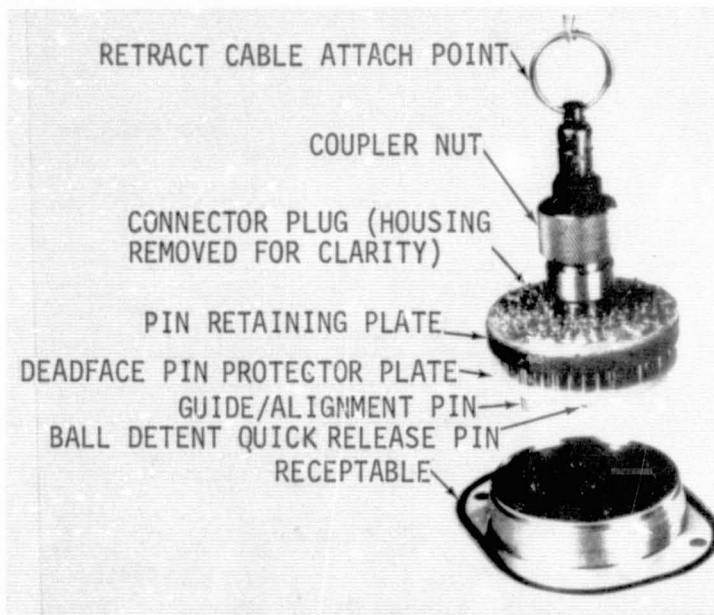ight hardware are discussed. The methods employed for mounting the low expansion quartz mirror with minimum distortion are also given. The paper concludes with the results of qualification and acceptance testing.

INTRODUCTION

The International Ultraviolet Explorer (Figure 1) is a stellar astronomical observatory which will be positioned over the Atlantic Ocean at synchronous altitude. The satellite will provide uninterrupted coverage of over 85% of the sky for ground observing facilities in the United States and Europe.

The scientific instrument is a Richey Chretien telescope (Figure 2) coupled with a dual spectrograph. The telescope assembly is a 45 cm diameter f/15 cassegrain design consisting of a beryllium concave hyperbolic primary mirror and a convex hyperbolic fused silica secondary mirror nine centimeters in diameter mounted on a focus drive mechanism. The function of the focus drive mechanism is to provide for precise axial positioning of the secondary mirror to optimize image size in orbit. The application also requires close control of tilt and decentering over the full range of axial adjustment.

FOCUS DRIVE MECHANISM

The focus drive mechanism is shown in Figures 3 and 4. The secondary mirror is mounted on a beryllium platen (described in detail later) which is attached at three points to the ends of ball screw. These three points define the mirror support plane which must be translated with a minimum of tilt and decentering errors. This is achieved by driving integral 64 tooth gears on the three ball screw nuts synchronously thru a common 94 tooth center gear. The center gear is driven by a size 11, $45°$ step, permanent magnet stepper motor through a 13 tooth pinion and 300 tooth reduction gear. The ball screw lead is .04 inches resulting in a linear motion of .0004 inches per step.

Each screw assembly has 2 individual ball nuts which are precisely shimed to a light preload to remove all axial play. Each ball nut assembly is rigidly supported by a duplex pair of preloaded bearings at one end, and a single spring preloaded bearing at the other end. This arrangement removes all sources of tilt error except for lead inaccuracy in the ball screws (less than 200 μ in) and the backlash of the center gear mesh reflected to the output (less than 10 μ in). The mechanism drives smoothly and at low torque (less than 2 in oz at the center shaft) despite the rigid constraint on undesired axial and decentering motions. The specifications for the ball screws and support bearing are given in Tables 1 and 2.

The gears and ball screws are lubricated with a light coat of low vapor pressure Krytox grease. The bearing retainers are vacuum impregnated with Krytox 143 AB oil with an additional 1.5 mg of free oil added to the raceways. The entire mechanism is sealed by "O" rings and flexible metal bellows on each ball screw as an added precaution against loss of lubricant.

MIRROR SUPPORT

Considerable attention was given to the secondary mirror mount to achieve stress free support over a wide temperature range. The mirror (the back of which is ground flat) is supported on three pads on a beryllium platen which is lapped flat to better than 50 μ in. The mirror is clamped by three elastomer (solithane 113) pads on the front of the mirror symetrically located with respect to the platen support areas to avoid bending stresses in the mirror. The elastomer pads are bonded to "C" shaped clamps which are adjusted to give a compressive force of 20 lb at each support which assures that the mirror does not lift off during launch shock and vibration. The clamps also center the mirror and are shimed to provide .001 inch of clearance at the edge of the mirror to accommodate the differential expansion of the fused silica mirror and beryllium structure over the design temperature range.

There are six heaters mounted in series and parallel on the back of the mirror to maintain the temp of the mirror at 0°C during flight.

POSITION READOUT

The position of the platen supporting the secondary mirror is monitored by a Linear Voltage Differential Transformer (LVDT). The housing of the LVDT is attached to the body of the mechanism while the position slug is attached to the platen, then any movement of the platen is indicated by a voltage change in the LVDT. The focus drive is aligned for flight such that the LVDT reads zero voltage in orbit focus position. Therefore steps in either the plus or minus direction indicate shortening or lengthening the intervertex distance of the telescope. One step of the focus drive give a 40 millivolts change in the readout of the LVDT.

PERFORMANCE

The performance specifications are given in the following table

FOCUS DRIVE MECHANISM
PERFORMANCE SPECIFICATIONS

Size	4 inches diameter x 4 inches max length
Weight	2.5 lbs maximum excluding secondary mirror
Focus Incrument	.00042 inches
No. of Focus Steps	180
Focus Range	.0756 inches
Tilt Angle Tolerance	20 arc-seconds maximum
Centering Tolerance	.001 inches maximum
Torque Margin	5 to 1
Detent Capability	150 lbs. minimum
Step Repeatability	Better than $\pm$ 0.1 step
Operational Temp. Range	-20°C + 50°C
Leak Rate	less than 1 x 10-6 cc helium/sec.

ENVIRONMENTAL TEST

The focus drive was subjected to the following environmental tests:

1. Sinusoidal Vibration

   20 g's 0 to peak maximum (thrust axis)

2. Random Vibration

   $.05g^2/Hz$ max

3. Shock

   300 g's maximum at 1500-4000 Hz

4. Thermal-Vacuum

   Heat Soak

   $+50^\circ C$ 1 x 10-5 torr vacuum for 24 hrs.

   Cold Soak

   $-30^\circ C$ 1 x 10-5 torr vacuum for 24 hrs.

The mechanism was required to demonstrate cold start capability at least 3 times during the 24 hour cold exposure. Due to the increased viscosity of the lubricant at cold temperature, the mechanism required a 5 minute warm up period at $-30^\circ C$ before stepping. At $-20^\circ C$ the mechanism stepped without a warm up period.

TABLE 1

BALL BEARING SCREW AND NUT
ASSEMBLY SPECIFICATIONS

Type	Beaver Precision Products No. B-15468 Duplex Preload Ball Nuts
Material	440C Stainless Steel
Lead Accuracy	.0005 inches/ft. for .05 inches
Preload	Zero backlash to one oz.-inch max. drag torque
Gear	to be intergral part of duplex nut housing
Gear Diametral Pitch	72
No. of Teeth	61
Pitch Diameter	0.8472 - .0010
Outside Diameter	0.8750 - .002

TABLE 2

BALL SCREW SUPPORT BEARINGS
SPECIFICATION

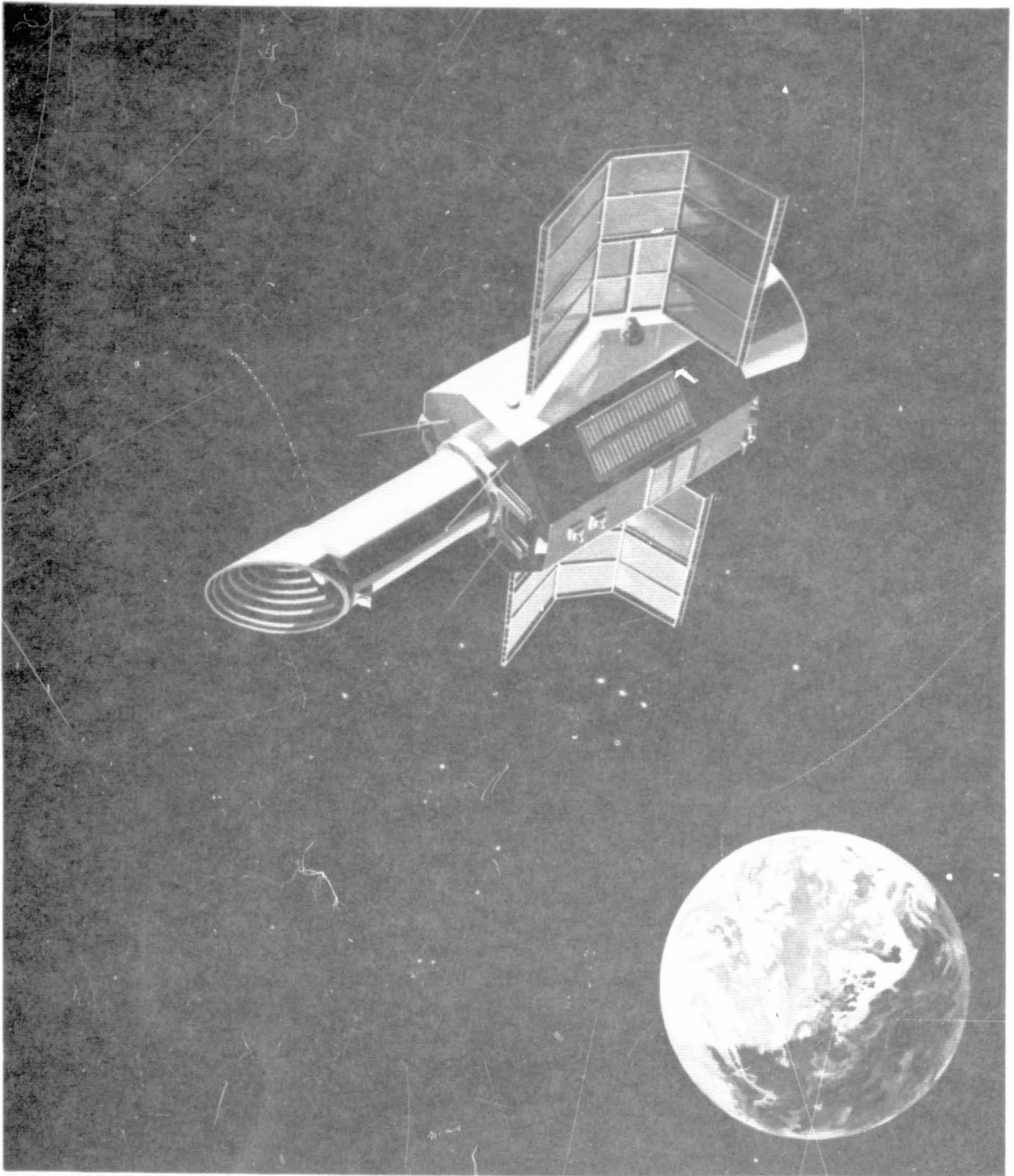| Manufacture	Split Ball Bearing Co.
Type (Duplex) (Single)	3 TAWR 12-19-63 3 TKRSS 21-28-136
Outside Diameter	1.1875 inches
Inside Diameter	0.7500 inches
No. of Balls	18
Ball Diameter	0.125 inches
Radia Play	0.0009-.0013 inches
Contact Angle	25°
Precision	ABEC-7
Duplex Preload	15 lbs.
Mean Hertz Stress @ 500 g's load (350,000 psi allowable)	177,000 psi
Retainer Material	Phenolic
Ball & Race Material	440C
Lubricant	Krytox 143AB
Shield	Double

Capacity
   Dynamic Radial
   Static Radial
   Static Thrust
	
	 690 lbs
	 432 lbs
	 880 lbs

Weight (each)	0.037 lbs.

Figure 1. IUE Scientific Instrument
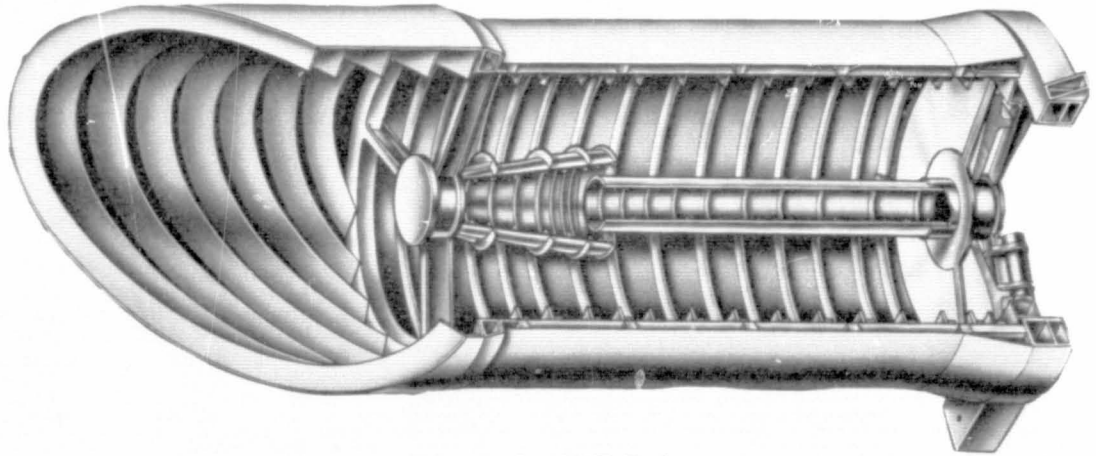
Figure 2. IUE Telescope
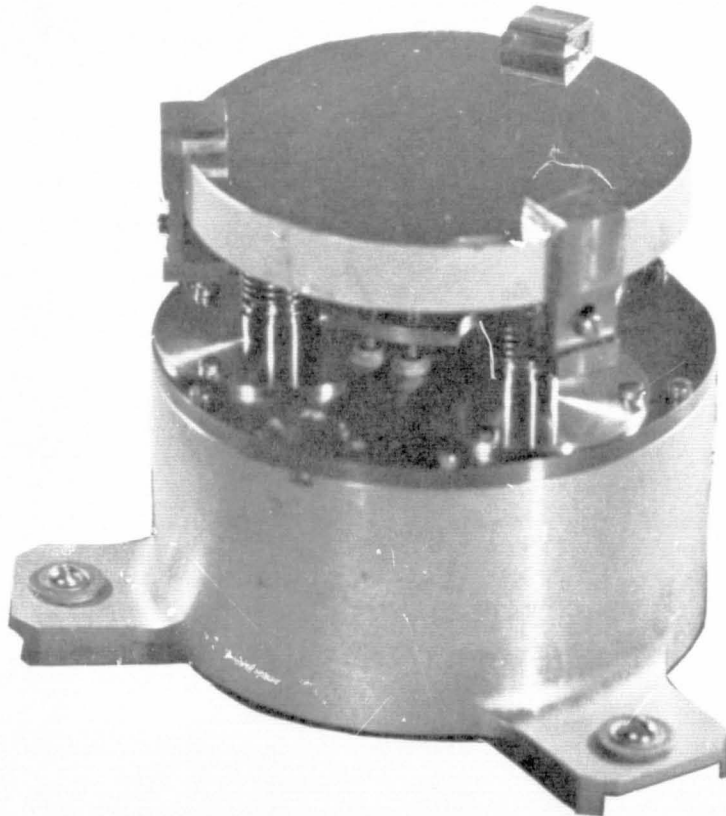
Figure 3. Focus Drive Mechanism
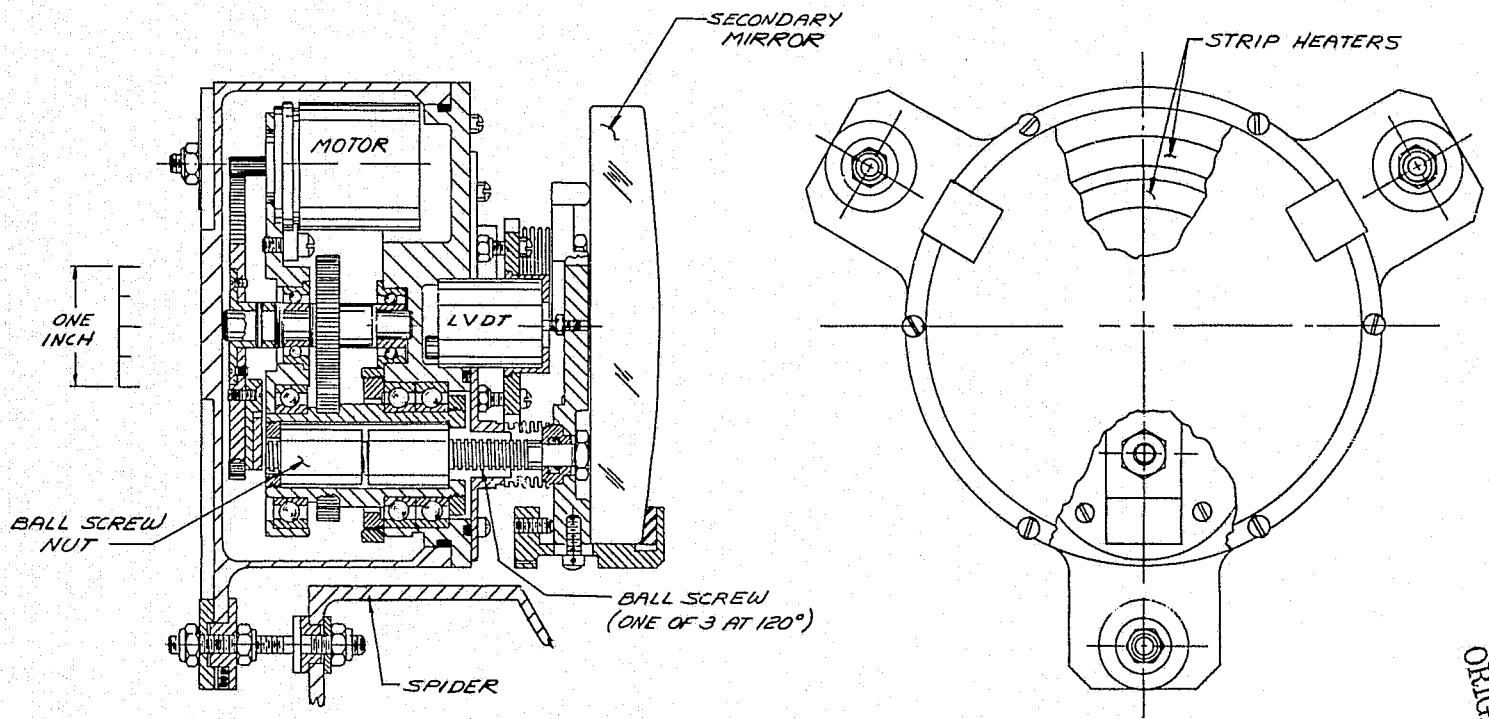
Figure 4. IUE Focus Drive Assembly

DESIGN AND DEVELOPMENT OF A SOLAR ARRAY DRIVE

By Terence Rees and John M. Standing

Space Division
Hawker Siddeley Dynamics Limited,
Stevenage, Hertfordshire, England.

ABSTRACT

The design and development of a dry lubricated direct drive solar array pointing mechanism is discussed from its inception in 1970 to its present development into a flight mechanism for use on the Orbital Test Satellite (OTS), MAROTS, European Communication Satellite (ECS) and others. Results of life testing the original prototype and the OTS mechanism are presented together with an appraisal of expected future development.

INTRODUCTION

Since 1970, the European Space Agency has been concerned with developing the technology required for three-axis stabilised geostationary communications spacecraft. The Orbital Test Satellite (OTS) is scheduled for launch on a Thor-Delta in June, 1977, and associated contracts for the maritime version of OTS, MAROTS, and the European Communications Satellite (ECS) are in progress. In aniticipation of these programmes, ESA placed a design and development contract for prototype Low Speed Mechanisms (LSM), the purpose being to establish the technology of slow speed despin mechanisms and solar array drives. At the start of this development precise requirements linked to a spacecraft application were not available, and in order to ensure that future applications would not cause fundamental changes in philosophy, severe design requirements were imposed. Within the LSM programme two mechanisms were manufactured and tested successfully providing the basis for the design of the Solar Array Drive for OTS. This OTS design is being applied, with little or no modification, to the Ariane Test Satellite, EXOSAT, MAROTS and ECS.

DESIGN OF THE LOW SPEED MECHANISM

Early in the LSM programme it became evident that the likely application was as a solar array drive. Consequently, emphasis was placed on a normal operational speed of 1 revolution/day and an acquisition, or slew speed of 1°/sec. The basic design requirements are given in Table 1.

The design of the LSM was conceived to be of modular form, that is, a self contained bearing and motor assembly with the slipring and brush blocks cantilevered from one end, allowing changes to the ring configuration as required. The overall assembly is shown in Figure 1. As can be seen, the drive is direct, with an Aeroflex brushless motor acting on the driven shaft. This approach was selected as it promised simplicity and low mass. Detailed analogue simulations were made to demonstrate the feasibility of the control concept.

The low speed and long life in a vacuum environment are requirements that can best be met by dry lubricants, as there is no advantage from an elastohydrodynamically generated film normally associated with medium to high speed oil lubricated applications. During the design phase suitable lubricants were found; the ESA sponsored lead film for ball bearings, and a molybdenum disulphide/silver/copper composite brush material. Use of these lubricants avoids the need for reservoirs and molecular seals.

The specified temperature range and shaft to housing differential temperatures required careful selection of materials and the method of preloading the bearings. Duplex bearings provide good stiffness but are sensitive to temperature differentials in regard to preload and friction torque. The bearing arrangement selected has two angular contact bearings, one with inner and outer races clamped to the shaft and housing, the other being clamped to the shaft but having its outer race supported by a flexible diaphragm. This diaphragm takes up any axial differential expansions between the housing and shaft and is also used to apply a preload of 45N by means of a built-in deflection. Preload changes over the design temperature range are less than 10%.

The effect of having a hot shaft and colder housing is to reduce the internal clearances in the bearings with possible seizure of the mechanism. For the analysis it is assumed that the bearing races follow the radial expansions of the housing and shaft. Figures 2 and 3 show the effect of temperature differentials for combinations of beryllium for both the housing and shaft and aluminium for the housing and shaft. Beryllium is clearly superior. The bearing fits into the housing and allows a radial clearance of some 5 to 15 μm, the outer race being clamped by a plate. Friction between the race and the clamp plate will cause the bearing to distort by 1.5 to 5 μm radially before interfacial slip occurs. These distortions are detrimental to bearing torque. Similar remarks can be made about the fit to the shaft. Thermal modelling has shown that temperature differentials between the races and the corresponding mounting surfaces to be less than 10°C. Using beryllium to match the coefficient of expansion of the bearing steel therefore produces minimal bearing distortion. Titanium is competitive with beryllium but does not offer the mass advantages. The design finally selected employs beryllium for the housing and shaft with a titanium diaphragm integral with the carrier of the inboard bearing outer race. In the event this produced a bearing mounting and a preload loop which was highly insensitive to temperature.

Separable angular contact bearings are used so that the rotating assembly is stiff in one direction, and, due to the diaphragm, compliant in the other. To prevent the mechanism 'rattling' under the launch environment, and to avoid damage to the diaphragm the bearing system is caged. The off-loading mechanism comprises a conical face at the outboard bearing which meets a seat in the housing when in the launch configuration. To achieve this the shaft is displaced axially through 0.13mm by a pivoted lever which applies a preload to prevent separation of the conical faces. Release is obtained by pyrotechnic action.

Slipring design is conventional with an epoxy-moulding carried on a central aluminium tube. The contact surface at the slipring is electroplated silver and each ring has redundant brushes with separate running tracks. Both brushes are arranged to trail.

ESA were interested in correlating friction with angular position and required a shaft position readout to within 0.1°. This was accomplished over the full temperature range by use of a Gray code optical encoder giving 4096 counts per revolution. The encoder features a 15 track chrome on glass pattern illuminated by redundant light emitting diodes (LED) acting through a fibre optic bundle to provide a slit source. Operation of this encoder at the higher temperature proved troublesome due to the reduction in output from the LED's. However, improved heat sinking overcame this problem. Dissipation from the LED's forced the adoption of pulsed operation at 400Hz with a duty cycle of 5%, the position being sampled and stored between pulses. The encoder output is used to provide an error compared to a clock demanded position and also to commutate the Aeroflex brushless dc torque motor. Use of this encoder was limited to the research programme and development into a flight item was not foreseen, but the use of incremental encoders of the Moire fringe type promise low mass and high accuracy.

TEST HISTORY OF THE LSM

Prior to thermal vacuum testing correct operation was demonstrated for a range of solar paddle characteristics. The solar paddle simulators are suspended on a small bearing so that a weightless load is obtained with only a slight increase in friction. Flexibility is obtained by coupling the load to the mechanism by a torsion bar. The first simulator corresponded to a large solar array at 20 kgm^2 inertia and 0.5 Hz torsional frequency and was used to test the number one LSM. For the second LSM a simulator having a range of frequencies of 0.06 to 3.6Hz with an inertia of 2.8 kgm^2 was used.

The first LSM was subjected to qualification levels of vibration and thermal vacuum testing prior to an accelerated life test equivalent to 10 years operation. A speed of 1 rev/hour was used, this being felt to be justified since the normal motion is stepped and a times 24 increase in speed merely increases the step frequency and does not change the motion within a step.

It was not possible to simulate the solar paddle inertia and flexibility in the test chamber but the sliprings did carry power. The life test cycle is shown in Table 2. Throughout testing the insensitivity of the mechanism to temperature was demonstrated. Figure 4 gives a typical trace obtained during the eclipse simulation, in which the drive flange temperature is reduced from 60 to -20°C in 72 minutes with the radiation 'sink' surrounding the mechanism held at 35°C. The variation in lag angle is ±1 encoder division (±0.09°), that is approximately ±0.0002Nm friction torque variation.

Strip down of the mechanism was carried out on completion of the 10 year equivalent life test. The condition of the mechanism was found to be excellent, with very little evidence of wear.

The second mechanism has completed over two years of testing at 1 revolution/ day, the test cycle being as shown in Table 2 part B. Of some significance, is the data collected to date which shows a gradual reduction in friction. This is discussed below, together with similar findings from the OTS solar array drive. Table 3 summarises the real time test data.

SYSTEM PHILOSOPHY FOR A FLIGHT ARRAY DRIVE

Due to the criticality of the solar array drive system to mission success, particular attention had to be paid to reliability and the elimination of single point failures. Other areas of concern are minimising spacecraft body perturbations resulting from array motion, the impact of spacecraft contaminants on the performance of the array drive sliprings and the ability to control array sun pointing in the absence of the prime control signals.

A number of candidate solutions were investigated and included a stepper motor drive controlled by a spacecraft 'clock', a brushless or brushed d.c. motor controlled by a clock and a shaft position indicator, such as a resolver or optical encoder. The system finally chosen was to have a totally redundant sensing and drive system with the control signals being generated by solar array mounted sun sensors. A block diagram of a single channel is shown in Figure 5.

Each sensor provides two outputs, one being level detected within the electronics to indicate that the sun lies within the field of view of the sensor, the other giving a measure of the angle between the satellite sun vector and the normal to the array. In the normal sun tracking mode (with sun angle less than 2°) this error signal is amplified and chopped to give amplitude modulated current pulses from unidirectional power amplifiers. The pulses are sequentially routed to the drive motors of the North and South BAPTA's to give a stepped motion of the array.

The design of the OTS array system (BAPTA subsystem) is such that each of the two solar arrays may be independently rotated about the spacecraft pitch axis by

use of a ground command 'inhibit' signal. A further feature of the subsystem is
that the arrays can independently offset from the satellite sun vector, either lagging
or leading in incremental steps of 1.53 degrees up to maximum offsets of 21° (equinox)
and 30° (solstice). Whilst the original reason for this capability was for an orbital
experiment to induce 'windmill' drifts, it is also possible to use this mode of
operation as a simulated error to control BAPTA orientation in the unlikely event of
a catastrophic failure of the sensing circuits.

Analogue simulations of the spacecraft pitch loop and BAPTA subsystem were
performed parametrically to predict BAPTA and spacecraft performance under a
variety of conditions. In a friction stabilised system such as the OTS BAPTA it is
essential that friction is both predictable and stable. In normal mode operation,
that is when the BAPTA is sun tracking, the value of friction is relatively unimportant,
but in certain back-up modes where the spacecraft is required to slew to reacquire the
sun, then friction is necessary, in order to hold the array position with respect to the
spacecraft body. In order to satisfy this condition the BAPTA friction F would need
to be greater than the expression below assuming a rigid array on spacecraft body:

$$F = \frac{I_A \cdot T_J}{I_{S/C}}$$

where I_A = Array inertia

T_J = Couple generated by the spacecraft control thrusters

$I_{S/C}$ = Inertia of the spacecraft about the pitch axis

In practice of course the expression is more complex to take account of the
array flexibility.

Array inertias of up to 100 kgm² were simulated together with friction levels
between 0.04 and 0.24Nm.

FLIGHT MECHANISM DESIGN

Having satisfactorily demonstrated the feasibility of the direct drive principle,
it was necessary to refine and implement the essential features of the LSM into a
flight solar array drive, referred to as the BAPTA (Bearing and Power Transfer
Assembly). From the experience gained during the LSM programme the following
main conclusions were drawn:-

●   Selection of material for the bearing housing and shaft together with the
     preload system was critical. The design of the LSM was such that the
     mechanism friction torque remained insensitive to thermal gradients.

- The lead lubrication of the bearings together with the silver/copper/molybdenumdisulphide composite brushes gave excellent results.

- The use of silver sliprings was questionable due to atmospheric corrosion problems.

- Because of the low duty cycle of the operational BAPTA, a brushed motor drive can be used.

The design of the BAPTA is best examined by reference to Figure 6. The design shares many of the features of the LSM particularly with respect to points 1 and 2 mentioned above. The common features are the bearings and preload system, lead lubrication, use of an off loading mechanism, beryllium main housing and shaft and finally the cantilevered modular slipring assembly. Significant changes are the deletion of the position encoder, this function being performed by the solar array sun sensor, and the use of a brushed d.c. motor. A short discussion of the major modifications follows.

Off-Loading Mechanism

An off-loading mechanism of similar design to that of LSM has been embodied into the BAPTA. The major difference being the use of a pyrotechnic pin puller in preference to the cable cutter as the prime release mechanism. The off-loading lever is held in position by means of a calibrated spring washer reacting through the BAPTA housing via the pin puller.

The pin puller is of the dual cartridge single bridgewire type, with each cartridge having the capacity to activate the off-loading mechanism. Leakage of the gaseous pyrotechnic products is prevented by a double 'O' ring seal.

Sliprings

Two major changes to the slipring design were made:-

- Trailing and leading brushes were replaced with symmetrically seated brushes because of the desire to maintain interchangeability between north and south BAPTA's.

- A gold plated slipring replaced the silver slipring to eliminate the progressive atmospheric corrosion experienced with silver.

This latter point was of particular concern in that the OTS BAPTA is controlled by signals derived in the array mounted sun sensor and then transmitted to the control electronics by means of the BAPTA sliprings. In normal mode operation

a 7mV signal can be expected, giving rise to currents in the order of a few micro amps. Although contact resistances of tens of thousands of ohms would be needed to cause significant sun following errors it was considered desirable to avoid use of materials which could result in high impedance contact resistances. Consideration was also given to the possibility of high electrical resistance polymers being produced due to the rubbing action of the brushes and sliprings in an organic atmosphere.

In the spacecraft it can be expected that low concentrations of organic vapour, resulting from outgassing of hydrocarbon based materials, will exist, however these low concentrations together with low rubbing rates are unlikely to give rise to polymer type film. Tests are, at the time of writing, being conducted on a standard slipring system in an environment simulating the spacecraft in terms of organic vapours. The test fluid for these tests has been collected from various spacecraft thermal vacuum tests.

For the OTS BAPTA application 4 pairs of power sliprings carry up to 3 amps with a further pair of power sliprings available for other OTS derivatives. Thus for the 31 slipring combination, 12 sliprings are sized for power and 18 have been sized for signal with respect to the lead wires only. The remaining 1 ring is for earth bonding. The rings and brushes themselves have all been designed to carry current up to 6 amps giving an overall theoretical transfer capacity of 4.5k watts.

Motor Drive

A brushed d.c. Inland motor is used to drive the BAPTA with a redundant motor housed at the outboard end of the BAPTA.

The copper commutators are gold plated to prevent atmospheric corrosion and the brush material is identical to that used for the slipring brushes i.e., silver/ molybdenum disulphide/copper.

MECHANISM TEST AND DEVELOPMENT

The principle objectives of the OTS BAPTA development test programme were:-

- To demonstrate BAPTA performance was insensitive to the thermal environment.

- That the signal sliprings, particularly the BAPTA control slipring would not degrade due to self contamination or spacecraft contamination arising from the use of various hydrocarbon and silicon based materials.

●   To demonstrate by means of accelerated life testing that BAPTA friction is predictable over a life time of 7 years.

One Engineering and four flight BAPTA's have been built. One of these BAPTA's, the Qualification Unit, was subjected to qualification level vibration and thermal vacuum testing prior to being put onto a 7 year accelerated life test. In addition to these five units a further dummy BAPTA with representative sliprings and brushes was built for special spacecraft compatibility tests, aimed at proving the integrity of the sliprings whilst working in an organic vapour atmosphere. At the time of writing these tests were not completed, but no problems relating to slipring performance had as yet been experienced.

Functional testing of the BAPTA under the ambient conditions within a clean area, were carried out using a solar array simulator whose inertia and first mode natural frequency was represenative of the OTS flight array, i.e., 2.2kgm² and 1.9Hz.

During these tests a typical sensor output signal of 7mV was transferred across the sliprings and in series with a representative load impedance of 30k ohm. These tests were carried out to demonstrate that with low currents of the order of a few micro amps, the contact resistance would remain constant. No measurable change in contact resistance was noted even when control signals of 0.1mV were used in the tests. Typical average contact resistances were 5m ohm per brush.

Average motor current during these pre thermal vacuum tests was 117mA with an average Sun following error of 0.78 degrees.

Thermal vacuum tests could not be conducted easily with a representative load inertia, but offered the advantage that in the steady state case with low inertia the current taken by the motor is directly representative of BAPTA friction torque. This offered an opportunity to monitor BAPTA friction directly.

From Figure 7 (which is a graph of motor current/BAPTA friction torque against various operational environments), two points emerge which are worthy of note.

The BAPTA friction torque apparently reduces when exposed to vacuum and only after a short period of running. The reduction in friction experienced at this stage of testing is probably not due to a running in phenomenon, the number of revolutions being small compared for example to the ambient pressure functional tests.

Secondly, the BAPTA friction was apparently insensitive to the thermal environmental temperature, with the friction torque being comparable at -20°C soak to +50°C soak.

All of the 4 flight BAPTA's exhibited very similar friction characteristics during acceptance testing.

At the time of writing the life test BAPTA had completed 3 years of accelerated testing the results of which are presented in Figure 8.

From Figure 8 the average motor current during 3 years of accelerated life testing was 30.33 milliamps (0.071Nm) with a standard deviation of 2.31 milliamps (0.005Nm).

The friction level at the beginning of life testing was similar to that at the completion of the qualification programme. A rapid fall in friction resulted during the first few days of the 1 rev per hour test, after which the friction level apparently remained fairly constant. No significant trend in friction could be identified as a result of wear or long term vacuum exposure or due to changes in the environmental boundary temperatures.

FUTURE DEVELOPMENTS

The OTS BAPTA is at present being examined to identify the growth potential for power transfer and load carrying capacity. To date these investigations have shown that power transfer capability of up to 4.5kW is feasible but requires some minor modifications to the slipring wire gauges and the BAPTA thermal model.

Thus all combinations of signal rings and power rings up to a total of 31 rings are possible with minimum modifications. Because the slipring assembly is of modular design, being cantilevered off the shaft, it is also possible to extend the length of the slipring assembly and embody additional rings possibly up to 40 in total.

In the OTS BAPTA configuration 7 of the 18 signal rings are used for control of the BAPTA Sun pointing vector. In order to allow greater flexibility to the Power subsystem designer, it is proposed in future to use a 1200 step stepper motor thus vacating 7 additional rings for use as power or signal transfer.

A stepper motor driven BAPTA is expected to undergo test in August, 1977.

Table 1

LSM Design Requirements

Operating Speed	Normal 4 rev/day, Acquisition 1 deg/sec.
Life	In orbit 7 years, Ground Running 50 hours
Slipring	6 Channels (Double Circuit) 2.5A Nominal 5A Peak 1 Bonding Channel 12 Channels 0.05A.
Qualification Environment	
Static Load	A single load of 1750N at the drive flange. Applied for 5 mins. along six directions corresponding to an orthogonal axes set containing the rotational axis.
Constant Acceleration	18g applied for 5 mins. Axes as above.
Sinusoidal Vibration	Axes as above. Sweep rate 2 octaves/min. 5 to 15Hz.; 9mm zero to peak displacement. 15 to 200Hz.; 8g zero to peak acceleration.
Random Vibration	Axes as above. Duration 5 mins. each axis. 25 to 100Hz.; 3dB/Oct. increasing to $0.2g^2$/Hz. 100 to 2000 Hz.; $0.2g^2$/Hz. flat.
Thermal Vacuum	T_1 = Shaft temperature at drive flange $^\circ$C. T_2 = Shroud or radiation sink temperature $^\circ$C.

Duration Hours	T_1	T_2
8	20	-25
8	80	15
8	80	80
8*	70	45

*During this period, four 72 minute eclipses are required to be
submitted by decreasing T_1 to -30°C whilst maintaining T_2 at 45°C.

Table 2

LSM Life Test Schedules

T_1 = Temperature of Drive Flange

T_2 = Enclosing shroud or sink temperature

(A)   Accelerated Test

Total test duration 15 cycles each comprising:-

8 Eclipse simulations with T_2 = 22.5°C, T_1 varying from 60 to -20°C
in 72 minutes.   Speed 1 rev/day.   Each Eclipse followed by an acquisition
of 1 revolution at 1°/sec.

10 Days at 1 rev/hour with T_2 = 22.5°C, T_1 = 60°C for odd number cycles.

10 Days at 1 rev/hour with T_2 = 22.5°C, T_1 = 10°C for even number cycles.

Total number of revolutions including qualification testing = 3911.

(B)   Real Time Life Test

Speed - 1 rev/day.

Cycle period is 26 weeks each cycle comprising:-

6 weeks (of 5 days) with 1 Eclipse simulation per day having T_1 varying
from 60 to -20°C in 72 minutes and T_2 = 22.5°C.   Mechanism then completes
1 revolution.

20 weeks with T_2 = 22.5, T_1 = 60°C for odd number cycles.

20 weeks with T_2 = 22.5, T_1 = 10°C for even number cycles.

Number of cycles completed 5 ($2\frac{1}{2}$ years).

Table 3

LSM Real Time Test Data (Averaged Values)

Cycle	Week	T_1 (°C)	Pressure (Torr)	Error (Degrees of Arc)	Torque Nm	MP (Watts)
1	1	60	1×10^{-6}	-3.7	0.104	1.3
	13	60	3×10^{-7}	-3.0	0.084	1.1
	26	60	1.8×10^{-7}	-3.0	0.084	1.1
2	1	60	1.6×10^{-7}	-3.0	0.084	1.2
	13	10	3.5×10^{-8}	-2.5	0.070	1.0
	26	10	3.0×10^{-8}	-2.4	0.067	1.0
3	1	60	1.8×10^{-7}	-2.8	0.078	1.0
	13	60	1.5×10^{-7}	-2.4	0.067	0.8
	20	60	1.0×10^{-7}	-2.9	0.081	0.7
	26	60	8.1×10^{-8}	-2.4	0.067	0.8
4	1	60	8.2×10^{-8}	-2.4	0.067	0.8
	7	10	2.2×10^{-8}	-2.5	0.070	0.8
	13	10	1.7×10^{-8}	-2.25	0.063	0.6
	20	10	1.5×10^{-8}	-1.9	0.053	0.6
	24	10	1.7×10^{-8}	-2.1	0.058	0.6
5	1	60	6.6×10^{-8}	-2.6	0.073	0.7
	7	28*	3.3×10^{-8}	-2.4	0.067	0.7
	12	28*	2.7×10^{-8}	-2.4	0.067	0.7
	15	28*	3.5×10^{-8}	-2.4	0.067	0.75
	16	60	3.5×10^{-8}	-2.4	0.067	0.75

* Due to heater failure.

Table 4
Key Features of BAPTA Subsystem

- Totally redundant sensing and drive channels (i.e. Sun sensors, electronics and motor).

- Control signals derived from solar array mounted Sun sensors.

- Normal mode Sun tracking error less than 2°. Initiation of normal mode is by ground command only. Loss of Sun presence in either acquisition or normal mode causes arrays to stop until the next ground command.

- Automatic failure detection which disconnects BAPTA control electronics from the AOCS.

- Independent variable offset facility of 1.53^o slip up to a maximum offset of 30°.

- Independent inhibit modes.

- Nominal slew rate of 1° second.

- Saturated torque demand at 2°.

- Sequential North/South actuation to minimise spacecraft pitch disturbances.

- Open loop slew mode of operation operated by ground command.

- Catch up time after exit from 18 degree eclipse will be a maximum of 15 minutes.

Table 5. Summary of BAPTA Key Features

- Mass	-	4.2kg including pyrotechnics, redundant motors and all connectors.
- Motors	-	2 brushed d.c. motors (1 being redundant) torque 0.71Nm (stall) current 0.3A at stall voltage 50 volts
- Speed	-	1 rev/day, normal mode 1°/sec Sun acquisition
- Power Consumption	-	Normal mode - 0.04W Acquisition - 0.85W
- Nominal Friction	-	0.07Nm (vacuum)
- Slip Rings	-	12 power rings 3 amp. 18 signal rings 1 earth bonding
- Growth Potential	-	30 power rings 6 amps. 1 earth bonding
- Launch Loads	-	1200N (OTS)
- Array Latch Loads	-	100Nm
- Stiffness, Caged	-	Axial 100×10^6 Nm Radial 40×10^6 Nm/rad.
Operational	-	Axial 1×10^5 Nm Radial 20×10^3 Nm/rad.
- Temperature Limits	-	-45 to +55°C Shaft 0 to +55°C Housing
- Environmental Test	-	Acceleration ± 18g Vibration along 3 principal axes

Sine	15 to 21Hz	7.5g
	21 to 100Hz	2.5g
Random	20 to 60Hz	0.05g²/Hz
	60 to 300Hz	3dB/octave to 0.25g²/Hz
	300 to 1200Hz	0.25g²/Hz
	1200 to 2000Hz	decrease at 6dB/octave

PURGE VALVE

BRUSHLESS
D.C. MOTOR

OFF-LOADING MECHANISM

THERMAL CONTROL
RADIATOR

OPTICAL ENCODER

ARRAY MOUNTING FLANGE

ANGULAR CONTACT
BALL BEARING

BERYLLIUM SHAFT

CONICAL SEATING FOR
OFF-LOADING

SIGNAL
SLIP RINGS

POWER
SLIP RINGS

TITANIUM DIAPHRAGM

BERYLLIUM HOUSING
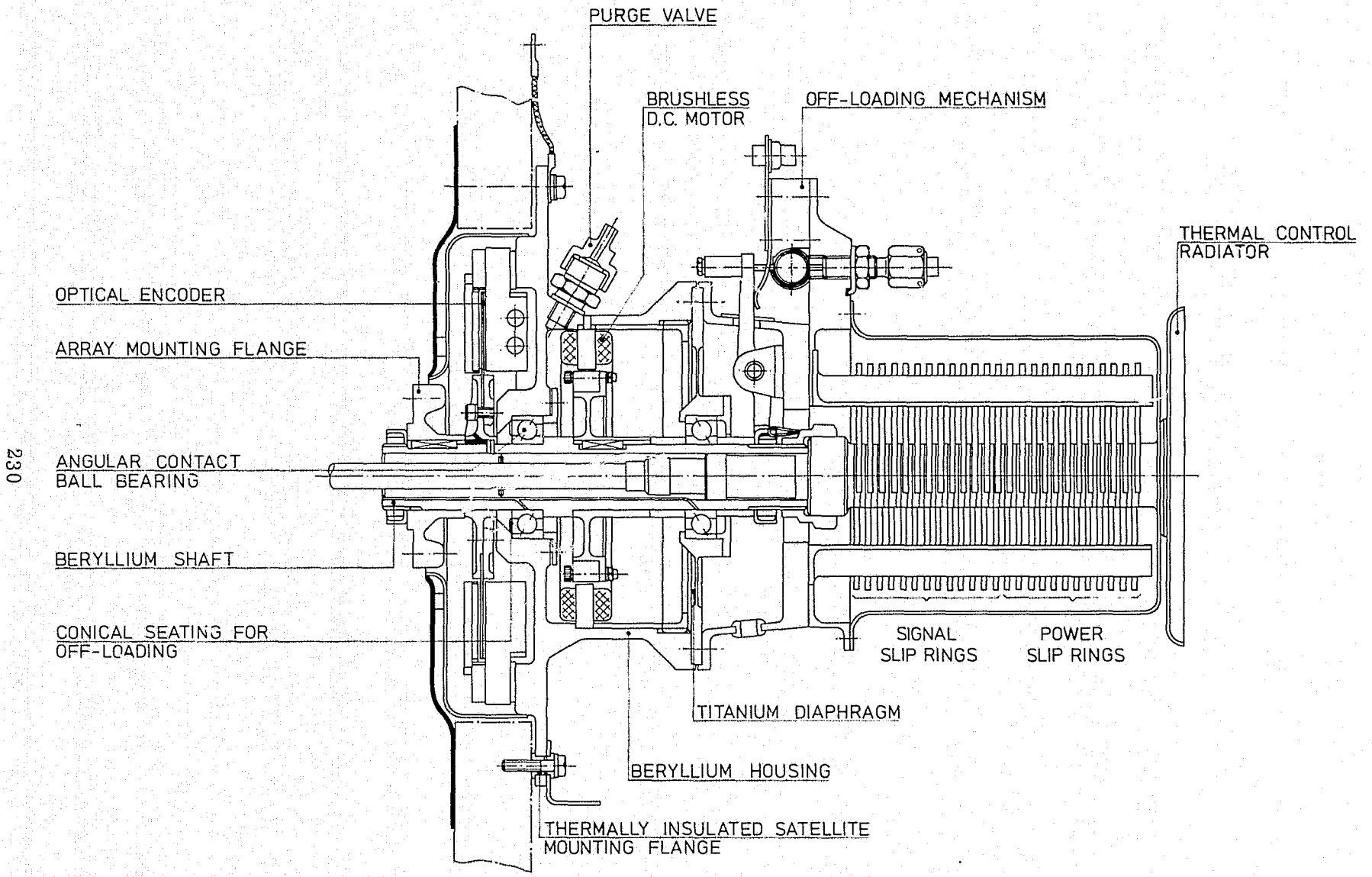
THERMALLY INSULATED SATELLITE
MOUNTING FLANGE

Figure 1. Overall Assembly of Low Speed Mechanism
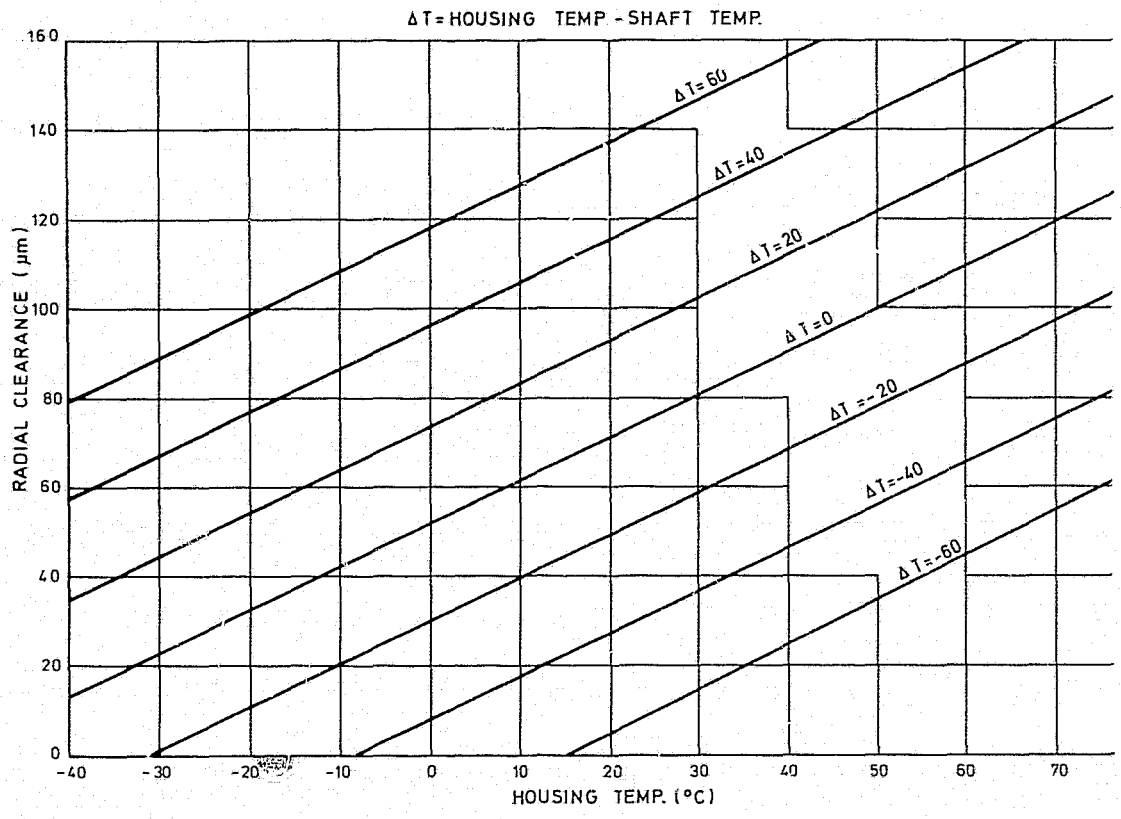
Figure 2. Bearing Radial Clearance Vs Temperature (Al/Al)
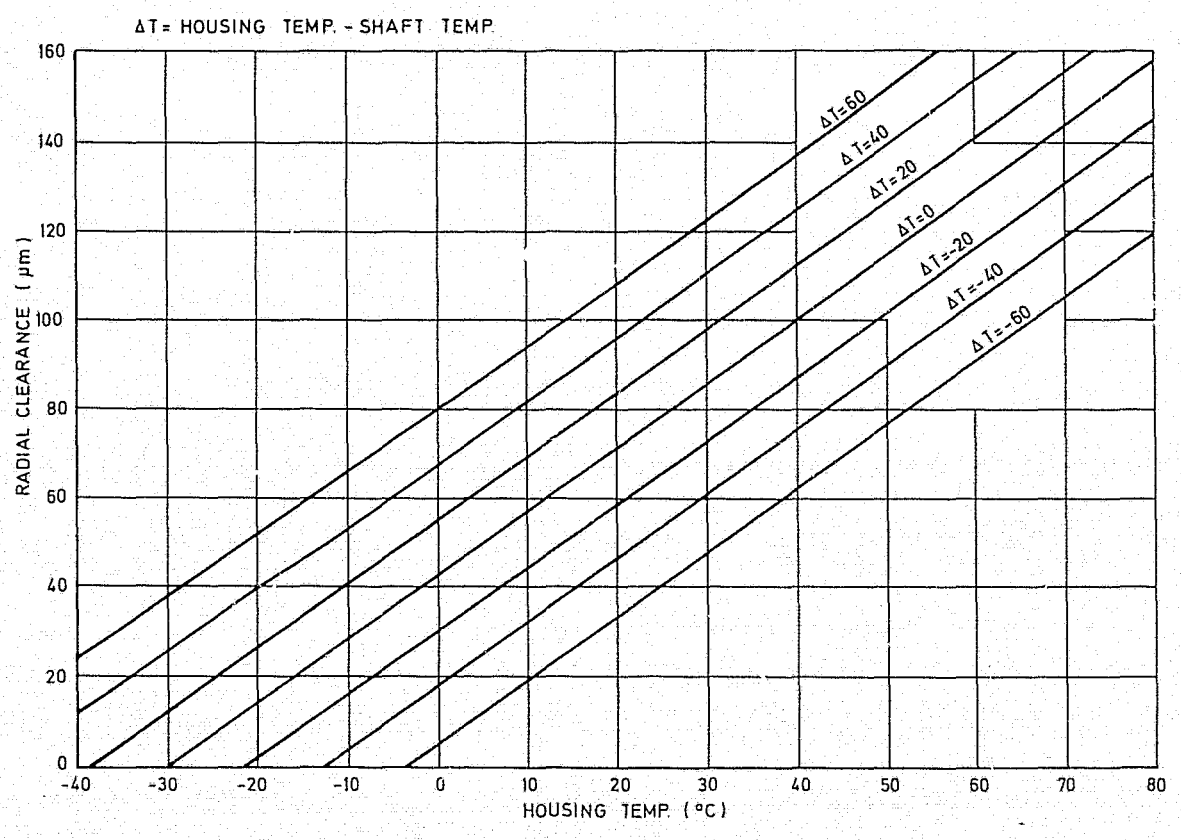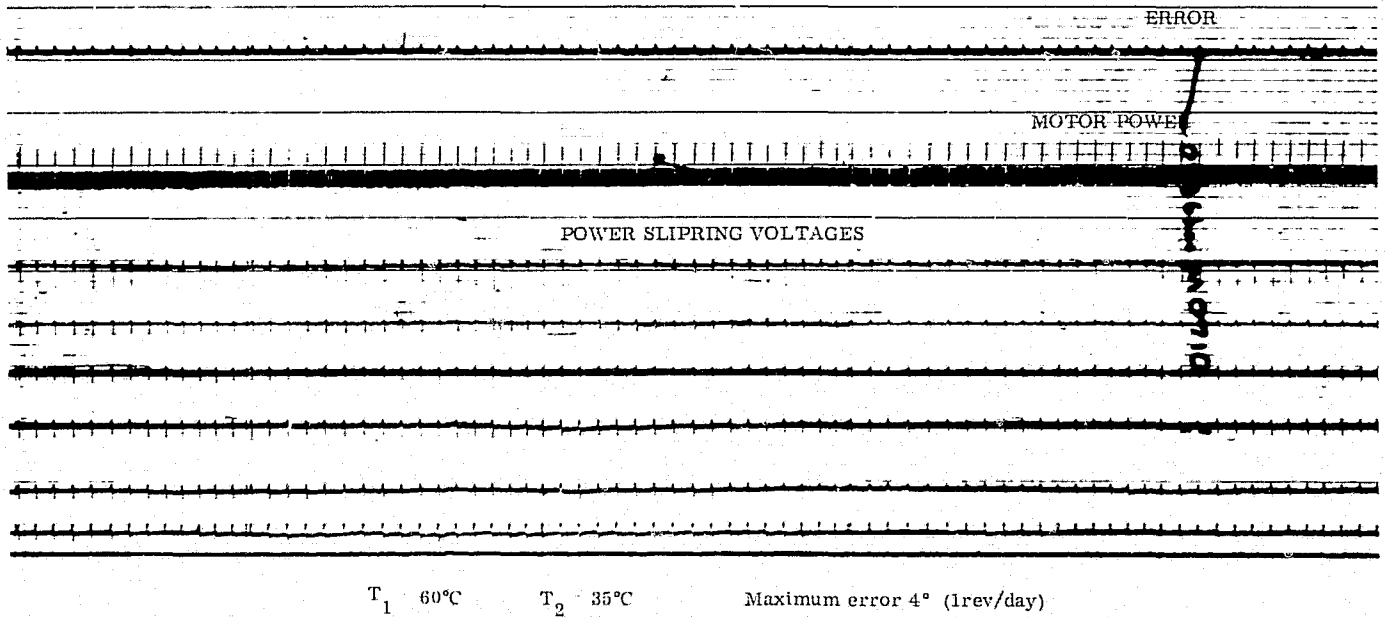

Figure 3. Bearing Radial Clearance Vs Temperature (Be/Be)

231

ERROR

MOTOR POWER

POWER SLIPRING VOLTAGES

T_1 60°C T_2 35°C   Maximum error 4° (1rev/day)

Figure 4. LSM Following Error During Eclipse Simulation
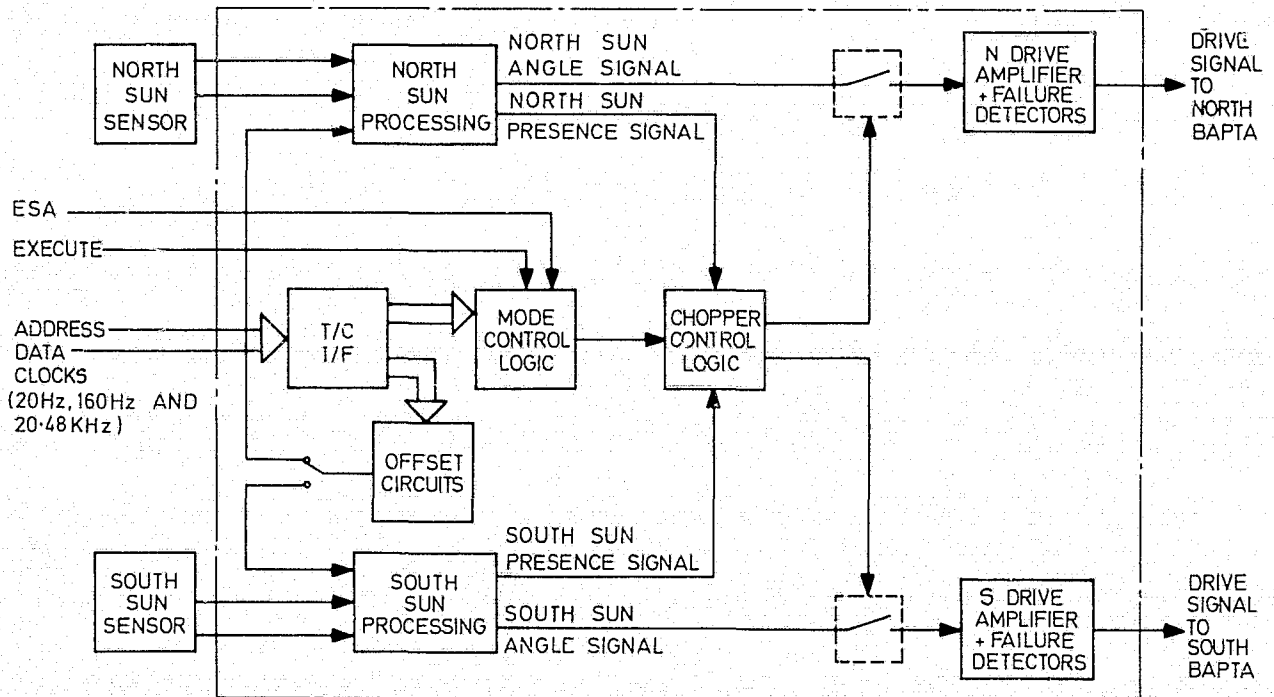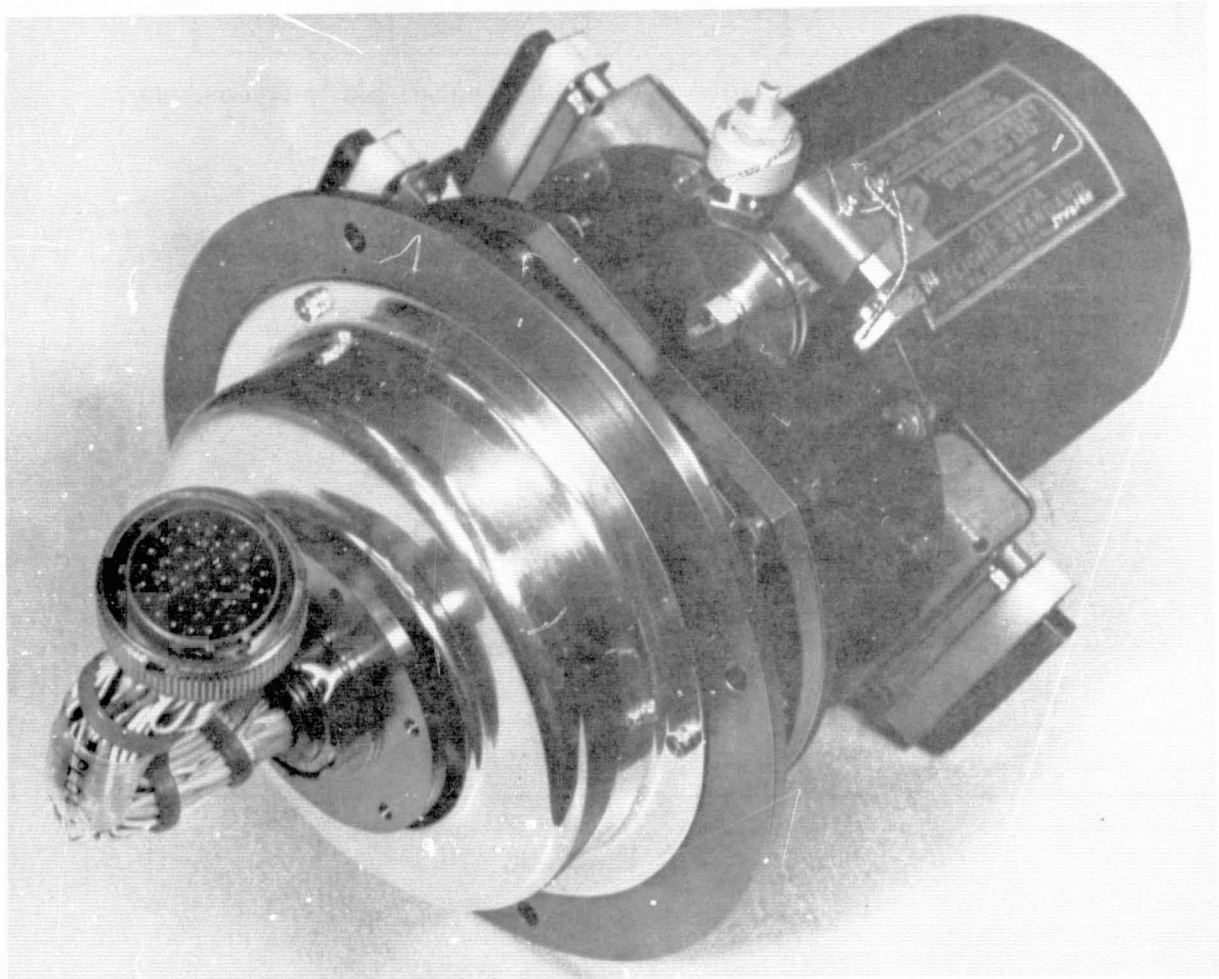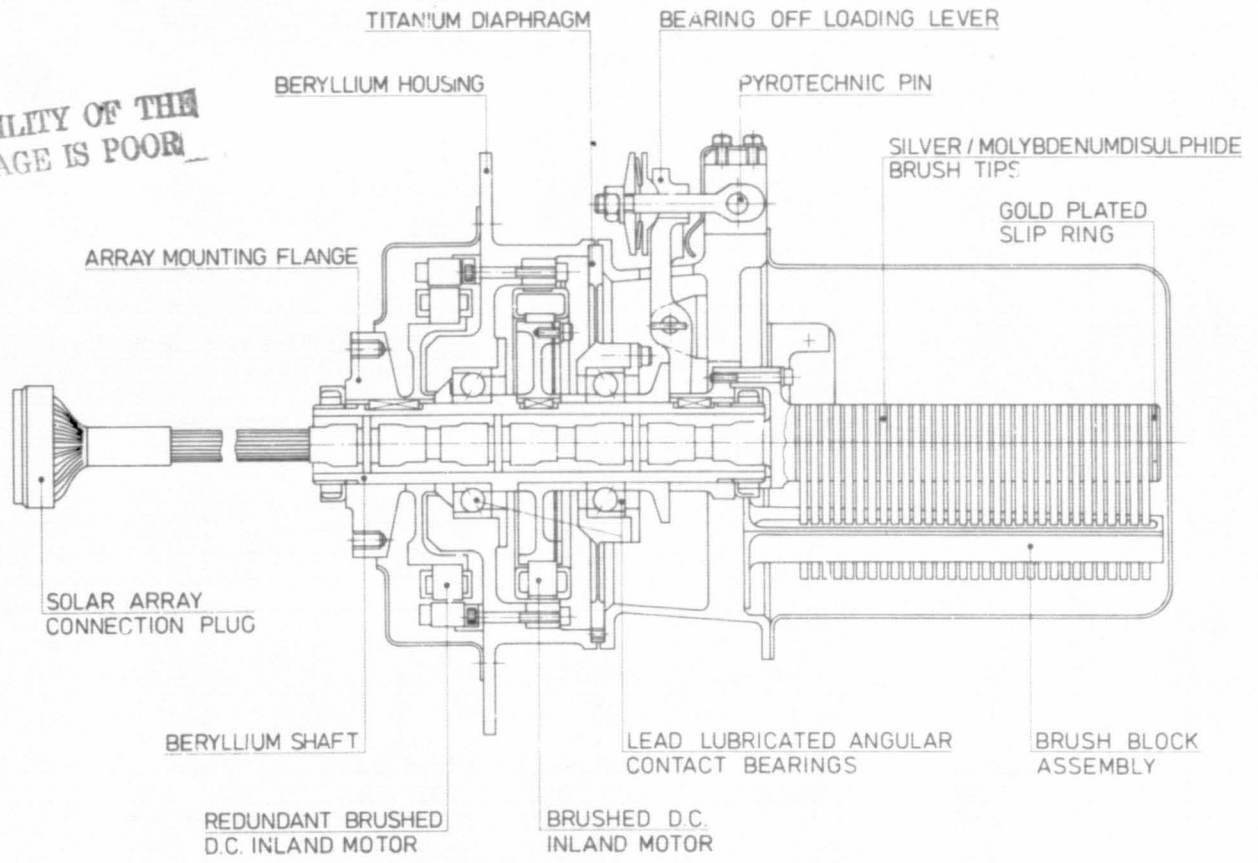

Figure 5. System Block Diagram

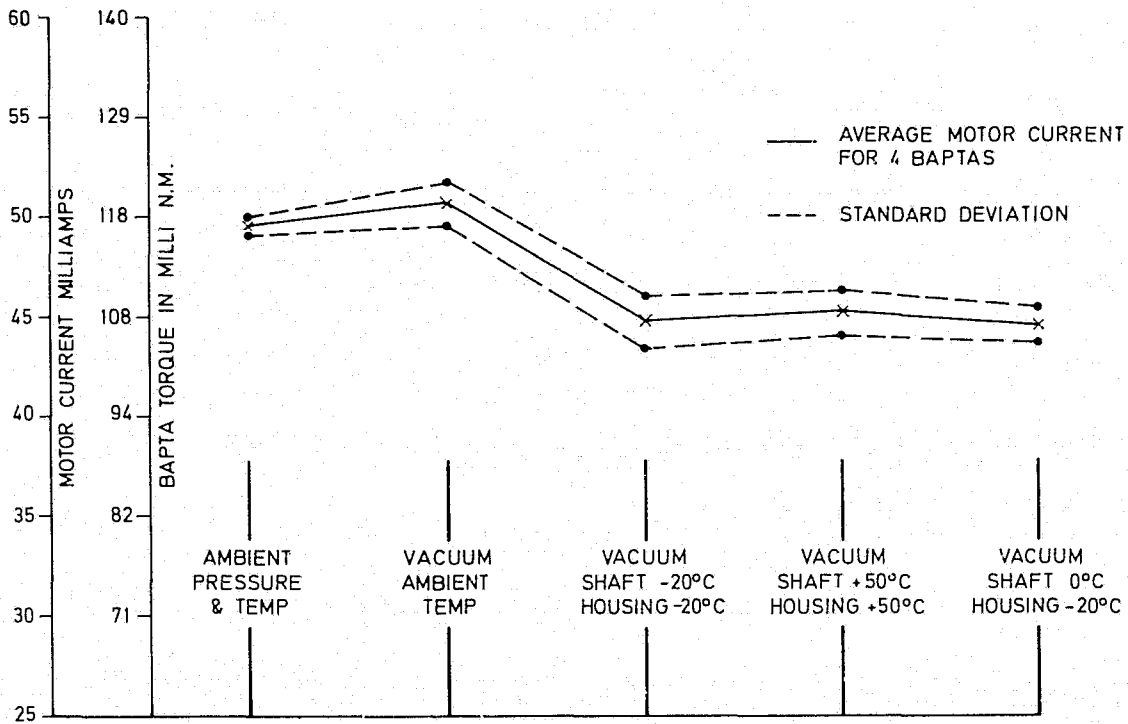Figure 6. OTS BAPTA General Assembly

233

Figure 7. BAPTA Friction for Various Operational Environments
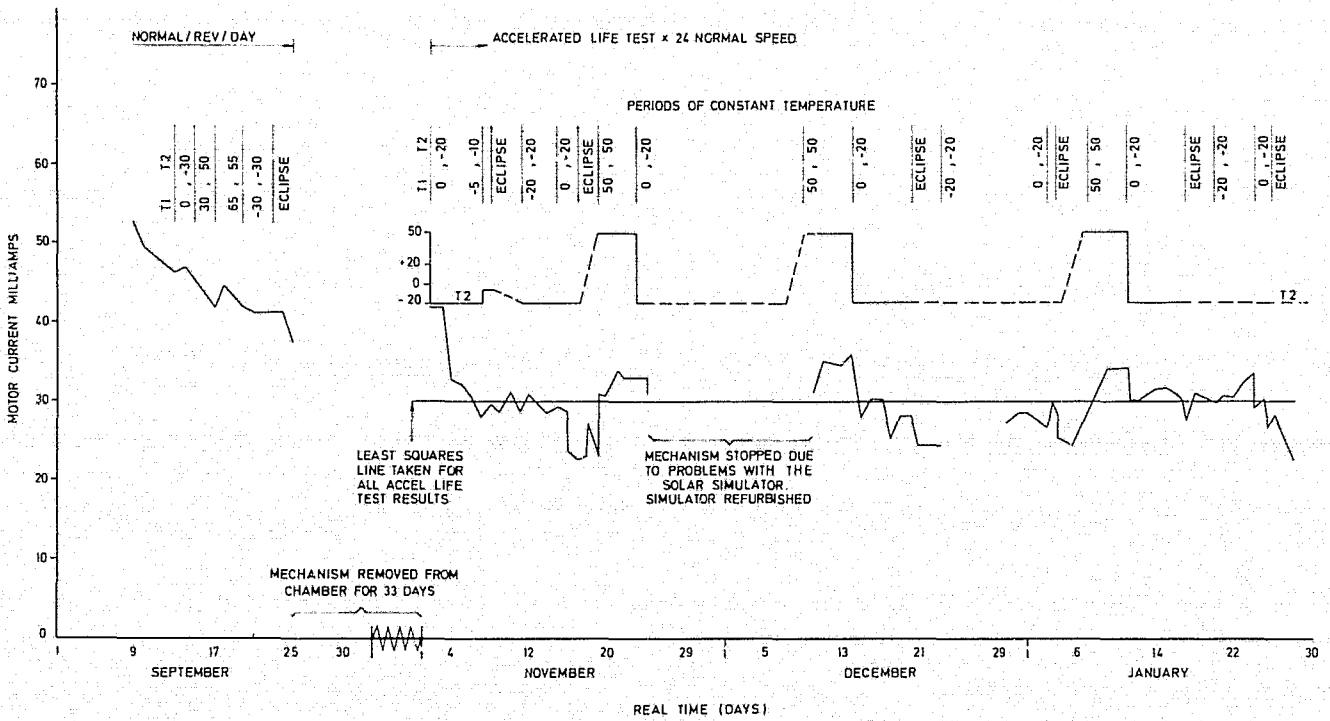

Figure 8. BAPTA Life Test Results

234

VIKING MECHANISMS: A POST MISSION REVIEW

Vernon P. Gillespie
NASA, Langley Research Center

During the summer of 1976 the United States successfully landed two Viking Spacecraft

on the surface of Mars. This feat and the subsequent scientific exploration was made

possible by the successful operation of numerous aerospace mechanisms on both the

landers and the orbitors. The goal of the NASA Viking program is to learn more about

the planet Mars with the primary emphasis on biological, chemical, and environmental

aspects which are relevant to the existence of life.

This presentation will review the current scientific results of the Viking mechanisms.

Special attention will be given to the four known mechanism anomalies. Reflecting on

the success of the Viking spacecraft, the author will discuss recommendations for the

design of future aerospace mechanisms.